POPE JOHN PAUL II STATE SCHOOL
OF HIGHER EDUCATION
IN BIAŁA PODLASKA

FACULTY OF ECONOMIC AND TECHNICAL
DEPARTMENT OF TECHNICAL SCIENCES

MODERN MATERIALS, INSTALLATIONS AND CONSTRUCTION TECHNOLOGIES

Ed. by Stanisław Fic

BREST (BIELARUS) – ODESSA (UKRAINE) – SIMFEROPOL (UKRAINE) – BIAŁYSTOK (POLAND) - BIAŁA PODLASKA (POLAND)

Biała Podlaska, 2013

POPE JOHN PAUL II STATE SCHOOL
OF HIGHER EDUCATION
IN BIAŁA PODLASKA

FACULTY OF ECONOMIC AND TECHNICAL
DEPARTMENT OF TECHNICAL SCIENCES

MODERN MATERIALS, INSTALLATIONS AND CONSTRUCTION TECHNOLOGIES

Edited by

Stanisław Fic

BREST – ODESSA – SIMFEROPOL – BIAŁYSTOK – BIAŁA PODLASKA
(BIELARUS) (UKRAINE) (UKRAINE) (POLAND) (POLAND)

Biała Podlaska, 2013

MONOGRAPH
ISBN 978-83-61044-39-0

Liczba arkuszy wyd.: 10
Nakład: 110 egz.

Published by
Pope John Paul II State School of Higher Education
in Biała Podlaska

Wydawnictwo PSW JPII
ul. Sidorska 95/97, p. 231R
21-500 Biała Podlaska
www.pswbp.pl

Skład, druk, projekt okładki/ Printing, binding and cover design:
Agencja Reklamowa TOP, ul. Toruńska 148, 87-800 Włocławek,
tel.: 54 423 20 40, fax: 54 423 20 80, www.agencjatop.pl

Introduction

A rapid development in the field of materials, installations and construction technologies has been observed for decades. Consequently, the research carried out in terms of various categories allows for the implementation and application of many innovative solutions to the construction.

The construction development is primarily determined by the availability of new materials and their application, which becomes a major determinant of progress and innovation. Nevertheless, the interest in the introduction of new materials to the construction industry is not decreasing. Even though successively introduced European standards in Poland aim at imposing the requirements in terms of materials, while they still treat briefly the quality and quantity of the ingredients used in the composition. The knowledge of the physico-mechanical and physico-chemical properties of materials enables the selection of a more suitable and economical way of their application. At the same time, the properties of the materials must be related to the physical processes that occur in materials used to build various objects. Thus the materials determine such factors as the comfort of use, durability, safety, impact on man and the surrounding environment. Consequently, while introducing new materials and technologies, it is necessary to take sustainable development into account since it reduces CO_2 emissions and becomes more environmentally friendly for man.

This monograph constitutes a collection of articles in the area of materials, installations and construction technologies.

In more than 20 articles, the authors present examples of solutions that allow to obtain a lot of information and knowledge on materials which are important from both the scientific and technical point of view. More importantly, the solutions are copyrighted since they result from experiments and theoretical research related to the areas of concern.

The information and solutions described in the articles can be used as a study aid not only to students of architecture and civil engineering, but also for civil engineers involved in the design and construction of buildings and specialists in the area of engineering science.

Acknowledgments:

The initiative to publish the monograph is held under the patronage of His Magnificence Ph.D Full Professor Józef Bergier, Rector of Pope John Paul II State School of Higher Education in Biala Podlaska, whom I am very grateful.

I express sincere thanks to the authors of the articles, the reviewers and the Scientific Committee for their hard work and professional preparation. I wish you success in your personal and scientific life.

Sincerely
Stanisław Fic

Contents:

THE INFLUENCE OF LEAKAGE OF INSULATING LAYER ON THERMAL PARAMETERS OF ETICS SYSTEM

Orlik-Kożdoń Bożena

Silesian University of Technology, Faculty of Civil Enginering,
Akademicka St. 5, 44-100 Gliwice, Poland
e-mail: Bozena.Orlik-Kozdon@polsl.pl

Summary:
The purpose of this paper is to show a part of results of research in examination of rigid material used for thermal insulation with modified structure. Modification of the material was relying on making of parallel perforations to the direction of the heat and moisture flow. The base solid material was an expanded polystyrene (15EPS-70-040) with board thickness of 5 cm. In the base material the circular perforations with diameter of 1, 3 and 5 mm were done, on the 2 cm x2cm grid (for 15EPS-70-40 material additional samples were done with perforations 7,9 and 11 mm). The researches were divided to preliminary and essential ones. The scope of research included the measurement of water vapour factor's transfer as well as the measurement of heat conductivity factor; the thermographic control of bulkhead insulated by solid and perforated Styrofoam, the simulation of thermal-moisture phenomena in analyzed bulkheads. The essential research was conducted in the Laboratory of Solar Energy Usage in the Faculty of Architecture. Two wall arrangements were analyzed in the research. The common element was the wall's carrying construction. The first bulkhead was insulated by the material with a modified structure - the styrofoam with 5mm perforation. The relative temperature and humidity of external and internal air was registered, on the border of the bulkhead layers as well. The external climate parameters were registered by the Kombi weather station. In the framework of research the mathematical model of coaxial transport processes was verified. Moreover, selected thermal-moisture parameters of wall arrangements were specified. These were as follows: the heat conductivity factor U, the dimensionless temperature of internal surface f_{Rsi}, the water vapour flow

Keywords: thermal insulation, thermal conductivity factor, water vapour factor, thermal-moisture process in bulkhead

Introduction

The styrofoam is today, alongside the mineral wool, the most common material used in thermal insulation. Its physical properties as a thermal insulation material used in architectural engineering were researched as early as 30 years ago. One of its physical properties – the low water vapour penetrability – was at these times acknowledged as disadvantageous. The good thermal insulation, easiness in treatment, low absorption capacity and low density cause that this material found its implementation in the jointless thermal insulation systems of buildings (ETICS, Instruction 447/2009). The styrofoam, as each building material, has its disadvantages. The low water vapour penetrability is one of them. The fast pace of building works and willingness for putting to use the newly erected buildings cause that styrofoam is often used in bulkheads containing large (considerable)

amounts of technological moisture (such as the newly erected walls made from the close dimensional elements). In case of using the styrofoam as a thermal insulating material in the newly erected walls there may be concern of water vapour condensation in the plane of bulkhead, or on its internal surface. The low water vapour penetrability of styrofoam may be in these cases the obstruction in the process of drying of the newly erected wall, or the reason of moisture growth in the cause of thermal insulation of the existing wall.

One of the possible structure modifications of the analyzed material such as the styrofoam used for thermal insulation was, in order to change its properties bound up with water vapour penetration, the making of holes in boards. The argument of selection of the diameters, the spacing and the inclination of holes as well as their influence on thermal and diffusive properties in reference to the water vapour was the main object of the Author's research.

Measured amounts and their analysis

Heat conductivity factor of the material

The studies were conducted for material called: solid material and perforated material. The base material was a solid expanded polystyrene board (EPS-70-040) of 5 cm thickness. The base material was perforated using 2 cm x 2 cm grid pattern in parallel to the direction of the heat and moisture flow. The perforations in the boards were made with the help of the heated up rods. Thanks to that the smooth, circular holes were obtained with diameters accordingly as follows: 1, 3 and 5 mm (additional samples with diameters 7, 9 and 11 mm for material EPS-70-040 were also made).

At the first phase of research the heat conductivity of the material was specified, with usage of the HFM 8301 board apparatus.

The apparatus is equipped with automatic control arrangement of parameters serving for determination of heat conductivity factor, which calculates its value also. The control arrangement assures the quick acquisition of the stationary heat flow in the sample. The other values such as heating and cooling plates' temperature, heat flow's density, sample thickness and the time from the moment of start of the measurement program are also displayed.

The measurements were conducted for the samples with dimensions of 0.30 m x 0.30 m with board thickness of 0.05 m. the field of measurement amounted 0.18 m x 0.18 m. There were constant thermal-moisture conditions in the measurement room – the external air temperature of 22°C and the cooling plate temperature of 0°C. The stabilisation of the heat's flow came up in approx. 30 minutes. After that time came up the reading of the parameter's values such as the temperature of the plates, heat's flow density, the decrease of temperature on particular plates. The readings came up every 3 minutes.

The research was conducted for the three samples arrangement, representing both the solid material and the every type of perforated one. The goal for acquisition of the high accuracy of results was to make the samples a subject of the multiplied measurements in the apparatus. The values of the heat conductivity factor were determined on the base of heat's flow density value, flowing through the sample as well as on the base of values read from the apparatus at the time of research.

The research of the heat conductivity was also conducted using samples with diameters φ7, φ9, φ11. The goal of these studies was to check to what borderline the hole diameter can be increased without decreasing the value of the heat conductivity factor (λ)

– by simultaneous increase of the material's diffusion. The results of the research show (Fig. 1) (Orlik, Ślusarek) that the borderline value is diameter of 5 mm, because the heat conductivity factor increases along with the growth of perforation. Analyzing the values of the heat conductivity factor for various types of diameters (Fig. 1), we may suspect that in case of perforations with diameter φ1, φ3 mm we have to deal with conductivity in the apertures, what causes the decrease of the lambda factor value. In the holes with diameter of φ5 mm there might occur the phenomenon of the convectional heat transfer, what causes a slight increase of the heat conductivity.

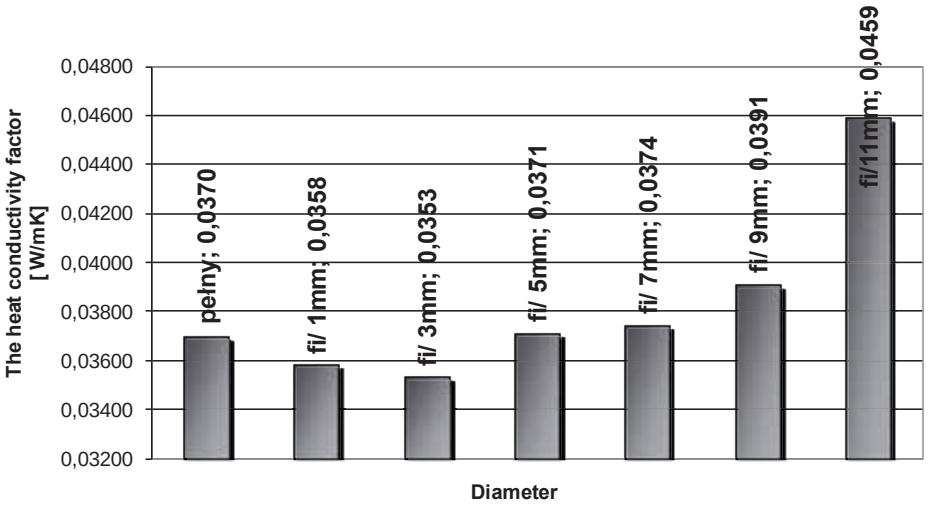

Fig. 1. Values of the heat conductivity factor for various types of perforations

Aiming at thinking through of the heat transfer phenomena in the researched material the simulation model was done using Therm 7beta computer program. This program was based on MES.

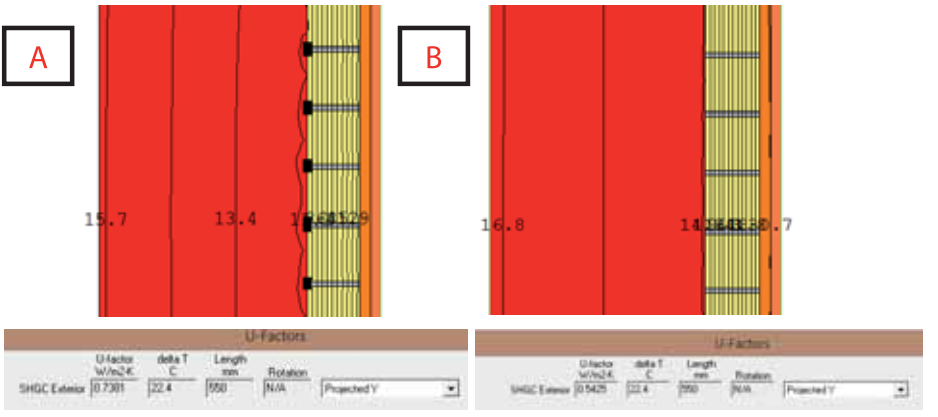

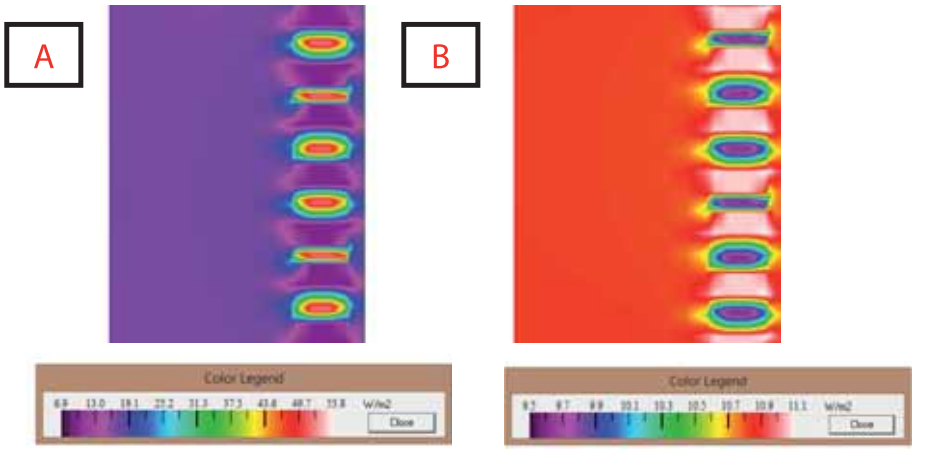

Fig. 2. The arrangement of isotherms and heat flow density in the bulkhead insulated with perforated material with hole diameter of 5 mm. Variant A) straight conductivity in the apertures; Variant B) conductivity in the apertures plus the free convection.

For further analysis of that phenomenon the mathematical model of the flow based on Jacob's empirical relations was formulated (Wiśniewski 1997). During the little intensive heat transfer we observe a straight conductivity, and after the occurrence of the convective currents the conductivity and convection came within a definition of the equivalent heat conductivity factor λ_r (Fig.3). The relation of the λ_r/λ factors (λ – air factor) is characterized by the potentiation of the heat exchange intensity caused by the free convection, in relation to straight heat conductivity. For analyzed apertures their dimensions such as thickness and height were taken into account. In the description of the phenomena the Jacob's empirical relations were put to use (Bloem 1996, Wiśniewski 1997):

$$\frac{\lambda_r}{\lambda} = 0.18 \cdot Gr^{0.25} \left(\frac{H}{l}\right)^{-\frac{1}{9}} \tag{2.1}$$

where:

λ – heat conductivity factor for the gas filling the aperture [W/mK],
λ_r - equivalent heat conductivity factor [W/mK],
l – width of the aperture [m],
H - height of the aperture [m].

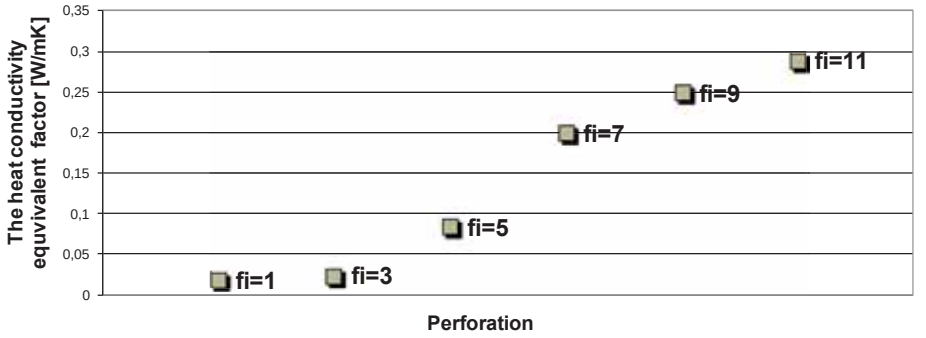

Fig. 3. Equivalent heat conductivity factor in analyzed bulkheads

The Grashof's number determines the free convection's intensity. As the theoretical arguments and experimental researches have shown, the movement in the liquid appears only when the critical value of Rayleigh's number Ra_{kr} = 1700 will be exceeded (Bloem 1996, Wiśniewski 1997):

$$Ra = \Pr \cdot Gr \tag{2.2}$$

where:

Gr – Grashof's number,
Pr – Prandtl's number
Ra - Rayleigh's number.

At the 1700 < Ra < 45 000 the movements in liquid are appearing. When the Ra > 45 000 the liquid's flow goes through laminar into turbulent one, the liquid's movements became irregular (Bloem 1996, Wiśniewski 1997, Bergman 2011).

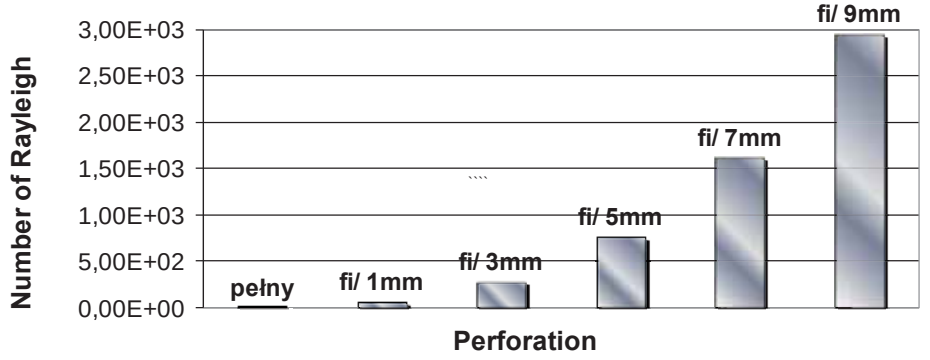

Fig. 4. Calculated Rayleigh's number for analyzed bulkheads

At the picture No. 4 the values of Rayleigh's number for analyzed bulkheads are shown. Its value increases proportionally to the diameter size of the holes. According to (Klemm, Collective work: Physics of the buildings, 2005; Wiśniewski 1997) at the 7 mm thickness of the air aperture the convection doesn't occur and we have to deal with the straight heat conductivity (the calculations shown confirm this). The closed air aperture serves as an insulator. For apertures from the range of φ7 mm ÷φ11 mm we already observe the appearance of movement in the aperture, what probably causes the increase of heat conductivity. Additionally, the heat flow as a result of radiation as well as the radiational characteristics of the surfaces adjoining to the sample affects on the results of the researches. That's why the heat's flow property incorrectly called the heat conductivity – calculated from the determined formulas and results of the heat's flow measurement as well as the difference of temperatures and sample dimensions – should be called the heat exchange factor.

3.2. Bulkhead's heat infiltration factor

The designation of the heat infiltration factor was done relying on heat flow's density researches (Fig. 7 – example – P2 bulkhead) for both types of bulkheads, according to the procedure included in the ISO 9869:1994 norm: *Thermal insulation. Building elements. In situ measurement of thermal resistance and thermal transmittance* (9).

In the researches two wall arrangements were analyzed: P1 – the wall insulated by the solid material; P2 – the wall insulated by the perforated material (Orlik, Ślusarek 2010). The density measurement was done by the gauge with sensor type *auxiliary wall* (Brandtke 1958, Bloem 1996, Taler 1995).

The researches of such a scale were conducted in the field conditions on the measurement station consisting of three separate chambers, where one of these was modernized for the purpose of the research. On the selected wall of the chamber the insulation was laid , made from solid and perforated research material. The used measurement system allowed registration of the data such as relative humidity and temperature distribution in particular bulkhead planes and in the chamber. Additional measurement apparatus installed on the building allows for measurement of quantities which characterize the external environment: wind speed, insolation, amount of rainfall, relative humidity and external air temperature – the weather station type Kombi WS 2305.

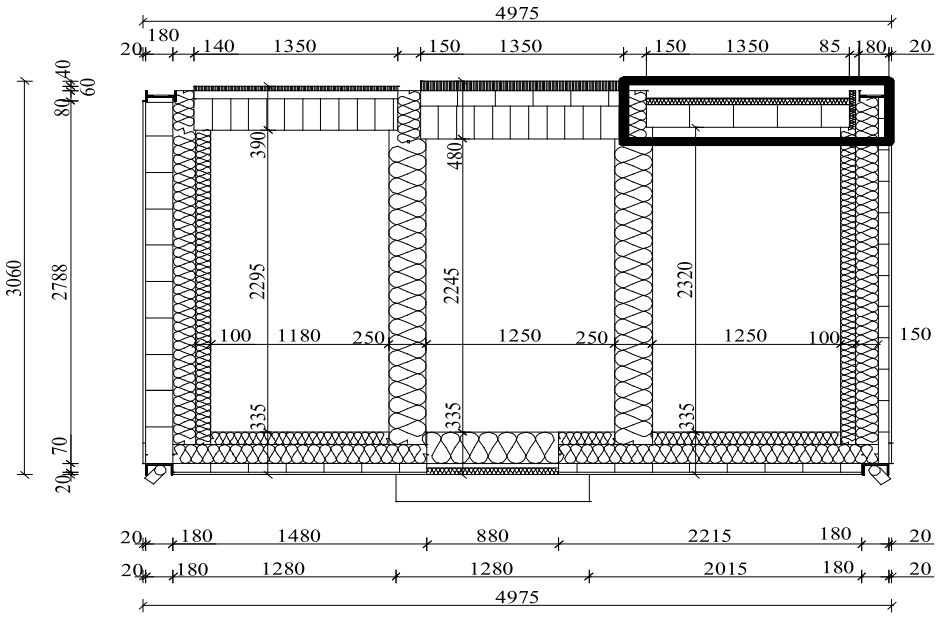

Fig. 5. Projection of a research station with a bulkhead under research marked

Fig.6. Picture of a research station in the laboratory of an Architectural Engineering Faculty of a Silesian Technical University [author's photo]

The chamber was situated against points of compass in order to expose the researched wall elements to the south. The internal bulkheads separating the rooms were designed as adiabatic ones in order to prevent the heat's flow among them. In the rooms three independent heating-cooling arrangements were used. The research station was equipped with computer – assisted registration and data gathering system, describing the basic thermal-moisture parameters of the analyzed chamber and its bulkheads. The measurement apparatus which was put to use on the research station is:

Fig. 7. View of the research station

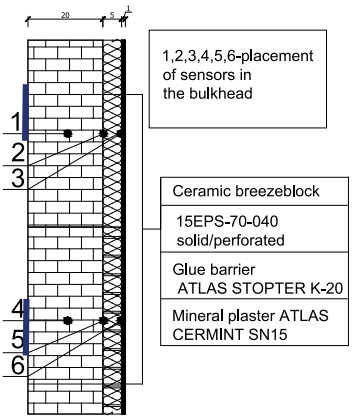

Fig. 8. Scheme of the analyzed bulkheads and arrangement of the sensors on their surfaces

The goal of these measures was to calculate the real thermal resistance R as well as the heat infiltration factor U for the researched bulkheads. In case of conducting of the continuous measures in time not shorter than 72 hrs, for calculations should be used the formulas included in the ISO 9869 (Bloem 1996, Haupt 2008, ISO 9869). The complete thermal resistance should be calculated from the formula ISO 9869):

$$R_n = \frac{\sum_{j=1}^{n} T_{sij} - T_{sej}}{\sum_{j=1}^{n} q_j} \tag{3.1}$$

where:

R_n – complete resistance of the bulkhead's surfaces without taking into consideration the resistances of heat's interception on the surfaces of the bulkhead [m^2K/W],
T_{sij} – measured temperature on the internal surface of the bulkhead [^oC],
T_{sej} – measured temperature on the external surface of the bulkhead [^oC],
Q_j – measured heat's flow density on the surface of the bulkhead [W/m^2].

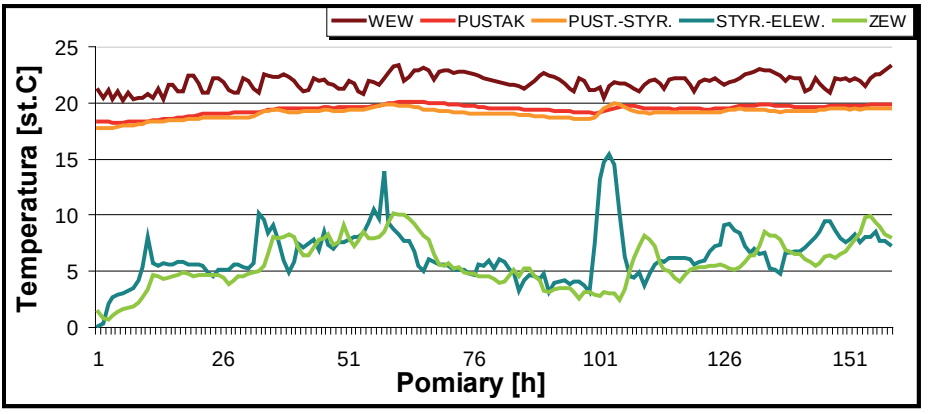

Fig. 9. The process of temperature's alternation in layers of a bulkhead insulated with solid material

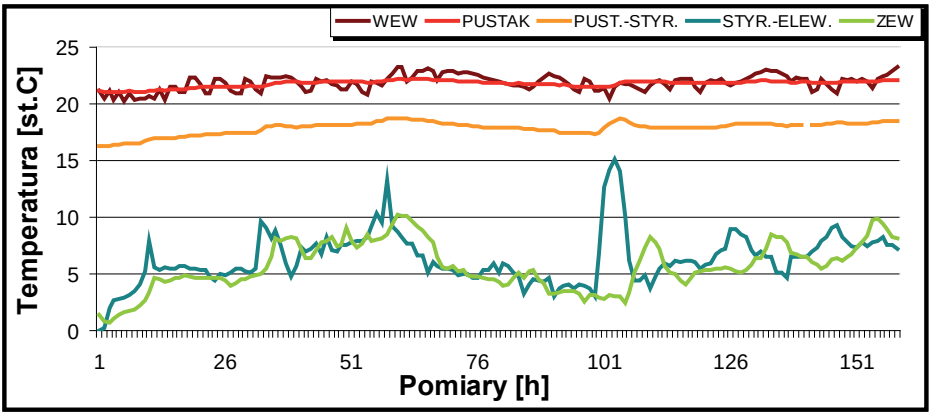

Fig. 10. The process of temperature's alternation in layers of a bulkhead insulated with perforated material

On the graphes illustrating the proceeding of temperaturę's alternation on the surfaces of bulkhead insulated by the solid material, the significant discrepancies in temperature distribution on the surfaces of the analyzed bulkheads can be observed. For the bulkhead insulated by the perforated material on the surface of ceramic block, the temperature obtains the value between 1,5°C÷4°C, which is higher than on the same surface in the wall insulated by the solid material. On the point of junction of the ceramic block – the styrofoam the sudden decrease of temperature follows in the bulkhead insulated by the perforated material, it is bound up with simultaneous increase of moisture on that surface and accruing of it in the direction of the external environment (Orlik, Ślusarek).

As a result of application of the 3.1 formula, as well as the values gained within the measures, the following values were received for the analyzed bulkheads:

R_{n1} = 1,144 m²K/W R_{n2}= 1,476 m²K/W

The complete thermal resistance of the bulkhead R_T taking into account the resistances of the heat's interception on the surfaces of the building bulkhead amounts to:

R_{T1} = 1,314 m²K/W R_{T2} = 1,649 m²K/W

where:

R_{T1} – complete resistance of the P1 bulkhead [m²K/W].

R_{T2} - complete resistance of the P2 bulkhead [m²K/W].

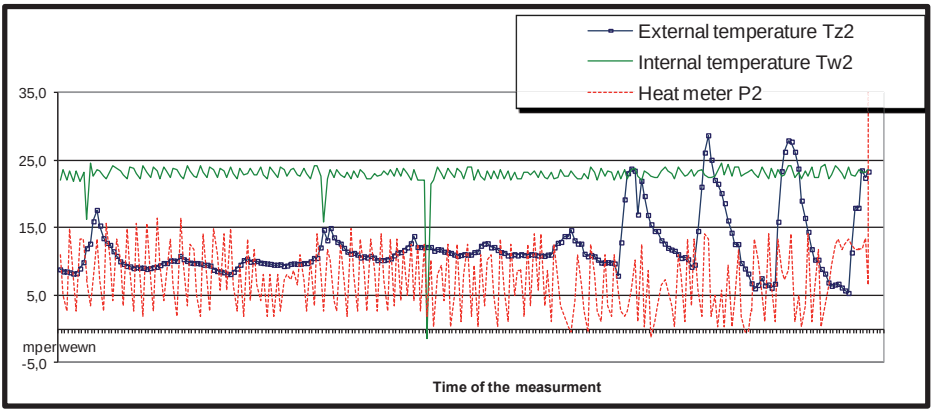

Fig. 11. Track record of the temperatures and heat's flow density for the bulkhead insulated by the P2 perforated material

According to the PN EN ISO 6946 (PN EN ISO 6946) the heat interception factor U is calculated in the compliance with the formula:

$$U = \frac{1}{R_T} \tag{3.2}$$

$U_1 = 1/R_{T1}$ = 0,76 W/m²K $U_2 = 1/R_{T2}$ = 0,61 W/m²K

4. Loss of heat by the analyzed bulkheads

The complete loss of heat in the heating season by the building bulkhead can be calculated according to the norm PN-B-02025:1999 *Calculating of the seasonal demand for the warmth for heating of the habitable and public utility buildings*, by the formula:

$$Q_u = 8{,}64 \cdot 10^{-5} \cdot S_d \cdot A \cdot U \quad [GJ/year] \tag{4.1}$$

where:

Q_u - loss of the heat in the heating season [GJ/year],

S_d - number of grading days (calculated according to the above norm for the nearest meteorological station - Katowice, S_d = 2616.6),

A - surface field of the bulkhead [m^2],

U - complete heat infiltration factor [$W/(m^2K)$].

Both researched bulkheads can be qualified as the solid walls without windows and doors. For the purpose of calculations the field of surface A=100 m^2 was accepted.

$$Q_{u1} = 8{,}64 \cdot 10^{-5} \cdot 2616{,}6 \cdot 100 \cdot 0{,}76 = 17{,}1 \text{ GJ/year}$$
$$Q_{u2} = 8{,}64 \cdot 10^{-5} \cdot 2616{,}6 \cdot 100 \cdot 0{,}61 = 13{,}7 \text{ GJ/year}$$

where:

Q_{u1} - loss of the heat in the heating season for the bulkhead P1 [GJ/year],

Q_{u2} - loss of the heat in the heating season for the bulkhead P2 [GJ/year],

According to the requirements known in *Technical conditions* the bulkhead of this type should be characterized by the heat infiltration factor U not bigger than 0,30 [W/m^2 K].

$$Q_u(WT) = 8{,}64 \cdot 10^{-5} \cdot 2616{,}6 \cdot 100 \cdot 0{,}30 = 6{,}78 \text{ GJ/year}$$

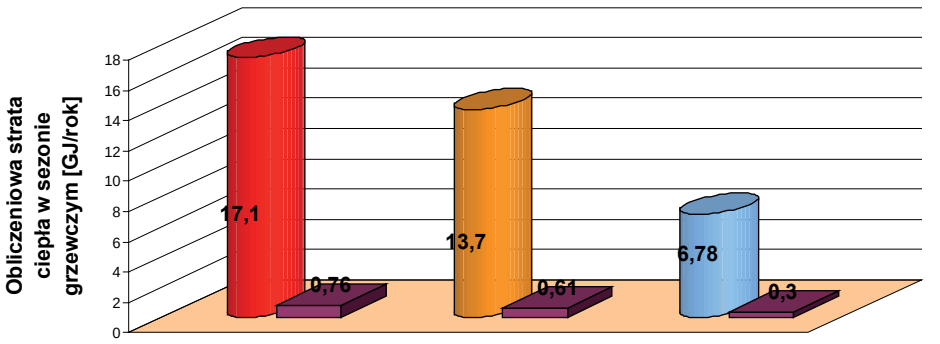

Fig. 12. Computational heat loss trough 100m^2 bulkhead

Summary

The researches presented in this paper are a part of the whole research cycle on the material with modified structure and about the behavior of this material in the bulkhead (Orlik, Ślusarek). Part of this research, dedicated to determining of the thermal parameters of the material and its behaviour in the wall, has shown that the modified boards beneficially cooperate with the whole wall arrangement, improving its thermal parameters (U factor). It should be remembered that the implementation of the new materials and technologies requires a full recognition of the very important physical conditions accompanying the associated phenomena of the heat and mass transfer. The observation and analysis of the water vapour diffusion phenomena through the analyzed wall arrangements, characterized by the discontinuity in the styrofoam layer, considerably increase the possibility of the water vapour flow, changing the moisture potential of the whole bulkhead. The further analyses show, that the places of the intensive water vapour flow due to the difference of the partial pressures, may contribute to the weakening of the plaster's layer adhesion to the base in places of the perforation. As a result of the thermal – moisture phenomena the emerging tensions may cause the damage of the elevation layer, what in turn may cause a greater penetration of the moisture into the particular bulkhead layers. The usage of a rigid insulating materials (styrofoams) in the methods of the thermal insulation should be preceded with additional research connected with the obsolescence of the whole arrangement, so as to eliminate the disadvantageous phenomena of the weakness of the external layers (glue, netting, plaster) in the places of the styrofoam's perforation.

References:

1. Bradtke F., Liese W.: Climatic measurements inside and outside of the buildings; Hand-book; Arkady 1958.
2. Bloem J.J.: System identification applied to building performance data; Institute for systems engineering and informatics;.Fundamentals of Heat and Mass Transfer; Incropera/DeWitt/Bergman/Lavine, 1996.
3. Bergman, Lavine, de Witt: Fundamentals of Heat and Mass Transfer; Incropera, 2011.
4. Haupt P.: Bauphysik; Klima Warme Feuchte Schall; Grundlagen, Anwendungen; Beispiele; Ernst&Sohn, 2008.
5. Orlik-Kożdoń B., Ślusarek J.: Processes of heat and moisture transfer in the building's bulkheads with the complex structure; Monography; Gliwice 2010.
6. Collective work under the management of asisstant professor doctor engineer P. Klemm: General architecture; vol. 2; Physics of the buildings ; Arkady 2005.
7. Taler J.: Theory and practice of the heat transfer identyfication ; Zakład Narodowy Imienia Ossolińskich 1995.
8. Wiśniewski S., Wiśniewski T.S.: Heat exchange; Wydawnictwo Naukowo-Techniczne; Warsaw 1997.

Norms and associated documents:

1. ISO 9869: 1994 Thermal insulation. Building elements. In situ measurement of thermal resistance and thermal transmittance.
2. Statuory instrument of the Ministry of Infrastructure in case of technical requirements for buildings and their situation , Journal of Acts No. 75 from 15.06.2002, pos. 690 with further changes.
3. PN-EN ISO 6946:1999. Building components and elements of the buildings. Heat resistance and heat infiltration factor. Method of calculation.
4. Complex systems of thermal insulation of the external walls of the ETICS building. The rules of design and realization, Warsaw

TECHNICAL AND ECONOMIC ANALYSIS OF THERMAL MODERNISATION PROCESS OF A DETACHED HOUSE

[1]Ewa Zarzeka-Raczkowska, [2]Andrzej Raczkowski, [2]Piotr Pomorski

[1]Pope John Paul II State School Higher Education in Biala Podlaska,
Department of Engineering Sciences, Department of Civil Engineering
Sidorska St. 95/97, 21-500 Biała Podlaska, Poland
e-mail: e.zarzeka-raczkowska@pollub.pl,
[2]Collegium Mazovia Innowacyjna Szkoła Wyższa w Siedlcach
Sokołowska St. 161, 08-110 Siedlce,
e-mail: araczkowski@mazovia.edu.pl,

Summary:
The aim of this paper is to analyse the cost-effectiveness of thermal modernisation of a detached house, making use of different technologies. In order to reduce heat losses three thermo-modernisation options are considered. In the first option the exterior walls are insulated with 10 cm thick Styrofoam and the roof is insulated with 15 cm thick mineral wool. This produces the following heat transfer coefficients: for the exterior wall U = 0.213 W/(m^{2}K) and for the roof U = 0.214 W/(m^{2}K). In the second option, additionally to the wall and roof insulation, the windows whose heat transfer coefficient is U=0.9W/(m^{2}K) are replaced. In the third option all the work as in the second option is done and a new, state-of-the-art boiler of the 93 % efficiency is installed.
The heat calculations for the thermal modernization of the detached house are performed with the computer program PURMO OZC v 4.80b. To cost the thermo-modernisation works the computer program Norma Pro v 4.03 – pricelist for the April-July quarter 2013 is used.
The thermal modernization of the existing detached house encompassing insulating external barriers, replacing old windows with new tighter ones and installing a new more efficient boiler resulted in a considerable reduction of the heat demand coefficient (EA) and allowed classifying the house as energy-efficient.
The scope of the thermo-modernisation in the three options increases as well as the costs incurred. The third option is twice as expensive as the first one, yet the payback period is similar - approximately nine years. The most profitable is the third option of thermo-modernisation because in a twenty-year period the owner can save about 41324 PLN as compared to the costs incurred currently.

Keywords: thermo-modernisation, mechanical ventilation, recuperation

Introduction

In recent years the rising costs of maintaining and operating a residential building, together with increasingly restrictive regulations in residential construction as well as growing environmental awareness of Polish society have all forced designers, investors and occupants to apply technologies which will enable to achieve the most cost-effective and energy-saving building solutions.

The value which assesses the building in energy-consumption terms is the coefficient of seasonal heat demand (EA). This value enabled to create energy-consumption classification of buildings (Table 1) (Sas-Micuń 2006).

Tab. 1. Energy-consumption classification of buildings (www.termoexpert.com.pl)

Type	Residential Building	Coefficient EA [kWh/m2 year]
A	Highly energy-efficient	20 - 45
B	Energy-efficient	45 - 80
C	Medium energy-efficient	80 - 100
D	Medium energy-intensive	100 - 150
E	Energy-intensive	150 - 250
F	Highly energy-intensive	over 250

In order to improve the energy-efficiency of a building, i.e. to limit the amount of energy supplied mainly by heating, ventilation and hot water systems, which entails the reduction of maintenance costs, it is advisable to thermo-modernize the building and to carry out its energy audit.

Thermo-modernisation lies in refurbishing a building in such a way as to reduce its consumption of energy needed to maintain constant pleasant living temperature and the consumption of energy needed to heat water as well as preventing exterior walls from freezing and enhancing the look of the building (Bogacki M., Osicki 2011, Dreger 2006).

Heat losses in a building bring about a number of unfavourable phenomena for the building itself as well as its occupants. One of them is insufficiently heated rooms. According to the regulation PN-82/B-02403 the pleasant living temperature for rooms should be 20^0C. Occupants, to reduce building maintenance costs, significantly lower the temperature even down to 15^oC - 17^oC. This, apparently, reduces the costs but dramatically diminishes thermal comfort. Another threat is overheating of rooms, which may derive from an inadequate heating system in the building. The old, over-exploited and badly chosen interior heating system, without the possibility of adjusting the heat supply results in heat surplus. This may lead to frequent airing of rooms and unreasonably high heat loss. This, in turn, leads to unjustified costs incurred by the occupant to heat the premises.

Far more heat energy needs to be supplied to maintain the desired temperature in older buildings than in new buildings. This requires supplying far more fuel. In Poland the most popular fuel sources are coal, oil and natural gas. Prices of these fuels are independent of the occupant and strictly dependent on the political and economic situation. As a result, an underheated building makes the occupant cover considerable costs to buy energy.

An acute problem of inadequately insulated house is the problem of freezing walls in winter time. On the internal surface of a cold building wall moisture turns up. This is an ideal environment for fungi and mold to spread, which is hazardous to human health. Damp barriers and moisture penetrated walls result in a significant drop in heat accumulation by construction materials used for facades. This leads to the deterioration of wall surfaces and manifests itself by water stains and peeling off plaster (Norwisz 2006).

Thermal modernisation of a building consists in insulating walls, roofs and ceilings, replacing windows and doors, upgrading or replacing the heating system, upgrading the ventilation and water heating system as well as using renewable energy sources.

The most beneficial in thermal modernisation is performing all the possible refurbishment works simultaneously. The profitability of each operation is presented in Table 1.

Thermal modernisation is a fairly costly operation. In Poland investors planning to modernise thermally their houses can seek financial support. Pursuant to the Thermo-modernisation and Refurbishment Support Act dated 21.11.2008 (Dz. U. Nr 223, poz. 1459) investors may receive financial support with a view to repaying part of the thermo-modernisation loan on several conditions, one of them being the reduction of building energy consumption (Dylewski, Adamczyk 2008).

The document required to obtain a thermo-modernisation loan is a building energy audit. This document is an analysis of thermo-modernisation solutions trying to find the best technical and economic solution for the building, which will minimize the maintenance and operational costs as well as reducing the energy consumption. In other words, the investment must be cost-effective, whereas the repaid loan cannot be higher than the savings generated through the thermo-modernisation.

Tab. 2. Cost-effectiveness of thermo-modernisation works - www.muratordom.pl

Thermo-modernisation work type	Approximate savings compared to before modernisation [%]	Approximate payback period [years]
Roof and ceiling over attic insulation	5 – 15	6 – 8
Wall insulation	10 – 20	8 – 12
Ceiling over basement insulation	2 – 5	10 – 20
Window replacement	10 – 15	15 - 25
Heating installation upgrade	10 – 20	4 – 8
Boiler room automatisation	5 – 10	3 – 5
Boiler replacement	10 – 20	8 – 12

The correct energy audit is performed in order to indicate the best technological solution to the investor or prospective occupant and to enable a conscious choice of employing the best thermo-modernisation method for the building in question.

Methods

The detached house is situated in Siedlce in Sokołowska Street. It was erected in 1985. It is a two-storey house with a basement and an unusable attic. The area which needs to be heated is 372.5 square metres. The building was constructed using traditional building methods. Three-layered exterior walls have the heat transfer coefficient of U = 0.39 W/ (m^2K), the ceiling under the unheated attic has the heat transfer coefficient of U = 0.5 W/ (m^2K), and the wooden-frame double-glazed windows have that of U = 2.6 W/ (m^2K).

Numerous heating calculations were carried out for the building. Their aim was to evaluate the annual maintenance cost of this detached house before modernization and to analyse the cost-effectiveness of thermo-modernisation in three different options (Dylewski, Adamczyk 2008, Koczyk et al. 2005).

In the first option the exterior walls are insulated with 10 cm thick Styrofoam and the roof is insulated with 15 cm thick mineral wool. This produces the following heat transfer coefficients: for the exterior wall U = 0.213 W/ (m^2K) and for the roof U = 0.214 W/ (m^2K) (Wysocki 2007).

In the second option, additionally to the wall and roof insulation, the windows whose heat-transfer coefficient is U=0.9W/ (m^2K) are replaced.

In the third option all the work as in the second option is done and a new, state-of-the-art boiler of the 93 % efficiency is installed.

The calculations were performed taking the following into consideration: convection heating system, low building tightness, location in the third climatic zone for which the predicted outdoor temperature is that of -20^{o}C in winter time. Average annual temperature for the building location is t=7,6^{o}C. The data for the calculations came from the actinometric weather station in Mikołajki.

All the calculations were carried out in compliance with the Polish regulations:

PN-EN ISO 6946 Construction components and building elements. Heat resistance and heat transfer coefficient. Calculation method.

PN-EN 12831:2006 Heating installations in buildings. Calculation method of design heat load.

PN-B-02025: Calculation of the seasonal heat demand for single-family and multi-family residential buildings.

The heat calculations for the thermal modernization of the detached house were performed with the computer program PURMO OZC v 4.80b. To cost the thermo-modernisation works the computer program Norma Pro v 4.03 – pricelist for the April-July quarter 2013 was used.

Results and discussion

The calculations allowed determining the design heat load for the building, the seasonal heat demand EA indicator and investment costs for each thermo-modernisation option. The results are presented in Table 3.

Tab. 3. Results of the building heat load F_{hl}, seasonal heat demand EA indicator and investment costs

Building state	Present state	1st Option	2nd Option	3rd Option
Investment costs PLN	-	16511.18	25188.73	32017.08
Heat load $F_{hl,}$ [W]	19610	17722	16330	16330
Seasonal heat demand EA indicator, [kWh/(m²*year)]	88.3	72.3	65.1	65.1
Annual heating maintenance costs PLN	10022.42	8213.71	7388.10	6355.35

The enhancement of external barrier insulation in the first and second options resulted in a considerable reduction of design heat load respectively by 9.6% and 12.7 %. It also resulted in the reduction of the seasonal heat demand EA indicator respectively by 18.1% and 26.3% and the reduction of annual heat maintenance costs by respectively 19.0% and 26.3% compared to the maintenance costs of the building in the present state.

The values of the seasonal heat demand EA indicator and the annual heat maintenance costs are directly proportional to each other; therefore their decrease is the same. The replacement of the heat source in the third option does not influence the further reduction of the design heat load and the seasonal heat demand EA indicator because it does not affect the heat loss values, yet it brings about the reduction in fuel consumption. Therefore, it directly reduces the annual heat maintenance costs by 36.6% as compared to the maintenance costs of the building in the present state. (Figure 1)

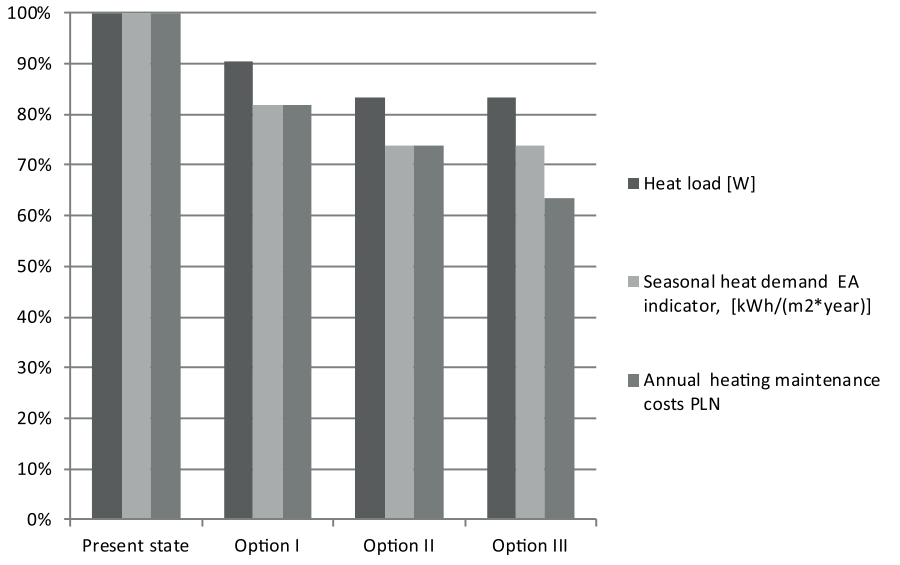

Fig. 1. Reduction in design heat load, seasonal heat demand EA indicator and heat maintenance costs.

On the basis of the calculated seasonal heat demand EA indicator which is 88.3 kWh/ (m^2year), the house in Siedlce has been classified as medium energy-efficient. The first and second thermo-modernisation options reduced the seasonal heat demand EA indicator respectively down to 72,3 kWh/ (m^2year) and 65,1 kWh/ (m^2year), which meant that the building could be classified as energy-efficient (Figure 2).

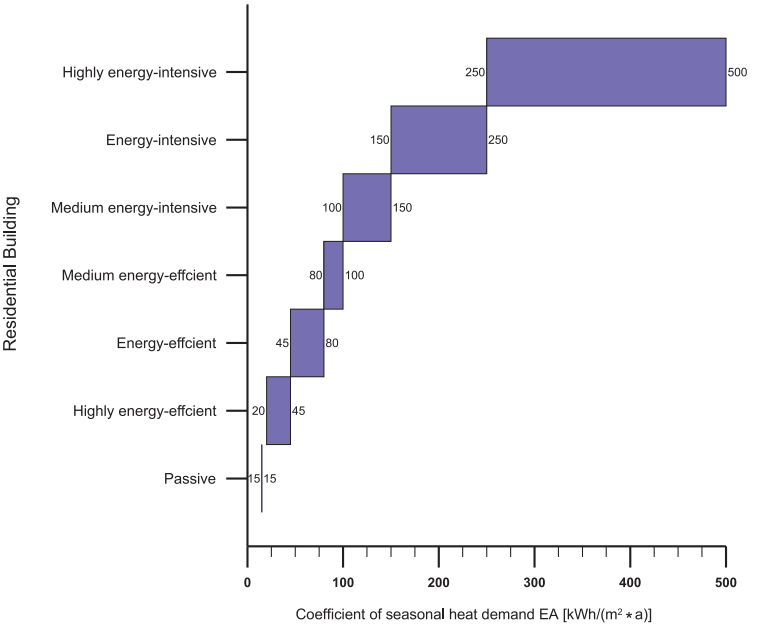

Fig. 2. Energy classification of buildings including the house in Siedlce

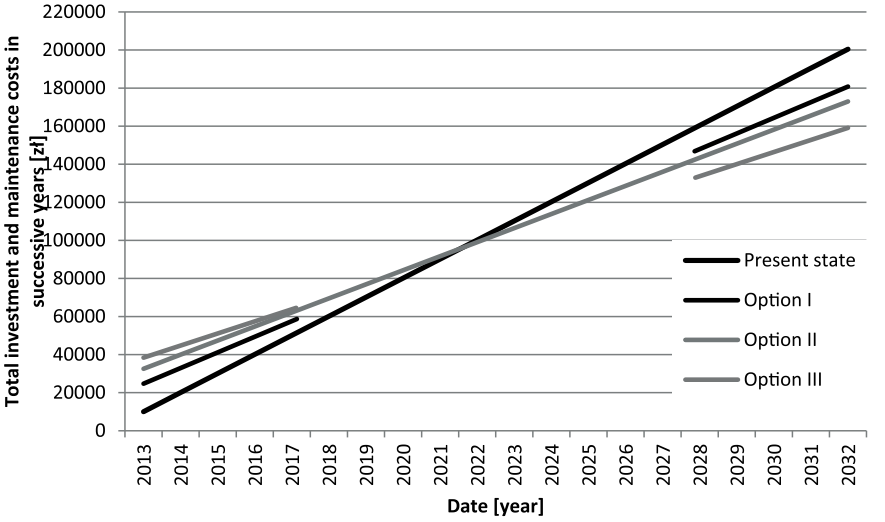

Fig. 3. Total investment and maintenance costs in successive years for the three modernisation options

The analysis of the aggregated investment and maintenance costs in the successive years (on condition that energy prices and efficiency of the existing solutions do not change) showed that the payback period for the first and third options is nine years, while for the second option is ten years. In a twenty-year period the third option will prove to be the most profitable as it will give 41324 PLN in savings (Figure 3).

Conclusions

The house in Siedlce in the present state has been classified as medium energy- efficient. The scope of thermo-modernisation works in the second option significantly reduces the value of seasonal heat demand EA indicator and as a result, the house meets the criterion of being energy-efficient. Further heat reduction is feasible through the improvement of the ventilation system and central heating system by means of automatisation.

The scope of the thermo-modernisation in the three options increases as well as the costs incurred. Despite the costs increase, the third option is twice as expensive as the first one, yet the payback period for all options is similar - approximately nine years. The most profitable is the third option of thermo-modernisation because in a twenty-year period the owner can save about 41324 PLN as compared to the costs incurred currently.

References:

1. Bogacki M., Osicki A. (2011), Termomodernizacja w świetle dyrektywy o charakterystyce energetycznej budynku. Fundacja na rzecz Efektywnego Wykorzystania Energii. Katowice.
2. Dreger M. (2006), Właściwa grubość izolacji, Materiały Budowlane, No 3, 7-8.
3. Dylewski R., Adamczyk J. (2008), Wpływ kosztów ogrzewania na dobór termoizolacji, Ciepłownictwo, Ogrzewnictwo, Wentylacja, No 6, 20-24.
4. Koczyk H., Antoniewicz B., Basińska M., Górka A., Makowska-Hess R., (2005), Ogrzewnicwo praktyczne- projektowanie, montaż, eksploatacja, Wyd. Systherm Serwis, Poznań.
5. PN-B-02025:2001 Obliczanie sezonowego zapotrzebowania na ciepło do ogrzewania budynków mieszkalnych i zamieszkania zbiorowego.
6. PN-EN 12831:2006 Nowa metoda obliczania projektowego obciążenia cieplnego.
7. PN-EN ISO 6946 Komponenty budowlane i elementy budynku. Opór cieplny i współczynnik przenikania ciepła. Metoda obliczania.
8. Praca zbiorowa pod redakcją dr hab. inż. Jana Norwisza (2006), Termomodernizacja budynków dla poprawy jakości środowiska. Narodowa Agencja Poszanowania Energii, Gliwice.
9. Rozporządzenie Ministra Infrastruktury z 6 listopada 2008r. w sprawie warunków technicznych, jakim powinny odpowiadać budynki i ich usytuowanie.
10. Rozporządzenie Ministra Infrastruktury z dnia 15 styczna 2002 roku w sprawie szczegółowego zakresu i formy audytu energetycznego (Dz. U. Nr 12, Poz. 114).
11. Rozporządzenie Ministra Infrastruktury z dnia 17 marca 2009 roku w sprawie szczegółowego zakresu i formy audytu energetycznego oraz części audytu remontowego, wzorów kart audytów, a takŜe algorytmu oceny opłacalności przedsięwzięcia termomodernizacyjnego.

12. Rozporządzenie Ministra Infrastrukturyz 12 kwietnia 2002r. w sprawie warunków technicznych, jakim powinny odpowiadaćbudynki i ich usytuowanie (Dz. U. 2002 nr, 75 poz.690).
13. Sas-Micuń A. (2006), System oceny energetycznej budynków – proponowane rozwiązania prawne. Materiały Budowlane 1/2006.
14. Ustawa z dnia 21.11.2008 r. o wspieraniu termomodernizacji i remontów (Dz. U. Nr 223, poz. 1459, z późn. zm.)
15. Wysocki K. (2007), Docieplanie budynków, Wyd. „KaBe", Krosno.

MODELLING OF FREEZING AND THAWING EFFECT ON THE DEFLECTIONS OF RC BEAMS MADE OF RECYCLING AGGREGATE CONCRETE

Andrzej Łapko, Andrzej Baj

Chair of Building Structures, Faculty of Civil & Environment Engineering,
Bialystok University of Technology, Wiejska St. 45e, 15-351 Bialystok, Poland
e-mail: lapko@pb.bialystok.pl; a.baj@pb.edu.pl

Summary:
Concrete resistance to cyclic freezing and thawing is typically controlled on the samples in an unloading state. Very few experimental tests have been only conducted on the concrete samples subjected to combined static load and frost effects. An experimental program was undertaken by the research team of Bialystok University of Technology to study the behaviour of structural members made of recycling aggregate concrete (RAC) subjected to long term static load and freezing and thawing cycles. In the paper the authors describe an innovative testing procedure for RC model beams made of RAC under constant bending moment and cyclic freezing and thawing. The aim of such studies was to clarify the effects of interaction of climatic and mechanical load on the deformability and cracking state of RC beams made of recycling aggregate concrete. The beams located in the climatic chamber have achieved over doubled deflection values in comparison with analogical beams loaded in room temperature. The tests made on an innovative beams made of recycled aggregate concrete with an insert of high strength concrete showed significantly increased RC beam's stiffness, reducing their deflections by over 30%. The results of current, as well as further planned research will let us develop the guidelines for using recyclable materials in concrete structural elements. Both adopted technical solutions and research procedure, as entirely innovative designs, were enclosed in submission to the patent register.

Keywords: recycled concrete, freezing and thawing cycles, static and thermal loads, RC beam deflections

Introduction

In accordance to sustainable development of the building industry and, furthermore, increasing demand for building materials and raising amount of construction concrete wastes (produced for example as a result of demolitions or rebuilding the existing structures), the need of recycling such wastes becomes even more sensible, also demanded by the EU (Council Directive 91/156/EEC, 1991). One of the responses to this need is the use of recycled aggregate concrete (RAC). The previous studies done by some researches (Ajdukiewicz and Kliszczewicz, 2012), (Xiao and Zhang, 2007), (Rahal, 2007) or (Lapko and Grygo, 2013) showed that the application of concrete waste for recycled aggregate concrete (RAC) revealed some significant differences in the behavior of structural elements made of RAC compared to members totally made of natural aggregate. The beams made of RAC cracked earlier and showed greater deflections at comparable loads, as well as grater shrinkage strain and creep characteristics.

The previous studies shows that the use of RAC in structural members is associated with an increased risk for the building structures. The study on application of RAC in structural members like RC beams were conducted in the Bialystok University of Technology (Lapko and Grygo, 2010, 2013). Apart from the compressive and tensile strength of RAC, the durability of such concrete is a very important aspect, influenced by freezing/thawing effect (Yao et al., 2012). The research of the RAC carried out up to now was conducted on the unloaded samples. Very few experimental tests have been only conducted on the concrete samples subjected to combined static load and frost effects, (Mu et al., 2002), as can be seen in Fig. 1. The use of such materials in structures requires a brand new approach, taking into consideration the interaction of stress state and deformation of sample elements subjected to static load and freezing/thawing cycles.

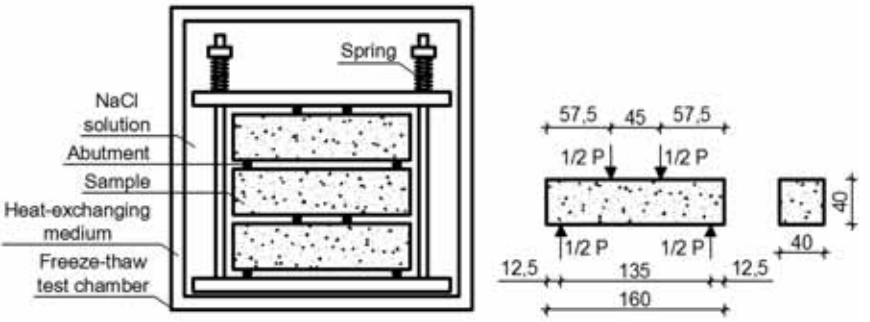

Fig.1. Combination of mechanical load with freezing and-thawing cycles and chloride penetration (Mu et al., 2002)

Essence of research, shown in the figure above, make up determine the influence of combination different kind of loads: static, climatic and physical-chemical effects. In Fig. 2 there are presented schematically research concrete stands for testing of concrete beams (1800×130×180mm) reinforced with glass FRP composite bars (Laoubi et al., 2006). The beams were exposed to 100, 200 and 360 freeze/thaw cycles (−20°C to +20°C) either in an unstressed state or loaded in bending to cause a tensile stress equals to 27% of the ultimate tensile strength of the GFRP bar. The conditioned beams were tested up to failure in a four-point bending set-up over a clear span of 1500 mm.

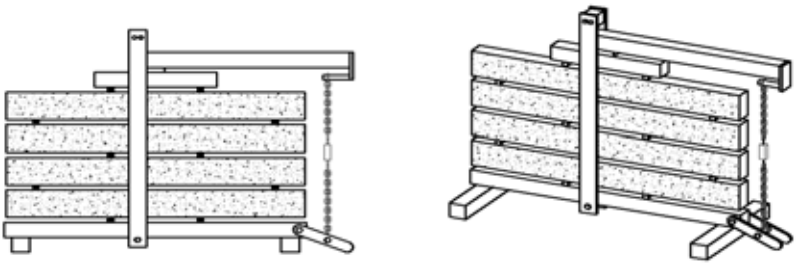

Fig. 2. Method of testing of concrete prisms under freeze-thaw cycles and sustained load (Laoubi et al., 2006)

The deep overview of recent scientific publications on deformability (deflections, strains and crack widths) in RC beams made of recycling aggregate concrete (RAC) shows that there is the lack of tests results for members under combined sustained static load and on freezing and thawing cycles.

An experimental program has undertaken by the research team of Bialystok University of Technology to study the behaviour of structural elements made of recycled aggregate concrete (RAC) in response to long-term static load and freezing/thawing cycles (Lapko et al. 2013). In the paper the authors describe an innovative testing procedures for RC model beams made of RAC under constant bending moment and cyclic freezing and thawing. The aim of such studies was to clarify the effects of interaction of climatic and mechanical load on the deformability and cracking state of RC beams made of recycling aggregate concrete.

Conducted research

The experimental investigation on RC model beams has been conducted with the use of following types of model RC beams:

- SR - RC beams entirely made of recycled aggregate concrete,
- SN - reference RC beams entirely made of natural aggregate concrete,
- SRW - innovative RC beams made of recycled aggregate concrete with the insert of high-strength concrete (HSC) located in the compression zone (Fig. 3).

The concept of such innovative beams was developed in the Bialystok of University of Technology (Grygo et al., 2013).

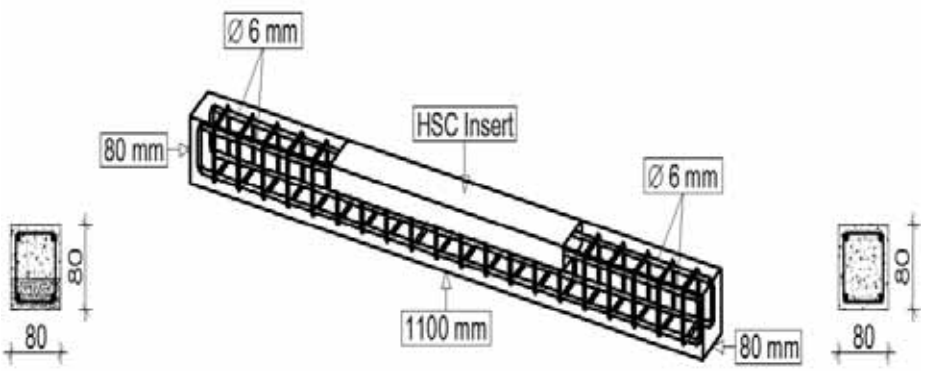

Fig. 3. Scheme of innovative SRW beam made of recycling aggregate concrete with HPC-HSC insert (identical dimension and reinforcement was applied in all SR and SN beams)

After 28-days-curing of concrete, the compressive strength, bending strength and modulus of elasticity of concrete were tested. The loading forces causing the cracks appearance was also defined. The results of the material tests are given in the Table 1.

Table 1. Properties of concrete used in the tested RC model beams after 28 days of curing

CONCRETE PROPERTIES	SN	SR	HSC
Mean compressive strength [MPa]	30,68	31,20	109,63
Mean values of concrete modulus of elasticity [GPa]	29,75	27,73	48,63

For the purposes of the studies on influence of the freezing/thawing cycles on the RC beams deflections an innovative stand shown in the Fig.4 has been designed. The three-point loading scheme was assumed. The tested free standing model beams were turned back during the long term tests so that the tensioned zone was located in the upper part of model beam.

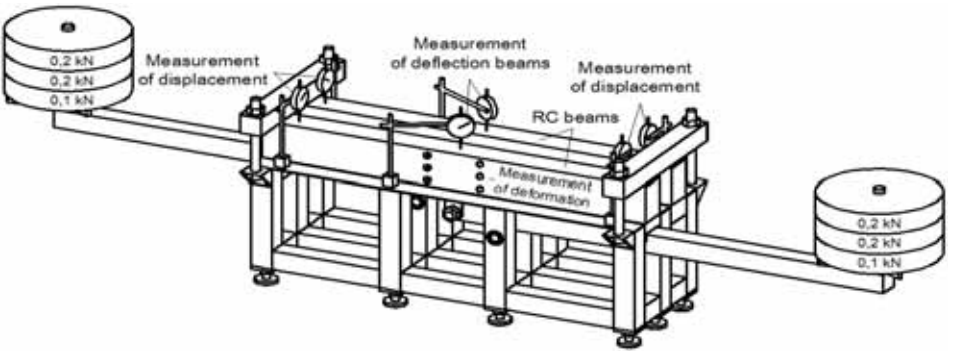

Fig. 4. The scheme of research stand with two tested model beams under static load and freezing and thawing cycles (Lapko et al., 2013)

The stands were located in the climatic room (with the working place of 2000 x 3000 mm), allowing the temperature changes from -20 ºC to +25ºC in a 4-hour period. Three stands were placed inside the climatic room, while the fourth - the reference one - was located outside the climatic chamber in room temperature. Two model beams were placed on every stand. The tested RC beams were subjected to the concentrated loading force of 3.50 kN passed on by the 7:1 lever ratio extension arms with the load of 0.50 kN placed on their ends (Fig. 5).

The conducted research has been planned for 200 full cycles of freezing and thawing, with the continuous measurement of beams deflections (in the mid span and on the supports) using waterproof dial indicators. There were also measured concrete strains by the use of Demec extensometer in the mid span of the tested beams (see Fig.4). The program of a continuous research enclosed an initial measurement of concrete compressive strength, flexural strength and value of elasticity module, repeated for every 25 cycles. The plan of experimental works are schematically shown in Fig. 6.

Fig. 5. The research stands with the model RC beams in the climatic room during the tests

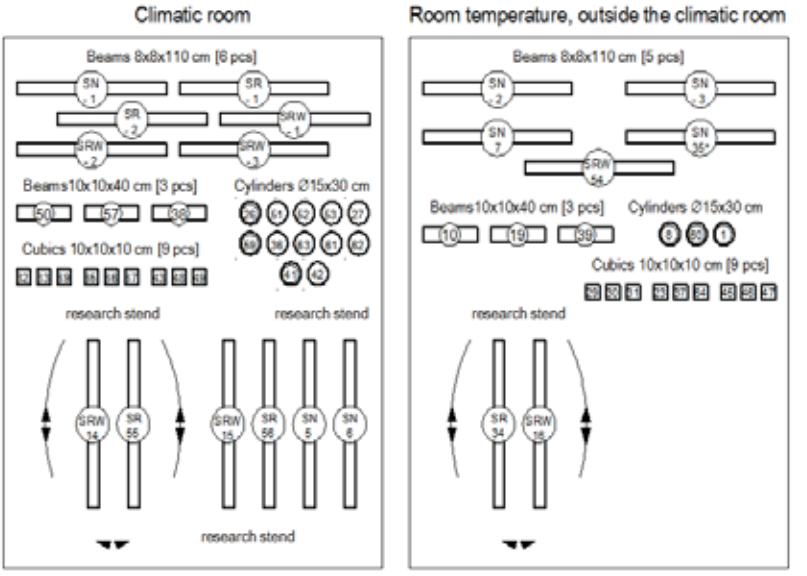

Fig. 6. Plan of experimental tests for combined static load and freezing and thawing cycles

The properties of recycling aggregate concrete (cube and cylinder strength for compression and flexural tension using concrete prisms) were successively tested for every 25 cycles of freezing-and thawing cycles.

Chosen test results

In this paper the results of registered twenty-four-hour deflection changes of the RC model beams subjected to the static load equal to 350 kN combined with freezing/thawing cycles (in the case of beams located in the climatic room). The diagrams of beam deflections versus number of freezing/thawing cycles values are presented in Fig.7 for beams made of RAC (series RW) and innovative beams with an reinforcing HPC-HSC insert (Series of SRW).

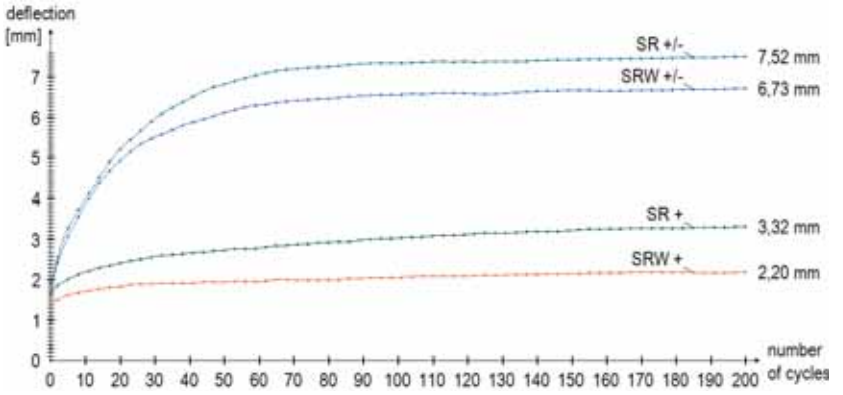

Fig. 7. Diagrams of the beams deflections versus number of cycles for the beam types: SR+/- and SRW+/- (tested in climatic room) and reference beams SR + and SRW+ (tested outside of climatic chamber in constant room temperature)

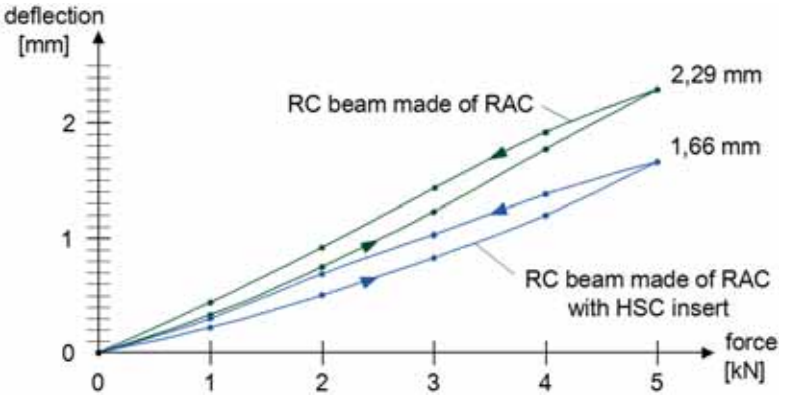

Fig. 8. The changes of deflections versus loading force for the beams type SR and SRW after 50 freezing/thawing cycles (from tests in the testing machine) (Lapko et al., 2013)

Moreover, an additional research procedure was carried out, on the basis of deflection and deformation measurement in accordance to these beams, which were exposed to the same static and thermal loads. After 50 freezing/thawing cycles, the beams were released and subjected to the loading forces in the testing machine outside the climatic room. The results of these tests are shown in Fig. 8.

After 95-days- curing of concrete samples in freezing/thawing conditions (after 200 cycles), the results of concrete compressive strength are presented in the Table 2.

Table 2. Mean compressive strength of concrete [MPa] used in the tested beams after 95 days of curing in different temperature condition

Time of curing - Series of samples	28 days (room temperature)	95 days (constant room temperature)	95 days 200 cycles of freezing/thawing
normal concrete - Series SN	30,68	38,33 ↑ 25%	33,19 ↓ 13%
RAC - Series SR	31,20	43,13 ↑ 38%	35,64 ↓ 17%
HPC - HSC	109,63	125,50 ↑ 14%	124,20 ↓ 1%

It can be clearly seen the increase of concrete compressive strength obtained for samples kept 95 days in constant room temperature compared to the age of 28 days, whereas the samples located in the climatic room with freezing/thawing cycles revealed visible decrease in concrete compressive strength in comparison with reference samples.

The results of the elasticity module of concrete tests (repeated every 25 cycles) are given in the Table 3.

Table 3. Changes of module of elasticity of concrete [MPa] depending to number of freezing/thawing cycles

Samples in climatic room	28 days	25 cycles	50 cycles	75 cycles	100 cycles
SN +/-	28	28	29	30	31
SR +/-	27	26	28	29	27
HSC +/-	49	50	51	50	52
Samples in constant room temperature	28 days	42 days	56 days	70 days	84 days
SN +	31	31	33	34	36
SR +	28	28	29	29	31
HSC +	49	52	52	53	54

Some number of samples are still in climatic room under freezing/thawing cycles and the tests on modulus of elasticity will be continued till to minimum 200 cycles.

Conclusions

1. The results, obtained so far confirm a significant influence of interaction of static load and freezing/thawing cycles on RC beams deflections. The RC beams made of recycling aggregate concrete located in the climatic room with changing temperature have achieved over doubled deflection values compared to analogical reference beams loaded outside climatic chamber in constant room temperature. This effect can be explained on the basis of decrease of beam stiffness due to destruction of concrete.

2. The tests made on an innovative beams made of recycled aggregate concrete with an insert made of HPC-HSC showed significantly increased RC beam's stiffness, reducing their deflections by over 30%.

3. The results of current, as well as further planned research, will elaborated the guidelines for the use of recycled aggregate concrete (RAC) in structural elements taking into account the durability criterion depending on effects of RAC resistance against freezing and thawing cycles.

References:

1. Ajdukiewicz A., Kliszczewicz A. (2012), *Properties of structural concretes with the recycling aggregates.* 58th National Scientific Conference, Rzeszów - Krynica, pp. 173-180 (in Polish).
2. Council Directive 91/156/EEC (1991), amending Directive 75/442/EEC on waste.
3. Grygo R., Lapko A., Chyży T. (2013), *Modeling of RC precast composite beams made of recycled aggregate concrete strenghtened by HSC inserts*. "Central Europe Towards Sustainable Building 2013: Sustainable building and refurbishment for next generations", Praha, Czech Technical University, pp. 337-340.
4. Laoubi K., El-Salakawy E., Benmokrane B. (2006), *Creep and durability of sand-coated glass FRP bars in concrete elements under freeze/thaw cycling and sustained loads*. Cement and Concrete Composites, pp. 28:869-878.
5. Lapko A., Grygo R. (2010), *Long term deformations of recycled aggregate concrete (RAC) beams made of recycled concrete.* Modern building materials, structures and techniques: the 10th International Conference, Vilnius, Lithuania, May 19-21, 2010, pp. 367-372.
6. Lapko A., Baj A., Wasilczyk R. (2013), *Response of recycling aggregate concrete of RC beams under static load and freezing and thawing cycles*. "9th Central European Congress on Concrete Engineering: CCC 2013: Concrete Structures in Urban Areas", Dolnośląskie Wydawnictwo Edukacyjne, Wrocław, p. 324-327.
7. Lapko A., Grygo R. (2013), *Structural behaviour of RC flexural members made of recycling aggregate concrete*. Materialy V Mezdunarodnoy Konferencii „Aktualnye problemy Arhitektury i Stroitelstva", Sankt Petersburg (Russia), 25-28 06 2013, Vol.1. pp. 295-301.
8. Mu R., Miao C., Luo X., Sun W. (2002), *Interaction between loading, freeze-thaw cycles, and chloride salt attack of concrete with and without steel fibre reinforcement*. Cement and Concrete Research; 32, pp. 1061-1066.
9. Rahal K. (2007), *Mechanical properties of concrete with recycled coarse aggregate*. Building and Environment, 42 (1), pp. 407-415.
10. Xiao J., Li J., Zhang Ch. (2007), *On statistical characteristics of the compressive strength of recycled aggregate concrete*. Structural Concrete (12), pp. 149-153.
11. Yao Y., Wang Z., Wang L. (2012), *Durability of concrete under combined mechanical load and environmental actions: a review*. Journal of Sustainable Cement-Based Materials, Vol. 1, Nos. 1-2, March-June 2012, 2-15.

Acknowledgments

The studies were co-financed by the Polish National Centre of Research and Development (NCBiR) and Rector Project S/WBiIŚ/2/12

ON TAKING WIND-DRIVEN RAIN AND CAPILLARY CHARACTERISTICS OF MATERIALS INTO ACCOUNT WHILE CALCULATING DAMPNESS OF SHIELDING STRUCTURES FOR BUILDINGS

[1]Vadzim Nikitsin, [2]Beata Backiel-Brzozowska

[1] Pope John Paul II State School of Higher Education,
Faculty of Economic and Technical, Department of Technical Sciences
SidorskaSt. 95/97, 21-500 Biała Podlaska, Poland
[2] Bialystok University of Technology, Faculty of Civil and Environmental Engineering,
Wiejska St. 45E, 15-351 Bialystok, Poland
e-mail b.backiel@pb.edu.pl

Summary:
The first aim of this paper was to analyse some basic methods of determining the thickness of streams of rain water falling diagonally on vertical surfaces of shielding structures. It was shown that for determining the horizontal component of wind-driven rain, the standard ISO method yields the best results for low buildings, while in the case of buildings of the tower type, the best results gives the CFD model.
The main aim of this paper was to propose a method of determining the thickness of streams of moisture absorbed by vertical surfaces of shielding structures exposed to rain falling diagonally. The developed method takes into account the horizontal component of wind-driven rain, the water sorption coefficient, the actual material humidity and the material humidity in the capillary saturation state.

Key words: wind-driven rain, capillary-porous ma materials, water capillary transport, shielding structures dampness

Introduction

Negative results of external shielding structures for buildings, made of capillary-porous materials, becoming damp, are widely known (accelerating mechanical, chemical, and biological corrosion, lowering physical and chemical properties of materials, etc.). In a number of works (e.g. Witczak et al., 2003; Blocken and Carmeliet, 2004, Blocken et al., 2006; Ali et al., 2005); it is emphasised that one of the major reasons for shielding structures becoming damp is wind-driven rain (WRD). The phenomenon of rain falling diagonally (WDR), consisting in precipitation and wind simultaneously influencing the fragment of the surface of the external shielding structure for the building under concern, should therefore be taken into consideration while calculating the dampness level of shielding structures.

The applicable European standard EN 15026: 2007 (Hydrothermal performance of building component and building elements – Assessment of moisture transfer by numerical simulation) also recommends taking into account the phenomenon of wind-driven rain while calculating non-stationary moisture transfer processes in capillary-porous materials of shielding structures. As a result of this phenomenon, capillary rise of moisture takes place through the material surface into its walls. In order to start

calculations for the initial moment of time and the subsequent period of time, the w specific humidity of the given material [kg/m^3], and the weight of the liquid absorbed by one surface area unit of a given shielding structure during one unit of the period of exposure to wind-driven rain (the thickness of the stream of moisture), g_w, [kg/(m^{2}s)], have to be known. The value of g_w is directly connected to the weight of rain falling on one surface area unit of the shielding structure under concern during one time unit, g_p, kg/(m^{2}s), and it does not exceed the value of the thickness of the stream of water absorbed by the material on the shielding structure surface, $g_{w\,\max}$ (g_w=g_p if g_p<$g_{w\,\max}$). Pursuant to EN 15026: 2007, it is assumed, without any explanation, that:

$$g_w = \min(g_p , g_{w\,\max}) \tag{1}$$

The value of the g_p thickness of the stream of moisture depends on a number of factors defining the local climate (the precipitation density as well as the wind direction and speed), the geometry of the building under concern, and also on its surrounding (the neighbouring buildings and trees, and the topography of the city, town or village). The factors mentioned above are to a different extent taken into consideration by different models described, among others works by Blocken and Carmeliet, (2004) and by Blocken et al. (2011). These models make it possible to calculate, with various degrees of accuracy, the intensity of rain falling on vertical surfaces of shielding structures.

In determining the g_w thickness of a stream of moisture (g_w≤$g_{w.max}$, $g_{w.max}$≥0), the ability of the surface layer of a structure to absorb moisture, that is, the $g_{w.max}$ stream of moisture, needs to be taken into account. This indicator depends on the humidity of the material and its water sorption coefficient before it starts to rain, and also on the changes in these parameters as a result of wind-driven rain, as well as on the humidity of the material at the moment of capillary saturation (when it can be assumed that g_w=$g_{w.max}$=0). Neither EN 15026: 2007 nor any of the literature known to the authors of the present paper give information on the way how the previously mentioned features of capillary rise of water are to be taken into consideration in calculating the level of dampness for shielding structures exposed to wind-driven rain. It also has to be underlined that in a popular computer application for analysing heat and moisture phenomena in construction barriers, WUFI (Witczak et al., 2003), the value of the g_w stream of moisture is established using the equation

$$g_w = k \cdot g_p \tag{2}$$

where k – rain water absorption factor equal to 0.7.

It is clearly visible that applying one of the dependencies, (1) or (2), might result in inaccuracy while determining the level of dampness for shielding structures exposed to wind-driven rain.

The present paper discusses and analyses some basic methods of determining the thickness of streams of rain water falling diagonally on vertical surfaces of shielding structures, and proposes a method of determining the thickness of streams of moisture absorbed by vertical surfaces of shielding structures exposed to rain falling diagonally.

Modelling wind-driven rain

According to Blocken and Carmeliet (2004), quoting 303 literature sources, scientists working within the field of construction have been investigating the phenomenon of wind-driven rain (WDR) and the results of its influence on shielding structures of buildings for over 60 years now, and in order to determine the intensity of free and non-free (falling on shielding structure surfaces) rain, empirical, semi-empirical and computational (computer simulations) methods have been developed so far.

If it is assumed that all raindrops have identical sizes, and that wind blows from the same horizontal direction at the same speed and it is always perpendicular to vertical surfaces, then, according to Blocken and Carmeliet (2004), a simple theoretical equation is obtained for determining the amount of free wind-driven rain R_{wdr}^{f} falling through one surface unit of a vertical plane of airspace (the horizontal component of wind-driven rain)

$$R_{wdr}^{f} = R_h \frac{U}{V_t} \tag{3}$$

where:

R_h – intensity of wind-driven rain falling on horizontal plane in one time unit, mm/h or l/(m²h),

U – wind speed, m/s,

V_t – final speed of falling rain drops, m/s.

The assumptions adopted when deriving the equation (3) on an ideal stream of rain are, however, not often met. Rain drops are of different sizes, they fall at different speeds and at different angles. They also crash into each other, thus becoming bigger or smaller. To take into account the aggregate range variability of falling rain drops in 1955 Hoppestad (Blocken and Carmeliet, 2004) suggested transforming the equation (3) to the following dependency connecting the value of R_{wdr}^{f} and the R_h horizontal component of free wind-driven rain

$$R_{wdr}^{f} = k \cdot U \cdot R_h \tag{4}$$

where k – free wind-driven rain factor, s/m.

If data concerning the values of U, R_h, and R_{wdr} are collected with the use of specific measuring devices (rain gauges and anemometers) in the open space at specified periods of time and when wind-driven rain is falling, then, on the basis of the equation (4), it would be possible to calculate the value of the k coefficient. Devices for simultaneous measuring of the indicators of free wind-driven rain R_h and R_{wdr} and questions pertaining to the accuracy of these devices are presented by Blocken and Carmeliet (2004). After having analysed the results of numerous experimental studies in 1965 Lacy R. E. increased the accuracy of the equation (4) suggesting adopting the mean value for the coefficient of free-falling rain k= 0.222s/m (Blocken and Carmeliet, 2004). Then

$$R_{wdr}^{f} = 0.222 \cdot U \cdot R_h^{0,88} \approx 0.222 \cdot U \cdot R_h \tag{5}$$

The equation (5) allows for determining the mean value of the thickness of free-falling rain R_{wdr}^{f} on the basis of standard U and R_h data measured by weather stations. It is emphasised in by Blocken and Carmeliet (2004) that results of numerous measurements of intensity of free-falling wind-driven rain are consistent with results obtained on the basis of calculations using the equation (5). This issue can be also solved on the basis of equation (3), after determining the $V_t(d)$ final velocity of falling rain drops (m/s). If the d rain drop diameter (mm) is known, then the following third order polynomial developed on the basis of experimental data and presented by Dingle and Lee (1972) and by Blocken et al. (2011) may be applied to determine the $V_t(d)$ final velocity:

$$V_t(d) = -0.166033 + 4.91844d - 0.888016d^2 + 0.054888d^3 \leq \frac{9.2m}{s} \quad (6).$$

In order to determine the mean diameter $\overline{d}$ (on the basis of the median), the equation proposed in 1950 by Best A. C. (Blocken et al., 2011) may be applied

$$\overline{d} = 1.105R_h^{232} \quad (7).$$

It has to be underlined that for k=0.222s/m, the final speed of rain drops of the same size, applied in equation (5), amounts to V_t=(1/0222)=4.5km/s, and that this speed, according to equation (6), corresponds to rain drops of the mean diameter of 1.2mm. A calculation performed on the basis of equation (7) revealed that rain drops of the same mean diameters (d=1.2mm) are formed for the rain intensity R_h=2mm/h. The calculated indicator is characteristic of moderate (medium intensity) rain for which the k coefficient of free-falling rain ranges from 0.2 to 0.25s/m. For drizzle, d≈0.5mm and k≈0.5s/m, and for heavy rain d≈5mm and k≈0.1s/m.

As a result of a complex interaction of free-falling wind-driven rain and vertical surfaces of shielding structures, the R_{wdr} intensity of wind-driven rain falling on the surface under study will differ from the R^{f}_{wdr} intensity of free-falling rain and will be unevenly distributed on the surface of the building façade it falls on.

For determining the intensity of wind-driven rain falling on vertical surfaces of shielding structures, a number of models based on the same equation (7) were proposed

$$R_{wdr} = \alpha \cdot U_{10} \cdot R_h^{0.88} \cos\theta \quad (8),$$

where:

U_{10} – speed of wind at the height of 10m above the ground level, m/s,

θ – angle between the φ_{10} direction of wind at the height of 10m above the ground level and the normal to the vertical surface of the building façade

α – coefficient of wind-driven rain, s/m.

Input meteorological data used for calculating R_{wdr} on the basis of equation (8) are composed of mean values of U_{10}, φ_{10}, and R_h, measured simultaneously at one-hour or ten-minute intervals adopted as the Δt time interval. The only difference for each of the models considered further is the method with which the α coefficient is determined.

When the SB model developed by Straube and Burnett in 2000 is applied, the α coefficient is described with the following equation (Blocken et al., 2011)

$$\alpha = DRF \cdot RAF \cdot \left(\frac{Z}{10}\right)^{\beta} \cdot R_h^{0.12} \tag{9}$$

where:

DRF – driving rain function,
RAF – rain admittance factor,
Z – height above the ground level, m.

The value of *DRF* is inversely proportional to the V_t final speed of rain drops, determined on the basis of equation (6), taking into consideration equation (7). *DRF* depends on the R_h rain intensity which changes in time. The *RAF* factor does not change in time, and, irrespective of the building type or the fragment of the façade under concern, its values range from 0.2 to 1.0, see Fig. 3 in (Blocken et al., 2011). The third coefficient in equation (9), introducing *z* and *β*, takes into account the influence of the natural topography of the building location on the wind speed profile.

The α coefficient in the applicable ISO (International Organization for Standardization) standard EN ISO 15927-3:2009 takes on the following form

$$\alpha = 0.222 C_R \cdot C_T \cdot O \cdot W \tag{10}$$

where:

C_R – roughness coefficient,
C_T – topography coefficient,
O – obstruction factor,
W – wall factor.

The C_R roughness coefficient provides for changes in the mean wind speed, depending on the *Z* height above the ground level and the 'roughness' of the area in the direction that the wind is blowing from. The value of the C_R coefficient in the *Z* function is determined from one of the equations (Blocken and Carmeliet, 2004):

$$C_R(Z) = K_R \ln\left(\frac{Z}{Z_0}\right) \quad \text{for} \quad Z \geq Z_{\min} \tag{11}$$

or

$$C_R(Z) = C_R(Z_{\min}) \quad \text{for} \quad Z < Z_{\min} \tag{12}$$

where K_R (terrain factor) is the parameter, and Z_0 and Z_{min} (heights) are selected depending on the terrain category. There are four terrain categories. Thus, for terrains of category II (country town or village) from Table 1 in EN ISO 15927-3:2009 we obtain K_R=0.19, Z_0=0.05m, and $Z_{\min}$=4m. Then, for example, at the height of *Z*=10m > $Z_{\min}$=4m, the value of the roughness coefficient can be calculated from equation (11)

$$C_R(10) = 0.19 \ln\left(\frac{10}{0.05}\right) = 1.007,$$

and for *Z*=3m < $Z_{\min}$=4m, from equation (12) the following is obtained

$$C_R(3) = C_R(4) = 0.19 \ln\left(\frac{4}{0.05}\right) = 0.8326.$$

The C_T topography coefficient providing for changes in the wind speed over terrain elevations or slopes is determined taking into account the Φ tangent of the inclination angle of the hill under concern, the λ location on the hill, as well as the Z height. Thus, for the windward side of the hill (Φ=0.3) for Z=0 the following are obtained: x=0, C_T=1.6 at the top; (x=-1) C_T=1.03 at the foot, and (x=-05) C_T=1.18 at the middle of the hill slope. For flat areas, (Φ <0.05) C_T=1.0.

The O obstruction factor provides for the effect of walls being protected from wind by nearby obstacles (e.g. buildings, forests), and its value is adopted depending on the L distance from the shielding structure. For example, if L=4-8m, then O=0.2, and for L>120m (practically an open space) O=1.0. While determining the O factor, heights of shielding structures proportional to the height of the wall under study need to be taken into consideration. In addition, the fact that the presence of nearby buildings might result in creating such dynamic effects for which it is recommended to adopt the maximum value for the O factor (O=1), needs to be taken into account.

The W wall factor is an attempt to provide for the wall type (its height, roof overhang, etc.) and for unevenness of the distribution of the amount of rain on the surface of a façade, caused by streams of air around external edges of buildings. According to EN ISO 15927-3:2009, values of the wall factor can range from 0.2 to 0.5.

The considered values of C_R, C_T, O, and W are not dependent on time, which results from the fact that they are not connected to meteorological data of U_{10}, ϕ_{10}, and R_h, which are variable in time.

According to Blocken et al. (2011), the α coefficient in the CFD (Computational Fluid Dynamics) model has the following form

$$\alpha = \frac{\eta \cdot R_h^{0.12}}{U_{10} \cos\theta}, \tag{13}$$

where c is determined from the ratio R_{wdr}/R_h. It is easy to explain by substituting expression (13) to equation (8). Coefficient η values are determined by means of CFD simulation for each Δt time interval characterised by the mean values of U_{10}, φ_{10}, R_h, and for any fragment (point) on the surface of a shielding structure. Results of CFD simulation are presented in different forms, including the graphical form, for example in the form of an equal level line (Blocken and Carmeliet, 2006).

The forecasting abilities of the described methods in determining the R_{wdr} intensity of wind-driven rain were tested experimentally with the use of containers for measuring wind-driven rain, installed on walls of low (type I) and high (type II) structures (Blocken et al., 2011). The façade of the type I building with a flat roof was a surface measuring 4.26 x 11.25 m, facing west. Eight containers were installed on this façade. The middle of the lower row of these devices was located at the height of 1.4m above the ground level. On the façade of the high structure (a tower of 34.5m in height), facing north-west, 4 containers were installed – one at the height of 18m, and the remaining ones at the height of 29m above the ground level.

In order to determine the R_{wdr} and R_h components of wind-driven rain, 120 one-hour intervals were chosen for the type I building, whereas for the type II building 144 ten-minute intervals were applied. After having added the data from the particular intervals, the ΣR_{wdr} and ΣR_h accumulated amount of rain and also the ratio $\eta_s=(\Sigma R_{wdr})/(\Sigma R_h)$ were determined.

The results of comparing the η_s ratio determined by the measurements and calculations on the basis of the described models for type I and type II buildings proved to be significantly different. For example, for the type I building, the mean value of the $\overline{\eta_s}$ ratio, determined on the basis of eight measurement points, was best forecast with the ISO method (the calculated values exceeded the experimental data by +7.1%). The results provided by the CFD method were not as good (the computed values were lower than the experimental data by -19.5%). The SBmax model proved to be the worst for forecasting the $\overline{\eta_s}$ values, yielding a result which exceeded the experimental data by 96.1%. In the case of the type II building, the order of models which best forecast the mean value of $\overline{\eta_s}$, determined on the basis of four measurement points, was different. The measurement results were best reflected by the CDF model (-15.6%). The SBmax method gave a significantly increased result (+51.6%), and the least accurate value was the value obtained with the use of the ISO model – this value was 2.78 times smaller than the corresponding experimental data. On the basis of the performed comparison, it can be stated that for calculating the R_{wdr} horizontal component of wind-driven rain for type I buildings it is best to use the ISO model, while the CFD method is the best one for type II buildings.

For known values of R_{wdr} measured in mm/h (1mm/h=1l/(m^{2}h)=2.777·10^{-4}kg/(m^{2}s)), the thickness of streams of rain falling on vertical surfaces can be determined from the equation

$$g_p = 2.777 \cdot 10^{-4} R_{wdr} \tag{14}.$$

This value is used in assessing the g_w thickness of streams of moisture absorbed into a shield by its surface.

Modelling of streams of moisture absorbed by vertical surfaces of shielding structures during wind-driven rain

As it was already emphasised, in order to start calculations of the non-stationary process of moisture transfer in capillary-porous materials of shielding structures during wind-driven rain whose value of the horizontal component is equal to g_p, the g_w thickness of the stream of moisture absorbed by the vertical surfaces of shielding structures needs to be known. The ability of a material to absorb moisture from the surface of a shielding structure is described by the capillary characteristics of the material and its w specific humidity (kg/m^3), and in the issue under concern it is characterised by a stream of moisture moving into the shielding structure $g_{x=0}=g_{w\,max}$.

For totally dry materials (w=0), the $g_{w\,max}$ stream of moisture has the highest value, while for total capillary saturation ($w=w_k$) it has the lowest value (approaching zero). Such phenomena can be observed when a specified layer of water falls down a vertical

surface. Issues connected to modelling the process of liquids falling down vertical surfaces were considered in detail, among others, by Kutateladze and Styrikovič (1976). Using the dependency presented by Kutateladze and Styrikovič (1976), a calculation was performed which demonstrated that a layer of water of 0.25mm in thickness under room conditions falls down a vertical surface of a barrier at the speed of 0.2m/s under laminar conditions.

If it is assumed that, when wind-driven rain starts to fall, $g_p > g_{w\,max}$ (which is a rare case) and that there is a stable layer of water on the vertical surface of a shielding structure, and the material is completely dry, homogeneous, and isotropic, then the amount of water absorbed by the surface of an unlimited half-space during the τ period can be calculated from the equation

$$W = A \cdot \sqrt{\tau}\,, \tag{15}$$

where

A – water sorption coefficient, kg/(m^{2}s$^{0.5}$).

A graphical interpretation of this phenomenon is presented in Fig. 1, with the actual material humidity profile in the direction of the $w(x, \tau)$ capillary moisture transfer being replaced by the simplified, effective profile shown in Fig. 2. The size of the equivalent profile can be computed using the following equation

$$w_k \cdot x_e = \int_0^l w(x,\tau)\,dx = A\sqrt{\tau}, \tag{16}$$

where:

w_k – material humidity in capillary saturation state, kg/m^3,
x_e – boundary between dry and humid parts of material, m.

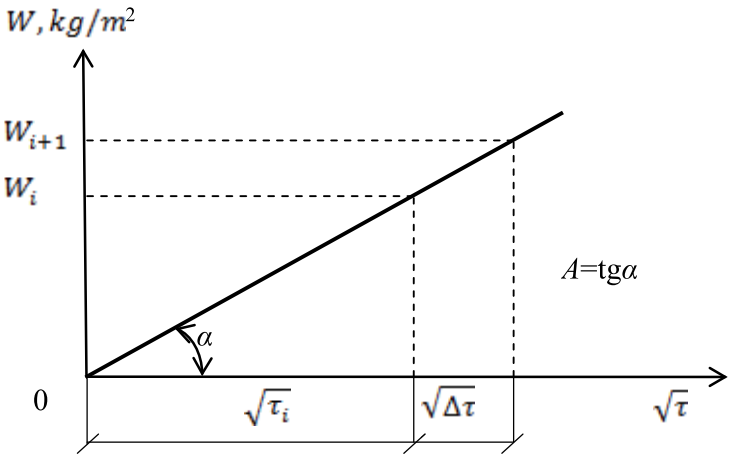

Fig. 1. Dependence of W amount of water absorbed by homogenous and isotropic capillary-porous material of unlimited thickness per surface unit

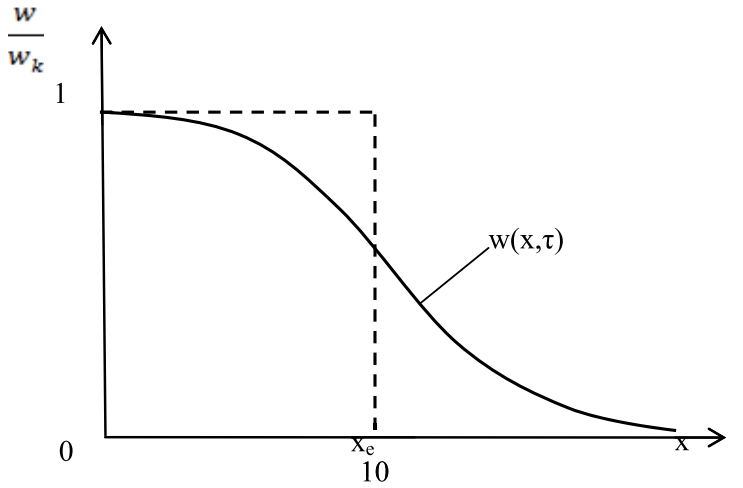

Fig. 2. Typical humidity profile of a sample of material of unlimited height $x=\infty$ for $w(x,\tau)$ capillary rise of water (solid line) and the substituting equivalent profile (dashed line)

A and w_k values are usually determined by special experiments in which the weight gain of water in a sample of $x=h$ in height and an unvarying cross-section in the process of one-direction capillary rise of water is monitored. The issues of determining the A and w_k coefficients experimentally are described with sufficient precision, among others, by Janz (1997), Nikitsin et al. (2005) and Nikitsin and Backiel-Brzozowska (2012).

The $g_{x=0}$ thickness of a stream of moisture transferred through the surface of a shielding structure for the entire x_e saturated layer is a derivative of the w value after the τ time

$$g_{x=0} = g_{w\max} = \frac{dW}{d\tau} \approx \frac{\Delta W}{\Delta\tau}, \tag{17}$$

where $\Delta\tau$ – computational time interval, s.

According to Fig. 1 and equation (15), for the $(i+1)$th stage of calculations, the following is obtained

$$g_w = g_{w\max} = \frac{\Delta W}{\Delta\tau} = \frac{W_{i+1} - W_i}{\Delta\tau} = \frac{A\left(\sqrt{\tau_i + \Delta\tau} - \sqrt{\tau_i}\right)}{\Delta\tau}, \tag{18}$$

From equation (18) it follows that the $g_{w\,max}$ thickness of a stream of moisture decreases in time, and that rain water absorption ceases after the humidity reaches the w_k value of capillary saturation in the elementary computational surface layer whose thickness is d. The humidity value in the computational layer whose thickness is d needs to be monitored at each stage of calculations, using the equation

$$w = \frac{W}{d}, \tag{19}$$

If no layer of water is present on the vertical surface of a shielding structure when wind-driven rain starts to fall (a typical situation), it means that the $g'_p \leq g_{w\ max}$ horizontal component of wind-driven rain as well as the rain water falling on the surface of the shielding structure under concern are entirely absorbed. In that case, for each (i+1)th stage of calculations in the $\Delta\tau$ time interval and for the d thickness of the surface material layer, the following holds true:

$$g_w = g'_p = \frac{W'_{i+1} - W'_i}{\Delta\tau} \text{ and } w = \frac{W'}{d}, \qquad (20).$$

As it was the case earlier, $w \leq w_k$. At the same time, at each stage of calculations, the g'_p and $g_{w\,max}$ values need to be compared. If $g'_p > g_{w\,max}$, then the g_w thickness of the stream of moisture absorbed by vertical surfaces of shielding structures is computed on the basis of equation (18).

Fig. 3 shows a graphical interpretation of the method of calculating the g_w thickness of a stream of moisture, using equations (18) and (20). It follows from Fig. 3 that in cases where the inequality g_p (or g'_p)$> g_{w\,max}$ holds (dashed line), the g_w value is established from equation (18). If, however, $g'_p \leq g_{w\,max}$, then equation (2) is applied in calculations.

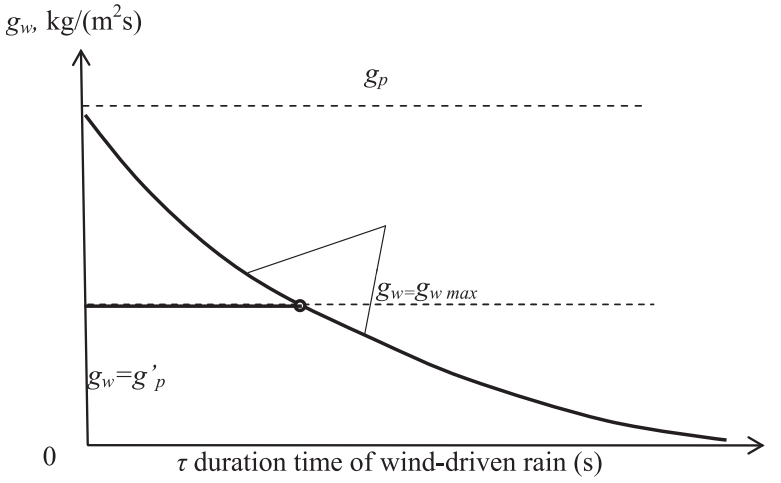

Fig. 3. Dependence of g_w thickness of stream of moisture absorbed by a vertical surface of a shielding construction during τ time for g_p (or g'_p) thickness of wind-driven rain

Summary

In the present paper, a few basic models for establishing the g_p thickness of a stream of wind-driven rain falling on vertical surfaces of shielding structures were considered on the basis of literature work. It was established that for determining the g_p horizontal component of wind-driven rain, the standard ISO method yields the best results for low buildings, while in the case of buildings of 18m in height and higher ones (of a tower type) this method is the one that provides the worst results. For a building of the latter type, the best results were obtained from the CFD model.

A method was developed for determining the g_w stream of moisture absorbed by vertical surfaces of shielding structures. The method takes into account the g_p horizontal component of wind-driven rain, the A water sorption coefficient, the w actual material humidity and the w_k material humidity in the capillary saturation state. In order to start calculations of non-stationary water transfer in capillary-porous construction materials during wind-driven rain, the g_w value needs to be known.

References:

1. Ali A. R., Nikitin V., Kofanov V. (2005), Wpływ odpadów atmosferycznych oraz parametrów przenoszenia wilgoci materiałów konstrukcji osłonowych na ich wilgotność. Materiały Budowlane, 12, pp. 24-26 (in Polish).
2. Blocken B., Abuku M., Nore K., Briggen P. M., Schellen H. L., Thue J. V., Roels S., Carmeliet J. (2011), Intercomparison of wind-drive rain models based on two case studies with full-scale measurements. Journal of Wind Engineering and Industrial Aerodynamics, 99, pp. 448-459.
3. Blocken B., Carmeliet J. (2004), A review of wind-driven rain research in building science. Journal of Wind Engineering and Industrial Aerodynamics, 92, pp.1079-1130.
4. Blocken B., Carmeliet J. (2006), On the validity of the cosine projection in wind-driven rain calculation on buildings. Building and Environment 41(9), pp. 1182-1189.
5. Dingle A. N., Lee Y. (1972), Terminal fall speeds of raindrops. Journal of Applied Meteorology, 11, pp. 877-879.
6. Janz M. (1997), Methods of measuring the moisture diffusivity at high moisture levels. Lund: Division of Building Materials, Lund Institute of Technology, University of Lund. Report TVBM-3076, p. 73 (in Swedish).
7. Kutateladze S. S., Styrikovič M. A. (1976) Gidrodinamika gazožigkostyh sistem. Moskva: Energiâ, p. 296 (in Russian).
8. Nikitsin V., Backiel-Brzozowska B. (2012), Anizotropia wyrobów ceramiki budowlanej a współczynnik wyrównywania wilgoci. W:Energy-saving and ecological materials, installations and technology in construction/ ed. Stanisław Fic. - Biała Podlaska: Wydaw. PSW JPII, pp. 19-30 (in Polish).
9. Nikitsin V., Backiel-Brzozowska B., Bołtryk M. (2005), Wpływ parametrów procesu wypalania na wskaźniki podciągania kapilarnego wody w tworzywach ceramicznych. Ceramika/Ceramics vol. 91, pp. 1223-1230 (in Polish).
10. Witczak K., Künzel H. M., Gawin D. (2003), Wpływ zacinającego deszczu na stan wilgotnościowy przegród budowlanych w Polsce. XLIX Konferencja Naukowa Komitetu Inżynierii Lądowej PAN i Komitetu Nauki PZITB, t. 4: Bezpieczeństwo pożarowe, fizyka budowli, konstrukcje murowe i drewniane, Oficyna Wydawnicza Politechniki Warszawskiej, Warszawa-Krynica, pp. 99-106. (in Polish).

ECOLOGICAL AND ECONOMIC ASPECTS OF THE IMPACT OF THE TYPE OF COARSE AGGREGATE ON STRENGTH PROPERTIES OF CONCRETE

Waldemar Budzyński, Jacek Góra

Lublin University of Technology, Faculty of Civil Engineering and Architecture
Nadbystrzycka St. 40, 20-618 Lublin, Poland
e-mail: w.budzynski@pollub.pl, j.gora@pollub.pl

Summary:
Solution proposed by authors of this paper is to change the type of coarse aggregate into the aggregate of higher quality in order to achieve better strength for a given concrete with a specific quantitative composition. Concrete classified in 3 groups was subjected to test: ordinary concrete of w/c = 0,70 and w/c = 0,58, and also high strength concrete of w/c = 0,28. In each group concrete was made using four different types of coarse aggregate. Comparing test results of strength properties it should be stressed that there is a significant effect of coarse aggregate on the values obtained, as confirmed by a statistical analysis. One can look for "concrete strength" in other sources than those consisting in a unit increase of cement content, through as shown, an appropriate choice of the type of coarse aggregate.

Keywords: concrete, coarse aggregate, strength

Introduction

Nowadays, the cement industry in Poland has become one of the most modern in Europe. This was possible due to investments, the value of which has exceeded 10 billion zloty over the last 20 years. The investments concerned not only improving technology and production efficiency, but also environmental protection. In the last five years, the expenditures on investments related to environmental protection in cement plants in Poland have exceeded the amount of 500 million zloty (Wiśniewska, 2013). Emission is nowadays much smaller than that set out in the European standards. In addition, about 50% of fuel needed for production of Portland cement clinker in all cement industry in Poland comes from combustion of alternative fuels (Wiśniewska, 2013). Despite many environmental-oriented activities and undeniably positive effects of their impact on the environment, cement plants in Poland are facing a major problem related to ecology. Currently, the CO_2 emission per ton of Portland cement clinker produced in our country is about 820 kg (Wiśniewska, 2013) and it exceeds the allowable limit of 766 kg per ton of clinker that has been set out in the European Union since 2013. In this situation cement factories must go for new investments or purchase licenses for the CO_2 emission. In both cases, production costs of clinker and cement are increased despite using alternative fuels and mineral supplements as a substitute for clinker. Additional costs will have to be somehow compensated by an increase of cement price, which in turn will affect the price of concrete. Basically, the production of clinker (cement) is not ecological, therefore it would be advisable to obtain high quality concrete at a minimum consumption of cement.

With regard to concrete, important parameters considered in quality assessment are compression and tensile strength. As usual, the value of these properties is primarily conditional on the value of the w/c ratio. Thus, in order to achieve better strength for a given concrete with a specific quantitative composition, it is necessary to decrease the w/c value which means an increase of cement content in a volume of $1m^3$, thus its bigger use in the production of concrete. One may also use or increase the content of superplasticizer admixtures, which will allow for reducing batch water, while maintaining the assumed mixture consistency, and as a result thereof lowering the w/c value without the need to increase the cement content. Another solution proposed by some authors is to change the type of coarse aggregate into the aggregate of higher quality.

It is undisputed that the type of coarse aggregate has a substantial effect on the properties of concrete, including strength ones. Neville (Neville, 2000) indicates that not only the strength can be conditioned by the type of aggregate, since low quality aggregate cannot make strong concrete, but also the properties of aggregate have a significantly effect on duration and behavior of concrete in the structure. The studies on concrete made from basalt, granite, gravel and used more and often carbonate aggregate, conducted so far show that changing the type of coarse aggregate results in a difference in compression strength class even by two classes (Piasta W. and others, 2011). The latter type of aggregate deserves special attention. An increase in the number of projects implemented in the recent years in construction engineering has led to a certain deficiency in the market dealing with aggregate. Periodic shortages of aggregates among those traditionally used, were supplemented with carbonate aggregates, although they are not credited with much of the reliance in building practice. Most likely this is so for fear of adverse effects of alkali-carbonate reactions that may occur, and the fact that these aggregates are characterized by high porosity and weak strength parameters. It should be noted, however that in some scientific studies conducted abroad (Baalbaki and others, 1991; Mehta, 1986; Roy, Jiong, 1992; Wu and others, 2001; Zimbelmann, 1985), as well as in the country (Bukowski, Kuczyński, 1972; Mierzwa, 2000; Piasta J., Piasta W., 1994; Piasta J., Piasta W., 1992; Piasta J., Piasta W., 2002) extensive usefulness of carbonate aggregates of adequate quality is justified for high-strength concrete of compression strength f_{cm} amounting to 120 MPa (Fig. 1).

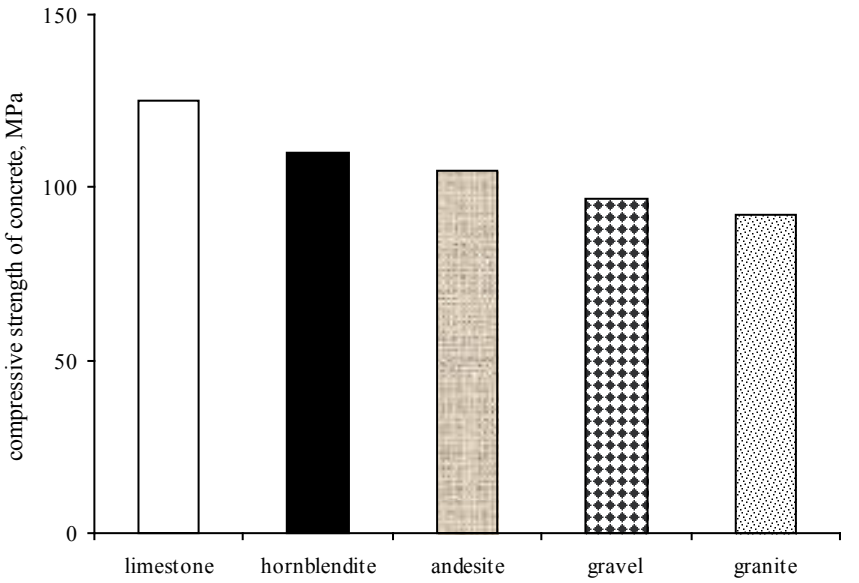

Fig. 1. Compression strength of high performance concretes with different aggregates (Roy, Jiong, 1992)

Although they are undervalued, carbonate aggregates distinguish themselves among crushed aggregates from compacted rocks (usually a mixture of calcite and dolomite at different proportions) characterized by low porosity which less than 3%. Due to their mineral composition they are able to react with cement paste, which brings favorable changes in the contact layer (e.g. formation of monocarboaluminate, portlandite crystals disorientation, reducing porosity and pore size, increasing layer strength). An external effect is, in most cases clearly visible on the basis of higher values of strength and elasticity modulus of concrete. The longer the time of curing the better improvement of the properties of concrete from carbonate aggregates.

Variability of properties of concrete made with different aggregates results from both different physical and chemical properties of the rock, from which the aggregate was made, as well as from diverse structure of the transition layer paste-aggregate, recognized by the vast majority of researchers for the weakest "link" in the structure of concrete. Aggregate plays a vital role in forming the structure of the transition layer, and therefore it has a significant impact on many properties of concrete determining its suitability in terms of construction adequacy and durability of the material.

Tests results and discusion

The following types of aggregate were taken for compression and tensile strength tests: aggregate made from igneous rocks - basalt and granite grit from inland beds having been used for many years, for the use in structural concrete of top classes and aggregates made from sedimentary rocks – dolomite grit, and also gravel, the most commonly used for concrete of different classes of strength.

Concrete classified in 3 groups was subjected to test: ordinary concrete of w/c = 0,70 and w/c = 0,58, and also high strength concrete of w/c = 0,28. In each group concrete was made using four different types of coarse aggregate of 2÷16mm fraction. Four different types of coarse crushed aggregates were applied in concrete: basalt from Gracze mine (B), granite from Graniczna near Strzegom (G), dolomite from Laskowa (D) and natural gravel from KSM Suwałki (O). Natural washed sand of 0÷2 mm fraction from KSM Suwałki was used as fine aggregate. Portland cement CEM I 42,5R was used in all types of concrete. In each group of concrete, the same volume of coarse aggregate was considered.

Aggregate composition of particular types of aggregate was formed from selected aggregate fractions 2÷4, 4÷8, 8÷16 mm 2 to 4, 4 to 8, 8 to 16 mm. In order the volume contents of each aggregate fraction was the same in the compared aggregates (within each group), different bulk density of aggregates was considered. Sand content of aggregate composition, expressed by volume, amounted to 37±1% in each case. In order to maintain a similar consistency of concrete mixtures, in HPC concrete one used the concrete admixture (superplasticizer) in the form of modified polycarboxylate. The consistency ratio of concrete mixtures was 10±3 cm, which corresponds to consistency classes of S2¸S3 according to PN-EN 206-1:2003. Air content in concrete mixtures, determined by means of a pressure method was 1,8±0,1%. Composition of concrete mixtures was given in table 1,2 and 3.

From each type of concrete, 10 cylindrical specimens were made, with a diameter of 150 mm and a height of 300mm (5 were allocated to compression strength testing and 5 to tensile strength at splitting). Specimens were tested after 28 days of curing in laboratory conditions. Upper surfaces of the specimens designed for tensile strength tests were polished to make them be parallel to the basis.

Tab. 1. Composition of ordinary concrete mixtures of w/c = 0,70

concrete components w/c = 0,70		Concrete marking (type of coarse aggregate)			
		B070-B (basalt)	B070-G (granite)	B070-D (dolomite)	B070-O (natural gravel)
Cement	kg/m^3	260	260	260	260
Sand	kg/m^3	697	697	697	697
Coarse aggregate	kg/m^3	1334	1221	1303	1221
Water	dm^3/m^3	182	182	182	182

Tab. 2. Composition of ordinary concrete mixtures of w/c = 0,58

concrete components w/c = 0,58		Concrete marking (type of coarse aggregate)			
		B058-B (basalt)	B058-G (granite)	B058-D (dolomite)	B058-O (natural gravel)
Cement	kg/m^3	325	325	325	325
Sand	kg/m^3	676	676	676	676
Coarse aggregate	kg/m^3	1274	1166	1245	1166
Water	dm^3/m^3	189	189	189	189

Tab. 3. Composition of high strength concrete mixtures of w/c = 0,28

concrete components $(w + w_{sp})/c = 0,28$		Concrete marking (type of coarse aggregate)			
		B028-B (basalt)	B028-G (granite)	B028-D (dolomite)	B028-O (natural gravel)
Cement	kg/m^3	479	479	479	479
Sand	kg/m^3	699	699	699	699
Coarse aggregate	kg/m^3	1258	1151	1229	1151
Water	dm^3/m^3	128	128	128	128
Superplasticizer	kg/m^3	10,5	10,5	10,5	10,5

In order to obtain a clear answer whether the type of coarse aggregate has a significant impact on strength properties of the tested types of concrete, the test results were subjected to one-factor analysis of variance test [ANOVA] at a significance level of $\alpha = 0,05$ (Sheskin, 1997). One test was performed for each group of concrete with the same w/c ratio. In all analyzes, the level of significance of $\alpha = 0,05$ was considered.

It should be noted that in all groups of concrete (of the same w/c) there is statistically significant effect of the type of coarse aggregate on the strength properties of concrete which was proved by means of the analysis of variance.

Additionally, in order to provide a detailed explanation of the significance of differences between the strength of concretes made from different aggregates, the least significant difference tests – "LSD" were carried out. The p-values indicating the existence of significant differences between the strength results of concretes being compared, were marked with bold letters in tables 4 to 9.

The results of the compression strength tests were presented in tables 4, 5 and 6, separately for each group of concrete. Average strength, variation ratios and LSD test results were given therein. Tables provide information about classes of the tested types of concrete based on compliance criteria according to PN-EN 206-1:2003.

Tab. 4. Average compression strength, variation ratio, class and LSD test results for concrete of w/c = 0,70

		Concrete marking			
		B070-B	B070-G	B070-D	B070-O
Compression strength	$f_{cm,cyl}$ [MPa]	34,5	28,7	36,1	32,0
	ν [%]	1,4	1,6	6,1	2,2
Class of concrete compression strength		C30/37	C20/25	C30/37	C25/30
p results of LSD test of compression strength of B070 concrete					
B070-B		—	**0,000373**	0,143909	**0,035194**
B070-G		**0,000373**	—	**0,000070**	**0,010215**
B070-D		0,143909	**0,000070**	—	**0,003204**
B070-O		**0,035194**	**0,010215**	**0,003204**	—

Tab. 5. Average compression strength, variation ratio, class and LSD test results for concrete of w/c = 0,58

		Concrete marking			
		B058-B	B058-G	B058-D	B058-O
Compression strength	$f_{cm,cyl}$ [MPa]	47,5	36,9	44,9	41,8
	ν [%]	3,6	3,2	1,0	2,5
Class of concrete compression strength		C40/50	C30/37	C40/50	C35/45
p results of LSD test of compression strength of B058 concrete					
B058-B		—	**0,000004**	**0,028384**	**0,000364**
B058-G		**0,000004**	—	**0,000032**	**0,000895**
B058-D		**0,028384**	**0,000032**	—	**0,012162**
B058-O		**0,000364**	**0,000895**	**0,012162**	—

Tab. 6. Average compression strength, variation coefficient, class and LSD test results for concrete of w/c = 0,28

		Concrete marking			
		B028-B	B028-G	B028-D	B028-O
Compression strength	$f_{cm,cyl}$ [MPa]	93,2	78,3	89,0	82,6
	ν [%]	2,9	4,7	1,6	4,1
Class of concrete compression strength		C80/95	C70/85	C80/95	C70/85
p results of LSD test of compression strength of B028 concrete					
B028-B		—	**0,000236**	0,115601	**0,002128**
B028-G		**0,000236**	—	**0,001940**	0,103868
B028-D		0,115601	**0,001940**	—	**0,027531**
B028-O		**0,002128**	0,103868	0,027531	—

In the case of ordinary concrete, the highest compression strength values were found with respect to concretes with grit basalt and dolomite, with some minor differences ranging from 4 to 6%. Compression strength of ordinary concrete with natural gravel and granite aggregate are statistically significantly lower than the strength of concrete with basalt and dolomite aggregate of corresponding relationships of w/c. The differences in the strength of concrete with natural gravel and granite aggregate in relation to the highest strength of the concrete in a particular group of w/c, were 11,4% and 20,5% respectively at w/c = 0,70 and similarly 12,0% and 22,3% at w/c = 0,58.

The above mentioned relationships, resulting from statistical interference, are exactly represented in assigning ordinary concrete to specific classes of strength. Concrete with basalt and dolomite aggregate belongs to the same class, C30/37 at w/c = 0,70 and C40/50 at w/c = 0,58, while concrete with natural gravel was classified to be one class below (C25/30 and C35/45 respectively), and concrete with granite aggregate two classes below (C20/25 and C30/37 respectively).

In the case of high performance concrete (HPC), the highest values of compression strength are also those of concrete with basalt and dolomite grit, at a statistically insignificant difference of 4,5% in favor of basalt. Considerably lower values, at differences statistically significant, were obtained in relation to concrete with natural gravel and granite aggregate, by 11,4% and 16,0% respectively, with regard to HPC concrete with basalt aggregate. However, the differences in concrete strength HPC concrete with natural gravel and granite aggregate are statistically insignificant (table 6).

Similarly as in the case of ordinary concrete, the relationships arising from statistical inference found in HPC concrete are confirmed by its assignment to particular class of strength. HPC concrete with basalt and dolomite aggregate belongs to the class of C80/95, while concrete with natural gravel and granite aggregate is classified one class below that is C70/85.

Results of tensile strength tests, separately for each group of concrete, were shown in tables 7, 8 and 9, in which one can find average tensile strength at splitting, variation ratios and axial tensile strength values calculated as 0,9 $f_{ctm,sp}$, (at dimensioning of concrete structures and reinforced concrete structures in accordance with PN-EN 1992-1-1:2008, it is advisable to use concrete strength in a state of uniaxial tension, and that is why the values of $f_{ctm,ax}$ corresponding to these test results were additionally included in the tables).

Tab. 7. Average tensile strength, variation ratios and LSD test results of concrete of w/c = 0,70

		Concrete marking			
		B070-B	B070-G	B070-D	B070-O
Splitting tensile strength\ (based on tests)	$f_{ctm,sp}$ [MPa]	2,76	2,29	2,93	2,71
	ν [%]	4,6	7,1	4,9	3,7
Axial tensile strength	$f_{ctm,ax}$ [MPa]	2,48	2,06	2,64	2,44
Concrete class		C30/37	C20/25	C30/37	C25/30
Standard axial tensile strength depending on the class according to EC2, MPa		2,9	2,2	2,9	2,6
p results of LSD test of tensile strength of B070 concrete					
B070-B		—	**0,000046**	0,053834	0,602767
B070-G		0,000046	—	**0,000001**	**0,000133**
B070-D		0,053834	**0,000001**	—	**0,018869**
B070-O		0,602764	**0,000133**	**0,018869**	—

Tab. 8. Average tensile strength, variation coefficients and LSD test results of concrete of w/c = 0,58

		Concrete marking			
		B058-B	B058-G	B058-D	B058-O
Splitting tensile strength (based on tests)	$f_{ctm,sp}$ [MPa]	3,25	2,75	3,36	2,87
	ν [%]	6,3	6,5	3,2	3,4

Axial tensile strength	$f_{ctm,ax}$ [MPa]	2,93	2,48	3,02	2,58
Concrete class		C40/50	C30/37	C40/50	C35/45
Standard axial tensile strength depending on the class according to EC2, MPa		3,5	2,9	3,5	3,2
p results of LSD test of tensile strength of B058 concrete					
B058-B		—	**0,000113**	0,295810	**0,001319**
B058-G		**0,000113**	—	**0,000014**	0,251135
B058-D		0,295810	**0,000014**	—	**0,000141**
B058-O		**0,001319**	0,251135	**0,000141**	—

Tab. 9. Average tensile strength, variation ratio and LSD test results of concrete of w/c = 0,28

		Concrete marking			
		B028-B	B028-G	B028-D	B028-O
Splitting tensile strength (based on tests)	$f_{ctm,sp}$ [MPa]	5,54	5,16	6,06	5,07
	ν [%]	2,8	3,1	4,6	2,3
Axial tensile strength	$f_{ctm,ax}$ [MPa]	4,99	4,64	5,45	4,56
Concrete class		C80/95	C70/85	C80/95	C70/85
Standard axial tensile strength depending on the class according to EC2, MPa		4,8	4,6	4,8	4,6
p results of LSD test of tensile strength of B028 concrete					
B028-B		—	**0,005900**	**0,000464**	**0,001090**
B028-G		**0,005900**	—	**0,000001**	0,434937
B028-D		**0,000464**	**0,000001**	—	**0,000000**
B028-O		**0,001090**	0,434937	**0,000000**	—

The highest values of tensile strength were determined with regard to concrete with dolomite and basalt aggregate, both in relation to ordinary and high strength concrete, likewise compression strength values. In each case (at all w/c) the differences between the strength of these types of concrete are maintained at a level of 3-9% in favor of dolomite (at statistically significant difference with respect to HPC concrete). Therefore, concrete with dolomite and basalt aggregate can be regarded as equivalent in terms of tensile strength. Relating to those values, the strength of concrete with granite aggregate and natural gravel

is smaller by 18 ÷ 22% and 7 to 15% respectively in groups of ordinary types of concrete, and by 15% and 16% in HPC group, mostly at differences statistically significant. It should be noted that the difference in tensile strength values at a level of approximately 10%, corresponds to the change of one compression strength class in the case of ordinary concrete starting from C25/30 class, and in the case of high-strength concrete the difference is only about 4%. Therefore, it must be concluded that the use of natural gravel or granite aggregate instead of dolomite or basalt aggregate results in substantial reduction of not only compression strength but also tensile strength of concrete.

A general regularity needs to be emphasized that the lowest values of tensile strength were achieved in the case of concrete with granite aggregate, only in the case HPC concrete there is a slight advantage in favor of granite grit compared with natural gravel, however at a difference statistically insignificant. Nevertheless, in ordinary concrete OC of w/c = 0,70 the strength of concrete with granite aggregate is weaker than that with natural gravel by even 15,5%, and in relation to the strength of concrete with basalt aggregate by 17,0%. Similar relationships, although at smaller differences, 4,2% and 15,4% respectively, occur in ordinary concrete OC of w/c = 0,58. The highest tensile strength values were obtained with regard to concrete with dolomite grit.

Comparing test results of strength properties it should be stressed that there is a significant effect of coarse aggregate on the values obtained, as confirmed by a statistical analysis. The differences caused by the type of coarse aggregate, reaching up to about 22%, result in a change in the classification of concrete at the level of the two classes of compression strength (Fig. 2). The similar situation is in the case of tensile strength.

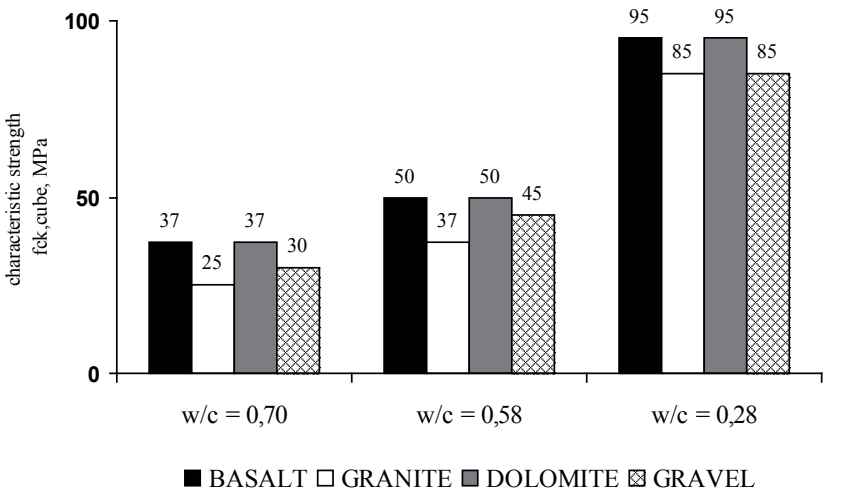

Fig. 2. Compressive strength of concrete with different types of aggregate and at different w/c values. Results obtained in tests

Weak strength test results of concrete with granite aggregate are to be found quite surprising. Granite rock aggregate is generally considered to be at least of good quality, however some of these rocks may be subject to quite considerable weathering, which leads to deterioration of aggregate properties (Jamroży, 2003; Neville, 2000; Piasta., Piasta W., 1994). In warm and humid climate, weathering of granites leads to formation of kaolin, the beds of which were formed in the Miocene period, mainly in strzegom and strzelin massif. Consequently, this may lead to deterioration of aggregate, and thus the properties of concrete. Negative differences obtained in the tests, compared to basalt and dolomite aggregates, may also be associated with different mineral composition and properties of the granite rock (coarse texture) and also aggregate (the breaking rate of granite is 2-4 times higher than that of basalt and dolomite respectively).

Summary

Considering the differences in strength classes of concrete obtained in tests due diversity of concrete composition by the type of coarse aggregate only, it needs to be adopted that this factor should be considered an alternative in the search for better strength properties of concrete, in relation to increasing the cement content. According to what has been said in the introduction, speaking more generally, increasing the proportion of cement in the production of concrete exerts a negative impact on the environment through, among others, an increase of CO_2 emission. This has also got a purely economic aspect for cement and construction industry in general. One can look for "concrete strength" in other sources than those consisting in a unit increase of cement content, through as shown above, an appropriate choice of the type of coarse aggregate. Moreover, given the results of strength tests, it seems to be feasible to use high-quality carbonate aggregates with properties comparable with basalt aggregates.

References:

1. Baalbaki W., Benmokrane B., Chaallal O., Aïtcin P. - C., Influence of Coarse Aggregate on Elastic Properties of High Performance Concrete, ACI Materials Journal, No 5/1991
2. Biliszczuk J., Beton - tworzywo do budowy mostów, Prace Naukowe Instytutu Inżynierii Lądowej Politechniki Wrocławskiej Nr 32, Seria: Monografie Nr 10, Wrocław 1986
3. Bogue R. H., Chemistry of Portland Cement, Reinhold, New York 1955
4. Bukowski B., Kuczyński W., Budownictwo betonowe, t. I, cz. 1 i 2, Arkady, Warszawa 1972
5. Jamroży Z., Beton i jego technologie, Wydawnictwo Naukowe PWN, Warszawa 2003
6. Mehta P. K., Concrete. Structure, Properties and Materials, Englewood Cliffs, NJ: Prentice-Hall, 1986
7. Mierzwa J., Niektóre aspekty wpływu kruszywa na właściwości wytrzymałościowe betonów, Konferencja „Beton na progu nowego milenium", Polski Cement, Kraków 2000

8. Neville A. M., Właściwości betonu, Polski Cement, Kraków 2000
9. Piasta J., Piasta W. G., Beton zwykły, Wydawnictwo Arkady, Warszawa 1994
10. Piasta J., Piasta W., Kruszywa a betony wysokiej wytrzymałości, Przegląd Budowlany nr 8-9/1992
11. Piasta J., Piasta W., Rodzaje i znaczenie kruszywa w betonie, XVII Ogólnopolska Konferencja Warsztat Pracy Projektanta Konstrukcji, Ustroń 2002
12. Piasta W., Budzyński W., Góra J., Wytrzymałość na rozciąganie betonów zwykłych i wysokiej wytrzymałości z kruszywami ze skał magmowych i osadowych, Przegląd Budowlany 10/2011
13. PN-EN 1992-1-1:2008 Eurokod 2. Projektowanie konstrukcji z betonu. Część 1-1: Reguły ogólne i reguły dla budynków
14. PN-EN 206-1:2003 Beton. Część 1: Wymagania, właściwości, produkcja i zgodność
15. Roy D. M., Jiong W., 9th International Congress on the Chemistry of Cement, Vol. 6, Poster Session, New Delhi 1992
16. Sheskin David J., Handbook of Parametric and Nonparametric Statistical Procedures, CRC Press 1997
17. Wiśniewska K., Sytuacja i perspektywy przemysłu cementowego. Materiały budowlane 5/2013
18. Wu K.-R., Chen B., Yao W., Zhang D., Effect of coarse aggregate type on mechanical properties of high-performance concrete, Cement and Concrete Research, Vol. 31/2001
19. Zimbelmann R., A Contribution to the Problem of Cement-Aggregate Bond, Cement and Concrete Research, Vol. 15/1985

REVIEW OF RESEARCH ON RECYCLING OF WASTE MATERIALS TO PRODUCE BRICKS THROUGH FIRING

Danuta Barnat – Hunek, Anna Kowalczyk, Katarzyna Stankiewicz

Pope John Paul II State School of Higher Education,
Faculty of Economic and Technical, Department of Technical Sciences
SidorskaSt. 95/97, 21-500 Biała Podlaska, Poland
e-mail: d.barnat-hunek@pollub.pl

Summary:
This paper presents a review of global research on the use of waste materials for production of ceramic building bricks through firing. Main objectives of the directive of the European Parliament and of the Council on waste materials and recycling thereof have been presented herein. Brick production technologies, that have been developed, contribute to improving the natural environment due to the use of waste materials in these technologies. The concept of production of ceramic materials based on waste materials aims at raising awareness with respect to energy saving and environmental protection.

Keywords: waste management, recycling, ceramic brick

Introduction

Poland has faced the necessity to implement solutions oriented towards energy saving and environmental protection due to the EU directives which are becoming more and more stringent. Directive of the European Parliament and of the Council 2008/98/EC of 19 November 2008 on waste materials establishes the legal frameworks concerning waste management in the EU. It defines the key concepts such as wastes, recycling and utilization and it establishes the essential requirements within waste management. It specifies the main principles of waste management in a way that does not have a negative impact on the environment or human health. Main strategy of the Directive is to focus on prevention of generating waste materials and their recycling. There is a great need for recycling and utilization of wastes, finding a recycling method feasible to be generally used. According to the Directive, one should be encouraged to give waste materials for recycling and to use the recycled materials in order to protect natural resources. Every three years the Member States inform the Commission on the implementation of the Directive.

These reports include the assessment of feasibility to implement, at a Community level, programs and measures related to recycling and activities directed towards the recovery of materials and energy, which can contribute to a more efficient use of them, for example in the construction sector for production of building materials which are environmentally friendly (the Directive).

According to the environmental policy of Poland, the objectives of the National Programme for Municipal Wastewater Treatment and the National Waste Management Plan, the amount of waste in Poland is regularly increasing. The priority is to create and use innovative and energy-efficient solutions in construction engineering using building mate-

rials made from waste materials. Due to the legislation and standardization requirements of the European Union concerning environmental protection, the management of waste has become a major economic, environmental and technical concern. This increases the need to look for new methods of their utilization, in addition to the existing solutions. There have been a lot of works carried out on waste management projects in all over the worlds in recent years. The increase in the degree of development of civilization and technology has increased the quantities, properties, and harmfulness of the waste generated. This is particularly important due to the presence of, for example heavy metals in wastewater sludge, which is a result of the discharge of municipal and industrial wastewater jointly. Industrial ecology is important from an academic perspective. One of the methods for using waste materials may be to actually use them in production of building bricks after prior having met the conditions set out in PN-EN. Building depots of building materials which are commonly used in building engineering, such as concrete are subjected to modifications, and also the proportions of raw materials for production of lightweight aggregate or ceramic bricks are changed.

Replacing basic components with waste materials causes changes in the structure and physical and mechanical characteristics of the material. Alternative materials allow to lower the production costs and energy consumption, as well as to dispose of waste, however they do not substantially alter the performance of the final product.

Modern technologies allow for the safe management of waste without having a negative impact on natural environment, and the field that the building engineering represents, offers unlimited possibilities of their utilization.

The paper presents a review of the literature on the use of different waste materials to produce traditional building bricks through their firing.

Production of bricks from waste materials – literature research

Along with the occurrence and development of the concept of sustainable development, there has been an increase of public awareness with respect to processing and recycling of waste. This trend can be observed in building engineering, among others in production of bricks by using recycled waste. Worldwide research is being conducted on the properties of waste materials and the feasibility of reusing them. For environmental protection and sustainable development, many researchers have studied the utilization of waste materials

to produce bricks. A wide variety of waste materials have been studied, including fly ash, mine tailings, slags, construction and demolition (C&D) waste, wood sawdust, cotton waste, limestone powder, paper production residue, petroleum effluent treatment plant sludge, kraft pulp production residue, cigarette butts, waste tea, rice husk ash, crumb rubber, and cement kiln dust (Zhang, 2013).

The research on methods for producing bricks from recycled materials can be divided into categories such as firing, cementing and geopolymerization.

First method uses mine tailings or fly ash to substitute a portion or entire amount of clay. Then, the formed products are kiln fired at a high temperature in a traditional way.

Cementing method does not require kiln firing but it is based on cementing from waste or other added cementing materials.

Geopolymerization is a method that relies on chemical reaction of amorphous silica, alumina, solids rich with alkaline solutions at ambient temperature or slightly increased temperature (Zhang, 2013).

Beneficial chemical and mineral composition of waste materials seems to be an interesting alternative both from the industrial and environmental point of view, to produce ceramic materials such as: clay brick.

A wide range of waste materials is used in production of bricks, which include, inter alia, fly ashes which increase tightness. Various industrial wastes such as urban sewage sludge, bagasse, and sludge from the brewing industry, olive mill wastewater, and coffee ground residue were blended with clay to produce bricks.

Municipal solid waste and slag decrease the rate of water absorption, reduce shrinkage formed during firing. Waste foundry sand, due to high level of silica contained therein improves the hygroscopic properties of the samples (Lin, 2006).

Waste glass has got a positive effect on mechanical properties of the material as it reduces its porosity, limits the absorption of water and decreases sintering temperature thus reducing energy consumption (Dębska, 2010).

Paper processing residues, as well as cigarette butts can be used in the production of light and porous bricks due to the low mass and reduced thermal conductivity (Aeslina and others, 2010).

Rice husks reduce linear shrinkage due to the lower water content (Rahman, 1987)

Petroleum effluent treatment plant sludge reduces water content needed for the production of bricks (Faria and others, 2012)

Cleaned river sediments improve the compressive strength of specimens, decrease their porosity and water absorption and reduce the possibility of shrinkage occurrence (Samara and others, 2009).

Marble dust had a positive impact on physical, chemical and mechanical properties of the produced industrial brick (Bilgin and others, 2012)

Using "Waelz" slag supports plastic properties of the tested material, decreases water absorption, limits porosity and reduces the emission of CO2 and NOx during the process of firing (Quijorna and others, 2012).

Sugar cane waste consists mainly of crystalline silica particles, which can be used as filler in brick (Faria and others, 2012).

Next part presents the method of making bricks from waste materials through firing and the tests that the produced samples were subjected to as well as results of analyzes observed.

Tab. 1. Research on recycling of waste materials to produce bricks through firing

Waste material		Tests conducted	Fiving condition	Scientist
1.	Saw dust (0-10%), spent earth from oil filtration(0-30%), compost (0-30%), marble(0-20%)	Compressive strength, water absorption, bulk density, apparent porosity	Specimens of 30x10x60 mm fired in a laboratory furnace at 3°C/min and at 950-1050°C for 4 hours	D. Eliche-Quesada, FA. Corpas- Iglesias , L. Pérez-Villarejo, FJ. Iglesias-Godino
2.	Municipal wastewater sludge (15%), sugarcane bagasse (2,5%), oil production residues (6,5%), coffee ground residues (3%)	Linear shrinkage, bulk density, water absorption, compressive strength, thermal conductivity	Specimens oven dried at 110°C for 24 hours, then weighted and cooled for 24 hours in water. Dried with cloth and weighted again. Specimens weighted every 24 hours.	D. Eliche-Quesada, C. Martínez-García, M.L. Martínez--Cartas, M.T. Cotes-Palomino, L. Pérez-Villarejo, N. Cruz-Pérez, F.A. Corpas-Iglesias
3.	Hematite tailings (77-100%), fly ash (0-8%)	Compressive strength, water absorption, bulk density	Cylinder specimens of 50x50mm dried at 105°C for 6-8 hours and then fired in an electric furnace at 850-1050°C for 2 hours.	Y. Chen, Y. Zhang, T. Chen, Y. Zhao, S. Bao
4.	Fly ash (0, 50, 60, 70, and 80%)	Compressive strength, water absorption, bulk density, apparent porosity, cracking due to lime, frost and frost-melting	Specimens of 60x60x25mm dried at ambient conditions for 2 days, at 60°C for 4 hours, at 100°C for 6 h, and fired in an electric furnace at 100°C/h below 500°C, 50°C/h from 500°C do1000, 1050 or 1100°C, and at the highest temperature for 8h.	X. Lingling, G. Wei, W. Tao, Y. Nanru
5.	Class C fly ash (0%, 20%, 40%, and 60%)	Compressive strength, water absorption	Specimen of 95x45x45mm dried at ambient conditions for 2 days, and then fired in a laboratory at 850 and 1000°C respectively for 24 h,	S.Kute, SV. Deodhar

6.	Class F fly ash (0-60%)	Compressive strength, water absorption, leaching	Specimen of various sizes fired like bricks of clay	MI. Chou, CJ. Laird, KK Ho, SF. Chou, V. Patel, MD. Pickering, JW. Strucki
7.	Fly Ash (100%)	Compressive strength, water absorption, modulus of rupture, density, bond strength, durability	Dried for 3 days, and then fired at 1000-1300°C	O. Kayali
8.	Granite sawing wastes (0-60%)	Compressive strength, water absorption, modulus of rupture	Various sizes of filings fired at different temperatures between 750a1200°C	RR. Menezes, HS. Ferreira , GA. Neves , HdL. Lira, HC. Ferreira
9.	Municipal solid waste incinerator, slag (0-40%)	Compressive strength, water absorption, density, firing shrinkage, weight loss on ignition, TCLP	Specimens of 50x25x50mm air-dried at room temperature for 24 hours, then oven--dried at 80°C for 24 h, and finally fired at 800, 900, or 1000°C for 6 hours	KL. Lin
10.	Gold mill trailings (0-75%)	Compressive strength, water absorption, linear shrinkage	Specimens of 100x100x76mm dried at room temperature for 2 days, in the sun for 3 days, and then fired in an electric furnace at 750, 850 or 950°C for 9 hours	S. Roy, GR. Adhikari, RN. Gupta
11.	Kaolin fine quarry residue (50%), granulated blast-furnace slag (10-40%), granite-basalt fine quarry residue (10-40%)	Compressive strength, water absorption, bulk density	Specimens of 50x50x50mm dried in an electric dryer at 80°C for 24 h, and then fired at different temperatures 1100,1125, 1150 and 1175 oC at 5 °C / min and 4h soaking time in a muffle furnace under oxidizing conditions	MS. El-Mahllawy

12.	Paper production residues (0%, 10%, 20% and 30%)	Compressive strength, water absorption, bulk density, apparent porosity, thermal conductivity	Specimens of 85x85x10mm held overnight at room temperature followed by drying at 45°C for 1 hour in an oven, and then fired in an electric furnace at 2,5°C/min until 600 °C and then at 10°C/min until 1100 °C, for 1 hour	M. Sutcu, S.Akkurt
13.	Cigarette butts (0%, 2,5%, 5% and 10%)	Compressive strength, water absorption, density, thermal conductivity, leaching	Specimens of 300x100x50mm dried at 105 oC for 24 h, and then fired in a furnace at 1050°C	AK. Aeslina, M. Abbas, R. Felicity, B. John
14.	Rice husk ash (0%, 5%, 10%, 15% and 20%)	Compressive strength, water absorption, density,	Specimens dried in the sun at 30°C for 8 days, at 105°C up to 24 h in an oven and then fired in a furnace continuously at 250, 500, 750°C for 2h, and finally at 1000 °C for 2, 4 or 6 h	MA. Rahman
15.	Petroleum effluent treatment plant Sludge (41%)	Compressive strength, water absorption, leaching	Specimens of 280x130x170mm dried at room temperature, and then fired in a coal-fired brick kiln at 1000-1100°C	P. Sengupta , N. Saikia, PC. Borthakur
16.	Kraft pulp production residue (2,5%)	Compressive strength, water absorption, density	Dried at 21°C for 72 hours at 105°C in an oven, and subsequently fired at 2°C/min until 600°C, and then at 5°C/min until 900°C for 30 min	I.Demir , MS. Baspinar, M. Orhan

17.	Waste tea (5%)	Compressive strength, water absorption, density	Specimens of 100x70x40mm dried at 21°C for 72 hours and then at 105°C in an oven, and subsequently fired at 2 oC/min until 600°C , and then at 5°C/ min until 900°C for 2 hours	I.Demir
18.	River sediment (15%)	Compressive strength, water absorption, porosity, firing shrinkage, leaching, permeability, freeze-thaw	Specimens of 60x220x22mm dried through a tunnel drier at 80°C , and then fired through a tunnel kiln with a maximum temperature of 1000°C	M. Samara, Z. Lafhaj, C. Chapiseau
19.	PC and TV waste glass (<2%)	Bending strength, water absorption, open porosity, bulk density, firing shrinkage, leaching	Specimens of 100x20x10mm dried at ambient temperature for 48 hours and then in an electric oven at 100°C overnight, and finally fired in an electric chamber kiln at 100°C / h until 900, 950 or 1000°C for 4 hours	M. Dondi , G. Guarini, M. Raimondo, C. Zanelli
20.	Municipal solid waste incineration fly ash (20%)	Compressive strength, water absorption, porosity, shrinkage, leaching,	Dried at around 60°C and then fired at 950°C	Z. Haiying, Z. Youcai, Q. Jingyu
21.	Foundry by-products (0-50%)	Flexural strength, water absorption, density, apparent porosity	Specimens of 150x30x15mm fired in a muffle furnace at 2°C/min up to 850, 950 or 1050°C for 3,5 h	R. Alonso-Santurde, A. Coz, JR. Viguri, A. Andrés
22.	Waste marble powder (20-100%)	Flexural strength, water absorption, bulk density, apparent porosity	Specimens of 41x8x8mm fired in an electric furnace at 5°C/min up to at 900, 1000 or 1100 for 3 h	N. Bilgin, HA. Yeprem, S. Arslan, A. Bilgin, E. Günay, M. Marsoglu

23.	Slag and waste foundry sand (20-40%)	Flexural strength, water absorption, density, open porosity, leaching	Objects of 100x80x20mm dried at 96-104°C in an industry tunnel kiln to a maximum 850°C	N. Quijorna, A. Coz, A. Andres, C. Cheeseman
24.	River sediment (100% or 50%)	Compressive strength, water absorption, firing shrinkage, freeze--thaw	Dried in an oven at temperature gradually increasing from 25 to 110°C until no change in mass, and then firing in an electric laboratory furnace at different temperatures from 900 to 1000°C with variations in heating rate holding duration at the maximum temperature	A. Mezencevova, NN. Yeboah, SE Burns, LF. Kahn, KE. Kurtis
25.	Sugarcane bagasse ash waste (up to 20%)	Linear shrinkage, water absorption, apparent density, tensile strength	Dried at 110°C for 24h then fired in an electric kiln at 1100°C (24h cold to cold)	KCP. Faria, RF. Gurgel, JNF. Holanda

Analyzing the above table one can see that many researchers have used different types of waste materials in their studies concerning the production of bricks.

Numerous tests have been conducted on the manufactured bricks in order to evaluate the diversity of their properties. The firing temperature ranged from 950 to 1300°C. The physical, chemical and mechanical properties of the bricks were evaluated.

The compressive strength and water absorption are two basic parameters that define the usefulness of the manufactured product to be used in construction.

The research shows that adding municipal wastewater sludge, brewing industry sludge, bagasse creates pores decreasing the compressive strength, but increasing the thermal insulation properties of the bricks.

Maintaining the compressive strength while improving the thermal properties can be achieved by means of using olive mill wastewater and coffee ground residue.

Lighter products with the same physical properties can be achieved by adding such materials waste as sawdust or compost. Adding this type of material improves the porosity and the compressive strength, thus reducing the absorption of water.

Fig. 1. Ceramic brick produced with sawage sludge (Herek and others, 2012).

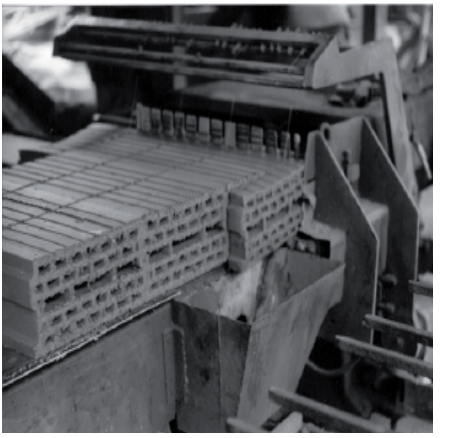

Fig. 2. The industrial production of the ceramic materials made of clay, sewage sludge and forest waste (Devant and others, 2011).

The results show an improvement in the compressive strength and an decrease of water absorption of bricks which are made by means of using fly ash, due to its fine structure.

Using marble dust has a positive impact on the physical, chemical and mechanical properties of the produced industrial brick due to an increase in size while increasing the porosity and decreasing the mass.

Summary

This paper presents a review of research on utilization of waste materials to produce bricks. In the worldwide literature one may find many examples which prove the feasibility to use waste materials in the production of building ceramics i.e. wastewater sludge from galvanization wastewater, municipal wastewater sludge, polymers waste, slag, industrial ashes, vegetable waste for example sawdust, sugar cane, linen hemp, river sediments and many others.

Examples of the use of waste produced as a by product in mining, municipal, agricultural and other industry presented in this paper confirm the feasibility of their ecological and economic development in the production of ceramic bricks.

The utilization of waste materials used for production of energy-saving building materials used in passive housing is feasible. The proposed technologies of firing the bricks combine the feasibility to dispose of waste and to produce new type of bricks, fully environmentally friendly and safe. Heavy metal compounds present e.g. in wastewater sludge are permanently built into the structure of the formed aluminosilicate due to high temperature of the thermal synthesis process.

The use of waste results from the need of the waste-free management of waste materials, decreasing their number, reducing thermal and electrical energy consumption in incinerators, reducing the feasibility of dioxins occurrence in flue gas due to the higher temperature of ceramics heat treatment than during the combustion of the waste itself.

Developed technologies contribute to improving the environment due to the use of waste materials stored in specially designated areas such as wastewater treatment plants. This will allow for reduction of storage costs. It should be noted, however that the obtained products must comply with the European quality standard requirements for building materials, be in line with the policy of the EU directives implementation. The initiative taken by developing the concept of production of ceramic materials from raw materials derived from waste aims at raising the awareness with respect to energy saving and environmental protection, as well as implementation of environment-friendly technologies in traditional and passive housing.

Continuation of the research on the feasibility to use waste in building engineering will allow for promoting and implementing the best standards and practices with regard to energy efficiency and environmental protection. On the basis thereof there will be optimal energy efficient solutions developed in building engineering.

For wide production and utilization of bricks from waste materials, further research and development is needed, not only on the technical, economic and environmental aspects but also on standardization and public education (Zhang, 2013).

References:

1. Dyrektywa Parlamentu Europejskiego i Rady 2008/98/WE z dnia 19 listopada 2008 r. w sprawie odpadów oraz uchylająca niektóre dyrektywy. Dziennik Urzędowy Unii Europejskiej L312, 22.11.2008
2. Zhang Lianyang „Production of bricks from waste materials – A review", Construction and Building Materials 47 (2013) 643–655
3. Lin KL., „Feasibility study of using brick made from municipal solid waste incinerator fly ash slag" J Hazard Mater 2006;137(3):1810–6.
4. Dębska Bernadeta „Materiały budowlane produkowane z wykorzystaniem odpadów'', Izolacje 5/2010
5. Aeslina AK, Abbas M, Felicity R, John B. „Density, strength, thermal conductivity and leachate characteristics of light weight fired clay bricks incorporating cigarette butts" Int J Civ Environ Eng 2010;2(4):179–84.
6. Rahman MA. „Properties of clay–sand–rice husk ash mixed bricks", Int J Cem Compos Lightweight Concr 1987;9(2):105–8.
7. Faria KCP, Gurgel RF, Holanda JNF. „Recycling of sugarcane bagasse ash waste in the production of clay bricks". J Environ Manage 2012;101:7–12.
8. Samara M, Lafhaj Z, Chapiseau C. „Valorization of stabilized river sediments in fired clay bricks: factory scale experiment" J Hazard Mater 2009;163 (2–3):701–10.
9. Bilgin N, Yeprem HA, Arslan S, Bilgin A, Günay E, Marsoglu M. „Use of waste marble powder in brick industry", Constr Build Mater 2012;29:449–57.
10. Quijorna Natalia, Coza Alberto, Andresa Ana, Cheesemanb Chris „Recycling of Waelz slag and waste foundry sand in red clay bricks", Resources, Conservation and Recycling 65 (2012) 1– 10

11. Lingling X, Wei G, Tao W, Nanru Y. „Study on fired bricks with replacing clay by fly ash in high volume ratio". Constr Build Mater 2005;9:243–7.
12. Kute S, Deodhar SV. „Effect of fly ash and temperature on properties of burnt clay bricks". J Civ Eng 2003;84:82–5.
13. Chou MI, Patel V, Laird CJ, Ho KK. „Chemical and engineering properties of fired bricks containing 50 weight per cent of class F fly ash". Energy Sources 2001;23:665–73
14. Kayali O. „High performance bricks from fly ash". In: 2005 World of coal ash(WOCA). Lexington, Kentucky, USA: Center for Applied Energy Research; 2005.
15. Menezes RR, Ferreira HS, Neves GA, Lira HdL, Ferreira HC. „Use of granite sawing wastes in the production of ceramic bricks and tiles". J Eur Ceram Soc 2005;25(7):1149–58.
16. Roy S, Adhikari GR, Gupta RN. „Use of gold mill tailings in making bricks: a feasibility study". Waste Manage Res 2007;25:475–82.
17. El-Mahllawy MS. „Characteristics of acid resisting bricks made from quarry residues and waste steel slag". Constr Build Mater 2008;22:1887–96.
18. Sutcu M, Akkurt S. „The use of recycled paper processing residue in making porous brick with reduced thermal conductivity". Ceram Int 2009;35:2625–31.
19. Sengupta P, Saikia N, Borthakur PC. „Bricks from petroleum effluent treatment plant sludge: properties and environmental characteristics". J Environ Eng 2002;128(11):1090–4.
20. Demir I, Baspinar MS, Orhan M. „Utilization of kraft pulp production residues in clay brick production". Build Environ 2005;40:1533–7.
21. Demir I. „An investigation on the production of construction brick with processed waste tea". Build Environ 2006;41:1274–8.
22. Dondi M, Guarini G, Raimondo M, Zanelli C. „Recycling PC and TV waste glass in clay bricks and roof tiles". Waste Manage (Oxford) 2009;29(6):1945–51.
23. Haiying Z, Youcai Z, Jingyu Q. „Utilization of municipal solid waste incineration (MSWI) fly ash in ceramic brick: product characterization and environmental toxicity". Waste Manage (Oxford) 2011;31:331–41.
24. Alonso-Santurde R, Coz A, Viguri JR, Andrés A. „Recycling of foundry by products in the ceramic industry: green and core sand in clay bricks". Constr Build Mater 2012;27:97–106.
25. Mezencevova A, Yeboah NN, Burns SE, Kahn LF, Kurtis KE. „Utilization of Savannah harbor river sediment as the primary raw material in production of fired brick". J. Environ Manage 2012;113:128–36.
26. Herek Luciana C.S, Hori C. E., Reis M. H. M., Mora N. D., Granhem Tavares C. R., Bergamasco R., „Characterization of ceramic bricks incorporated with textile laundry sludge". Ceramics International 38 (2012) 951–959.
27. Devant M., Cusidó J. A., Soriano C., „ Custom formulation of red ceramics with clay, sewage sludge and forest waste". Applied Clay Science 53 (2011) 669–675.

DESIGN REQUIREMENTS FOR WATER SUPPLY AND SEWAGE SYSTEMS IN THE ENERGY SAVINGS CERTIFICATES IN THE CONSTRUCTION INDUSTRY

Jarosław Chudzicki, Agnieszka Malesińska

[1] Warsaw University of Technology, Faculty of Environmental Engineering,
Nowowiejska St. 20, 00-653 Warszawa,
e-mail: jarek.chudzicki@is.pw.edu.pl, agnieszka.malesinska@is.pw.edu.pl

Summary:
The paper presents problems related to the design and installation of systems for greywater use in indoor installations in buildings in Poland. These problems are related to the lack of references in the current legislation, appropriate technical terminology in Poland, and appropriate design guidelines and regulations for the dual installations.
The study was based on the most popular in the world certification systems according to which investors obtain green certificates of buildings. In these rules, in addition to a whole range of requirements are also requirements for indoor installation, including dual installations. The second issue is putrescibility time for grey wastewater. For this purpose, samples were taken and measurements of their putrescibility time were made depending on the chemical composition.
Dual Installation enables a significant saving of drinking water. Unfortunately, in Poland there is no clear regulations governing the design and construction of this type of installation. Often the cost of the installation exceeds the economic benefit of saving water.

Keywords: dual installation, grey wastewater, ecological certification in buildings

Introduction

The idea of a dual system is closely linked to the concept of "green construction" that began in the 70s of the last century. Just then there was the first severe energy crisis. At that time, attention was drawn to the growing problem of environmental pollution. Those unfavorable processes have forced people to change their perception of available energy sources and to notice the fact of irreversible environmental degradation. Then there were first attempts to reduce the negative effects of human impact on the environment.

One form of such activities is an establishment of associations developing guidelines for obtainment of green certification (ecological) for buildings.

Specific to designs and buildings with this certificate is a significant decline of energy consumption within their whole life cycle. Recently, also in Poland that investment processes, using procedures to reduce energy consumption of buildings, started to be employed. The authors present in this paper the selected legal, technical and terminological aspects, related to the design and implementation of dual systems in our country.

Brief overview of ecological certification systems for construction works

The most popular ecological certification systems in the world are currently the following:

BREEAM (*Building Research Establishment's Environmental Assessment Method*) – Great Britain [2] [6][8][17],

LEED (*Leadership In Energy and Environmental Design*) – USA [7][13][17],

CASBEE (*Comprehensive Assessment System for Built Environment Efficiency*) – Japan [6] [16],

DGNB (*Deutsche Gesellschaft fur Nachhaltiges Bauen*) – German Sustainable Building Council –Germany [5].

The German DGNB certificate is the youngest of the reviewed certificates. It was developed by the German Sustainable Building Council, and it seems to be the most transparent system of multi-criteria evaluation of buildings. It is worth mentioning that this is the only certification system which strongly emphasizes the need for facilities for disabled. The DGNB certification could be used virtually in every building, because of its unique criteria. These criteria can be applied either to office buildings, residential, schools or kindergartens. This gives us almost unlimited possibility of use, which in a short time could translate into a large growth of popularity and applicability of this young certification system [5].

There has been no environmental certification system developed yet that would be dedicated only for Polish conditions, and because of that we use certificates, which are based on the most popular worldwide LEED and BREEAM [2] [17] systems.

Currently the LEED system gives an opportunity to certificate almost every investment, both newly built and existing objects undergoing renovation. Various types of buildings can be certified: industrial, office, schools, hotels or multi-family residential buildings. Exceptions are only detached houses, which could be certified only in the USA [7][13].

For the European version of the BREEAM system certification is possible only for office, industrial and commercial buildings. Any other type of building has to be certified basing on the criteria prepared individually by BRE[1]. Because of the specificity of developing ecological certification criteria, the requirements included there are related to the conditions characteristic of a relevant country. Consequently these criteria differ considerably [8][13] [17]. Of the entire group of differences resulting from the application of the type of certification we can mention two, which will have a direct impact on the design of internal water supply and sewage systems (dual systems), namely:

- ✓ building regulations:
  - – according to the BREEAM regulations – European standards apply with the possibility of adapting to local regulations,
  - – according to the LEED regulations – American regulations required, without the possibility of adapting to local regulations,
- ✓ system
  - – according to the BREEAM regulations – European standards apply,
  - – according to the LEED regulations – ASHRAE[2] standards apply.

[1] BRE - *Building Research Establishment's* –British organization dedicated to sustainable construction.

[2] A set of standards prepared by ASHRAE (*American Society of Heating, Refrigerating and Air-Conditioning Engineers*). This specific set of standards includes regulations and guidelines for various branches used in building

One of the elements to be certified is the water supply system for a building, and more specifically the size of demand for drinking water and the possibility of limiting this value by replacing a certain amount of water used for purposes other than drinking and for hygienic purposes with greywater supplied by a dual system. Below is presented the method of calculating water requirements for the purposes of certification of an object according to the BREEAM [2] and LEED [7] criteria.

Water saving in the BREEAM certification

A design or a building to obtain the green BREEAM certificate has to get a required number of points from various environmental categories, including water saving.

The number of points is awarded depending on the evaluation of e.g. innovation level, but mainly of the savings made, in this particular case the drinking water consumption savings during the annual operation of the building. The value of the savings is expressed as a percentage, and it correspondents to the indicated number of points (Table no. 1). The percentage of drinking water conserved is evaluated in the relation to baseline values of usage provided by the BREEAM.

In calculations of either forecasted water usage or of its demand the following draw-off points and sanitary utensils in the internal systems in the assessed building should be included:

- toilets,
- urinals,
- shower baths,
- sinks,
- baths,
- dishwashers,
- washing machines.

Tab. 1. The points awarded depending on the volume of drinking water savings [2].

The volume of drinking water saved [%]	**BREEAM certification points**
12,5	1
25	2
40	3
50	4
55	5
65	above expectations

Since demand for water is closely linked to a commercial use of a building, and equally the percentage indicator of water saving decides about the number of points awarded in the certification, in the BREEAM specification is given a formula of how to calculate the savings ratio for various ways of using the surface in one building.
For this reason the below relationship should be used:

objects – from lighting, to mechanical devices' performance, to the methodology of energy calculation. In the case of requirements for the systems in buildings energy efficiency calculations are carried out using the Quest program.

$$I = 100 * \left[1 - \frac{(T_{1Act} * T_{1Occ}) + \cdots + (T_{nAct} * T_{nOcc})}{(T_{1Base} * T_{1Occ}) + \cdots + (T_{nBase} * T_{nOcc})}\right]$$

where:

T_{nAct} – actual water consumption for every type of utilization, [dm^3/ (number of persons x number of days)],
T_{nBase} – referential water usage for the corresponding type of utilization, [dm^3/ (number of persons x number of days)],
T_{nOcc} – load factor for the relevant surface type, [-].

Based on the I – the savings' percentage indicator calculated a proportionate number of points in the BREEAM certification is being awarded. Buildings are being assessed according to the baseline standards. If the assessed building deviates from the generally accepted standards, it has to be assessed individually through a comparison with guidelines developed by the BRE Global[3].

The table no. 2 shows both the baseline values of water consumption for a given sanitary utensil and the number of points, dependable on the size of reducing drinking water consumption in relation to the baseline values shown in the BREEAM system.

Tab. 2. Baseline values, points awarded for the size of reducing water consumption [2].

Utensil	Baseline value	Points					Unit
		1	2	3	4	5	
Toilet	6	5	4,5	4	3,75	3	dm^3
Sink	12	9	7,5	4,5	3,75	3	dm^3/min
Shower bath	14	10	8	6	4	3,5	dm^3/min
Bath	200	180	160	140	120	100	dm^3
Urinals (2 items and above)	7,5	6	3	1,5	0,75	0	dm^3/(items x h)
Urinals (only 1 item)	10	8	4	2	1	0	dm^3/(item x h)
Greywater/rainwater	0%	0%	0%	25%	50%	75%	% coverage of demand for toilets and urinals by grey and rain water
Draw-off point in kitchenette	12	10	7,5	5	5	5	dm^3/min

[3] BRE Global (*Building Research Establishment's Global)* – these are guidelines created individually for the analyzed building. The guidelines are created by the BRE organization which deals with the sustainable green construction [17].

Kitchen draw-off point in restaurant	10,3	9	8,3	7,3	6,3	6	dm^3/min
Household dishwashers	17	13	13	12	11	10	dm^3/cycle
Household washing machines	90	60	50	40	35	30	dm^3/usage
Garbage disposal units	17	17	0	0	0	0	dm^3/min
Commercial dishwashers	8	7	6	5	4	3	dm^3/drawer
Industrial washing machines	14	12	10	7,5	5	4,5	dm^3/kg

Water saving in the LEED certification

The in line with the American guidelines certification assumes the water demand for a given draw-off point according to the data included in the table no. 3 for uninhabited buildings or in the table no. 4 – for residential housings.

Tab. 3. How many times sanitary utensils in uninhabited buildings were used [7].

Type of appliance	Working time [s]	Usage /day			
		FTE	Temporary	Retail customers	Students
Toilets (Women)	n/a	3	0,5	0,2	3
Toilets (men - if there are urinals)	n/a	1	0,1	0,1	1
Urinals (women)	n/a	0	0	0	0
Urinals (men)	n/a	2	0,4	0,1	2
Sinks in toilets	30	3	0,5	0,2	3
Shower bath	300	0,1	0	0	0
Kitchen sinks	15	1	0	0	0

FTE – *Full Time Equivalent* – an indicator of usage of a utensil in the whole work cycle of a building,
for example an assumption of usage for 3 times for 24 hrs is a 100 % utilization of the work cycle, which means FTE = 100%

Tab. 4. How many times sanitary utensils in residential housings were used [7].

Type of appliance	Working time [s]	Frequency of use [1/24 hrs]
Toilet (Women))	n/a	5
Toilets (men)	n/a	5
Sinks in toilets	60	5
Shower bath	480	1
Kitchen sinks	60	4

In order to determine the size of water demand according to the LEED system, the total volume of water used should be calculated. The calculation should be made by knowing the normative outflow for both the given draw-off point and a utensil. For example, the volume of 1,6 US gallons is presumed for one usage of a lavatory bowl according to the American guidelines, and when flashing the bowl with a smaller amount of water– then 1,1 US gallons[4].

The American guidelines allow the reduction of the drinking water demand by covering water volume necessary for flashing of lavatory bowls with the use of the local water sources, e.g. rivers or lakes.

The following could be also used for this purpose: condensate of an air conditioner, rainwater and greywater.

Legal aspects of applying ecological certificates in Poland

The proposed and recommended solutions in the introduced ecological certificates for the construction industry usually do not comply with the technical specifications for buildings and their components in the country (for example, can be not economically justified) or are not in these requirements taken into consideration.

Sanitation services, evaluating the design documentation, are placed in a difficult situation, because there is no any legal basis in Poland for certain technical ecological solutions, such as systems reusing grey wastewater.

These aspects are the reason that the investor, who wants to build a building that meets very high environmental requirements; low consumption of energy, water and other utilities, may not obtain the building permit in the traditional way.

Fortunately for investors who want to build a building in our country in accordance with the LEED or BREEAM certifications the design documentation of such a facility can be treated in accordance with the Building Materials Act, Article 10, paragraphs 1 and 2 of that Act [14] as individual design documentation. Such a classification of design documentation is associated with an innovative concept of technical solution in that design, for example, water supply and sewage systems allowing reusing some of the processed water in the designed building.

[4] One gallon = 3,785 dm^3.

An additional problem of using dual systems is the lack of single-valued terminology for such technical solutions. In the case of wastewater terminology, the following definitions of the sewage systems standards are the base [9]:

grey water – does not include faeces and urine,

blackwater –includes faeces and urine.

Unfortunately, the definitions do not cover all terms necessary in dual systems. An example of this would be here colloquial use of the alternate wording for grey wastewater - greywater. This term is often used in marketing materials for producers of dual systems appliances and also in everyday language.

Some justification of this status can be a faithful translation of the term in English: *greywater - grey water*.

It should be noted, however, that the term "*sewage*" has a synonym in English: wastewater, which in a free translation is "water *worn*". Of course, in the field of water supply and sewage systems such a translation is not applied, the term *wastewater* translates into domestic sewage or municipal waste (not to be confused with rainwater).

An additional problem is terminological distinction between grey water incoming from sanitary utensils, such as sinks, and grey water purified and reused in a separate system, distributed, for example, to flushing cisterns. The latter wastewater type has a totally different qualitative composition (this is connected with the use of various treatment processes).

For the purposes of both technology description and technical solutions used in dual systems, adopting separate terms for these two types of greywater can be considered, namely:

Grey wastewater – wastewater incoming to the storage reservoir before its treatment,

Grey water – grey wastewater after purification and disinfection processes, ready to be reused in a construction work.

In national regulations, relating to building systems, there is no clear reference to dual systems. General requirements for water supply and sewage systems, however, can be interpreted.

An important reference to the possibility and the purposefulness of the dual systems usage is the PN-EN 12056-1:2002 standard [9], in which a sewage system discharging by separate circuits grey wastewater and blackwater (the so-called IV system) has been classified.

Among the national standards the PN-EN 1717:2003 standard [10]should be mentioned, the standard that is on the protection of water supply systems transporting drinking water against the risk of secondary pollution through a backflow. The dual systems consist of at least two duct systems, which transport grey wastewater (greywater) and drinking water. It should be noted that any joints of these systems may be achieved only through an air break (protection of the A group).

At this point, we should also mention the Regulation of the Minister of Infrastructure on the conditions to be met by buildings and their location [11]. This document includes the transcript (§126, section 3) about the possibility of use of rainwater in buildings

for domestic purposes (watering the green around the house, washing, flushing lavatory bowls, etc.). There is no transcript, however, about the possibility of reusing grey wastewater for these purposes.

In this respect, the national legal status will be changed in the near future. At the present time (2012 – 2013), there are ongoing works on the amendment to the mentioned regulation, which is the basic legal act in the case of buildings under construction. In terms of substance, changes are being prepared by the Modern Buildings Association[5] delegated by the Ministry of Infrastructure. From many modifications made, there is also a transcript introduced about the possibility of using dual systems in buildings, in which grey wastewater is to be reused. An introduction of the amendment to the regulation is planned at the end of this year.

Technical problems when using dual systems

Our country, when it comes to designing, executing and exploitation of dual systems reusing grey wastewater, does not have any of the following: technical guidelines, recommendations, technical literature and practical experience. Hence the designers out of necessity are looking for the designing data in the foreign regulations and guidelines. Most often used for this purpose are the British standards for the design and requirements for the systems transporting grey wastewater [3] [4]. However, taking the recommendation and guidelines developed for other countries without adjustments might be a problem not only when designing but also during the assembled dual system's operation. It is necessary to remember that the standards and technical guidelines of other countries have been developed taking into account many specific criteria, such as tradition of using water, cultural habits of the inhabitants, weather conditions, etc.

Because of the special nature of dual system operation a very important issue is grey wastewater stability, namely its putrescibility time. This parameter is influenced by many factors, such as composition of grey wastewater (e.g. type of used tensides), temperature, etc. The data from the studies conducted in other countries may be unreliable in the relation to the real composition of grey wastewater in our country.

In order to estimate the stability of grey wastewater depending on the source of its formation, there has been conducted time measurement of putrescibility [12]. For this purpose, samples of grey wastewater from a single-family house have been examined. This wastewater has arisen as a result of using the following: baths, shower baths, sinks and washing machines. The tests were conducted in two stages. In the first stage the putrescibility time of wastewater samples coming only from one sanitary utensil was being analyzed. In the second stage there was analysis carried out of mixture of wastewater coming from the above mentioned utensils. The wastewater combinations chosen for the tests are typical for wastewater from daily use of the mentioned utensils both in a household and in public buildings.

Table no.5 presents putrescibility time of the analyzed samples and of their mixtures of specified proportions.

[5] Modern Buildings Association (www.snb.org.pl) - An Internet website of interdisciplinary collaborative platform of experts for improvement of regulations and implementations of laws in construction for the effective use of developments in the field of energy-saving and innovative solutions, and for ensuring respect for sustainable development.

Tab. 5. Putrescibility times for grey wastewater of different composition [12].

Wastewater source	Sample 1	Sample 2	Sample 3	Sample 4
	putrescibility [24 hrs]			
Bath/Shower	5	2	4	3
Sink	3	2	4	2
Washing machine	1 – for one test			
Mixture 2:3 Bath/Shower + Washing machine	1 – for one test			
Mixture 5:1 Bath/Shower + Sink	1 – for one test			
Mixture 2:2:1 Washing machine + Bath/Shower + Sink	1 – for one test			

The wastewater putrescibility time was found to be closely dependent on the content of biodegradable substances. The reason of different sustainability of analyzed wastewater samples coming from one utensil was the use of different chemicals. Designations of those indicators are very essential in determining the time of the possible detention of grey wastewater in a storage tank, which is part of a dual system.

Summary

This paper presents some of the problems encountered in the design of dual systems, which are becoming more and more attractive because of significant potential to reduce drinking water consumption for buildings of different types of ecological certifications.

Technical solutions to save water and other media supplied to the designed building are so expensive that often have no economic justification compared with the projected savings.

Often such solutions are implemented “by brute force”, without any rational justification, and investor and the designer go only by the ability to obtain a very prestigious certificate for themselves.

An example here might be the method of calculating the balance of water demand and the participation of some grey wastewater in this balance for an office building located in one of the largest Polish cities according to the LEED standard. The designer had assumed that about 80% of the employees of the building will commute to work by bicycles (the designer has in this way additional LEED points for the decline in the number of parking spaces in the basement of the building), and on the arrival they will take a shower. In this way, in the balance has been obtained a sufficient amount of gray wastewater, which then could be reused for flushing lavatory bowls.

During the summer season (approx. 4-5 months) such a forecast is possible to be performed. The problem, however, will occur in the winter season, because traveling by two-wheel vehicles in our climate zone will be quite difficult.

Praca naukowa finansowana ze środków Narodowego centrum Badań i Rozwoju w ramach projektu rozwojowego nr PBS1/B9/15/2012.

Scientific work was financed from the measures of National Center of Research and Development as a research project No. PBS1/B9/15/2012.

References:

1. BRE_Global –Breeam Europe_Presentation-Bre Global (2010 Edition).
2. BREEAM New Construction, Non-Domestic Buildings, Technical Manual SD5073-2.0:2011.
3. BS 8525-1:2010. Greywater Systems – Part 1 Code of Practice.
4. BS 8525-2:2011. Greywater systems – Part 2: Specification and method of test for treatment equipment.
5. Jackowska B. Certyfikacja DGNB w pigułce. Portal Budownictwa Ekologicznego (www.ecosquad.pl/certyfikacja-dgnb-w-pigu-ce-.html), aktualizacja 05.04.2013 r.
6. Juchimiuk J. Certyfikacja ekologiczna BREEAM w warunkach polskich - trzy budynki biurowe Trinity Park III, Crown Square, Katowice Business Point. Przegląd Budowlany 5/20011, str. 88-95.
7. LEED Green Building Rating System For Core & Shell Development Version 2.0 (July 2006, www.usgbc.org, lipiec 2012).
8. M. Gawroński. Innowacyjny według certyfikatu BREEAM, www.muratorplus.pl/technika/zrownowazony-rozwoj/innowacyjny-wedlug-certyfikatu-breeam_79455.html .
9. PN-EN 12056-1:2002. Systemy kanalizacji grawitacyjnej wewnątrz budynku, Część 1: Postanowienia ogólne i wymagania.
10. PN-EN 1717:2003. Ochrona przed wtórnym zanieczyszczeniem wody w instalacjach wodociągowych i ogólne wymagania dotyczące urządzeń zapobiegających zanieczyszczeniu przez przepływem zwrotnym.
11. Rozporządzenie Ministra Infrastruktury z dn. 12 kwietnia 2002 r. w sprawie warunków technicznych, jakim powinny odpowiadać budynki i ich usytuowanie (Dz. U. nr 75, poz. 690 z późn. zm.).
12. Sobieraj K. Badania wskaźników zanieczyszczeń ścieków szarych pod kątem ich wykorzystania w instalacjach dualnych. Praca dyplomowa magisterska. Promotorzy: J. Chudzicki, K. Umiejewska. Wydział Inżynierii Środowiska Politechniki Warszawskiej, Warszawa 2012.
13. U.S. Green Building Council LEED 2.0 Specifications (www.usgbc.org, lipiec 2012).
14. Ustawa o wyrobach budowlanych z dnia 16 kwietnia 2004 r. (Dz. U. z 2004 r. Nr 92, poz. 881).
15. Water Use Reduction. Additional Guidance. (July 2012, www.usgbc.org, lipiec 2012).
16. Witryna internetowa Japan GreenBuild Council (JaGBC) i Japan Sustainable Building Consortium (JSBC) (http://www.ibec.or.jp/CASBEE/english/overviewE.htm), aktualizacja 05.04.2013 r.
17. Zrównoważony rozwój. Porównanie najbardziej popularnych systemów certyfikacji energetycznej BREEAM i LEED. Artykuł w witrynie www.murator.pl (http://www.muratorplus.pl/technika/zrownowazony-rozwoj/porownanie-najbardziej-popularnych-systemow-certyfikacji-energetycznej-breeam-i-leed_66921.html), Polish Green Bulding Council (PLGBC), ostatnia aktualizacja 15/03/2010.

MODELING OF CRACKING BEHAVIOUR OF R/C-MEMBERS BASED ON THE BOND-SLIP RELATION FOR BONDED REINFORCEMENT

[1]Viktor Tur, [2]Aliaksei Drahan

[1]Department of Concrete Technology and Building Materials, Faculty of Civil Engineering, Brest State Technical University, 224017 Moskowskaja St. 267, Brest, Belarus
e-mail: vvtur@bstu.by
[2] Department of Town Development and Architecture, Faculty of Civil Engineering, Brest State Technical University, 224017 Moskowskaja St. 267, Brest, Belarus
e-mail: alexdragan@yandex.ru

Summary:
In this article is presented the new approach for design procedure for crack width calculation, received on the basis of experimentally-theoretical research of axially-loaded reinforced concrete tensile elements. This new approach (calculation method) based on studying of the mechanism of interaction and internal forces redistribution between reinforcement and surrounding concrete. It was possible to establish laws of crack formation in reinforced concrete elements, to receive the equations to establish strain distributions of reinforcement and tension concrete on the length of an element and to receive an analytical equation for definition of the length of the strain redistribution zone for the various bonding conditions, to receive a relation for calculation of average crack width (w_m).

Keywords: crack width, reinforcement, concrete, strain distributions, length of the strain redistribution zone

Introduction

Currently, there is a large number of calculation methods proposed for determining of crack resistance of reinforced concrete elements. Based on analysis performed by the authors the following calculations methods were proposed:

- Empirical relationships (ACI 224.2R-86 1986; Gergely i in., 1968, Mulin 1974, Gusha 1976, etc.);
- Expressions based on the theory of fracture mechanics (Piradov i in., 1991, Guzeev 1991, Oh i in.1987, Shah 1995, etc.);
- Expressions based on the theory of «tension stiffening» (TSE) (CEB-fib MC 2010, EN 1992-1, Pedziwiatr 2008, SNB 5.03.01-02, Murashev 1962, Nemirovskij 1970, etc.);
- Relationships obtained from the analysis of the stress-strain state of reinforcement and surrounding concrete along the length between sections with cracks (Holmberg 1984, Farra 1992, Noakowski 2004, Alvares 2004, a proposed approach, etc.).

In the modern theory of crack resistance of the concrete element last two approaches are most widely used. Expressions of these groups what described the mechanism of crack formation are similar. The main difference between of two calculation methods consists of to determining the strains distribution and crack space. In the expressions derived on the basis of TSE-method, the strain difference of reinforcement and concrete between sections with cracks is determined by multiplying the value of strain in the

cracked cross section and dimensionless coefficient of ψ, which characterizes the uniform distribution of the mean strains along the length between sections with cracks. The mean crack spacing (s_{rm}) traditionally obtained as follow. In general, the expression for determining s_{rm} may be obtained from the equilibrium conditions, compiled for the block concluded between the cross-section with a crack and section located in the middle of the block, and is corrected multiplying by empirical coefficients.

The expressions obtained in the framework of the fourth group models can most fully describe the real development of cracks, because they are based on the physical laws of interaction of materials under load. Obviously, the accuracy of the results obtained using the expressions of this group, directly depends on the adequacy of the idealized diagrams used in calculation models to describe physical laws (strain-stress diagram, bond-slip diagram).

Basic provisions of the proposed approach

General view on crack development in RC-elements

The behavior of reinforced concrete elements under tensile load will be considered on the example of a symmetrically reinforced concrete elements subjected to axial tension. Tensile load applied on the section in the end of element, which conditionally can be considered as crack. The whole tensile load is perceived by reinforcement bar. For intermediate points what situated between end section and middle section of an element tensile force is transferred from the reinforcement to the concrete by bond forces. Such mechanism of strain redistribution between the reinforcement bars and the surrounding concrete corresponds to a gradual reduction of the value of strains of reinforcement and, consequently, to an increase in strains of concrete diagrams (Fig. 2.1a).

In a section, located at a distance of l_t from the end of element reinforcement and concrete strains are equal ($\varepsilon_s=\varepsilon_{ct}$). Thus, along the length of the reinforced concrete element under the axially applied tensile load two characteristic zones can be identified (Fig. 2.1):

1. zone of equal strains – $\varepsilon_s=\varepsilon_{ct}$;
2. zone of strain redistribution – l_t.

In accordance with the mechanism of strain-stress redistribution presented above, the formation of cracks in this element can occur only within the zone of equal strains, when tensile strains in concrete reaches ultimate value (ε_{ct1}) (see Fig. 2.1).

The formation of the first(-s) crack in any of sections of zone 1 is equally probable, because throughout its length is a homogeneous stress-strain state take place. The most unfavorable case is observed when the smaller number of cracks is formed along the length of the element. In this case, the crack width value will be the maximum. Suppose that will be formed only one crack in the cross section, located exactly in the middle of equal strain zone (zone 1, Fig. 2.1).

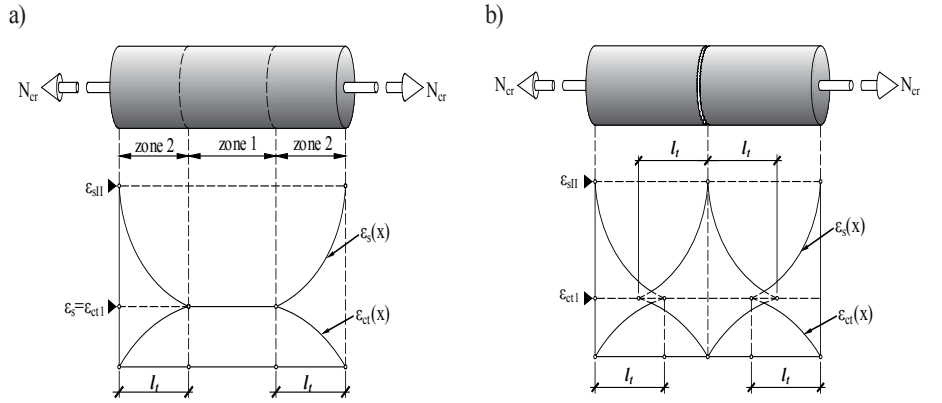

Fig.2.1. Strain distribution along of concrete element with allocation of characteristic zones: a) –before cracking; b) – after cracking;

The development of cracks is progressive and the cracks number increases as the load increases until a stabilized cracking condition is reached. The stabilized cracking is characterized by the overlapping of strain redistribution zone of two neighboring cracks (Fig. 2.1b). In any sections along the length of block observed a difference in the strains, which leads to slippage of reinforcement. It should be noted that the formation of new cracks in the already allocated blocks is possible only when strains in the middle section along the length of the block reached the ultimate value (ε_{ct1}).

After a stabilized cracking condition is reached further increase of tensile load leads to an increase in the difference between values of the strains of reinforcement and concrete in each section along the length of the element, and as a consequence, increase reinforcement slippage, which in turn causes an increase in crack widths (see Fig. 2.2).

The length of strain redistribution zone

As follows from the mechanism of stress-strain state formation in reinforced concrete elements at different loading stages the key factors what influencing at development of cracks are as follows:

1. length of the strain redistribution zone l_t;
2. functions, what describing the distribution of strains of reinforcement $\varepsilon_s(x)$ and the concrete $\varepsilon_{ct}(x)$ along the length of the redistribution zone.

Under the length of strain redistribution zone authors mean a conditional length, which for each stage of loading is required to transfer a part of the tensile force from the reinforcement to the concrete by bond and measured between section with a crack, (where $\varepsilon_{sII}=N/(A_sE_s)$ and $\varepsilon_{ct}=0$) and the section with equal strains of reinforcement and concrete ($\varepsilon_s=\varepsilon_{ct}$). Strain redistribution zone length depends on the following parameters:

– value of axially applied load;
– bond conditions;
– the geometric parameters of RC-element;
– mechanical characteristics of concrete and reinforcement.

Introduction of "conditional length" concept is based on and justified by the fact that the length of this zone increases as applied load is increased and in some cases may exceed the length of the reinforced concrete element under consideration. (see Fig. 2.2).

Basic assumptions of the proposed approach

The design crack width can be determined using the following expression:

$$w = \int_L \left[\varepsilon_s(x) - \varepsilon_{ct}(x) \right] dx \,, \tag{2.1}$$

where L – block length between cracks; $\varepsilon_s(x)$ – function, describing the reinforcement strain distribution; $\varepsilon_{ct}(x)$ – function, describing strains distribution of surrounding concrete in tension;

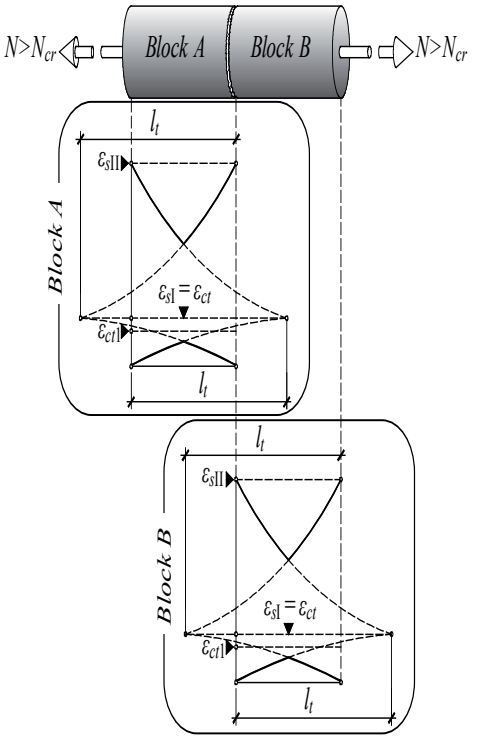

Fig.2.2. Strain distribution in reinforcement and concrete along the length of an element (calculation case: redistribution zone length is longer than the block allocated by cracks)

In addition to the functions $\varepsilon_s(x)$ and $\varepsilon_{ct}(x)$ is necessary to determine the final (maximum) length of the block between neighboring cracks, where crack development is impossible. According to the provisions given in (2.1), the formation of following crack in the block is possible if at least in one section along the length the value of reinforcement and concrete strains are equal, i.e. $\varepsilon_s = \varepsilon_{ct}$. Such a case is possible if the

block length L is equal to the twice length of the strain redistribution zone when tensile load is equal N_{cr}, i.e.($L=2l_{t,cr}$). After the crack formation the block will be divide into two new blocks with the length $l_{t,cr}$ and expression (2.1) takes the following form:

$$w = \int_{l_{t,cr}} \left[\varepsilon_s(x) - \varepsilon_{ct}(x)\right] dx \tag{2.2}$$

The numerical algorithm was proposed for evaluation of analytical expressions for calculating the length of the strain redistribution zone l_t and functions $\varepsilon_s(x)$ and $\varepsilon_{ct}(x)$ a planar coordinate system with origin in the cross-section with condition $\varepsilon_s=\varepsilon_{ct}$ is accepted. The positive direction of the horizontal axis taken in the direction of the cross section with a crack. Using an iterative numerical method for the elementary interval Δx, allocated by along the horizontal axis is searched for distribution of concrete and reinforcement strains, satisfying the of equilibrium equations (see Fig. 2.3):

$$\begin{cases} \sigma_{s\,i} - \sigma_{s\,i-1} - \Delta x \cdot \left(\dfrac{\tau_{b\,i} + \tau_{b\,i-1}}{2}\right) \cdot \dfrac{4}{\varnothing_s} = 0 \\ \sigma_{ct\,i-1} - \sigma_{ct\,i} - \Delta x \cdot \left(\dfrac{\tau_{b\,i} + \tau_{b\,i-1}}{2}\right) \cdot \dfrac{4 \cdot A_s}{\varnothing_s} \cdot \dfrac{1}{A_{ct,netto}} = 0 \end{cases} \tag{2.3}$$

Solution of the equations (2.3) can be determined with using following laws:
- for the reinforcement – by the elastic part of relationship "σ_s-ε_s";
- for the concrete – by the ascending branch of the strain diagram of concrete in tension;
- for the bond– according to the diagram CEB-fib-MC 2010.

a) b)

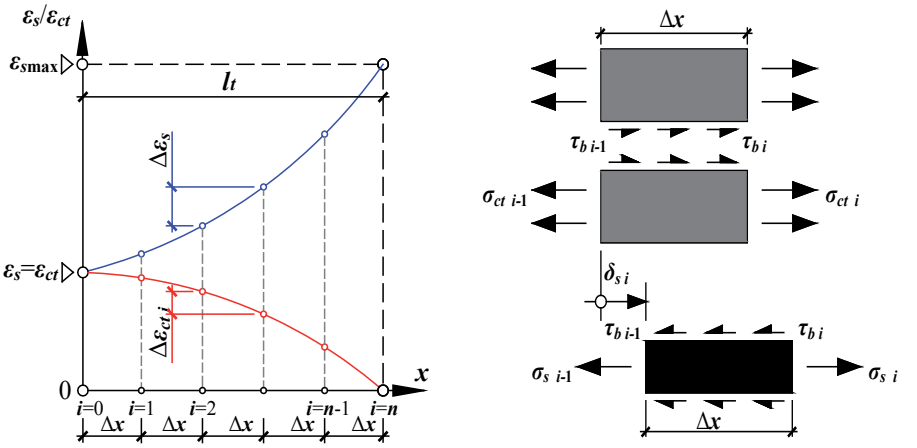

Fig. 2.3. To making the calculating algorithm:
a) – to definition of increments of stains;
b) – conditions of equilibrium for an elementary segment Δx.

The condition for complete the calculated procedure of the algorithm to determine the position of the cross section for which would have the next equations:

$$\varepsilon_{ct} = 0 \quad \text{and} \quad \varepsilon_s = \frac{N}{A_s \cdot E_s} \tag{2.4}$$

Numerical investigation using of special computer program containing the calculating procedures of presented algorithm was performed. On the basis of a computer program containing the calculating procedures of the presented algorithm was performed computational experiment, which program included determination of analytical expressions to determine the length of there distribution zone, as well as functions describing the strains redistribution of reinforcement $\varepsilon_s(x)$ and the concrete in tension $\varepsilon_{ct}(x)$ within this zone. During the computational experiment was carried out varying of the following parameters:

The following parameter was carried out varying of following parameters:

- diameter of reinforcement – 10 ... 40 mm;
- type of surface of bars – ribber bars, smooth bars;
- effective reinforcement ratio – 0.25...4.0%;
- the average strength of concrete – 1.3...2.9 MPa.

Based on the analysis results of computer simulation for the calculation the length of the strain redistribution zone following expression was obtained:

$$l_t = k_p \frac{N_{ult}}{u \cdot \left(1 + \rho_{eff} \cdot \alpha_E\right)} \cdot \sqrt{\frac{N}{N_{ult}}} \tag{2.5}$$

where

k_p –factor, which takes in account bond properties of reinforcement, mm^2/N;
N_{ult} – value of ultimate tensile force, kN;
u – perimeter of contact between reinforcement and surrounding concrete;
ρ_{eff} – the effective reinforcement ratio;
A_s – the reinforcement area;
$A_{ct,eff}$ – the effective tension area of concrete;
α_E – a ratio of modules of elasticity of reinforcement and concrete.

To describe the strain distribution of reinforcement and surrounding concrete the following equations were received:

$$\varepsilon_s\left(x\right) = \varepsilon_{sII} \cdot \left[a \cdot \left(\frac{x}{l_t} \right)^{\frac{1+\alpha}{1-\alpha}} + b \right] \tag{2.6}$$

$$\varepsilon_{ct}\left(x\right) = \varepsilon_{sII} \cdot \left[1 - \left[a \cdot \left(\frac{x}{l_t} \right)^{\frac{1+\alpha}{1-\alpha}} + b \right] \right] \cdot \rho_{eff} \cdot \alpha_E \tag{2.7}$$

where e_{sII} – strain of reinforcement assuming a cracked section; a and b – dimensionless coefficients are defined by:

$$a = \frac{1}{1+\rho_{eff}\cdot\alpha_E} \quad \text{and} \quad b = \frac{1}{1+\frac{1}{\rho_{eff}\cdot\alpha_E}} \tag{2.8}$$

Inserting obtained relationships into (2.2) and performing the appropriate transformations, expression for determining crack width takes the form:

$$w_m = 0{,}15\cdot k_p\cdot\varepsilon_{s\text{II}}\cdot\frac{\varnothing_s}{1+\rho_{eff}\cdot\alpha_E}\cdot\sqrt{\frac{\sigma_{s\text{II}}}{f_{yk}}}\cdot\left[1-\left(1-\frac{1}{2}\cdot\sqrt{\frac{f_{ctm}}{\sigma_{s\text{II}}\cdot\rho_{eff}}}\right)\right] \tag{2.9}$$

where

$\sigma_{s\text{II}}$ – reinforcement stress for cracked section; f_{yk} – characteristic strength of reinforcing steel, MPa; f_{ctm} – average tensile strength of concrete, MPa.

Experimental verification of proposed analytical model

For verification of proposed analytical model several tests series of axially reinforced concrete elements have been executed. At manufacturing of test specimens for various experimental series it was made by variation in reinforcing parameters (diameter of reinforcement (Øs=20, 25 and 36mm)); type of a surface of reinforcement (smooth bars and ribber bars) and strength characteristics of steel reinforcement and concrete of specimens.

To measurement of reinforcement bar strain within embedding length of concrete it was applied strain-gage method. As primary measuring devices have been used strain gages with base 5,0mm. Strain-gages were pasted in the grooves executed on a lateral surface of reinforcement bars along longitudinal edges of a profile, in chessboard order with step 50mm that has allowed equipping each bar with 41 gages.

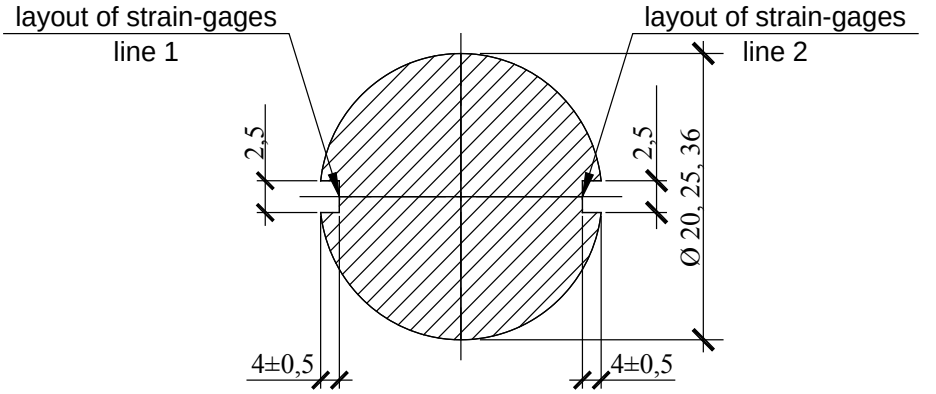

Fig. 3.1. Layout of strain-gages on the reinforcement bar

During the tests of experimental specimens at each stage registration of following parameters was made:

– reinforcement bar strains on embedded length in the concrete on the basis of strain-gage method at use of a measuring computer complex;
– crack width at use of microscope.

The results of comparison of experimental and analytical strain distributions of reinforcement for stages accordingly before and after crack formation are presented in Figure 3.2. It is necessary to notice that at the description of strain distribution for reinforcement $\varepsilon_s(x)$ and concrete $\varepsilon_{ct}(x)$ tensile load and of position cracked section were accepted according to experimental data.

The comparative analysis of the experimental and analytical data (Fig. 3.2) gives the grounds to draw a conclusion about legitimacy of hypotheses and the preconditions accepted by working out of model, and also about adequacy of dependences $\varepsilon_s(x)$ and $\varepsilon_{ct}(x)$, proposed for the description of stress-strain condition of reinforcement and the tension concrete of axially reinforced concrete element. Comparison of values of average crack width received during carrying out of tests, to the corresponding values calculated according to various calculating procedures: to a proposed method and standard method EN-1992-1 (2004), it is executed in Figure 3.3. The comparative analysis of results of calculation shows that the Eq. (2.9) proposed for calculation of the average value of crack width, provides comprehensible reliability of calculating values in relation to the experimental data. Besides, character of change of values of average crack width calculated according to proposed relation, is most close to the character taking place in the experiment.

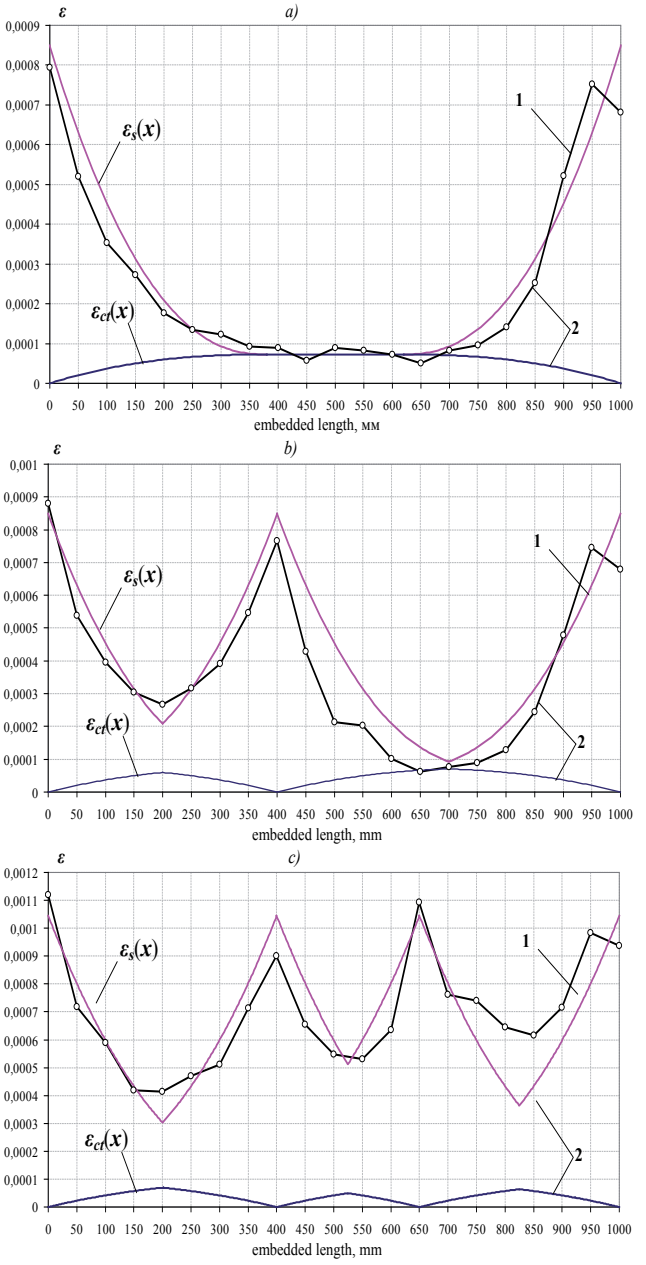

Fig. 3.2. Comparison of strain distributions, received experimentally (1) and analytically (2), for the specimen with following characteristics – 1Ø25S400; ρ_{eff}= 0,015; f_{ctm}=2,47N/mm^2
a) – before crack formation of (N=80kN); b) – after first crack formation (N=80kN);
c) – after second crack formation (98,4kN)

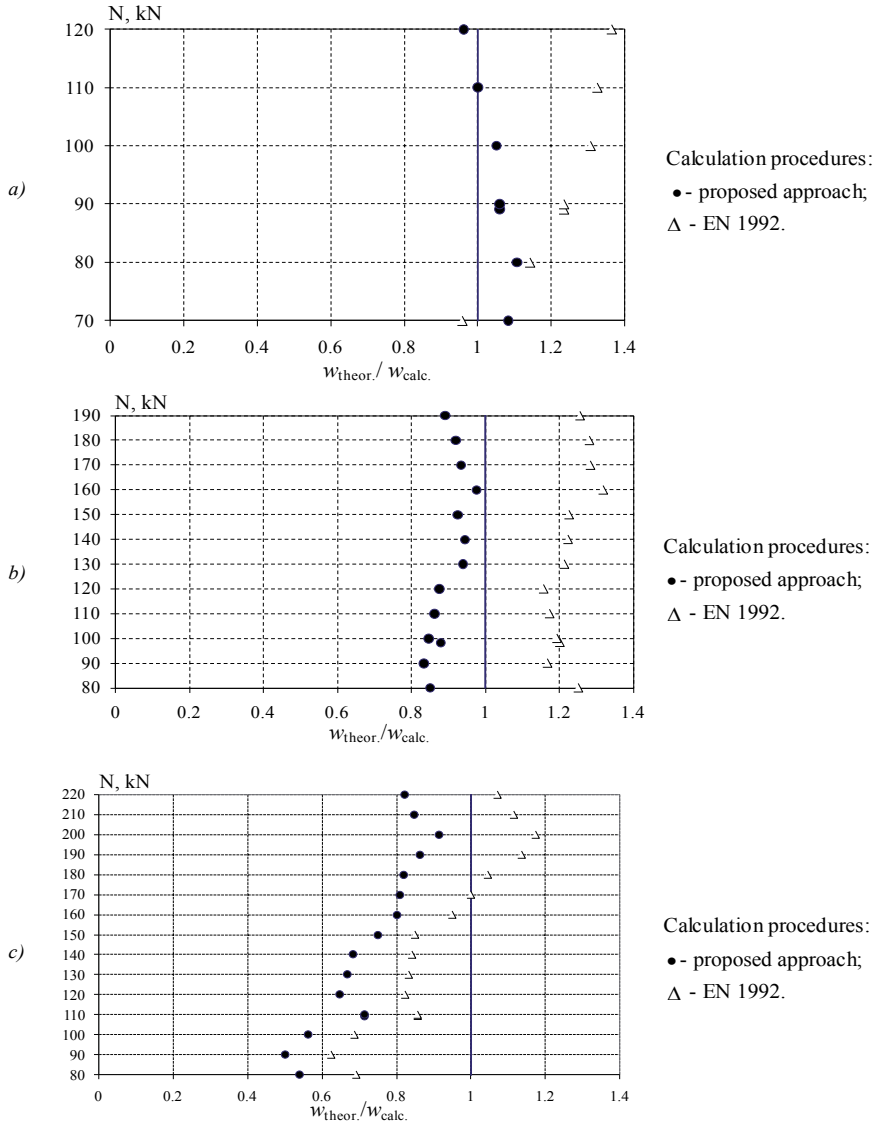

Fig.3.3 Comparison of average values of crack width
a) - experimental specimen with following characteristics – 1Ø20S400; ρ_{eff}= 0,01; f_{ctm}=2,47N/mm^2;
b) - experimental specimen with following characteristics – 1Ø25S400; ρ_{eff}= 0,015; f_{ctm}=2,47N/mm^2;
c) - experimental specimen with following characteristics – 1Ø36S400; ρ_{eff}= 0,03; f_{ctm}=2,47N/mm^2;

Conclusion

Proposed concept based on an analysis of strain-stress state of concrete and reinforcement qualitatively characterizing the conditions of crack formations in RC-elements under axially applied tensile load.

Based on the general provisions of the concept were obtained:

– equations describing the strain distribution of reinforcement and concrete along the length of the strain redistributions zone at any loading stage;
– relationship of the crack width and strains distribution in the reinforcement, the geometric parameters of tensile RC-element cross-section.

References:

1. Alvarez M. (1998), *Einfluss des Verbundverhaltens auf das Verformungsvermögen von Stahlbeton*. Institutfür Baustatik und Konstruktion, Eidgenössische Technische Hochschule Zürich.
2. American Concrete Institute Committee 224. *Cracking of concrete members in direct tension*. ACI 224.2R-86. ACI Journal., 84(1): 3–13, 1986.
3. CEB-FIP Model Code 2010: *Design Code. Comite–Euro–International du Beton*, London, 2010.
4. Eurocode 2: Design of Concrete Structures – Part 1-1: *General Rules and Rules for Building*. EN 1992–1:2004. European Committee for Standardization., Brussels, 2004.
5. Farra B., Jaccoud J.-P. (1992), *Bond behaviour, tension stiffening and crack prediction of high strength concrete*. Proceedings of International Symposium «Bond in Concrete», Riga.
6. Gergely P., Lutz L. A. (1968), *Maximum crack width in reinforced flexural members. Causes, Mechanism and Control of Cracking in Concrete*. American Concrete Institute SP-20: 87–117.
7. Gusha J.P. (1976), *Crack width in elements of reinforced-concrete constructers* / Limiting conditions of elements of reinforced-concrete constructers, s. 30–44.
8. Guzeev E.A. (1999), *Mechanics of destruction of concrete: theory and practice questions* Publishing house BPI, Brest.
9. Holmberg A. (1984), *Unbonded Portions Between Concrete Cracks*. Danish Society for Structural Science and Engineering, 55(4), s. 113-117.
10. Mulin N.M. (1974). *Reinforcement of reinforced-concrete members*. Stroyizdat.
11. MURASHEV V.I. (1962). *Reinforced-concrete structures.Publishing house of literature on building, architecture and building materials*.
12. Nemirovsky J.N. (1970), *Revision of some positions of the theory of crack opening*. Concrete and reinforced-concrete, s.13-16.
13. Noakowski P. (2004), *Determination of crack width: Simple and close to reality method considerating tensile strength of concrete and steel bonding*: Technology of Concrete. Supplement. – Gdansk.
14. Oh B. H., Kang Y-J. (1987), *New formulas for maximum crack width and crack spacing in reinforced concrete flexural members* . ACI Structural Journal, 85(2), s. 103–112.

15. Pedziwiatr J. (2008), *Tension stiffening effect a przyczepnosc na przykladzie osiowo rozciaganych elementow zelbetowych*. 54 konferencja naukowa: Problemy naukowo-badawcze budownictwa, Krynica, s. 241-248.
16. Piradov A.B., Gvelesiani, L.O. (1991).*Width and length of crack opening in elements of concrete designs at long loading*. Izvestijevuzov. 12, s. 88-90.
17. Shah S.P. (1995), *Fracture Mechanics of Concrete: Applications of Fracture Mechanics to Concrete*, Rock and Other Quasi-Brittle Materials. New York: John Wiley & Sons.
18. SNB 5.03.01–02. 2002. *Concrete and reinforced-concrete stuctures*. Minstrojarchitectura, Minsk.

POSSIBLE APPLICATIONS OF NATURAL FIBER AND STRAW OF FLAX AND HEMP IN THE CONSTRUCTION INDUSTRY

[1]Stanisław Fic, [2]Przemysław Brzyski, [2]Maciej Szeląg

[1]Pope John Paul II State School of Higher Education, Faculty of Civil Engineering,
Sidorska St. 95/97, 21-500 Biała Podlaska, Poland
e-mail: s.fic@pollub.pl
[2] Lublin University of Technology, Faculty of Civil Engineering and Architecture,
Nadbystrzycka St. 40, 20-618 Lublin, Poland
e-mail: p.brzyski@pollub.pl, maciej.szelag@pollub.pl

Summary:
High energy consumption, carbon dioxide emission, air pollution and slow depletion of conventional fuels contribute to the production of various building materials. The idea of sustainable development in the construction industry is to reduce these effects to a minimum by seeking alternatives such as ecological and energy efficient building materials and technologies of their production. More importantly, the economic dimension expressed by lower operating costs of energy efficient buildings is a relevant issue.
The purpose of this paper is to present the possibility of using natural resources in the production of building materials.
The article describes the characteristics of lightweight composites composed of natural fibers and straw from flax and hemp, on the lime binder modified with different additives and admixtures. The pilot study, executed in several European countries including our own, was described on the basis of world literature which focuses on mechanical and thermal properties of these materials [1,5]. In addition, other uses of flax and hemp, known in the construction industry for a long time, were presented.
As far as conclusion is concerned, the current progress in the study of these materials was evaluated. The obtained results indicated the direction for further development of research and allowed to assess the potential for wider application in construction industry.

Keywords: natural fibers, ecology, building materials

Introduction

Flax and hemp are fully biodegradable, non-waste materials with health and ecological properties [3]. Flax and hemp fibers have high tensile strength and resistance to abrasion and for this reason, they can be used as an alternative to synthetic materials. Even in ancient times and in the early centuries of our era, they were frequently used in construction. These fibers and linseed oil (the oil in flax) were added in order to improve the mechanical and physical properties of lime mortar used for instance, in the construction of aqueducts and water reservoirs. Linseed oil is used for the manufacture of linoleum flooring [7]. This environmentally responsible material is biodegradable and does not release harmful gases or toxins into the air as it breaks down, in contrast to common PVC flooring. Not to mention the fact that oil from flax preserves providing protection on wooden surfaces in buildings. Dry chopped stalks of flax and hemp after

the separation from fibers are used in the manufacture of chipboards. Flax straw is mainly used as a bio-fuel. It is a carbon neutral fuel. When the straw is burnt, carbon, in the form of carbon dioxide, is released into the air, where it can, once again, be used the following year in the production of straw. Flax fibers are more frequently used in the production of geotextiles as a substitute for common synthetic or coconut fibers whose transport costs are relatively high [7]. When the fibers are aggressively processed, they can be turned into quite soft, fine fibers. Whereas coarse and fine fibers can be blended and processed so as to produce insulation batts with insulating properties similar to the fiberglass batts, so commonly used to insulate walls and ceilings. More importantly, flax fibers can be used in place of fiberglass in many plastic composite applications. They are cheaper, lighter in weight and impart more springiness than fiberglass. In addition, such natural fibers require less energy in manufacture and are easier to be decomposed or burnt. The following images represent the fiber and the straw of flax and hemp.

Fig 1. Flax fiber and straw [8]

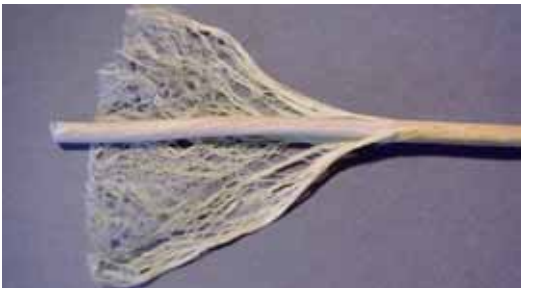

Fig 2. The fiber separated from the woody part of the hemp stalk [6]

The aim of this study is to evaluate the suitability of the use of these materials in the production of lightweight composite materials (wall materials); and to make a contribution to the development of sustainable construction by developing ecological material of reproducible natural resources.

The characteristic of the composite material

In the recent years in France and in the United Kingdom research has been conducted into the new application of hemp in construction focusing on their specific properties. Hemp is used in the production of composite building materials. The composite known as hemp lime consists of fast-growing and carbon sequestrating plant-based aggregates (hemp core chopped into short pieces of about 25 mm) with a lime-based binder [1]. Such a lightweight material is suited to various construction applications. The composite is formed by mixing together hemp aggregates and lime-based binder. The lime binds chopped hemp core together, giving the material modest structural strength and stiffness. However, this material has good thermal and acoustic performance, provides healthy microclimate and controls the level of indoor humidity. Lime also protects hemp from biological decay. By modifying the mix design and proportions of ingredients, lighter

or denser material can be obtained for various applications such as, under-floor or roof insulation and wall material. Moreover, this composite contributes to sustainable building since it can capture and accumulate carbon dioxide and lock it up into buildings [1].

Furthermore, hemp lime may be used in various ways – it can be cast like concrete within shuttering or sprayed (Fig. 4). It can also be cast into blocks (Fig. 3) and panels or cast as a floor screed and used as a plaster. In the case of solid hemp lime, a shuttering can be removed after 24 hours, although the material achieves quickly a self-supporting resilience. Block walls are denser and do not provide very good thermal insulation properties, nevertheless they have high thermal mass. Blocks can be used as infill inside a frame construction mainly made of timber [1].

Hemp lime composite walls need external weather protection provided by a finishing material such as, a lime render providing vapour permeability so that the material can breathe.

Fig 3. Hemp lime blocks [1]

Drying time of hemp lime is normally of about four weeks. A building constructed with the use of such a technology should be well ventilated while the hemp lime dries out. Hemp lime absorbs moisture and ensures breathing of walls. The moisture content in the material serves also as a thermal buffer. Such a hygroscopic performance has beneficial aspects which are the prevention of condensation and control of internal relative humidity. It has been proposed that hemp lime absorbs and releases energy, as moisture is released or absorbed, giving the material a unique apparent thermal mass. Breathable composite with lime provides a protection from biological pathogens and mould growth at the point of construction. The alkalinity of the lime reduces the potential for an attack by pests [4]. Another advantage of using hemp lime is lack of volatile organic emissions from the materials as it occurs in the case of synthetic materials.

Hemp lime solves the problem of thermal bridge because of the homogenous structure of the material. There are no cold points of wooden construction since all the timber frames are buried within the mass of the insulating material [1].

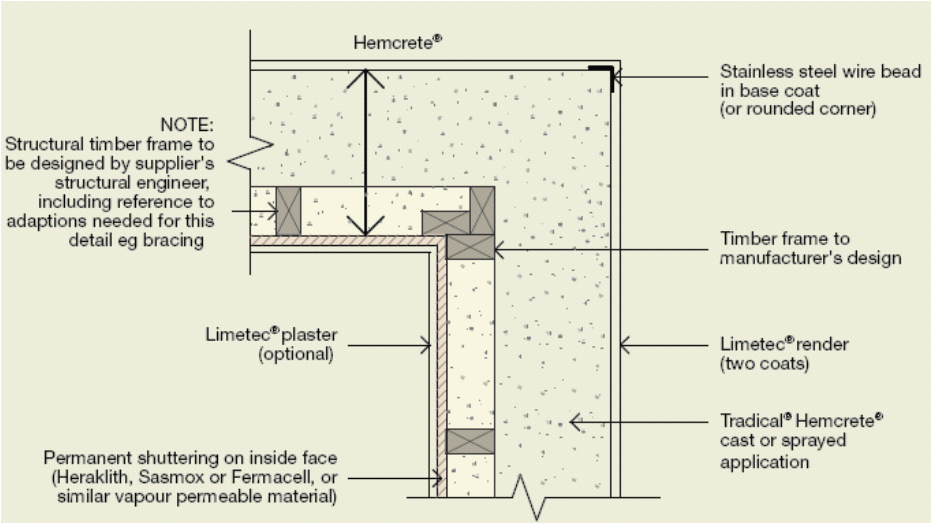

Fig 4. Permanent internal shuttering board and timber frame for spray application of hemp lime [1]

In Slovakia hemp is also used as an ingredient of the lightweight composite, yet on another binder which is described in more details in the next chapter. Whereas in Poland, studies have been undertaken on the possibility of the application of straw and flax fibers in building materials on lime binder.

It is also worth mentioning attempts to use other natural fiber in the construction industry, for instance, in Brazil, research was conducted into concrete wall bricks which were armoured with natural micro-reinforcement of sisal fibers [2].

Composites research and results

The research carried out in France, the UK and Slovakia [1,5]

Material was tested for thermal and mechanical properties. Thermal comfort is improved by the effect of hemp lime walls having a high surface temperature. It is caused by thermal mass and the ability of the composite to absorb moisture, regulate level of humidity and emit heat. The thermal conductivity of the materials was examined with different proportions of ingredients in the mix. Research produced the 'λ' values in the range of 0,08 to 0,09 W/mK that were subsequently taken on a wall which was 200 mm thick. Thermal resistance (the 'R' value) was calculated to be 2,75 m^2K/W taking plaster and surface resistances into account. On the basis of these figures, the research team agreed that a U-value would amount to 0.36–0.37 W/m^2K. A 300 mm thick wall would have a U-value of about 0,26 to 0,28 W/m^2K. It meets the new Building Regulations thermal standards.

Thermal properties are associated with the density and method of making the material. Due to the high heat capacity and the ability to absorb moisture, hemp lime reaches equilibrium in heat exchange only after 72 hours, whereas the temperature difference on the two sides of the wall amounts to 20 °C (black solid line in the Fig. 5). Whereas cellular concrete of the same thickness needs above 30 hours and the mineral wool 12 hours. Although the heat transfer coefficient of hemp lime wall is slightly smaller than the foregoing materials, the hemp lime wall provides more thermal comfort [1].

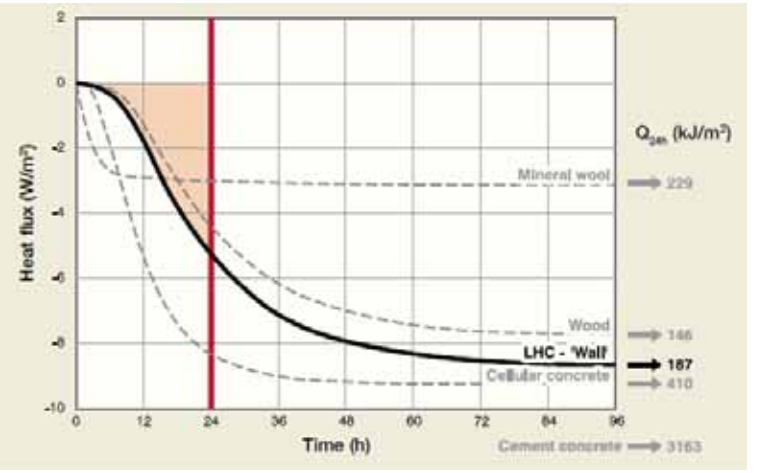

Fig 5. Heat flow through various materials [1]

Hemp lime achieved very good performance in the air tightness test. A building was tested by using a pressure and depressure test. It gave a performance of approximately 3 $m^3/h/m^2$, which is a satisfactory result against the Building Regulations target of 10 $m^3/h/m^2$. The material has good tightness, but there is no likelihood of mould growth, humidity or condensation owing to the vapour permeability of the material. Air tightness is improved with plastered finishes. A compressive strength test is extremely significant to the evaluation of the possibility of hemp lime use. In France, the material was tested on cylindrical specimens; 160 mm (diameter) x 320 mm (height) cylinders were used, whereas in the United Kingdom smaller 100 mm (diameter) x 200 mm (high) cylinders. Such a shape is better than cube for hemp lime because of the deformation characteristics of the material under load. In both cases, there occurs significant ductility in the behaviour of the material under load. Cylinders were tested in uniaxial compression under a steadily increasing load until the failure. Owing to the low stiffness, loading rate should be maintained constant, between 0.5% and 2% per minute to the failure. Specimens were formed by light compacting layers or by uniform static compaction. Hemp lime, like other lime-based materials, becomes significantly stronger with time, as the lime binder carbonates. It was tested after 90 days, which is recommended for lime-based materials. The values received from hemp lime cylinder tests were in the range of 1 to 2 MPa. After two years the 90-day strength doubled [1].

Previous research performed in France indicates that hemp lime under moderate stresses initial loading is inelastic - it does not fully recover when load is removed. However, on the reapplication of load, material behaviour is elastic or near elastic. The initial service loading compresses the open structure [1]. The results obtained from hemp lime cylinder tests in five specimens with various mixes are compared in a graph and table below:

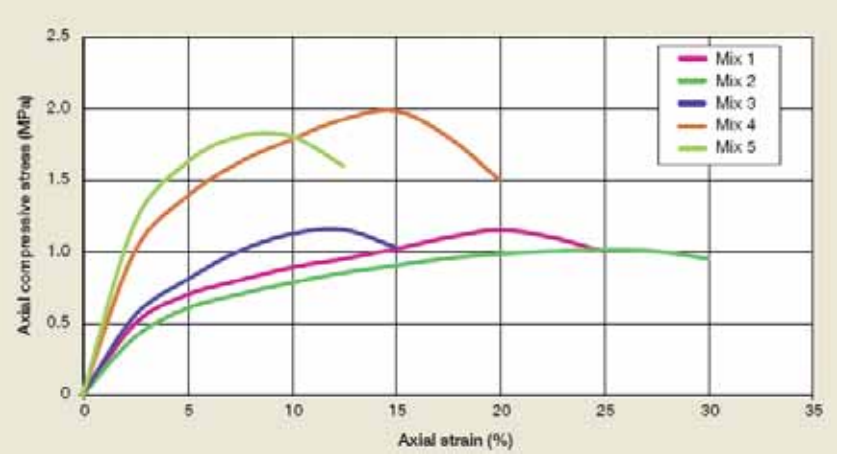

Fig 6. Stress-strain responses of hemp lime cylinders under compression loading [1]

Table 1. Comparative compression performance of hemp lime materials [1]

Mix	Mix proportions (by volume)	Dry density (kg/m^3)	Ultimate stress (MPa)	Axial strain at maximum load (% strain)
1	Lime: Hemcore*: water 1:3:0,9	620	1,15	22,5
2	Lime: Isochanvre**: water 1:3:0,9	500	1,01	25,0
3	Lime: Hemcore*: sharp sand: water 1:3:0,5:0,9	700	1,15	12,5
4	Tradical PH 70***: Hemcore*: water 1:3:0,7	610	1,98	15,0
5	Tradical PH 70***: Hemcore*: sharp sand: water 1:3:0,5:0,7	830	1,88	10,0
	* Hemcore – registered name for chopped hemp straw ** Isochanvre – registered name for mineralised hemp *** Tradical PH 70 – registered name for lime binder [9]			

There are no published data on bending and shear resistance and shrinkage, creep or settlement of hemp lime materials. Fire safety is an impostant requirement because of hemp and timber frame use in this technology. Fire tests have been carried out in France on 250 mm thick walls of hemp lime blocks, laid in a lime mortar. There were no emissions of toxic material and no re-ignition. The wall remained intact for 1 hour 40 minutes. The wall blocks were not damaged, but the mortar joints failed. This research indicates that the wall made of solid hemp lime mass has better fire performance than the wall made of hemp lime blocks. In addition, the composite meets building regulations of sound insulation. A research team tested a sound transmission between the two pairs of houses. The hemp house tests measured a sound reduction of 57 dB. The ability to absorb sound occurs due to the high porosity of this material [1].

Tests on building materials containing hemp were also performed in Slovakia [5]. The aim of the research was to check the influence of thermal loading on material with regard to mechanical, structural and thermal properties. Tested composite contained 'hemp shiv' in the mix (which is the waste from the production of hemp fibres), binder (containing caustic magnesite, silica sand, sodium hydrogen carbonate) and water. Material was prepared in steel cube forms with dimensions 100x100x100 mm. Samples were tested after 28 days of curing under laboratory conditions. Initially the composites were put inside furnace for thermal loading in temperatures of 20, 50, 100, 200°C in the period of time 48 or 72 hours. Mechanical properties of material were tested before and after different thermal loading [5]. Changes in compressive strength are shown in the graph below.

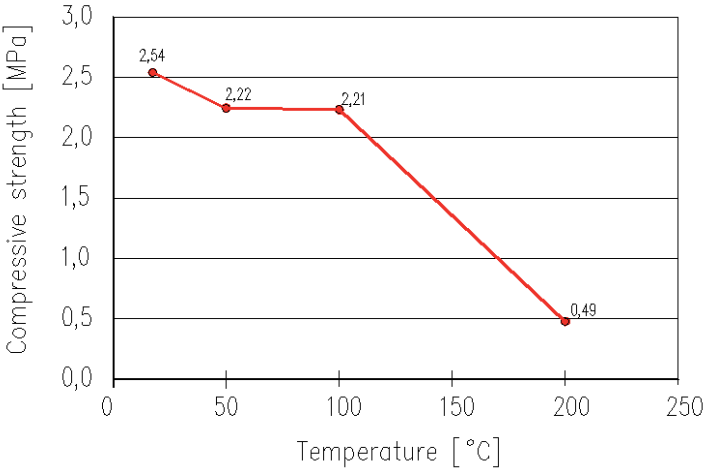

Fig 7. Compressive strength of composites before and after thermal loading [5]

The thermal conductivity coefficient measurement gave satisfactory results. For the material with a density of about 850 kg/m^3, the 'λ' value was about 0,07 W/mK and for density of about 1000 kg/m^3, it was about 0,1 W/mK [5]. A piece of original hemp shiv and sample of hemp shiv from composite loaded up to 200°C were examined under a

microscope, which showed the deterioration of fibers surface due to oxidation process of organic constituents after the higher thermal load. The research team also verified thermal stability at higher temperatures up to 800°C. The top of thermal decomposition of cellulose and lignin was observed at 280°C, whereas the loss of weight was of 56,49 wt.% [5].

Own research

In Poland, hemp cultivation gradually discontinued due to the general association of hemp with drugs. For this reason, greater chance of success has flax. A trial research on the possibility of using flax in construction is carried out whose aim is to obtain a lightweight composite which can be used as infill inside a timber-frame construction and which meets thermal building regulations for walls ('U' value below 0,3 W/m^2K). The subject of the study concerned composites containing chopped straw and fibres of the flax with the length of about 25 mm, lime binder with additions (for example, silica sand fraction of 0-1 mm, microsilica or lime powder) and water. Flax is very absorbable and it swells when it is soaked in water. To reduce the absorption, the flax straw was covered with linseed oil. Samples were obtained with a density of about 900-1000 g/dm^3. The volume of the flax straw and fiber in the mixture was 80% by volume of binder, whereas water volume was about 40-50%. Therefore, a material of relatively high density was obtained. The aim of further research will be a gradual reduction of the density of the composite.

The material was tested on cube specimens with dimension 100x100x100mm after 90 days of curing under laboratory conditions [Fig.8, Fig.9]. Samples were formed by light hand tamping of subsequent layers. Compressive strength was in the range of 0,4 to 1 MPa. It is difficult to estimate the maximum strength and the moment of damage of material due to the plastic behaviour of the composite under increasing strain. The sample is considered to be destroyed at the time of the collapse of the force-displacement graph. Displacement of the testing machine was 5 mm/min. At the time of destruction, the displacement was about 15mm.

Fot 8. Compressive strength test

Fot 9. Destroyed sample after the compressive strength test

The thermal conductivity of the samples stored in the laboratory conditions was also investigated. As a result, it amounted to about 0,20 W/mK. Further research will be aimed at reducing the value of λ, so that the use of additional insulation in the walls made of this composite is unnecessary.

Conclusions

The purpose of the article was to review the possibility of using natural resources, rapidly renewing, to the production of new green composites applicable in the construction industry both as a structural and filling element. This is an innovative use of flax and hemp. In Poland, in recent years the cultivation of hemp has become less popular because of its unprofitability. Many farms store the collections of flax from many years ago. New application of fiber and straw can change this situation, contributing to further development of sustainable construction. On the basis of the results, it can be concluded that the materials have good thermal properties, meeting building regulations in this regard. The mechanical properties are sufficient to erect self-supporting walls and to fill their skeleton structure.

Further research is required to evaluate the influence of the mix design, proportion of ingredients, curing conditions, material moisture content and loading duration on physical and mechanical properties of hemp lime. Moreover, the research should focus on seeking optimal recipes which provide greater compressive strength and rapid maturation of the mix, simultaneously maintaining the ecological character. Higher strength parameters give the possibility of extending the applications of these composites in construction, increasing the confidence among investors.

References:

1. Bevan R., Woolley T. (2010), *Hemp Lime Construction: A Guide to Building with Hemp Lime Composites*, Bracknell.
2. Izquierdo I.S., Ramalho M.A. (2013), *Elements of structural masonry reinforced with sisal fibers,* Journal of Civil Engineering and Architecture, vol.7/2013.
3. Kostic M., Pejic B., Skundric P. (2008), *Quality of chemically modified hemp fibers*, Bioresource Technology 99.
4. Osiecka E. (2006), *Wapno w budownictwie - tradycja i nowoczesność*, Kraków.
5. Stevulova N., Terpakova E., Lidalova L., Priganc S., Estokova A., Helcman M. (2011), *Hemp as potential component in suitable construction,* VI Konferencja Naukowo Techniczna: Zagadnienia materiałowe w inżynierii lądowej MATBUD'11, Kraków.
6. www.earthtechling.com
7. www.flaxcouncil.ca
8. www.flaxstalk.ca
9. www.lhoist.co.uk

CONFORMITY TESTING OF CONCRETE COMPRESSIVE STRENGTH BASED ON OVERLAPPING GROUPS

Elżbieta Szczygielska

Pope John Paul II State School of Higher Education in Biała Podlaska,
Department of Civil Engineering, Sidorska St. 95/97, 21-500 Biała Podlaska, Poland
e-mail: e.szczygielska@dydaktyka.pswbp.pl

Summary:
Conformity testing carried out according to the standard PN-EN 206-1 concerning compressive strength allows the use of two computational procedures. Standardized criteria are checked on a series of a fixed number, created with subsequent strength measurements. The series may overlap or be non-overlap. This paper presents the analysis of the risks borne by the manufacturer using these computational procedures carried out during the compulsory conformity testing. The risk assessment was carried out by means of the operating characteristic (OC-curve). Probabilities of acceptance have been determined using the Monte Carlo simulation method . The calculations of results have shown that the aggregation of data in the series does not affect the risk of rejection of a „good" concrete batch. The author recommends conformity control based on the results of overlapping sequences due to the possibility of early detection of non-compliance, which gives the opportunity to take corrective action as soon as possible.

Keywords: concrete, conformity criterion, overlapping groups

Introduction

Compressive strength of concrete is one of the basic parameters indicative of its quality. The basis of assessment of concrete quality are tests carried out in the framework of statistical quality control on a series of n strength test results obtained from standard samples. Fulfilling the standard conformity criterion forms the basis to confirm the strength of concrete produced with the characteristic strength adopted in the design of reinforced concrete construction. The European standard EN 206-1, functioning in Poland since 1st January 2004, allows two computational procedures used in the process of monitoring conformity concerning strength. In both methods, the results of the measurements are grouped into series of required number n, and the difference is in the way of creating the series. Series may form overlapping groups or be non-overlapping.

The changes in the Polish standardization concerning the assessment of concrete production and its control of the quality, which were introduced by the standard PN- EN 206-1:2003, have been extensively described by many authors (e.g. Kohutek 2002; Brunarski 2004; Bajorek 2006). There have also been a lot of comments on this standard (e.g. Czarnecki et al., 2004). In literature, one can find the patterns of conformity assessment sheets of specific assortment of concrete (Kohutek 2009; Bajorek, Betlej 2010). However, it is difficult to find the material which analyzes and assesses the risks borne by the manufacturer using the above calculation procedures carried out during the obligatory conformity testing. The results comparison of conformity assessment on compressive strength of concrete, carried out including both ways of results aggregation, were presented for the first time in Poland in 2009 by Zdzisław Kohutek (Kohutek 2009).

Conformity assessment according to PN-EN 206-1:2003

According to PN-EN 206-1:2003 Concrete - Part 1: requirements, properties, production and conformity assessment are carried out within the framework of conformity testing, which, in turn, is one of the components of production control. According to this standard, all standardized concrete parameters whose value is determined using the appropriate equipment or laboratory equipment are subject to conformity assessment. Tests are performed both at the stage of the concrete mixing as well as on the hardened concrete.

Figure1 presents the diagram of conformity testing, designed with the consideration of standard provisions.

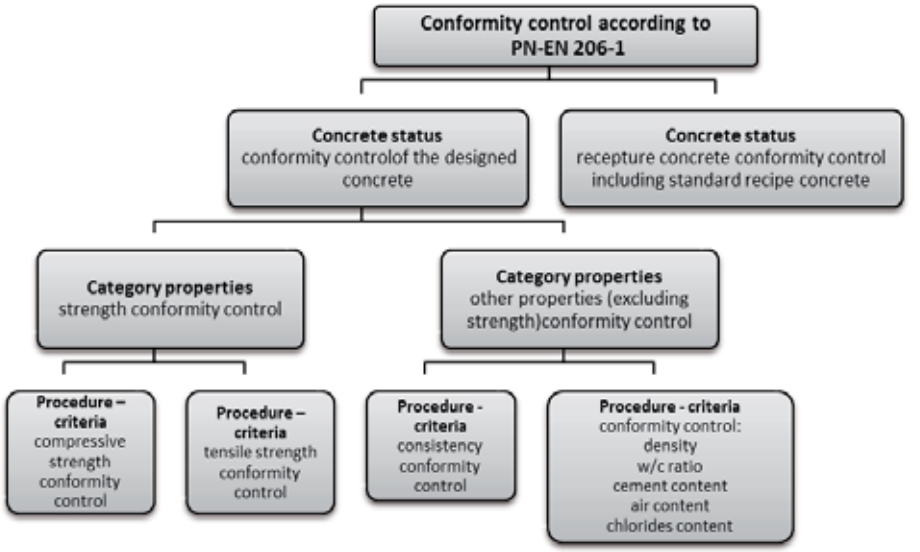

Fig. 1. Conformity control system of concrete properties (Kohutek 2009, s.178).

The article focuses attention on the conformity control of the designed concrete concerning its compressive strength. In the light of the applicable standard, such a control is performed by the manufacturer. The standard describes in detail the plan for the collection, preparation and examination of samples on the bases of which concrete strength parameters test is conducted. Citing provisions of the standard PN -EN 206-1:2003 "any concrete should be subject to the process of production control whose responsibility bears the producer". It is a producer who, having carried out conformity control, ensures a recipient of the quality of concrete available on the market. He declares that the concrete produced in the factory is of appropriate quality determined by the characteristic strength tested on cylindrical or cubic samples.

According to PN EN 206-1:2003 conformity control of concrete compressive strength is carried out with the consideration of two stages of production, initial and continuous. The initial production phase continues until collecting at least 35 results needed to

determine a preliminary estimate of the population standard deviation (σ). The standard requires that the manufacturing process, during which results used later to calculate point assessment estimator of parameter σ are collected, lasts longer than three months. After this time, assuming that there has been no more than 12 months, production goes into the stage called continuous production.

Depending on the stage of production and possessing the certificate of production control, appropriate sampling frequency is used. Sampling should be staggered while production. After the first three samples of the first 50 m^3 of production it is not recommended to collect more than one sample from each 25 m^3 of the mixture.

The analysis of conformity criteria of compressive strength

Conformity criteria concerning compressive strength are described in the chapter 8.2.1.3 of the standard PN -EN 206-1:2003. Results of strength measurements are processed according to numerical procedures, defined as criterion 1 and criterion 2 (Table 1). The fulfillment of both criteria simultaneously confirms conformity.

Tab. 1. Conformity criteria concerning compressive strength.

Production	Number „*n*" of test results used to assess conformity	Criterion 1	Criterion 2
		Mean of „*n*" test results (f_{cm}) N/mm^2	Any single test result (f_{ci}) N/mm^2
Initial	3	$\geq f_{ck} + 4$	$\geq f_{ck} - 4$
Continuons	15	$\geq f_{ck} + 1{,}48\sigma$	$\geq f_{ck} - 4$

Source: PN- EN 206-1:2003

The result of test can be the strength value (f_{ci}) obtained from a single cubic or cylindrical sample, or it may be the arithmetic mean of the measurements from at least two samples taken from the same sample of mixture and tested in the same age. In the second procedure of the calculation of (f_{ci}) result, one should skip the values different from the preliminarily calculated mean of more than 15%, unless the analysis of the case reveals any rational reason explaining the omission of a single test result.

Size (f_{ck}) means the characteristic strength defined as the quantile of order 0.05 of the distribution strength general population. This is the value at which concrete class is determined, for example: class C25/30 means that the minimum characteristic strength determined on the cylinder ($f_{ck,cyl}$) size:150x300 mm should be 25 MPa, and on the cube ($f_{ck,cube}$) of the edge 150 mm – 30 MPa.

The criterion 1 uses the arithmetic mean (f_{cm}) calculated from the series of results of three numbers at the initial production stage or 15 numbers at the continuous production. Series are created from the consecutive results (f_{ci}) and may be separate (Fig.2) or may overlap (Fig.3).

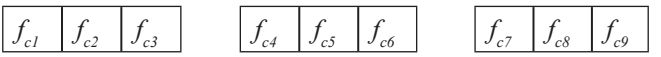

Fig. 2. Grouping scheme in the non- overlapping results sequence.

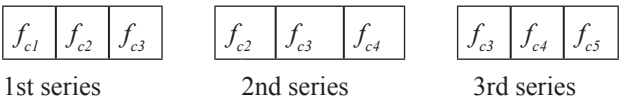

Fig. 3. Grouping scheme in the overlapping results sequence.

The arithmetic mean, calculated on the basis of overlapping sets of results (Fig.3) is a moving average sleeking a series of research results obtained during the production process.

The note, namely, the use of criteria to the overlapping results increases the risk of their rejection, is included in the standard. This would mean a higher risk attributable to the manufacturer. However, the calculations based on the overlapping results allow earlier detection of non-conformity. As a result, a producer has the chance to take earlier corrective action. It should be noted that the results are obtained with a delay compared in relation to concrete mixture production. Samples of hardened concrete are subjected to compression on 28th day of curing, and if the strength is specified for different age groups, then samples test is carried out at the specified age. This means that the producer receives a signal of the lack of conformity after about one month from the time when the concrete came to the site. If the assessment of conformity is based on non-overlapping sets of results, then this time is even longer. It is necessary to collect the required number of results in the series, i.e. 3 or 15. This may take several more days or even another month, depending on the volume of the produced concrete mix. The delay in the detection of non-conformity is, in turn, detrimental to the recipient. It increases the risk of purchasing concrete of lower class than that declared by the manufacturer. This may cause disadvantageous effects.

The standard PN-EN 206-1:2003 contains also the information that the conformity criteria are based on the overlapping results. It can be assumed that the producer, who has laconic information about the origin of developing the criteria and a warning about the increased risk of rejection of an "good" concrete batch, shall decide on the procedure for assessment of conformity based on overlapping sequences of test results. The priority may turn out to be economic reasons rather than safety.

The criterion 2, identical at both stages of production, is reduced to checking the minimum result in the series and it does not matter whether series overlap or not. Moreover, the standard also imposes the obligation to check the results dispersion of measurements of the compressive strength. When production goes into a continuous phase, it is necessary to control the spread of results using the standard deviation of s_{15} of the last 15 test results. The criterion 1 used at this stage of production uses the standard deviation σ, calculated from the results collected during the initial production (at least 35 results collected over a period longer than three months, obtained in the directly preceding period of production, during which conformity is to be checked). The control

of the dispersion of results is based on checking whether the estimator s_{15} "appropriately" estimates the adopted standard population deviation (σ) confidence level $1 - \alpha = 0.95$. Knowing the value of σ one can easily convert a relation (1):

$$\sqrt{\frac{(n-1)s_n^2}{\chi^2_{1-\frac{\alpha}{2},n-1}}} \leq \sigma \leq \sqrt{\frac{(n-1)s_n^2}{\chi^2_{\frac{\alpha}{2},n-1}}}, \quad (1)$$

describing the confidence interval for the standard deviation, where after having calculated the quantile of order $1 - \alpha/2$ from the chi–squared distribution and the number of degrees of freedom $df = n - 1$, for $n = 15$ and $\alpha = 0.05$, one obtains the relation:

$$0{,}63\sigma \leq s_{15} \leq 1{,}37\sigma \quad (2)$$

If the condition (2) is not fulfilled, one must specify a new estimate σ from the last available 35 test results. A new estimate σ determined in this way is to be used for the next period of conformity assessment.

Producer's risk assessment while using overlapping and non-overlapping sequence of results

According to the comments on EN 206-1, published in various sources (Harrison et al. 2001 Caspeele 2010) the assessment of concrete compressive strength procedures according to conformity criteria has been developed on the basis of data processing obtained by computer- generated random values (simulation method) and the analysis of the actual production of a few specific plants in Europe. Mathematical development of conformity criteria was described in detail by Lesław Brunarski (Brunarski 2009).

In the statistical procedures of quality control, along with accepted sampling inspection plans, Operating Characteristic Curve (OC-curve) is used. These OC functions represent the dependence of the probability of acceptance of tested product batches on the actual quality level of the batch, measured by defectiveness. One can assess the risk borne by the concrete producer by means of the Operating Characteristic if the actual level of production quality is known.

Based on the OC curves current values of the coefficients in the conformity criteria have been selected (Taerwe 1988).

Oparating Characteristic has been used by the author to investigate the problem, namely, how the aggregation of results affects the risk of rejection of a "good" batch of concrete.

Due to the complexity of the analytical structures, the construction of OC curves was performed using the Monte Carlo simulation.

Contemporary building standards treat the strength of the material as a random variable of normal distribution. Hence, this distribution has been adopted as the starting theoretical distribution.

First of all, two sets of series of random numbers conforming to the standard normal distribution were generated. For this purpose a random number generator implemented

in the Statistica program was used. The number of three-element series amounted to 100 000 whereas the number of 15-element series was 69905. This data made the base for the non-overlapping sequence of results. The number of overlapping groups created on this basis amounted to 299 998 and 1 048 561.

Taking concrete class C25/30 as a model and determined standard deviation (σ = *2, 3, 4, 5 and 6 MPa*) five different normal distributions were obtained. The probability of acceptance for the compound conformity criterion according to PN-EN 206-1 was calculated with a fixed defective fraction *w*, including the initial and continuous stage of production.

The shape of curves obtained for the initial production OC are shown in figure 4 and figure 5.

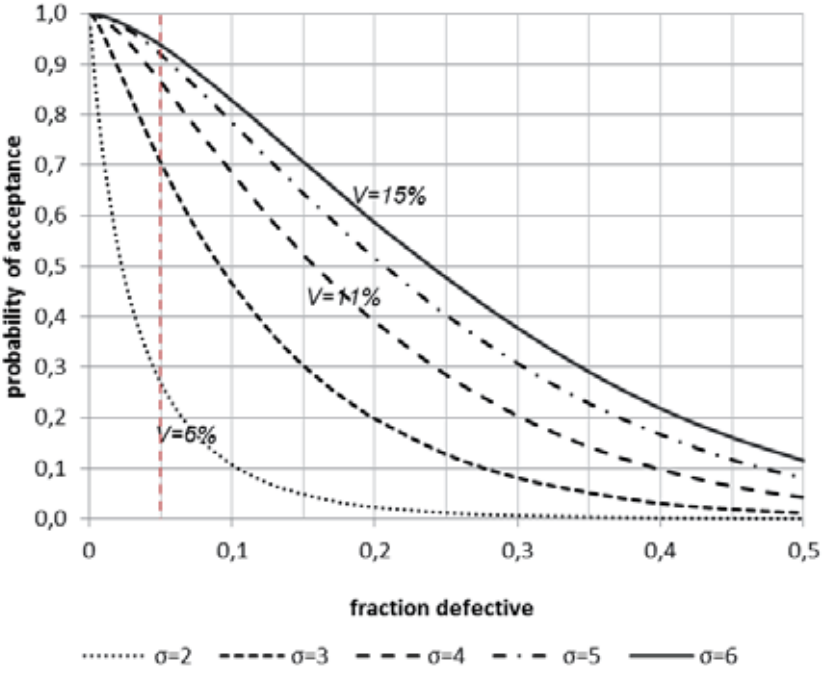

Fig. 4. OC curves compound conformity criterion in accordance with PN-EN 206-1 and different dispersions of normal distribution for the non-overlapping groups of results (number of results in a series n = 3).

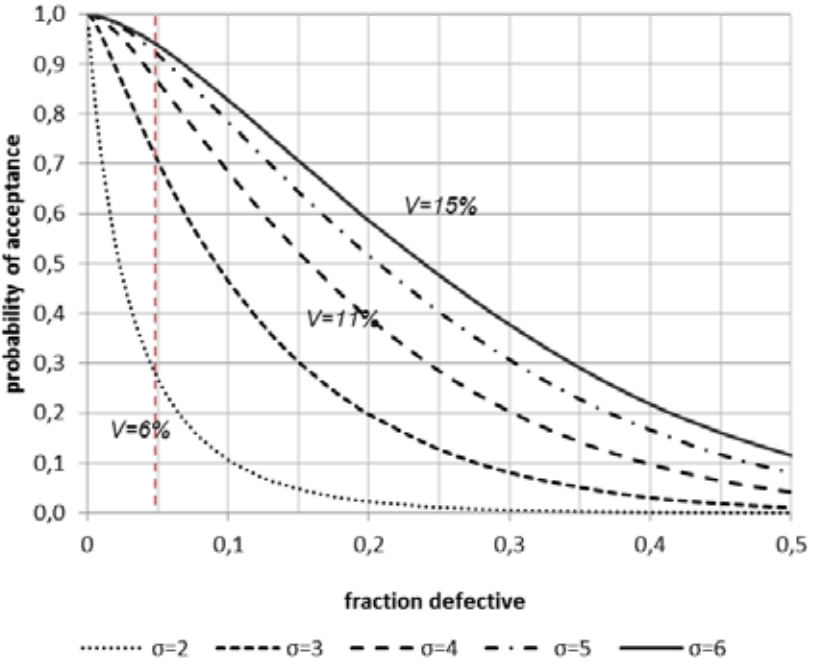

Fig. 5. OC curves compound conformity criterion in accordance with PN-EN 206-1 and different dispersions of normal distribution for the overlapping groups of results (number of results in a series n = 3)

Comparing the graphs presented above, it can be concluded that the way of result aggregation did not affect the shape of the OC curve. The exact values of obtained probabilities of acceptance at a fixed defectiveness level of, for example, 5%, can be traced by analyzing the data presented in Table 2. The differences between the values are minimal, of the order of one or a few ten-thousandths.

Tab. 2. Probability of acceptance of a double conformity criterion in accordance with PN-EN 206-1:2003 at a constant batch defectiveness $w = 0.05$ at the initial production phase (n = 3).

The way of grouping	Standard deviation (V – coefficient of variation)				
	σ = 2 V=6%	σ = 3 V=8,6%	σ = 4 V=11%	σ = 5 V=13%	σ = 6 V=15%
Non-overlapping groups	0,2695	0,7057	0,8650	0,9192	0,9375
Overlapping groups	0,2690	0,7053	0,8658	0,9192	0,9376

Source: own calculations

Owing to the lack of significant differences, one of the distributions has been selected, on the example of which the observed phenomena were presented. Normally the level of concrete compressive strength measurements diversity is about 11 - 13%, so for such a coefficient of variation a sample comparison of OC curves was presented, confirming the lack of influence of the results grouping on the probability of acceptance at the initial production phase (Fig. 6). The situation is the same for other analyzed distributions.

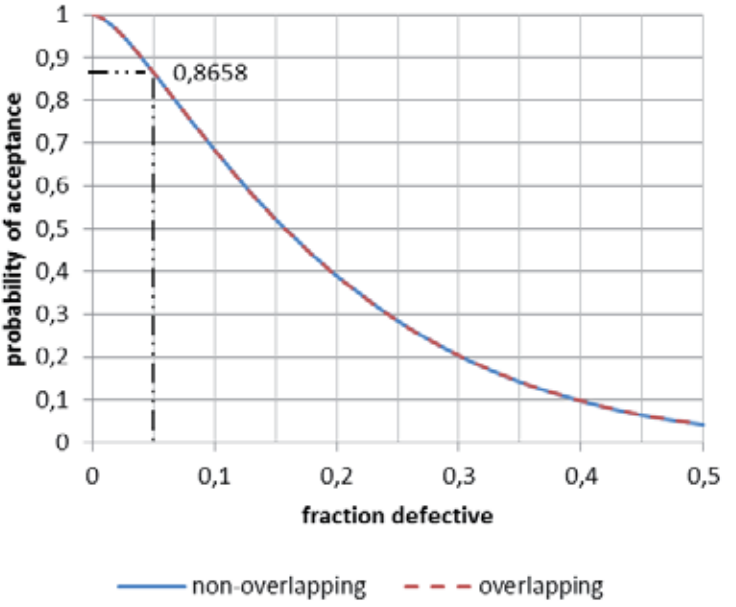

Fig. 6. OC curves for the overlapping and non-overlapping groups of results (n = 3, σ = 4).

Whereas, the dispersion of results clearly modifies the shape of graphs. Increasing dispersion leads to reducing the risk of rejection of a "good" batch of concrete. This problem was noticed by Woliński and Skrzypczak (Woliński, Skrzypczak 2006). In their view, such a situation may discourage producers to take steps aiming to ensure uniformity of production at the expense of increasing the average strength and it increases the risk of a recipient connected with the purchase of concrete batch of underestimated quality.

While using the conformity criteria at a continuous production stage it has not been observed that the aggregation of the results would increase the producer risk. The probability of acceptance calculated using a compound criterion: $f_{cm} \geq f_{ck} + 1{,}48\sigma$ and $f_{ç,min} \geq f_{ck} - 4$ with respect to non-overlapping and overlapping groups was almost identical. OC curves are shown in Figure 7 and 8.

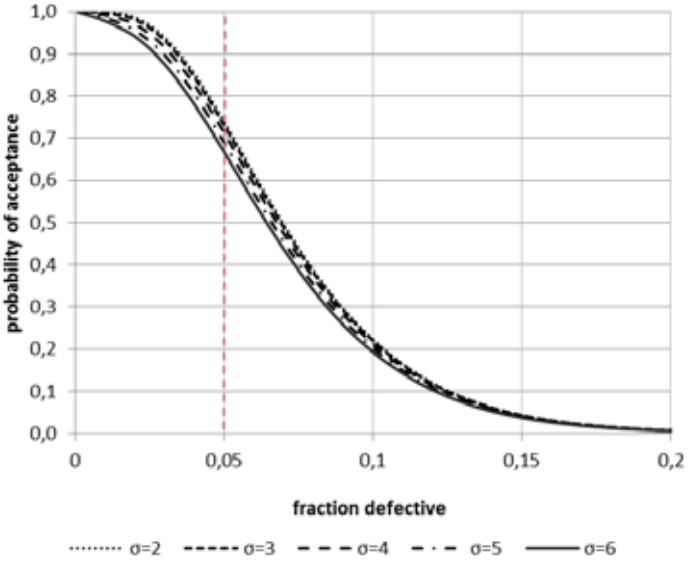

Fig. 7. OC curves of a compound conformity criterion in accordance with PN-EN 206-1 and various dispersions of normal distribution for the non-overlapping groups of results (number of results in a series n = 15)

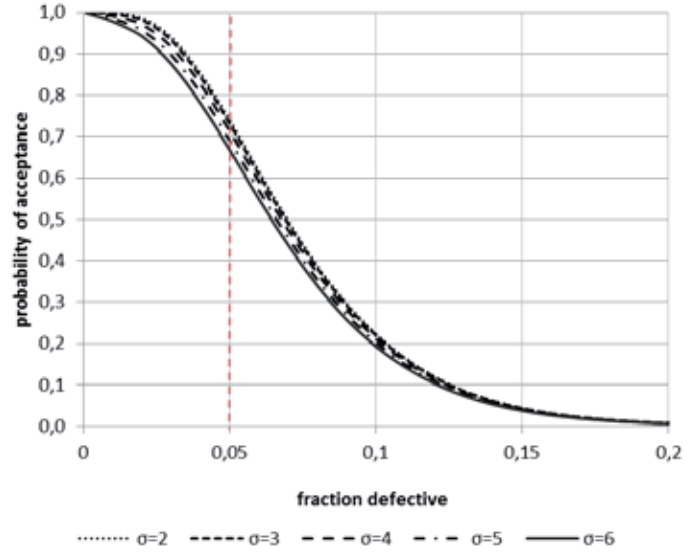

Fig. 8. OC curves of a compound conformity criterion in accordance with PN-EN 206-1 and various dispersions of normal distribution for the overlapping groups of results (number of results in a series n = 15).

The exact values of probability of acceptance with defective fraction of 0.05 are set in Table 3.

Tab. 3. Probability of acceptance of a compound conformity criterion in accordance with PN-EN 206-1:2003 at a constant batch defectiveness $w = 0.05$ at the continuous production phase (n = 15).

The way of grouping	Standard deviation (V – coefficient of variation)				
	σ = 2 V=6%	σ = 3 V=8,6%	σ = 4 V=11%	σ = 5 V=13%	σ = 6 V=15%
Non-overlapping groups	0,7373	0,7286	0,7111	0,6886	0,6658
Overlapping groups	0,7391	0,7305	0,7127	0,6899	0,6672

Source: own calculation

The differences in the values of probability of acceptance are already slightly higher than in the case of the criteria used for the initial production stage, but still minimal, of the order of several thousandths. Should one consider this difference as vital, more beneficial calculation procedure would be the one that is based on the overlapping sets of results.

OC curves of compound conformity criteria applied to overlapping and non-overlapping groups of results, presented in one coordinate system run almost identically to the same standard deviations, the differences are hardly noticeable. A graphical presentation of all these graphs, almost skipped in this article, has been limited to one. An example of the OC function graph of a compound conformity criteria for the standard deviation of 4 and $n = 15$, with a more detailed scale is shown in Figure 9.

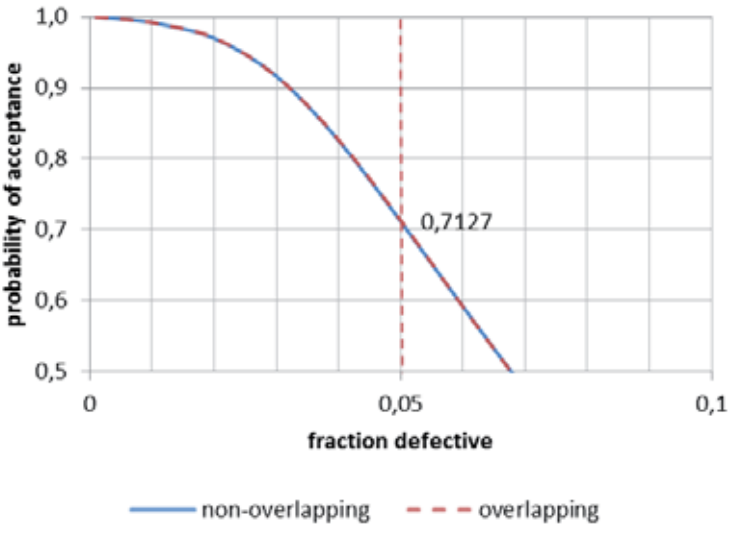

Fig. 9. OC curves for the overlapping and non-overlapping groups of results (n = 15, σ = 4).

In addition, it should be noted that the author has received the values of probability of acceptance very close to the results presented by Woliński S. Skrzypczak I. (Woliński, Skrzypczak 2006). However, the information on how to create a series of subsequent results was not provided in the description of the algorithm for calculating operating characteristic.

The calculations and analysis of the results let us draw the conclusion that the aggregation of overlapping or non-overlapping results in a series does not affect the producer's risk connected with the rejection of a "good" batch of concrete.

A different conclusion is drawn by Zdzislaw Kohutek (Kohutek 2009). He estimates as "more sensitive " sequence of overlapping results. As far as disjoint setting of series of subsequent results is concerned, he writes that "..it provides the added value since a possible single result, deviating excessively, spoils averaging only once, not repeatedly".

In the case of analyzing the data, including the empirical one, one can talk about the method sensitivity while comparing the frequency of detected relative nonconformities, not as described in the cited report, absolute frequencies. In the case of creating a sequence of overlapping series, the number of results increases according to the formula:

$$N^* = n \cdot (N - 1) + 1 \tag{3}$$

where:

n – the size of series ,

N – number of non-overlapping series,

N^* – number of overlapping series.

The increased number of series N^* must be included in the calculation of the frequency of detected relative nonconformities.

Conclusions

1. The standard PN-EN 206-1:2003 allows conformity assessment of concrete compressive strength according to two calculation procedures. Consecutive measurements are grouped in the series of the required number of *n*. These series may overlap or be separate (as non-overlapping groups). The choice of a procedure depends on the producer.
2. Probability of acceptance of a compound conformity criterion in accordance with PN-EN 206-1:2003, determined using the Monte Carlo method, does not depend on the grouping of results in the series.
3. The results of calculations performed on randomly generated "large" data sets provide the evidence that conformity control of concrete compressive strength carried out on overlapping groups of results does not increase a producer’s risk.
4. The author recommends to check conformity control of concrete compressive strength on the basis of overlapping sequences of results due to the possibility of early detection of non-conformity, which makes an opportunity to take corrective action as soon as possible.

References:

1. Bajorek G. (2006), Normowa kontrola zgodności w ramach kontroli produkcji. W: Materiały szkoleniowe Stowarzyszenia Producentów Betonu Towarowego w Polsce „Norma PN-EN 206-1: Beton…- bez tajemnic", Kraków, s.93-108.
2. Bajorek G., Betlej L. (2010), Normowa kontrola betonu według PN-EN 206-1. „Inżynieria i budownictwo", nr 3/2010, Fundacja PZITB, Warszawa, s.121-125.
3. Brunarski L. (2004), Nowe kryteria zgodności wytrzymałości betonu. „Budownictwo, Technologie, Architektura", nr 2/2004, Polski Cement, Kraków, s. 28-30.
4. Brunarski L. (2009), Podstawy matematyczne kształtowania kryteriów zgodności wytrzymałości materiałów, ITB, Warszawa.
5. Caspeele R. (2010), Probabilistic Evaluation of Conformity Control and the Use of Bayesian Updating Techniques in the Framework of Safety Analysis of Concrete Structures. PhD thesis, Ghent University, Ghent, Belgium, s. 129
6. Czarnecki L. i in. (2004), Beton według normy PN-EN 206-1 – komentarz. Wyd. Polski Cement, Kraków.
7. Harrison T. i in. (2001), Guidance on the application of the EN 206-1 conformity rules (ed. Harrison T.) Quarry products Association.
8. Kohutek Z. (2002), Ocena zgodności właściwości betonu oraz kontrola jego wytworzenia w świetle europejskiej normy EN 206-1 – cz.I: kontrola zgodności. „Cement – Wapno – Beton", nr 1/2002, Fundacja Cement, Wapno, Beton, Kraków, s. 28-32.
9. Kohutek Z. (2009), Testowanie zgodności parametrów wytrzymałościowych betonu. „Górnictwo i Geoinżynieria", r. 33, z.3/1, Uczelniane Wydawnictwa Naukowo-Dydaktyczne AGH, Kraków, s. 177-189.
10. PN-EN 206-1:2003. Beton – Część 1: Wymagania, właściwości, produkcja i zgodność.
11. Taerwe, L. (1988), Evaluation of compound compliance criteria for concrete strength. Materials and Structures 21(1), s. 13-20.
12. Woliński S., Skrzypczak I.(2006), Kryteria statystyczne zgodności wytrzymałości betonu na ściskanie. „Materiały Budowlane", 2/2006, Politechnika Rzeszowska, Rzeszów, s.20-25.

EFFECTIVENESS OF FLEXURAL BASALT REINFORCEMENT APPLICATION IN RC BEAM STRUCTURES

[1]Marek Urbański, [2]Andrzej Łapko

[1]Warsaw University of Technology, Faculty of Civil Engineering,
Armii Ludowej St. 16, 00-637 Warsaw, Poland
[2]Bialystok University of Technology, Faculty of Civil & Environment Engineering,
Wiejska St. 45e, 15-351 Bialystok, Poland
e-mail: [1]m.urbanski@il.pw.edu.pl, [2]lapko@pb.bialystok.pl

Summary:
Basalt bars for concrete reinforcement called Basalt Fiber Reinforced Plastic (BFRP) is a new material, so it is necessary to identify the differences and limitations of their use in relation to traditional steel reinforcement. The paper presents some chosen results of research on the flexural behavior of model beams reinforced with BFRP bars, compared to the reference beams with steel reinforcement. The tested beams were made of C30/37 concrete and flexural reinforcement of basalt bars with 8 mm diameter. The tensile test of BFRP bars has been conducted and the analyses of the beam deformability and flexural capacity have been performed. The results show the different character of the load-deflection dependence of basalt reinforced beams compared to traditionally reinforced beams, as well as the significant influence of the type and quality of anchoring on the basalt bars crack process.

Keywords: basalt rebar, BFRP, flexural capacity, reinforced concrete, deflections.

Introduction

Basalt fiber reinforced plastic (BFRP) is a quite new type of concrete reinforcing rebar that are stronger than conventional steel bars and at the same time are completely resistant to corrosion.

The current cost of repair and maintenance of infrastructure around the world is estimated to exceed more than 100 trillion euro's (fib Bulletin 40/2007). A large part of the costs is associated with providing durability of concrete structures. According to a study conducted by CC Technologies for the Federal Highway Administration (G. Koch et al. 2002) alone the costs of corrosion attack in road and bridge RC construction industry the U.S.A. government agencies estimate at $ 276 billion / year (about 3.1% of GDP). For example, in the period from 1987 to 1993 200 000 tonnes of steel bars epoxy-coated plates were used in the bridge, but a significant percentage of them is degraded (Hollaway 1993).

In today's world there is a wide range of available technologies delaying corrosion of reinforcement for concrete. Each of them has its own particular advantages and economics. The following types of protection against corrosion of reinforcement used in concrete structures could be specified:

- protective coatings and linings,
- metal coatings and linings,
- corrosion resistant alloys,
- corrosion inhibitors,

- cathodic and anodic protection
- corrosion resistant composites

Several enhancements methods (such as galvanizing and coating of steel rebar), as well as alternative reinforcement (such as carbon fiber reinforcement (CFRP) or glass fiber reinforcement (GFRP) were tested in the past. The recent introduction of composite basalt as reinforcing bars shows many advantages in comparison with conventional steel bars.

Basalt FRP bars are an excellent alternative as bridge girder spans due to minimizing the weight of the slab, reducing repairs and a significant increase in usability (Karbhari 2007).

Service life of concrete slabs with conventional steel reinforcement for the use in bridges, is estimated for 25 years. From the other hand the life of panels with FRP reinforcement is usually expected to be at least 75 years (i.e. the period of use of the bridge) (Hooks, O'Connor 2004). The study showed that after two years in tropical conditions and in highly alkaline environment physico - chemical properties of FRP reinforced platforms have not been degraded (Tomosawa, Nakatsuji 1997), (Clarke, Sheard 1998). Also, an inspection made at 20 and 25 years of use in Mondial House Building (built in 1974) has shown that the design of FRP reinforced plate elements is almost as good as new (Karbhari 2007).

In May 2008, Southeast University, Zhejiang GBF Basalt Fiber Co., Ltd. and Zhang Shi Shijiazhuang – both highway managing companies - developed a technology of continuous reinforcing process of building structures, using BFRP reinforcement to strengthen the road at the north and south ends of the Xingtang crossing bridge. The technology of constructing a continuous reinforcement eliminated the need for welded joints, thereby reducing shrinkage cracks of concrete blocks, but also solved the problem of corrosion of steel reinforcement effect due to de-icing salt, thereby positively affecting the quality and durability of highways and motorways and has reduced costs and shortened construction time (Wu Z. *et al*. 2012).

The problem of determining the real stress – strain relationship of reinforcement rebar made of composite-based materials, such as glass, aramid (Kevlar), or carbon fibers exists for the last two decades.

For example, in the SLS design the use of indirect methods for determining the width of the cracks on the bars distance basis, as a function of the tension in the reinforcement, and concrete cover is not recommended for the FRP bars.

For the service load the maximum width of the cracks may be assumed greater than that for conventional reinforced concrete, due to high BFRP resistance to corrosion. The recommended crack width limit values for FRP reinforced elements recommended by Canadian Standards (CSA 2002) are:

– for external reinforcement 0.5 mm (0.3 mm for steel),
– for internal reinforcement 0.7 mm (0.4 mm for steel).

Together with the implementation of FRP materials in the engineering structures it became necessary to determine their mechanical parameters. Due to the anisotropic structure of composite materials and isotopic steel reinforcement, the modified stress-strain relationships have to be considered.

Characteristics of basalt reinforcement (basalt fibers and basalt bars)

Basalt

Basaltic rock is one of the most common mineral in the world. Basalt is a fine-grained, volcanic rock with a dark color (green or black), which often glassy appearance, consisting mainly of three minerals, it is of plagioclase, pyroxene and olivine. Basalt rock is effusive fine and has a higher content of iron and magnesium than granite. Most of basalt, which can be found on Earth arose in just three types of rock formations:

1) oceanic rift zones,
2) hot spots oceanic,
3) mantle plumes and continental hot spots.

Basalt has good thermal properties, strength and durability. The density of basalt rock ranges from 2.8 to 2.9 g/cm^3. Basalt is a very hard rock with Mosh hardness of 5 to 9. Crushed basalt is commonly used for road foundations, as aggregate for concrete, aggregate for asphalt, aggregate railway and coal as a filter for surface drainage.

Basalt fibers

Basalt reinforcing rods are made of very thin basalt fibers which are similar to the carbon and glass fibers, but have better physical and mechanical properties than glass fibers, and are significantly less expensive than carbon fibers.

In the first stage of production basalt crushed volcanic rock is melted at a temperature of from about 1400 to 1700 °C. The molten rock is then extruded through special platinum nozzles for the production of continuous basalt fiber strands. The fibers due to their shape of a hexagonal chains are much more durable than steel or glass fibers (Van de Velde et al. 2002). As a result of the production of fibers there are no wastes in the environment. The fibers are non-toxic in use, and to recycle. Typically, basalt fibers consist of strands with the thickness 6, 9 and 13 micrometers. Initially, after World War II (in the former Soviet Union, the U.S.A. and Europe) basalt fibers used in military and aerospace industries. The first industrial production of continuous basalt fiber (BCF) was launched in Kiev, Ukraine in 1985. Many countries within the European Union, Japan, South Korea and China are working on basalt fiber technology. The current annual production of basalt fiber BCF is approximately 3000 - 5000 tonnes (Basaltex 2008).

BFRP basalt bars

Composite basalt rebars - Basalt Fiber Reinforced Plastic (BFRP) are made of continuous basalt fiber, epoxy and polyester using pultrusion process. 80% by weight of fibers made of basalt rock and 20% filler in the form of an epoxy resin, and winding improving the adhesion properties (Bank 2006). Often resin matrix for basalt fiber is used as a polymeric vinyl ester. Vinyl ester resin is a combination of epoxy resin and unsaturated polyester resin (Karbhari 2007). The advantage of vinyl ester resins is that they have similar physical properties of the epoxy resins and preferred characteristics required for the processing of the polyester resin. Structural composites may be defined as a system of heterogeneous material consisting of two or more components on a macroscopic scale, which in combination, can provide new improved properties that are

superior to the properties of the components. Thus, fiber reinforced polymer composite consists of fibers of high strength and rigidity of the polymer matrix embedded with a relatively lower strength and stiffness.

Generally, the fiber is the main support element and the polymer matrix is designed to provide the desired direction of the composite to facilitate the transfer of the load on the fiber and to protect the fiber from environmental factors associated with elevated temperature and ambient humidity (Hollaway 1993).

In contrast to steel, which is an isotropic material, the basalt bars (basalt composite) are anisotropic material, which implies a difference in mechanical properties in the longitudinal and transverse directions. Anisotropy of basalt bars causes that the longitudinal properties are determined by the properties of the fiber, while the transverse and shear properties are governed by the properties of the resin. A mechanism of basalt bars destruction after rupture shown in Figure 1 (Urbański et al 2013).

Fig. 1. Failure mode of the rupture of basalt bar (Urbanski et al 2013)

In the table 1 there are presented some chosen comparison of mechanical and physical properties of basalt and steel bars.

Tab. 1. Comparison of basalt and steel rebar (Basaltex 2008, RockBar 2010).

Nr	**Characteristics**	**Steel**	**BFRP**	**Comments**
1	Density, t/m^3	7,8	1,80	4 times lighter
2	Weight 1m bar in kg Ø10 Ø12	0,617 0,888	0,150 0,221	4 times lighter
3	Ultimate strength, MPa			
	In tension In compression	485 485	1200 420	above 2 times more
4	Young's Modulus, GPa	200	52÷57	
5	Thermal conductivity, kcal/(h m °C)	38	0,35 ÷0,59	66÷111 times less
6	Linear thermal expansion , 10^{-6} m/mK,	12	9 ÷12	similar

7	Length of 1 ton bar, m Ø10 Ø12	 1 621 1 126	 5 848 4 330	4 times larger (transport !)
8	Elongation , %	14,5	2,2÷2,5	6 times less
9	Poisson ratio, ν	0,3	x	

Some significant advantages of reinforcing bars made on the basis of basalt BFRP compared to the conventional steel reinforcement are listed below, as follows.

- Much higher (more than twice) the tensile strength of the reinforcement steel or GFRP glass fiber, at the same diameter (Bank 2012).
- BFRP bars do not corrode and therefore the thickness of the concrete cover may be reduced. This allows the use of thinner concrete sections, resulting in material savings and cost.
- BFRP bars are 89% lighter than steel reinforcing bars; one ton of basalt rebar reinforcement replaces 9.6 tons of reinforcing steel. One person can easily lift 150 m roll of 10 mm BFRP. Thus, there is no need to transfer the BFRP any cranes, forklifts and trucks.
- The low weight of BFRP allows faster construction and installation of reinforcement.
- Very high strength allows to use rebars of a smaller diameter (in many cases, the diameter of the reinforcement can be reduced by applying the BFRP).
- BFRP bars have a similar thermal expansion coefficient as for concrete and steel, therefore the BFRP bars expand and shrink at similar rate compared to the concrete. (Karbhari 2007).
- BFRP bars are inherently resistant to corrosion, rust, alkalis and acids (Bin Wei *et al*. 2010). Basalt rebar is indifferent to the high pH of the concrete. BFRP bars do not rust, so the concrete cracks due to swelling corrosion products are completely eliminated. In contrast to the GFRP bars BFRP bars do not need a special coating to protect against exposure to high pH of concrete.
- Basalt fibers do not absorb and do not send moisture, like glass fibers do (Wu Z. *et al*. 2012). Moreover, the protruding fibers do not form any paths for water, which could penetrate and destroy the concrete.
- BFRP bars do not conduct electricity, which prevents electrolysis in construction exposed to the sea.
- BFRP bars are non-magnetic and they do not induce any magnetic field when exposed to electromagnetic or radio frequency energy (RF). Therefore, they can be used in rooms with magnetic resonance imaging (MRI) and close to radio frequency identification reader (RFID) (Sim *et al*. 2005).
- Basalt fiber can be used in a wide range of temperatures, -260/-200 ° C to about 650/800 ° C, with a melting point of 1450 ° C. Although the content of the resin bars BFRP, limiting temperature range is from - 70 ° C to +100 ° C, and are therefore useful in applications that require resistance to fire. BFRP bars also have low thermal conductivity, are non-flammable and do not emit any harmful

substances in fire (Subramanian *et al*. 1977).

Disadvantages of BFRP bars

- BFRP bars are brittle in nature (do not extend as far as the steel bars before breaking off), so are not suitable for use in areas prone to earthquakes.
- Bending of the cross-sections is unacceptable; BFRP bars are not weldable.
- BFRP bars are designed primarily for reinforcement in tension zone elements.
- Compared to steel bars, BFRP bars have a lower modulus of elasticity, which results in some increase in the deflection elements.
- Cross cutting, cutting bars are not recommended cause rapid dulling and steel shear fracture as a result of crushing steel. Hacksaw or abrasive wheels may be a good alternative. The best choice is cheap, circular saw blade with a diamond inexpensive. Massive cuts may be made cutter or a saw blade, gas, mineral however wet cutting is more favorable.
- Contrary to steel bars, BFRP bars are not ductile and have brittle destruction when the ultimate tensile strength is reached. Therefore, it is important to keep the permanent load below the limit strength of an adequate margin of safety.
- BFRP bars cost may be higher than steel bars. However, the Russian Federation has produced basalt bars relatively cheaper than steel bars.

The study of flexural concrete members reinforced with basalt bars

Research assumptions

Warsaw University of Technology began research on the effectiveness of the application of basalt bars for reinforcement of flexural concrete structures. The primary objective of the study was to identify the main mechanical properties of reinforcing bars made of BFRP basalt fiber, and to determine their suitability as reinforcement for the beams subjected to bending. Determination of mechanical properties of BFRP bars 8 mm in diameter consisted of determining the tensile strength, strains at fracture limit, the average modulus of elasticity, and determining the stress limits of bond between the reinforcing bars and the surrounding concrete.

The research program contained a bending test of three model beams with bottom flexural reinforcement made of 3 BFRP bars with a diameter of 8 mm and 3 reference beams with bottom steel reinforcement. The simply supported beams with a clear span 1000 mm have the cross-section $b \times h = 80 \times 140$. Top reinforcement in the regions of supports of all tested beams consisted of 2 steel bars with a diameter of 8 mm. The scheme of the tested beam and the location of benchmarks are shown in Figure 2. In all the beams the central bottom bar was protruded on both end sides (as presented in the Fig.2) to enable the measurement of the slip during the loading process.

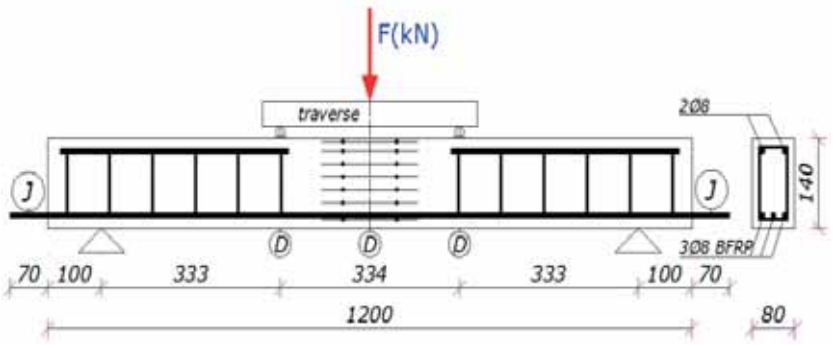

Fig. 2. Scheme of tested beam with bottom reinforcement (BFRP bars) and the location of benchmarks used to measure the concrete strains with an extensometer, J - slip measurement sensor, D - deflection measurement sensor, beam dimensions in mm

Reference beam reinforcement system (only reinforced with steel bars) was identical as in BFRP beams.

The testing procedures

Load was carried by the beam in the four point system made of steel traverse, respectively in the third and two thirds in the beam span.

In the first series the beams were subjected to load up to 10 kN, and then release to 5 kN. In the second cycle load was increased to 20 kN, and then released to 5 kN. In the last third cycle the beams were loaded until failure.

The Figure 3 shows the mode of failure of beam BFRP 3 in the final phase of the load equal to 45 kN. It is noteworthy that there was no rupture of the bottom reinforcement basalt bars. The destruction took place by shear in support zones of the BFRP beams and it had fragile nature. However, there was no sudden destruction due to continuous reinforcement preserved basalt. More detailed description of testing procedures are presented in the paper (Lapko and Urbanski 2013).

Fig. 3. The BFRP beam with flexural basalt reinforcement reaching critical load capacity equal to 45 kN (Lapko and Urbanski 2013)

Results of experimental tests

In the table 2 there are presented chosen results of BFRP beam deflections (vertical displacements in the mid span) with basalt reinforcement and the deflections of reference beams (SRC), depending on the load.

Tab. 2. Deflections of BFRP beams with flexural basalt bars and reference SRC beams with flexural steel reinforcement

Loading force, kN	Mid span beam deflections in mm					
	SRC1	SRC2	SRC3	BFRP1	BFRP2	BFRP3
5	0.97	1.81	1.61	3,21	3.04	3.10
10	1.71	2.23	2.06	4.35	4.11	4.23
20	2.45	3.30	3.14	7.33	6.99	7.21
30	3.48	4.43	4.24	12.63	11.58	12.01
40	x	x	x	-	19.54	19.03

In the case of SRC1 reference beam the measured deflections are different from the other two reference beams due to the different initial cycle of the load - strain.

In BFRP beams with basalt flexural bars, in contrast to the reference SRC beams the deformations of the reinforcement were linear, thus the increase of deflection in relation to the increase of loading force was practically constant, until the destruction of the element. Figure 4 shows for the tested beam BFRP3 and for comparison for the reference beam SRC3 the diagrams of the deflections versus beam loading forces.

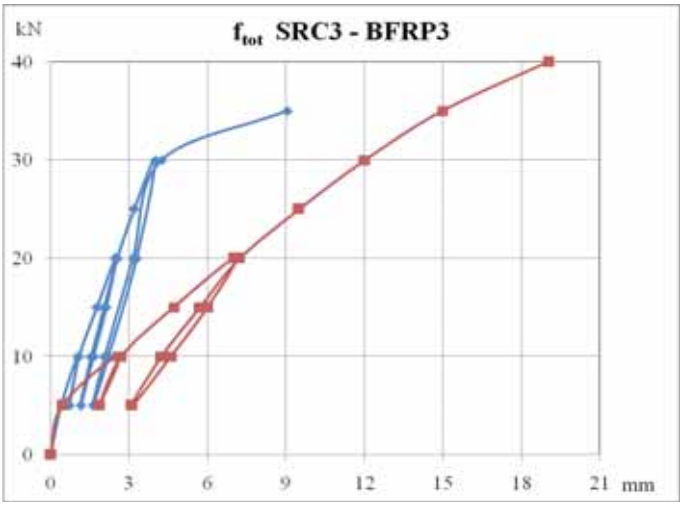

Fig. 4. The relationship: deflections versus loading force of the beam BFRP3 (squares) and the reference beam SRC3 (diamonds)

The increased deflections of beams with basalt reinforcement, compared to the reference beams with steel reinforcement can be clearly seen. The reason for the larger value of deflections of BFRP beams was its lower stiffness in relation to reference conventionally reinforced beams. Deflections in the mid span of beams with basaltic reinforcement for the loads 10, 20, 30 kN were equal to 4.2, 7.2, 12.1 mm, respectively, and were about 2.2, 2.4, 3.0 times larger compared to the reference beam deflections (with steel reinforcement).

In the table 3 there are presented chosen tests results of BFRP beams reinforced with 8 mm basalt bars (the maximum loading force Fu and moment MR, fl carried by the beam critical sections and their mean values $F_{u,m}$, $M_{R,fl,m}$, respectively) compared to the results of reference SRC beams with flexural steel reinforcement of the same diameter.

In this table there are also included maximal values of concrete strains ε_1 and ε_7, measured with the extensometer, respectively at 135 mm level from the bottom edge of the beams (in the compression zone) and at a distance of 20 mm (at the level of the flexural reinforcement), as shown in the Fig. 2.

Mean destructive force for reference beams with steel reinforcement was 37,6 kN, whereas for model beams with basalt reinforcement the mean destructive force was equal to 46,7 kN, it means that it was about 24% higher.

Tab. 3. Selected test results of model beams reinforced with basalt bars (BFRP) and reference beams reinforced with steel bars (SRC)

	Steel reinforced reference beams			Basalt reinforced beams		
	SRC1	SRC2	SRC3	BFRP1	BFRP2	BFRP3
F_u, kN	37.5	35.0	40.5	47.5	47.5	45.0
$F_{u,m}$, kN	37.6			46.7		
$M_{R,fl}$, kNm	6.3	5.8	6.8	7.9	7.9	7 .5
$M_{R,fl\,m}$, kNm	6.3			7.8		
ε_1, ‰	-1.58	-2.17	-2.02	-1.78	-2.60	-3.25
ε_7, ‰	4.18	5.69	6.52	9.43	13.60	7.76

Summary of research and conclusions

1. 1. It has been confirmed that, in contrast to the bilinear of the stress - strain relationship for the steel reinforcement, the basalt reinforcement has a linear relationship until the failure of the beam.
2. 2. It was noted that critical forces of tested beams reinforced with BFRP bars was much greater than the carrying capacity of beams with conventional reinforcement, which arose from the different degrees of mechanical reinforcement ratio in both types of beams.
3. Destruction of beams with BFRP reinforcement does not occur suddenly and was a result of transformation of the beam into a tie system.

4. Deflections of beams with BFRP reinforcement were significantly higher than the reference beam deflections, due to the much lower modulus of BFRP bars compared to steel bars.
5. Deformations of the basalt flexural reinforcement were considerably higher (average of 3 to 4 times) than the beams with steel reinforcement. However, in the final phase of the load above the difference decreased to 40% due to the phenomenon of plasticity in the beams of conventional steel reinforcement.
6. Due to the relatively lower elasticity modulus of basalt rods, compared to steel ones, both: the deflections and width of cracks can be a major factor in the designing the BFRP reinforced concrete beams.
7. From a practical point of view, in a properly designed BFRP reinforced beam, ultimate moment of capacity due to the tension reinforcement is much higher than the limit of capacity due to the crushing of the concrete.

References:

1. Bank Lawrence C. (2006), *Structural design with FRP materials, Composite for Construction*. John Willey and Sons Ltd.
2. Bank Lawrence C. (2012), *Progressive Failure of FRP Composites for Construction.* 13-15 June, CICE2012, Rome 2012, 10 pp.
3. Basaltex. (2008)*, The thread of stone.* Wevelgem, Belgium, http://www.basaltex.com
4. Basalt Rebar.(2010), *Technical info,* http://www.provenperformancechemical.com
5. Bin Wei, Hailin Cao, Shenhua Song. (2010),*Tensile behavior contrast of basalt and glass fibers after chemical treatment*. Materials and Design 31 (2010) pp. 4244–4250, http://dx.doi.org/10.3846/13923730.2011.6435343
6. CSA-S6-02. (2002), *Design and Construction of Building Components with Fibre-Reinforced Polymers*. CAN/CSA S806-02, Canadian Standards Association, Rexdale, Ontario, Canada, 177 pp.
7. Clarke J. L., Sheard P. (1998), *Designing durable FRP reinforced concrete structures*. Proceedings of the 1st International Conference on Durability of Fiber Reinforced Polymer (FRP), Composites for Construction (CDCC 1998), Shearbrooke, Quebec, Canada, pp. 13-24.
8. fib Bulletin 40. (2007), *FRP reinforcement in RC structures, technical report*. International Federation for Structural Concrete (fib). September 2007, 160p.
9. Hollaway L. (1993), *Polymer Composites for Civil and Structural Engineering*. first edition, Blackie Academic and Profession.
10. Hooks, J. and O'Connor, J. (2004), "*A Summary of Six Years Experience Using GFRP Composites for Bridge Decks*", Proceedings of the 21st International Bridge Conference. June 12-14, 2004, Pittsburgh, PA.
11. Karbhari V.M.(2007), *Durability of composites for civil structural applications*. Woodhead Publishing Ltd, Cambridge, England.

12. Koch, G.H., Brongers, M.P.H., Thompson, N.G., Virmani, Y.P., Payer, J.H. (2002), *Corrosion costs and preventive strategies in the United States*. Report no FHWA-RD-01-156,U.S. Department of Transportation, Federal Highway Administration, Washington D.C.
13. Lapko A., Urbanski M. (2013), *Problemy badania betonowych elementów zginanych zbrojonych prętami bazaltowymi*. [The problems of testing of concrete beams reinforced with basalt flexural bars], Materiały Budowlane, 2013/3. ISSN 0137-2971, (in Polish).
14. Sim, J., Park, Cheolwoo & Moon, Do Young. (2005), C*haracteristics of basalt fiber as a strengthening material for concrete structures.* Composites, Part B, 3**6(**6-7): pp.504-512.
15. Subramanian, R.V., Tang, T. J. Y. and Austin, H. F.(1997), *Reinforcement of Polymers By Basalt Fibers.* SAMPE Quarterly, 1977: p. 1-10.
16. Tomosawa F., Nakatsuji T. (1997), *Evaluation of ACM reinforcement durability by exposure tests*. Non- Metallic (FRP) Reinforcement for Concrete Structures, Proceedings of 3rd International Symposium, Sapporo 1997, Vol.2, pp. 75-82.
17. Van de Velde K., Kiekens P., Van Langenhove L., Cater S. (2002), *Basalt fibers as reinforcement for composites, Editorial.* International Composites News, March 2002.
18. Urbanski M., Lapko A., Garbacz A. (2013), *Investigation on Concrete Beams Reinforced with Basalt Rebars as an Effective Alternative of Conventional R/C Structures.* Procedia Engineering, Elsevier, Science Direct, Volume 57, May 2013, 1183-1191pp.
19. Wu Zhishen, Wang Xin, Wu Gang. (2012), *Advancement of Structural Safety and Sustainability with Basalt Fiber Reinforced Polymers*, 13-15 June, CICE2012, Rome 2012, 29 pp.

NEW APPROACH IN CONSTRUCTION OF THE WOOD-FRAMED RESIDENTIAL BUILDINGS

Mikołaj Malesza, Czesław Miedziałowski, Jarosław Malesza

Bialystok University of Technology, Faculty of Civil and Environmental Engineering
Wiejska St. 45E, 15-351 Bialystok, Poland
email: m.malesza@wp.pl

Summary:
Work presents actual directions in development of the wood-framed construction and examples of construction as well as the methods of industrial production of elements in practice.
Light wood-framed buildings constitutes significant percentage of constructed residential single family and multi families as well; as small commercial buildings realized in many countries. At about 47% building materials is based on wood and wood derivatives, in advanced technologically countries, while for their production is used 4% of total value of energy used in building industries. Buildings of this type are constructed in the form of large panels elements (walls, floors and roofs) or directly constructed on the site using previously made individual elements like studs, beams, lintels, bottom plates, rafters, top plates. Nowadays more buildings are constructed using large panel construction achieving better quality of industrially made elements and shorter time of assembling of building.
Problems of formation, static and dynamic analysis and construction of the light wood-framed varying structures are presented in the work. Due to specifics of these structures in the phase of construction and exploitation all problems shall be considered together. Special attention shall be paid to deformation of light wood-framed structure and their sensibility on environmental conditions, flammability. Adequate selection of analytical models in static analysis and models reflecting thermal and moisture behavior of timber structures are to considered at the stage of design. Quality of assembling at the site comparably to the quality of elements obtained from factory production shall be always considered because of high level of prefabrication.

Keywords: wood-framed structure, 3D behavior, modular structure, transport and lifting, analytical models

Introduction

Light wood-framed buildings constitutes significant percentage of constructed residential single family and multi families as well; as small commercial buildings realized in many countries. Economic transformation in Poland forced energy saving also in building industry. Search of new solution brought to conclusion, that the light wood-framed construction is one of the highest energy saving and ecological type of buildings. These kinds of buildings are commonly constructed in USA, Canada, Scandinavian countries, as well as in Australia and Japan (Asiz et al. 2005), (Breyer 1993), (Miedzialowski, Malesza 2006). Within last three decades industry and construction of these buildings is also developed in Germany and Austria (Schulze 1996), (DIN 1988). Lumber used in the wood-framed structure is a renewed material in case if management of forest resources is planned and provided according to economic roles, and in addition preserving pro-ecological activity. In advanced technologically countries, at about 47% building materials is based on wood and wood

derivatives, while for their production is used 4 % of total value of energy used in building industries. Hence, selection of wood as a building and structural materials is well grounded. Low own weight in the wood-framed construction in the range of 0,30 ÷ 1,00 kN/m^2 and its profitable proportion comparing to the live load increases effect of energy saving due to lower energy consumption within realization and assembling of building.

Light wood-framed buildings are constructed in the form of large panels elements (walls, floors and roofs) or directly constructed on the site using previously made individual elements like studs, beams, lintels, bottom plates, rafters, top plates. Actually more buildings are constructed using large panel construction achieving better quality of industrially made elements and shorter time of assembling of building. Structurally, the most sensitive elements provided on the site are all types of connections (Mohammad 2006).

Work presents actual directions of development of the wood-framed construction and examples of construction as well as the methods of industrial production of elements in practice.

Varying building construction on the base of timber

Timber is one of the oldest building material used in varying structures. Widely known buildings with timber bar (vertical) or timber log (horizontal) construction - figure 1a, solid timber posts and beams constructions with masonry bricks or hollow-blocks infill (Prussia masonry) - figure 1b, studs and beams construction with diagonal bracings – figure 1c, Wood-framed with sheathing – figure 1d.

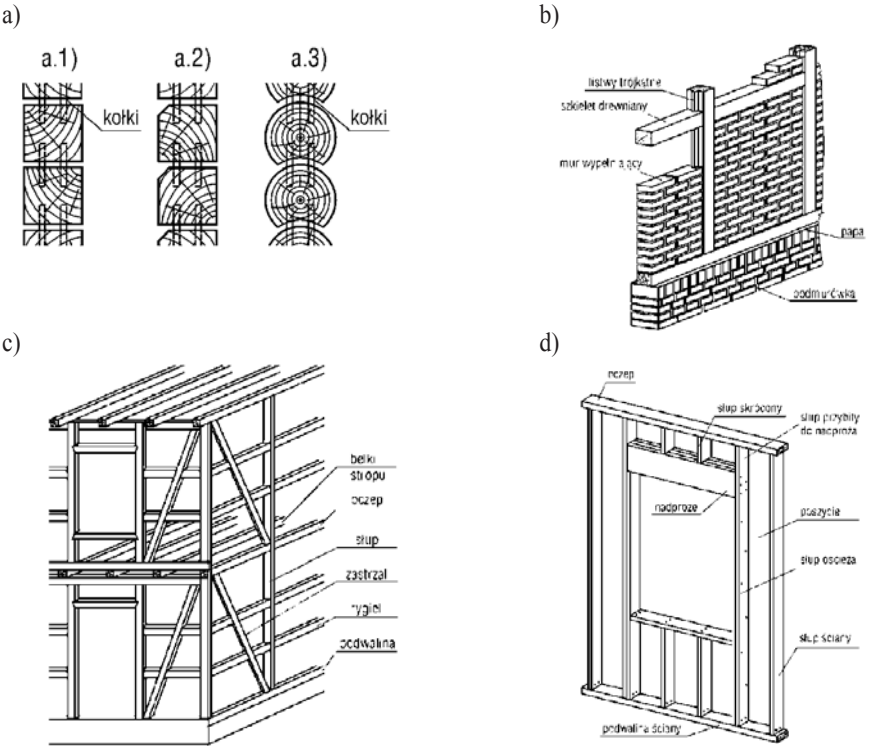

Fig. 1. Varying timber buildings construction [3].

Actually timber buildings are constructed in the wood-framed with sheathing technology, being the most economic and elastic in formation and technology. Low own weight facilitates their full prefabrication, hence industrial production of wall, floor and roof panels, decreasing time of elements production and whole building assembling. Assortment and products line of large wood-framed with sheathing elements: wall, floors and roof diaphragms raises quality of production, decreasing time of assembling of the buildings. Products line and varying light wood-framed elements do not need labor - consuming processes and intricate moulds or shuttering indispensable in reinforced concrete framed or large panel structures.

Different structure-technological systems of timber based construction were developed abroad. These systems can be divided into three groups:

- system of stud and beams as a separately constructed elements (assembler on the site studs, joists, girders, rafters and boards of sheathings),
- system of precast construction using plane elements (wall, floor and roof slabs) – slab-type of precasts,
- system of 3D spatial elements – modular construction.

Plane elements were industrially produced in Poland under name of Stolbud, Namysłów, Sępólno, Mikołajki, and lately were organized precast unit production plants: PRIBO in Suwałki, Danwood and UNIBEP in Bielsk Podlaski. At the beginning, systems of the wood-framed construction were mainly transferring without any objection examples from USA and Canada. In this way in dependence to the sections of elements and details of construction it is recognized an American or Canadian system of construction. It is very well known troubles in Poland with these construction due to their low stiffness and thermal-moisture problems.

Foundations of the light wood-framed buildings are similiar to those traditionally constructed, but there are to be considered the following factors:

- low dead load of the structure requires adequate anchorage in the foundations,
- wood sensitivity on moisture conditions, possibility of biological corrosion requires careful design of moisture protecting isolation, adequately high level of foundation setting and possibility of drying wood (specifically girder beams and ends of the floor joists),
- the thermal insulation of foundation should be carefully designer and constructed.

Three-dimensional behavior of buildings

In building of the light wood-framed, structure spatial 3D stiffness remains the main requirements in the process of the bearing structure design (Schmidt et al. 2000), (BS 1988), (BS 1991). The main principle in securing of the 3D stiffness in the framed or wall structures remains providing of the shear wall. This walls with big lateral stiffness, which are transferring all horizontal forces and loadings acting to building. Remaining structural elements in building like columns bearing the girders or bidding rafter (purlins) can be dimensioned for vertical load only. Lateral load is acting from different directions, what requires allocation of shear walls longitudinally and transversally in the building. These longitudinal and transverse stiffening walls create in joint and connections spatial sets of elements being stiff enough in both directions.

Floors cooperating with walls are acting as the horizontal diaphragms, securing uniform share in transfer ring the lateral load. This share is adequate to wall stiffness under bending in the wall plane. Check of the 3D building stiffness remains import ant part of static analysis of structure. Correctness of this computations depends on fulfilling of adequate structural requirements, specifically, connections continuity in vertical joint of walls and floors and walls in horizontal joints. Horizontally, ties along the walls are securing of spatial building stiffness and in case of girders, continuity of transferring load shall be secured on both sides of the bearing beam where wall diaphragms are to be adequately joined to the foundations or lower structure. Significant part in spatial stiffness of the light wood-framed building takes fire separating walls constructed as a masonry structure specifically in case of row building construction.

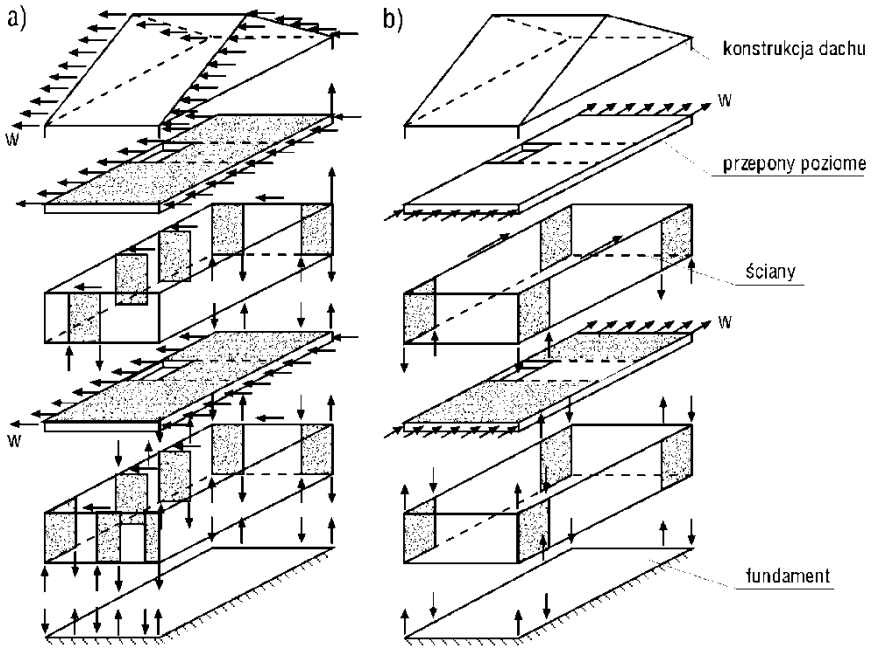

Fig.2. Redistribution of lateral loads to structural elements of building (Schulze et al. 1996), (Kuttinger et al. 1992): a) wind load to the longitudinal wall, b) wind load to the transversal wall.

Diagram of wind loading to building and arrangement of the stiffening walls as well as the principles of load distribution on individual walls is presented in figure 2.

Methods of analysis and design of modular structures are based on analysis of design of timber diaphragms with sheathing including in the process of design selected aspects of transportation, lifting and assembling. Construction of individual module in the range of vertical and horizontal loadings is similar to the assumption taken in the diaphragm of light wood-framed structure analysis according to figure 3. Specific approach is required

in case of lateral loading and stability problem, hence combination EQU in EC0 and PN-EN 1990 shall be included in analysis. In case of higher buildings (multi storey buildings) and adequately not high value of vertical loadings in adequate configuration and geometry of building, the tie-up module forces can arise and effect of anchoring shall be necessary. Proposals of assembling and stabilization of structure with securing of 3D stiffness of the structure is presented in (Schmidt et al. 2000).

Buildings in traditional construction

The first buildings in technology wood-framed Baloon Framing were designed and constructed at the beginning of XIX centaury. In this type of structure the external walls are continuously constructed from foundation bottom plate up to the horizontal top plate where roof rafters are supporting and the studs are not divided into the first (ground) and the second floor. In this solution consumption of lumber is rather low due to elimination of top plate in the wall of the first floor and bottom plate of the second floor wall. This solution shortens the time of assembling and makes lighter in result of use studs with smaller dimensions of the cross-sections than in the other types of construction. Diagram of building constructed in the Baloon Framing technology is presented in figure 3a.

Buiding in technology of panel construction

New solution developed in the wood-framed technology construction leads to industrial production of building elements. Platform Framing technology, where in sequence walls of the ground floor, floors over the ground floor and walls of the second floor and finally roof are installed, replaced the Baloon Framing technology at the beginning of XX centaury. This system of construction allows for higher degree of prefabrication and panels are built in industrial manner in factories-plants.

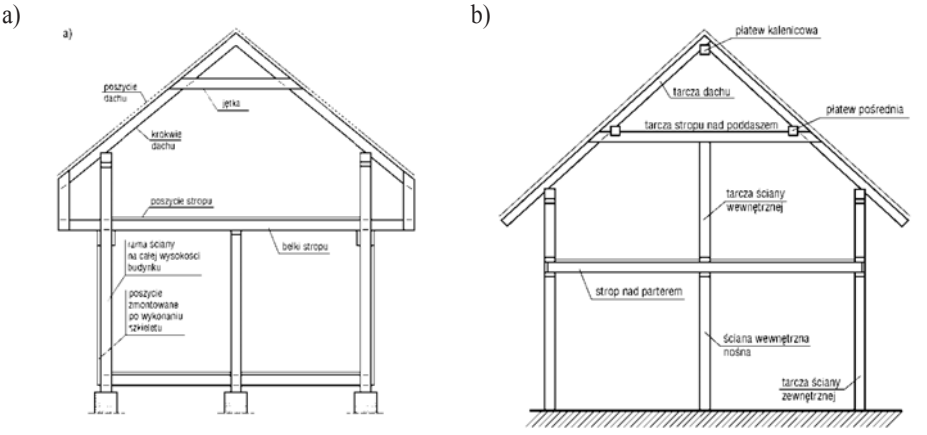

Fig.3. Diagram of buildings constructed in: a) Baloon Framing technology, b) platform technology.

As far as the dimensions are concerned, there are buildings constructed of large panels or small panels (figure 4).

a) b)

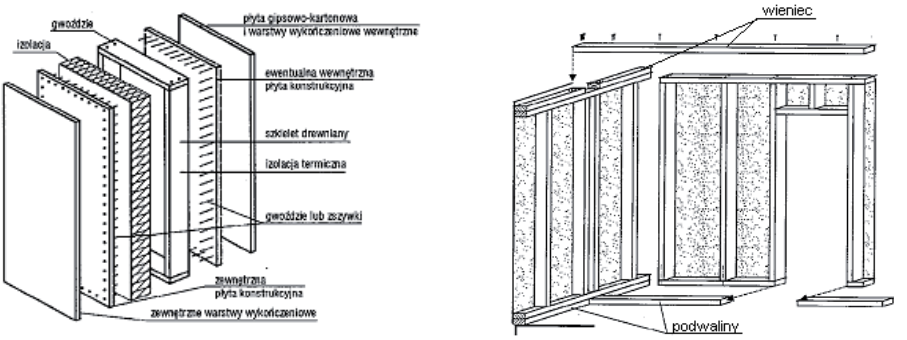

Fig. 4. Wall diaphragms (panel) construction in plate buildings construction:
a) structure of the single unit wall plate, b) joining of the neighboring walls using timber tie.

In the process of the light wood-framed buildings design, the long-term behavior of structure like: rheological factors, degradation of material parameters and influence of temperature and moisture shall be taken into account.

Plants processing elements used in the wood-framed structure is based on the stream method of production, stationary method or combined methods of panel construction. In the stream method, wall, floor or roof element moves to succeding workplace where they are completed. At the sequent workplaces elements are completed, obtaining final form of product. At the commencement of the process, elements are in horizontal position where studs and top and bottom plates are positioned giving the framing of diaphragms, and then the panel is positioned vertically for final completion and finishing phase of wall or floor.

Part of line with horizontally positioned elements is presented in figure 5a, while vertical stand is shown in figure 5b.

a) b)

Fig.5. Stands of stream line production: a) horizontal, b) vertical.

In the stationar method, the composition of diaphragm is conducted on one work-place, where all assembling operations are done sequently. These stands are horizontally positioned or they are inclined (tilt stand).

Industrially composed diaphragms are transported to the site and directly from the trucks they are assembler as it is show in figure 6.

a) b)

Fig. 6. Building assembling using large panel directly from the transportation truck.

Modular types of buildings

Modular buildings are prefabricated buildings consisting of so-called modules, the six sided boxes (cuboidal) constructed in a remote facilities, then transported to their intended site of assembling. The modules are set on the building's foundation and then joined together to make a residential, hotels, school, office or commercial building. Similar way of construction using three-dimensional modular reinforced concrete precast elements was used in Poland, but it was limited to the WC units and partly kitchen in multi storey large panel construction of block of flats. Low own weight of the 3D elements in use of the wood-framed structure allow to construct also multi storey residential buildings. The module are placed side-by-side, end-to-end or stacked up to four or five stories in height assembling various configuration and style in designed building layout.

Modular buildings should conform to all building codes for their expected use. Residential modular buildings can be built on the steel frame or in the technology of wood-framed with sheathing construction (CSA 1992), (NAHB 2002). The modular buildings may be used for long-term, temporary or permanent facilities in construction of different use. Modular components are typically constructed on assembly lines, and then completed modular segment is transported and assembled on the site, hence they are essentially indistinguishable from typical site construction structures. Materials used in modular homes are the same as site constructed homes. Wood-frame with sheathing floors, walls and roof are typical conforming to typical light wood-framed constructions. Usually modular structure is designed to be stronger than traditionally constructed building even when large panel construction. Nails and staples joints are usually replaced by screws in addition glued to help modules maintain their structural integrity while they are transported on trucks to the construction site. Prediction of building strength is rather difficult since the modules need to endure transportation stresses and assembling while handling by crane all segment, where the traditionally constructed houses never experience these stressing (Asiz et al. 2005). For this reason modular houses usually

contain higher use of lumber. On the opposite site it is obtained final result in the form of ready for finishing works building in shorter time than traditional or even large panel construction based on the wood-framed structure with sheathing.

Modules assembled wall-to-wall or one on the other in four to seven stories construction create buildings of varying configuration, geometry and architecture style. Figure 7 presents completion of module segment and assembling phase. Figure 7c presents assembling of traditional building structure composed of large dimension panel (Miedziałowski, Malesza 2006).

Design and method of analysis in case of modular structure is based on analysis of wood-framed diaphragms including some aspects of analysis concerning the handling, transportation and assembling as well as the dynamic aspects of analysis.

Strengthening of all structure and increase of its stiffness is required due to additional load resulting from lifting of module segment and process of transportation to the site of construction very often several hundred kilometres. Final product in the form of module building is ready for final finishing works in any possible time, even comparing to large panel technology, where industrially constructed in factory panels also reduce the works at the site. Modular segments consist light wood-framed horizontal, inclined as the roof or vertical diaphragms, hence they constructions are similar like individual panels. These diaphragm-panels are assembled in segment-building not at the construction site, but in the plant where they were provided, what is shown in figure 7.

Transportation phase depends on the distance from plant (CSA 1992), for example:

- transport by trucks to the other transportation equipment,
- railway transport or transport shipping,
- truck transport to the assembling site.

a)

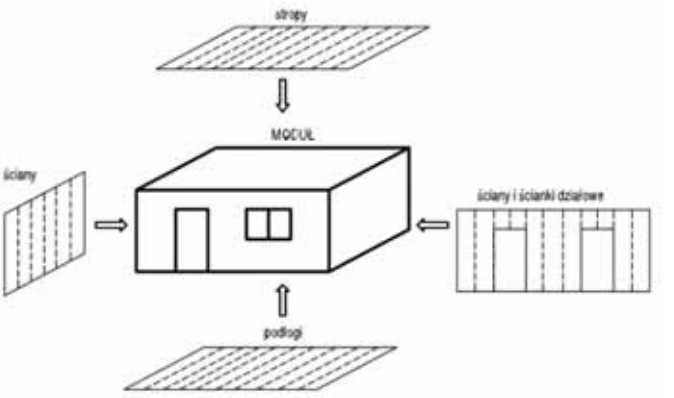

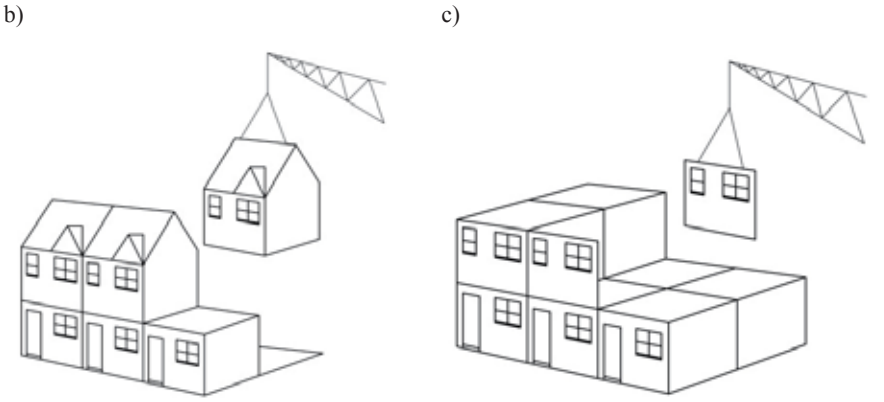

Fig.7. Completion and assembling of modular structure: a) completion of module, b) assembling of modular building, c) assembling of large panel building.

At each stage repeatedly occurs very sensitive lifting and handling of module by crane, and concurrent forces are acting on the 3D element. These forces and loadings are not acting in normal exploitation. There are for instance centrifugal forces during transport by the truck along the road horizontal curve (CSA 1992), or action to the module in result of impact or tilt during the see transport (NAHB 2002).

Prediction and evaluation of load bearing capacity of modular structure is complicated because structural module elements are subjected to stressing not only in exploitation but also within production, transportation and using crane. Traditional structures assembler at the site are not subjected these kinds of stressing under 3D form of module and acting varying forces.

Numerical model of the wood-framed with sheathing structure and selected results of experimental tests are presented in (Miedziałowski, Malesza 2006) to explain the behaviour of composite wood framed three-dimensional wall and floor panel. Wall and floor diaphragms as the three-dimensional composite structure are modelled applying plane shell elements representing framing and sheathing and beam element describing the fasteners. Experimental tests were conducted on typically disposed the wood-framed wall and floor diaphragms in residential housing in Poland. Associated tests of materials and connections and their results are also included in the paper. Nonlinear behaviour of fastener is examined in the numerical model. Results obtained from model and experiments conducted on wood framed panel construction are coincident.

Design and method of analysis in the range of exploitation, transport and assembling including lifting are completely different in the dynamic aspect of analysis. Analytical model of 3D structure is more complicated and cannot be conducted for individual diaphragms. Assembling of module is in stationary factories. Sub-assembling of individual module elements – ceiling, walls, floor is on the special automated production lines, and then they are completed and assembled in three-dimensional structure. Individual elements are assembled in stationary or stream system. Usually ceilings and floor diaphragms are sub-assembled on stationary stands while walls are sub-assembled in the stream system. Figure 8 presents sub-

assembling of module composing elements and their completion.

a)

b)

c)

Fig. 8. Stages of module assembling: a) sub-assembling of floor elements, production of wall panels, c) assembling of module structure (UNIBEP)

Phase of transportation is very often compared to repeated dynamic action, however the values of these action are not so high. Except typical transport conditions, during transportation; semi-trailer undergoes deformation, slide down of module from trailer or traffic collision causing additional loadings. Experience from varying countries (CSA 1992), ((UNIBEP) shows, that structure of module not always undergoes damages, sometime defects and failure occur in the finishing inside. Correct structure and construction play significant role in module behavior. The longest distance of transport is 400-600 km. The route of transport and Road existing engineering infrastructures are limiting the dimensions of module. Usually 485 cm wide and 410 cm height are limiting dimensions of module in case of road transportation due to keep clearance gauge of engineering structure existing along the route. The length is limited to 1830-1980cm. Figure 9 presents stage of trailer loading and unloading and readiness to transport, and figure 8 presents scheme of static behavior of segment in transportation.

a) b)

Fig.9. Loading (a) and transport of modules (b)

Modules at the site are assembled „one on the other", creating form of building. In this phase are used the same lifting sling like in phase of transport. Usually assembling from the wheels – directly from the trailer is used. At the site module require cranes dependely on number of floors and range of lifting.

Bolts along the ceiling and floor joists are used for connection, and twin-walls are linked with fasteners (BS 1988). Assembled and connected according to the arrangement modules are ready for finishing works. Modules with their installations and partly ferniture make 80-90% of whole work to be conducted with building. Module assembling is shown in figure 10.

Single module unit weight is equal to 15 – 16 tons (150 kN). Module should be designer as to fulfill ULS and SLS (CSA 1992), (PN-EN 2010) as the basic in design of according to limit state requirements. In all stages and in the phase of realization with lifting and transportation the stressing appearing within the exploitation phase is exceeding. Some parts of structure requires higher use of material then in traditional structure. In referencing sources are not described parts of structure overstressed and defected under overloading in the range of excessive deformations under transport and lifting. Hence, advanced 3D analysis of module structure and its loading or overloading is required and highly recommended. However, it shall be taken into account fact, that sometime not significant defects and discontinuity of connections may lead to unfavorable effects in exploitation of whole building. Also dynamic analysis of vibration influence on structure remains the significant element in analysis, especially when we consider the height of multi-storey modular building (NAHB 2002).

a) b)

Fig.10. System of lifting of module: a) System of lifting slings in the chase of lifting, b) assembling of modular building

Summary

Problems of formation, static and dynamic analysis and construction of the light wood-framed varying structures are presented in the work. Due to specifics of these structures in the phase of construction and exploitation all problems shall be considered together. Special attention shall be paid to deformation of light wood-framed structure and their sensibility on environmental conditions, flammability. Adequate selection of analytical models in static analysis and models reflecting thermal and moisture behavior of timber structures are to considered at the stage of design. Quality of assembling at the site comparably to the quality of elements obtained from factory production shall be always considered because of high level of prefabrication.

Design analysis are conducted according to the following models: beam on elastic supports, 2D diaphragm (plate) elastically supported and 3D - three dimensional discrete model. The idea of modelling is presented in figure 11.

Spatial 3D numeric model of modular building based on the light wood-framed with sheathing structure is the only tool, leading to reliable analysis in the phase of lifting and specifically unfavorable phase of transportation of modular structure. Experimental tests of connections and properties of materials are to be conducted in the investigations. This model should be built on the basis of experimental and numerical analysis of diaphragms and their stiffness characteristics. The advanced analytical model with implementation of super-elements can be built, what may facilitate the analytical solution of problem (Asiz et al. 2005), (Schmidt et al. 2000), (NAHB 2002).

a)

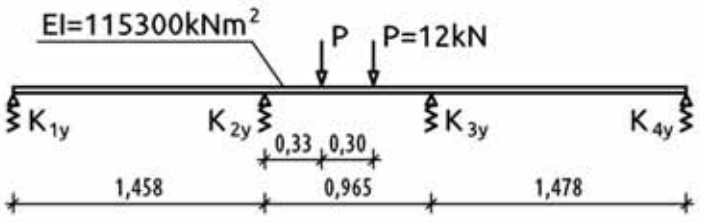

b)

c)

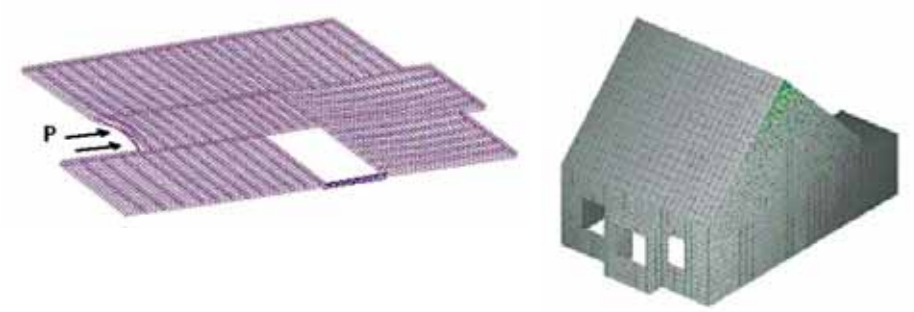

Fig.11. Analytical models used in design of the light wood-framed structures: a) beam model, b) diaphragm 2D (plate) model, c) 3D model

References:

1. Asiz, A., Iranpour, M. and Smith, I. (2005), *Analysis Of Structural Stresses During Handling And Transportation Of Factory-built Housing Construction.* Proceedings of 33rd Annual Conference of the Canadian Society for Civil Engineers, Vol. 2, CD-ROM, 8 pp.
2. Breyer D. E. (1993), *Design of Wood Structures*, Mc Graw-Hill, Inc. Third Edition.
3. Küttinger, G., u.a. (Bearbeiter). (1992): Holzrahmenbau. Teil I. 2. Auflage. Herausgeber: Bund Deutscher Zimmermeister. Karlsruhe
4. Miedziałowski Cz., Malesza M. (2006), *Budynki o szkielecie drewnianym z poszyciem*. Podstawy mechaniki konstrukcji oraz zagadnienia konstruowania i realizacji, PAN, Warszawa-Białystok.
5. Mohammad, M. (2006), *Connection Systems For Prefabricated Wall Panels*, *Final Report*, No.FCC25, Natural Resources Canada, Ottawa, ON.
6. Schmidt, R. J., Goodman, J. R., Richins, W. D., Pandey, A. K. and Larson, T. K. (2000), *Improved Design Of Manufactured Homes For Hazardous Winds*, Proceedings of World Conference on Timber Engineering, 31 July - 3 Aug, Whistler Resort, BC.
7. Schulze H. (1996), *Holzbau, Wande-Decken-Dacher*, B. G. Teubner, Stuttgart.
8. BS 5268, Section 6.1, (1988), *Structural Use of Timber*. Part 6, Code of practice for Timber Frame, walls. Dwellings not exceeding three storeys.
9. BS 5268, Part 2, (1991), *Structural Use of Timber*. Code of practice for permissible stress, design, materials and workmanship.
10. CSA - Canadian Standard Association. (1992), *Manufactured Housing/Mobile Homes*, Standard CAN/CSA Z240, CSA, Ottawa, ON.
11. DIN 1052 T. 1-3, (1988), *Holzbauwerke, Berechnung und Ausfurung*.
12. PN-EN 1995.1-1, (2010), *Design of Timber Structures*, EC 5, Part 1-1.
13. NAHB – National Association of Home Builders Research Center. (2002), *Advanced Panelized Construction - Year One Progress Report*, prepared for Partnership for Advancing Technology in Housing (PATH), Washington D.C., U.S.
14. http://unibep.pl UNIBEP S.A. Bielsk Podlaski

EXPERIMENTAL ANALYSIS OF HIGH PERFORMANCE FIBRE REINFORCED CONCRETE PLATES

Piotr Smarzewski

Lublin University of Technology, Faculty of Civil Engineering and Architecture,
Department of Civil Engineering, Nadbystrzycka St. 40, 20-618 Lublin, Poland
e-mail: p.smarzewski@pollub.pl

Summary:
The article presents the experimental results of bent plates made of high performance concrete and high performance fibre concrete. The test was performed for plate elements with reinforcement mesh of Φ8 mm rods. The main aim of the test was to define the influence of adding polypropylene and steel fibres on carrying capacity and deformability of fibre reinforced concrete plates. All plates had identical reinforcements and differed by the percentage of fibres. The research was performed into Zwick/Roell hydraulic press, with the load range from 0 to 3000 kN. During the tests, the rate of displacement increment was controlled. The load and deflection were registered. The analysis of the results was made on the basis of crack development, damage images and load – deflection relations. Experimental tests proved the usefulness of steel and polypropylene fibres in order to improve the ultimate tensile strength of high performance concrete in plates. Adding fibres changes the characteristics of high strength concrete – from a brittle, into elastic-plastic material. The analysis of the results proves that cooperation between the concrete matrix and fibres is very effective. With the increase of the number of fibres increased concrete tensile strength and maximum deflection of plates.

Keywords: reinforced concrete elements, high performance fibre concrete, plates

Introduction

The development of concrete technology and the research on its properties together with the idea to build safe and durable structures contributed to the development of numerous new building materials. In various cases they are the effect of improving previous solutions based on innovations in concrete properties. Such was the case of fibre concrete, in which the key element is to improve concrete tensile parameters by adding steel and synthetic fibres. More information concerning composite properties with fibre reinforcement and the directions of their improvement can be found in the works (Banthia, Gupta 2004, Brandt 1996, 2008, 2009, Chiaia et al. 2009, Domański, Czkwianianc 2006, Foster 2009, Glinicki et al. 2002, Glinicki 2008, 2010, Jamroży 2000, Prisco et al. 2009, Walraven 2009).

At the same time, searched for methods to improve concrete strength and durable through its modifications in dosing ingredients and concrete curing. The problems concerning the design and production of high performance concrete were described in papers (Aïtcin 1998, 2003) and (Kaszyńska 2002).

Experimental tests on plates made of reinforced high performance concrete with addition of steel and polypropylene fibres have been the subject of few works so far (Fairbaim et al. 2012).

Experimental investigations

Analysis of aggregate grading curve

Marking the gradations of aggregate was conducted in accordance with the norm EN 933-1:1997 for coarse aggregate and sand.

Prior to grade analysis the coarse aggregate was dried. The test samples weighting 3200 g was divided into 2 equal samples, 1600 g each. The test sieves meshes 8 mm, 4 mm, 2 mm, 1 mm, 0.5 mm, 0.25 mm, 0.125 mm, which were graded from the smallest to the largest was conducted. As a result of hand sieving, the agregate was segregated into fractions. The residue of each fraction was weighted. In order to examine quartz sand, an sample of 800 g was prepared. A sieves with meshes sized 2 mm, 1 mm, 0.5 mm, 0.25 mm, 0.125 mm were used. In order to prepare the plates, the aggregate was mixed in the following proportions: 66% of granodiorite aggregate and 34% of quartz sand, so that the contents of each fraction was within the range curves of the norm. Figure 1 presents the grading curves of aggregate within the norm curves.

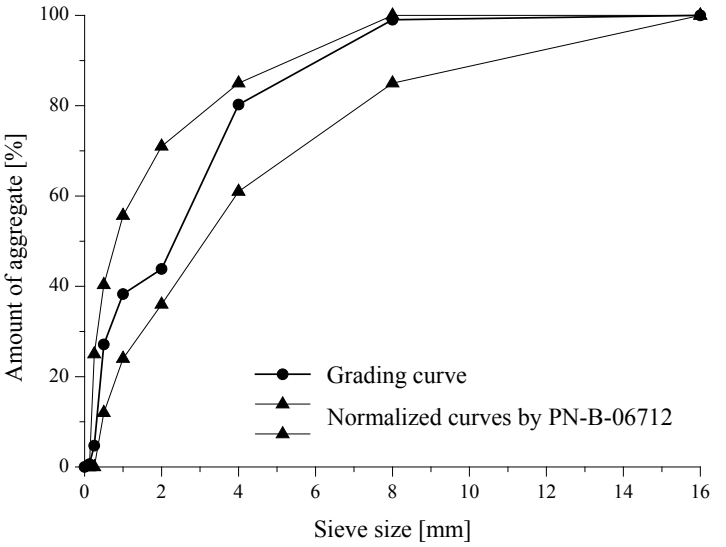

Fig. 1. Grading curves of aggregate

Properties of reinforcement steel

The test of a steel reinforcement bar, 8 mm in diameter and 300 mm of the length, was conducted with a material test system MTS 810 with the load range 0-100 kN, Fig. 2.

Fig. 2. MTS 810 material test system and steel bar during the axial tensile test

The bar was fixed with special holding jaws which prevented potential slide and incorrect measures. During the test current force, bar elongation and transverse displacement at rupture were measured. The graph load-axial displacement steel bar was shown in Fig. 3.

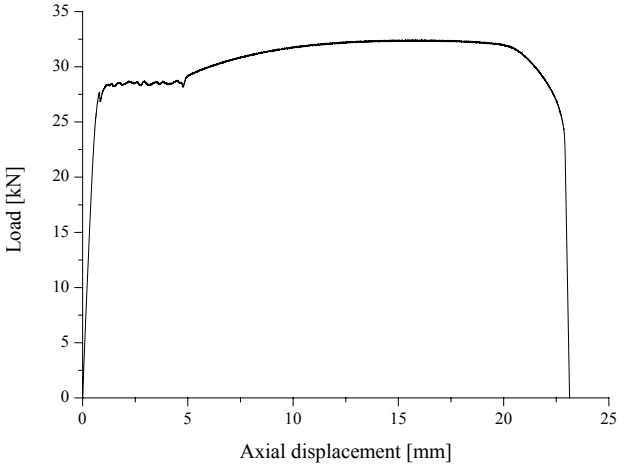

Fig. 3. Load-axial displacement relation for the 8 mm reinforcement bar

On the basis of these results yield stress f_{yk} = 567 MPa, ultimate tensile strength f_{tk} = 644 MPa and modulus of elasticity E_s = 206 GPa were calculated.

Properties of concrete and preparation of HPFRC plates

Table 1 presents composition of concrete mixtures for three reinforced concrete plates.

Table 1. Composition for concrete mixtures

Component		Mixture 1 [kg/m^3]	Mixture 2 [kg/m^3]	Mixture 3 [kg/m^3]
Cement CEM I 52.5R	C	596	596	596
Granodiorite 2-8 mm	K	990	990	990
Quartz sand	P	500	500	500
Condensed microsilica	M	59.6	59.6	59.6
Superplasticiser	S	20	20	20
Water	W	196	196	196
Steel fibres	W_{sf}	–	39	78
Polypropylene fibres	W_{pf}	–	0.5	0.5

The prepared concrete mixes are characterised by the following coefficients: water and the components of the bond $W/(C+M)=0.212$, aggregate to cement and condensed microsilica quantity $K+P/(C+M)=2.3$; $S\rho_s/(C+M+K+P)=1.1\%$, $\rho_s=1150$ kg/m^3, percentge of steel fibres for mixture 2 (M2), $V_{sf}=W_{sf}/\rho_{sf}=0.5\%$, $\rho_{sf}=7800$ kg/m^3, percentge of steel fibres for mixture 3 (M3), $V_{sf}=1\%$, percentge of polypropylene fibres for M2 and M3 $V_{pf}=W_{pf}/\rho_{pf}=0.056\%$, $\rho_{pf}=900$ kg/m^3.

Concrete samples were prepared according to the mixture 1 in the forms that meet the requirements of the standards. Compression tests were conducted on 150 mm cube samples. Bending tensile strength tests were performed on beam elements sized 600 x 150 x 150 mm. Concrete compression and tension strengths for M1 were f_c = 99.4 MPa and $f_{ct,fl}$ = 8.2 MPa respectively. Figure 4 presents load – displacement relation for three bent beams.

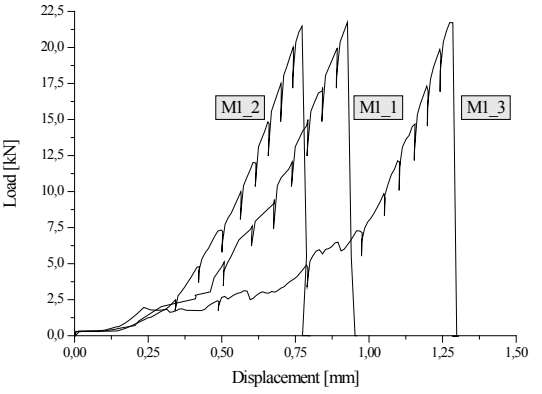

Fig. 4. Load – displacement relation for beam samples

The moulds of reinforced concrete plates were made of plywood. Reinforcement was prepared in a form of grids made of rods of 8 mm in diameter. The moulds were covered with antiadhesive liquid before concreting. After placing the mixtures in moulds, its were condenced on the vibratory table and the members were covered and cured for 7 days in damp conditions.

Investigations of HPFRC plates

The investigations of high performance fibre reinforced concrete (HPFRC) plates were carried into Zwick/Roell hydraulic press, with the load range from 0 to 3000 kN. During the tests, the rate of displacement increment was controlled and the load and deflection were registered.

The main aim of the test was to define the influence of adding polypropylene and steel fibres on carrying capacity and deformability of fibre reinforced concrete plates. All plates had identical reinforcements with grids and differed by the percentage of fibres.

Reinforced concrete plates were locally loaded with a centrally located steel plate, according to the scheme presented in Fig. 4.

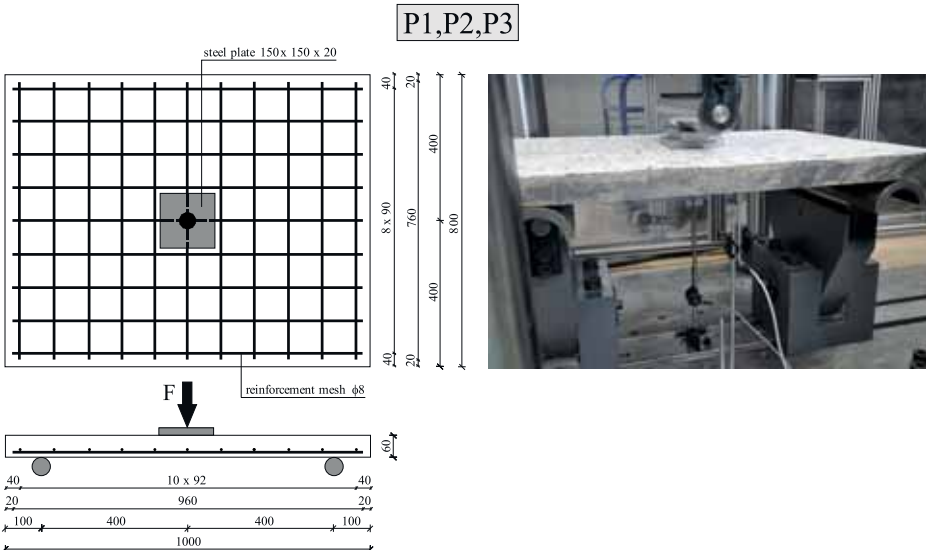

Fig. 4. Scheme of load and support plates

The plates were loaded at constant increment of press piston displacement. During the test, piston displacement and current load were measured.

Analysis of HPFRC plates experimental results

The images of failure development were made on the basis of detailed photographic documentation. Cracks propagations and damage images were presented in Fig. 5. The first cracks appeared at midspan of all elements. In case of plate P2 and P3 the cracks

appeared after the time that was twice as long as in plate P1. With the increase of load, the cracks were perpendicular to the width of the plate. The number and width of cracks were correlated with the percentage of fibres. At further stages of loading, was observed spalling of the concrete at upper surface of the plates.

(a)

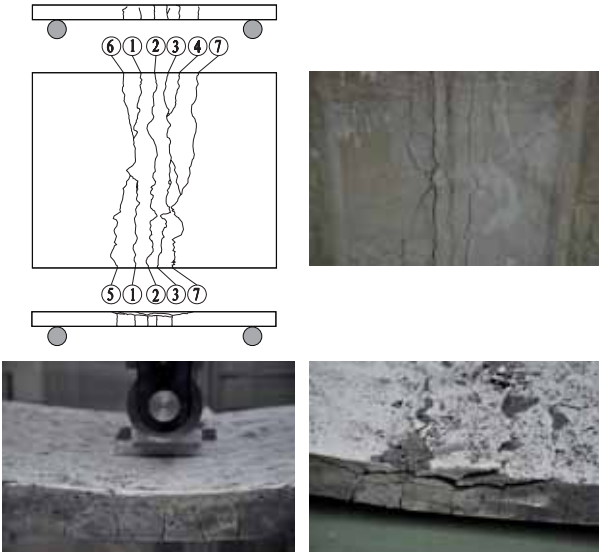

(b)

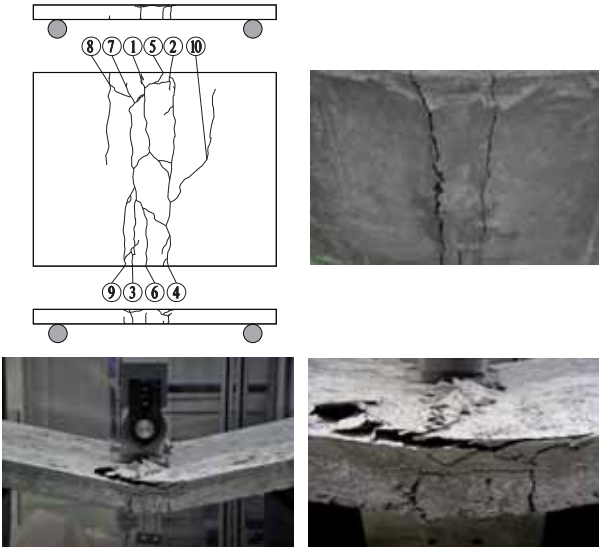

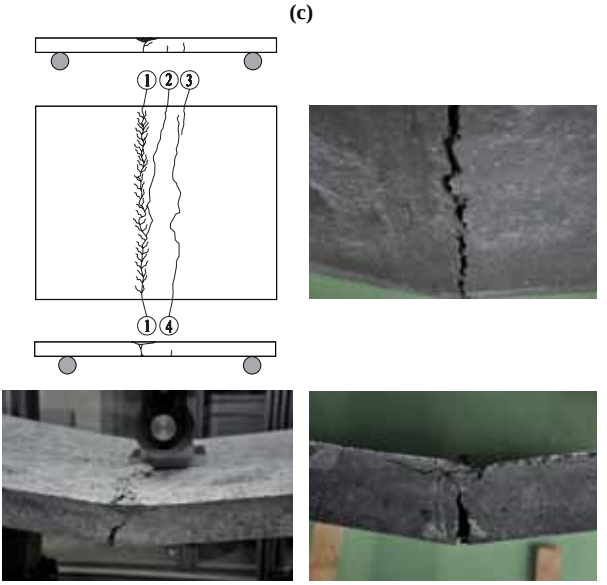

Fig. 5. Maps of crack development and images of damage in the final stage for plate a) P1, b) P2, c) P3.

The plate with 1% of steel fibres had a significantly different image of cracks. During the test only one crack increased width. Additionally in the final stage of loading small radial cracks appeared along its length, Fig. 5c. The research was carried out until the compression zone layers were completely crushed and the cracks in the tensile area were over 5 mm in plates P1, P2 and over 15 mm in plate P3.

Graphs of the load – deflection for the three research elements are shown in Fig. 6.

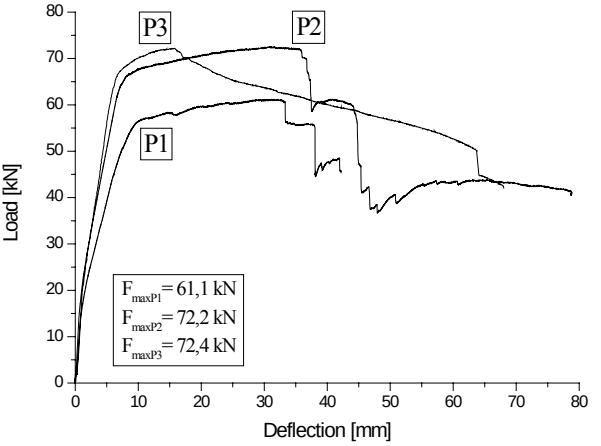

Fig. 6. The load – deflection relation for plates

On the basis of load – deflection relation, it was stated that at maximum load 61.1 kN, deflection plate P1 was equal to 31.2 mm. In case of plate P2 with 0.5% of steel fibres the response of the element was similar, but the largest load is higher by 18.5% at 31 mm deflection. In case of plate P3 with 1% of steel fibres it was observed that the deflection for the load of 72.2 kN was only 15.6 mm. After yield of the reinforcement, the decrease of load capacity is mild, without significant refractions, as steel fibres inhibit the evolution of cracks.

Conclusions

Experimental tests proved the usefulness of steel and polypropylene fibres in order to improve the ultimate tensile strength of high performance concrete in plates. The analysis of the results proves that cooperation between the concrete matrix, fibres and the reinforcement mesh is very effective. With the increase of the number of fibres increased the tensile strength of concrete and maximum deflection. The range of elastic work for all plates is similar covered in the range between 0 and 9 mm. In plate P3, with the contents of steel fibres of 1%, different character of element response was observed. Adding fibres changes the characteristics of high strength concrete – from a brittle, into elastic-plastic material. The evolution of cracks is slow progress, because each crack is bridged by fibres, what translates into a mild failure mechanism and high ductility of the elements.

References:

1. Brandt A.M. (1996), *Toughness of fibre reinforced cement based materials.* Archives of Civil Engineering, XLII, 4.
2. Jamroży Z. (2000), *Concrete and his technologies*. PWN, Warszawa-Kraków (in Polish).
3. Glinicki M.A., Litorowicz A., Zieliński M. (2002), *Experimental analysis of fracture mode I behaviour of fibre concrete*. Building Materials, No 3, 74-76 (in Polish).
4. Banthia N., Gupta R. (2004), *Hybrid fiber reinforced concrete (HyFRC): fiber synergy in high strength matrices*. Materials and Structures, Vol. 37, 707-716.
5. Domański T., Czkwianianc A. (2006), *Influence of fibre reinforcement on the mechanical parameters of the concrete.* Building Review 6 (in Polish).
6. Brandt A.M. (2008), *Fibre reinforced cement-based (FRC) composites after over 40 years of development in building and civil engineering.* Composite Structures 86, 3-9.
7. Glinicki M.A. (2008), *Investigation of fibre concrete property with the macro synthetic fibres, designed on industrial floors*. Cement Lime Concrete. No 4, 184-195 (in Polish).
8. Brandt A.M. (2009) *Cement Based Composites: Materials, Mechanical Properties and Performance*. Taylor and Francis. London and New York.
9. Foster S.J. (2009), *The application of steel-fibres as concrete reinforcement in Australia: from material to structure*. Materials and Structures 42: 1209-1220.

10. Walraven J.C. (2009) *High performance fiber reinforced concrete: progress in knowledge and design codes*. Materials and Structures 42: 1247-1260.
11. Prisco M., Plizzari G., Vandewalle L. (2009), *Fibre reinforced concrete: new design perspectives*. Materials and Structures 42: 1261-1281.
12. Chiaia B., Fantilli A.P., Vallini P. (2009), *Combining fiber-reinforced concrete with traditional reinforcement in tunnel linings*. Engineering Structures 31 1600-1606.
13. Glinicki M.A. (2010), *Concrete with the structural reinforcement*. XXV the Polish Workshops of Work of the Structural Designer, Szczyrk (in Polish).
14. Aïtcin P.C.: *High-Performance Concrete*. E & FN SPON 1998.
15. Aïtcin P.C.: The durability characteristics of high performance concrete: a review. Cement & Concrete Composites 25 (2003) 409-420.
16. Kaszyńska M. (2002), *HPC: possibilities, properties, applications*. XVII the Polish Workshops of Work of the Structural Designer, Ustroń (in Polish).
17. Fairbairn E.M.R., Toledo Filho R.D., Formagini S., Rosa J.I., Battista R.C. (2012), *Experimental analysis and modeling of ultra high performance fiber reinforced concrete plates*. 1-8.

Acknowledgment

This work was financially supported by Ministry of Science and Higher Education within the statutory research number S/15/2013.

THE ULTIMATE FATIGUE STATE OF RC STRUCTURES ACCORDING TO MODEL CODE 2010

Andrzej Łapko, Rafał Wasilczyk

Bialystok University of Technology, Faculty of Civil & Environment Engineering,
Wiejska St. 45e, 15-351 Bialystok, Poland
e-mail: lapko@pb.bialystok.pl; r.wasilczyk@pb.edu.pl

Summary:
The paper presents a review and discussion of CEB-FIP Model Code 2010 principles and rules of design proposed for the needs of verification of fatigue strength of RC structures, like concrete bridges, subjected to dynamic actions. It has been stressed that these rules are based on some different assumptions compared to Eurocode 2. The paper presents also an example of calculations performed to indicate the differences between the results of verification of the Ultimate Fatigue State according to the Model Code 2010, and the the Eurocode 2 and former Polish Codes. The differences are shown in relevant tables.

Keywords: Ultimate Fatigue State, RC structures, Cyclic loads. Model Code 2010

Introduction

The first complete draft of CEB-FIP Model Code 2010 was approved in October 2011 and the final version was published in 2012. This document has been elaborated by an international team of researches and experts aimed to define new and advanced solutions and directions in designing of reinforced concrete structures. It is characterized by different attitude to verifying the Ultimate Fatigue State (UFS) of RC structures for both concrete and reinforcement.

The aim of this paper is to present principles and rules for verification of the UFS of RC structures in accordance to CEB-FIP Model Code 2010. Additionally, example calculations were performed, which were the base for the comparison of CEB-FIP Model Code 2010 and former Polish Codes for bridges and other engineering structures discussed in some papers (Woliński, 1998, 1999); (Jankowiak and Madaj, 2011); (Siwowski and Michalak, 2013).

This paper was elaborated in the frame of state of art analysis of the dynamic fatigue behavior RC structural members made of recycled aggregate concrete subjected to cyclic load (including low-cycle fatigue). That problem is till now at the pilot phase and only very few papers are presented, e.g. (Gordon, 2011) or (Luo and Yao, 2011a, 2011b).

Methods of verifying of RC structures fatigue strength proposed in Model Code 2010

Model Code 2010 (MC 2010, 2012) includes in one document principles and rules for design RC buildings, as well as bridges and other engineering structures throughout their all the life cycles, beginning from designing to erecting, maintenance, strengthening and finally demolition.

In the section describing the ULS state for non-static loads, the rules for shaping structural elements due to fatigue strength have been enclosed. There are also presented a restrictions for reinforcing and prestressing steel as calculation procedures which can be applied for cyclic loads with number of at least 10^4 repeats. It should be mentioned however that the low-cycle fatigue is not enclosed in Model Code 2010 design procedures. Just like in current Eurocode 2 (PN-EN 1992-1-1, 2008), the verification of the UFS include separate courses for steel and concrete, where both conditions should be fulfilled. The Palmgren-Miner summation (Palmgren, 1945) or adequate S-N curves (Fig. 1), different than in PN-EN 1992, also have been applied here.

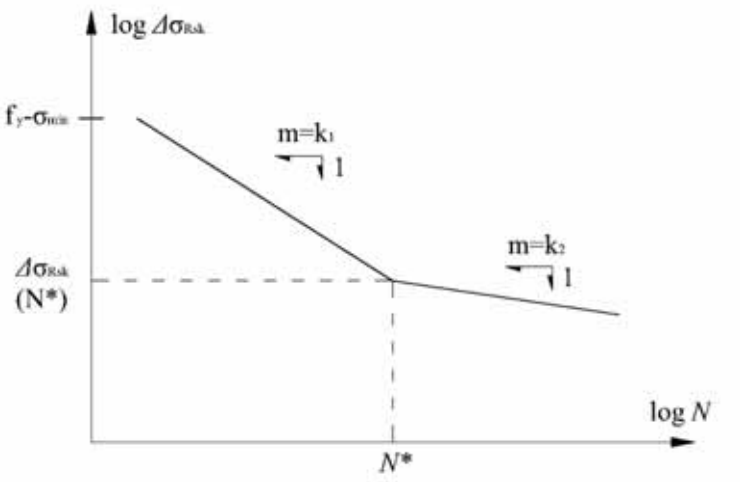

Fig. 1. Characteristic S-N curves for reinforcing and prestressing steel based on the CEB-FIP Model Code 2010 (described in Table 1 and 2)

Model Code 2010 presents 3 main methods with varied levels of accuracy.

- **Simplified procedure** can be used only in case of objects subjected to the number of loading cycles not higher than 10^8, with low stress range.

The reinforcement fatigue state requirements will be met if:

$$\gamma_{Ed} \cdot \max \Delta\sigma_{Ss} \leq \frac{\Delta\sigma_{Rsk}}{\gamma_{s,fat}} \tag{1}$$

where $\max \Delta\sigma_{Ss}$ is the maximum steel stress range under acting loads, $\Delta\sigma_{Rsk}$ is a characteristic value of fatigue strength under the number of 10^8 cycles given in Table 1 and 2, dependent on reinforcement type, its diameter, shape, environment, type of bond. Adopted value of load coefficient γ_{Ed} is 1,1, but in case if stress analysis is accurate enough and its results are confirmed with in-situ observation - $\gamma_{Ed} = 1{,}0$ can be adopted. Another parameter is steel fatigue coefficient $\gamma_{s,fat} = 1{,}15$ just like in Eurocode 2.

Tab. 1. S-N parameters for reinforcing steel in accordance to CEB-FIP Model Code 2010

Reinforcement type	N^*	Stress exponent		$\Delta\sigma_{Rsk}$ (MPa)[e]	
		k_1	k_2	at N^* cycles	at 10^8 cycles
Straight and bent bars $D \geq 25\varnothing$ $\varnothing \leq 16mm$ $\varnothing > 16mm$[a]	 10^6 10^6	 5 5	 9 9	 210 160	 125 95
Bent bars $D < 25\varnothing$[b]	10^6	5	9	–[c]	–[c]
Welded bars [b] including tack Welding and butt joints Mechanical connectors	10^7	3	5	50	30
Marine environment [b],[d]	10^7	3	5	65	40
The values $\Delta\sigma_{Rsk}$ represent the S-N curve of a 40 mm bar; for diameters between 16 and 40 mm interpolation between the values of this line and those of line above is permitted. Most of these S-N curves intersect the curve of the corresponding straight bar. In such cases the fatigue strength of the straight bar is valid for cycle numbers less than that of the intersection point. Values are those of according straight bar multiplied by a reduction factor depending on the ratio of the diameter of mandrel D and bar diameter $\varnothing$: $\xi = 0{,}35 + 0{,}026 \cdot D/\varnothing$. Valid for all ratios $D/\varnothing$ and diameters $\varnothing$. In cases where $\Delta\sigma_{Rsk}$ - values calculated from the S-N curve exceed the stress range $f_y - \sigma_{min}$, the value $f_y - \sigma_{min}$ is valid.					

Tab. 2. S-N parameters for prestressing steel in accordance to CEB-FIP Model Code 2010

Structure type	N^*	Stress exponent		$\Delta\sigma_{Rsk}$ (MPa)[b]	
		k_1	k_2	at N^* cycles	at 10^8 cycles
Pretensioning	10^6	5	9	160	95
Posttensioning Curved tendons Straight tendons Mechanical connectors	 10^6 10^6 10^6	 3 5 3	 7 9 5	 120 160 80	 65 95 30
In case where the S-N curve intersects that of the straight bar, the fatigue strength of the straight bar is valid. In cases where $\Delta\sigma_{Rsk}$ - value calculated from S-N curve exceeds the $f_y - \sigma_{min}$ stress range, the value $f_y - \sigma_{min}$ is valid.					

The reinforcement fatigue state is verified by the use of two conditions – appropriate to compression and tension:

$$\gamma_{Ed} \cdot \sigma_{c,\max} \cdot \eta_c \le 0,45 \cdot f_{cd,fat} \tag{2}$$

$$\gamma_{Ed} \cdot \sigma_{ct,\max} \le 0,33 \cdot f_{ctd,fat} \tag{3}$$

where $\sigma_{c,\max}$ and $\sigma_{ct,\max}$ are maximum concrete stress values caused by load combination under compression and tension accordingly, $f_{cd,fat}$ and $f_{ctd,fat}$ are concrete design fatigue tensile and compressive strengths, while η_c is the averaging factor considering the stress gradient.

Mentioned η_c coefficient can be calculated from equation below:

$$\eta_c = \frac{1}{1,5 - 0,5 \cdot \frac{|\sigma_{c1}|}{|\sigma_{c2}|}} \tag{4}$$

where $|\sigma_{c1}|$ and $|\sigma_{c2}|$ are accordingly the lower and the larger absolute values of the compressive stress within a distance of 300mm from the surface under the same load combination (Fig. 2).

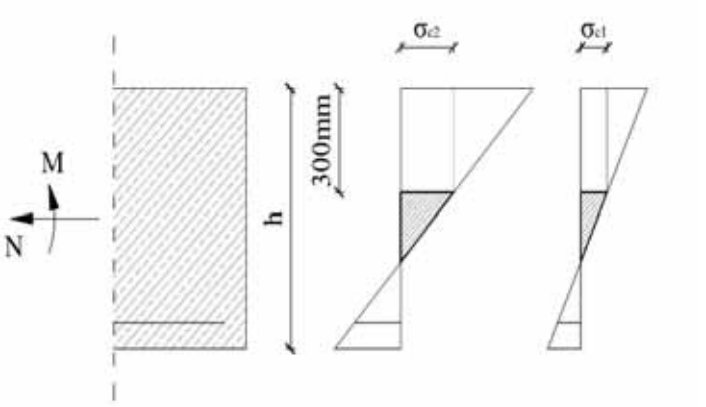

Fig. 2. Definition of the concrete $|\sigma_{c1}|$ and $|\sigma_{c2}|$ in accordance to CEB-FIP Model upper and lower value of compressive stress in Code 2010

The design fatigue reference strength of concrete under tension $f_{ctd,fat}$ is defined as 5-percentage of characteristic concrete tensile strength $f_{ctk,0,05}$ with the use of concrete material factor $\gamma_{c,fat} = 1,50$ as in equation below:

$$f_{ctd,fat} = \frac{f_{ctk,0,05}}{\gamma_{c,fat}} \tag{5}$$

The design fatigue reference strength of concrete under compression is defined taking into consideration: concrete reference strength $f_{cko} = 10MPa$, characteristic compressive strength f_{ck} and the $\beta_{cc}(t)$ coefficient which depends on the age of the concrete in days when the fatigue loading starts, what is shown, similarly to Eurocode 2, in equation:

$$f_{cd,fat} = \frac{0,85 \cdot \beta_{cc}(t)}{\gamma_{c,fat}} \cdot \left[f_{ck} \cdot \left(1 - \frac{f_{ck}}{25 \cdot f_{cko}} \right) \right] \tag{6}$$

$\beta_{cc}(t)$ factor is a function of development of concrete compressive strength in time (Eq.7), dependent on the age of concrete (in days) and factor s related to the class of cement used, which values are given in Table 3.

$$\beta_{cc}(t) = \exp\left\{ s \left[1 - \left(\frac{28}{t} \right)^{1} \right] \right\} \tag{7}$$

Tab. 3. Values of s factor depending on cement class according to Model Code 2010

Cement class	32,5 N	32,5 R 42,5 N	42,5 R 52,5 N 52,5 R
s	0,38	0,25	0,20

- The verification taking into consideration a single, constant range of stress velocity consists in relating the foreseen number *n* of cycles during the use of the structure to maximum fatigue effects *Q*, which, if estimated accurately enough, allows to perform more precise calculations than with the use of the simplified procedure. It is an innovation in comparison with polish codes.

In accordance to reinforcement steel, meeting the criteria is determined by following condition:

$$\gamma_{Ed} \cdot \max \Delta\sigma_{Ss} \le \frac{\Delta\sigma_{Rsk}(n)}{\gamma_{s,fat}} \tag{8}$$

where $\Delta\sigma_{Rsk}(n)$ is the stress range obtained from a characteristic fatigue strength S-N function, relevant to *n* cycles of variable loading.

The parameters of the S-N curve are shown in Table 1 and 2 and they depend on the reinforcement type, its shape, environment and bonds. Moreover, these are characteristic values, so material safety coefficients are not taken into consideration. Their accurate values should be authorized in proper approvals.

In case of concrete, there is a need to establish the conditions for centric compression, tension and both mixed together, where the verification of fatigue strength state is more indirect than in case of steel. Foreseen number of variable load *n* should be lower or equal to the limit number of cycles *N* that steel or concrete can bear. It is calculated with the use of logarithmic function. For axial compression, the following set of equations is used:

$$\log N_1 = \left(12 + 16 \cdot S_{cd,\min} + 8 \cdot S_{cd,\min}^2\right) \cdot \left(1 - S_{cd,\max}\right) \tag{9}$$

$$\log N_2 = 0,2 \cdot \log N_1 \cdot \left(\log N_1 - 1\right) \tag{10}$$

$$\log N_3 = \frac{\log N_2 \cdot \left(0,3 - 0,375 \cdot S_{cd,\min}\right)}{\Delta S_{cd}} \tag{11}$$

Defining the adequate value of *N* requires fixing the equations above into following conditions:

if $\log N_1 \le 6$, then $\log N = \log N_1$ should be assumed (12)

if $\log N_1 \le 6$ and $\Delta S_{cd} \ge 0,3 - 0,375 \cdot S_{cd,\min}$, then $\log N = \log N_2$ (13)

if $\log N_1 \le 6$ and $\Delta S_{cd} < 0,3 - 0,375 \cdot S_{cd,\min}$, then $\log N = \log N_3$ (14)

and the values $S_{cd,\min}$, $S_{cd,\max}$ of compressive stress and ΔS_{cd} compressive stress range nan be calculated from Eq.15:

$$S_{cd,\min} = \frac{\left|\gamma_{Ed} \cdot \sigma_{c,\min} \cdot \eta_c\right|}{f_{cd,fat}} \tag{15}$$

$$S_{cd,\max} = \frac{\left|\gamma_{Ed} \cdot \sigma_{c,\max} \cdot \eta_c\right|}{f_{cd,fat}} \tag{16}$$

$$\Delta S_{cd} = S_{cd,\max} - S_{cd,\min} \tag{17}$$

where $\sigma_{c,\min}$ is the minimum stress under the load combination.

It is essential to mention, that equations above refer to a case when $S_{cd,\min}$ is 0,0÷0,8. However, if $S_{cd,\min}$ is equal or above 0,8, the S-N curves should be used. The environmental conditions are also important. The calculations of N refer to elements working in sealed conditions or large sections of concrete characterized with low permeability. Slim elements which are allowed to dry can reach even higher fatigue strength. On the other hand, concrete structures, which are constantly under the water, can prove lower fatigue strength.

Verification of the ultimate fatigue state for centric and eccentric tension ($\sigma_{ct,\max} > 0,026 \cdot \left|\sigma_{c,\max}\right|$) requires only calculation below:

$$\log N = 12 \cdot \left(1 - S_{td,\max}\right) \tag{18}$$

where the maximum value of tensile stress $S_{td,\max}$ is considered as:

$$S_{ctd,\max} = \frac{\gamma_{Ed} \cdot \sigma_{ct,\max}}{f_{ctd,fat}} \tag{19}$$

In the case of compression with tension at the same time ($\sigma_{ct,\max} \le 0,026 \cdot \left|\sigma_{c,\max}\right|$), the verification is the same as before:

$$\log N = 9 \cdot \left(1 - S_{cd,\max}\right) \tag{20}$$

- The verification considering various stress ranges bases on the Palmgren-Miner summation and it is presented in the Model Code 2010 as most accurate. Similarly as in the Eurocode 2, single damages caused by *j* stress ranges are added altogether. According to that, structural fatigue damage D is following:

$$D = \sum_{i=1}^{j} \frac{n_{Si}}{N_{Ri}} \tag{21}$$

where n_{Si} is a number of acting load cycles connected with stress range in steel and current stress range in concrete. N_{Ri} describes the limit number of cycles leading to damage of the structure. In accordance to steel, the limit number of cycles is defined minding increased stress range $\gamma_{Ed} \cdot \gamma_{s,fat} \cdot \Delta\sigma_{Esi}$. N_{Ri} for concrete is calculated with methods mentioned above and it does not require any additional increasing. The use of proper calculating methods (for ex. rain flow) allows to reach the limit fatigue damage $D_{\lim} = 1,0$.

The example of ultimate fatigue state verification

Assumptions common to all variants of example are shown below.

The calculations were performed for a RC bridge slab, subjected to a multiple variable load with constant amplitude (number of cycles = 10^6). Design assumptions are listed in Table 4. They were chosen and calculated in such way, that all of the ultimate states (except for fatigue) were fulfilled with a reserve not higher than 10% (according to PN-EN). Such action gave the opportunity to show the need of verification of the ultimate fatigue state in structures under the dynamic load. In order to compare calculating procedures with outdated Polish Codes and the Eurocode, the same set of characteristic stresses in steel and concrete was assumed (in the span section), what is shown in Table 5. The example is made the way that minimum stress comes from constant load, while the maximum stress is caused by both constant and variable loads. Depending on the case, they were multiplied by reliable coefficients.

Tab. 4. Design assumptions used in RC slab example calculations

Concrete class	C35/45 (PN-EN 206-1:2003+AP1:2004)
Steel type	B500SP
Cross section $h \times b$	900x1000 [mm]
Reinforcement sectional area	$A_{s,prov} = 80,40cm^2 \left(10\varnothing 32\right)$
Concrete cover	$C_{nom} = 45mm$
Effective depth	$d = 819mm$
Span of the slab	$L = 1800mm$

The results of all variants calculations with Model Code 2010 are set in table below (Table 5). The example presents that on the base of CEB-FIP proposal, the fatigue requirements may not be met. However, it is noticeable that load-bearing capacity of steel was surpassed by 6%. Such effect is the outcome of wide range of acceptable stress $\Delta\sigma_{Rsk}\left(n\right)$ for 10^6 loading cycles. The final stresses in accordance to PN-EN are 162,5 MPa, while in MC 2010 - 210 MPa.

Tab. 5. Results of calculations of the RC slab example

Code	Result of steel verification	Result of steel verification
PN-B-03264:2002	Ultimate state exceeded in 20%	Ultimate state exceeded in 80%
PN-91/S-10042	Ultimate state filled with reserve of 6%	Non checkable
PN-EN 1992-1-1:2005+AC:2008	Ultimate state exceeded in 28%	$\sigma_{cd,\max} > f_{cd,fat}$
PN-EN 1992-2:2005+AC:2008	Ultimate state exceeded in 86%	$\sigma_{cd,\max} > f_{cd,fat}$
CEB-FIP Model Code 2010	Ultimate state exceeded in 9%	$\sigma_{cd,\max} > f_{cd,fat}$

Referring to the safety reserves that fatigue compressive strength of concrete $f_{cd,fat}$ include, the Model Code 2010 confirmed a huge discrepancies between the results of resaerch on the concrete fatigue.

Summary

The article characterizes requirements of the Model Code 2010 for verifying the ultimate fatigue state of RC structures made of normal concrete, however the structures made of recycling aggregate concrete are not included in this Standard.

The results of calculation on the basis of Model Code 2010 set in Table 6 confirm the remarkable influence of the fatigue on the structure's load-bearing capacity. The Eurocode 2 and Model Code 2010 procedures have a similar attitude to the material fatigue, using the S-N curves, design values of fatigue forces and Palmgren-Miner summation of destructions.

In the Model Code 2010 there are no proper rules or calculating methods for the low-cycle fatigue given in the Model Code 2010 and it still requires a respectable research.

Defining the parameters of S-N curves for reinforcing steel, the MC 2010 proposes a case of marine environment, which significantly lowers durability of the structure.

References:

1. Gordon P.M. (2011) *Low cycle fatigue behavior of concrete with recycled concrete aggregates*. A Thesis presented to the Faculty of California Polytechnic State University, San Luis Obispo. In Partial Fulfillment of the Requirements for the Degree Master of Science in Civil and Environmental Engineering.
2. Jankowiak I., Madaj A. (2011). *Obliczanie na zmęczenie betonowych konstrukcji mostowych wg PN-EN*. Archiwum Instytutu Inżynierii Lądowej / Politechnika Poznańska, Nr 10, 105-127.
3. Luo X., Yao H. (2011a). *Deformation and deformation and acoustics parameters feature of recycled concrete under cyclic loading*. Applied Mechanics and Materials, Vols. 80-81, 213-216.
4. Luo X., Yao H. (2011b). *Ultrasonic Propagation Characteristics and Damage Evolution of Recycled Concrete under Dynamic Loading*. Advanced Materials Research, Vols. 163-167, 956-960.
5. Miner, M.A., "*Cumulative Damage in Fatigue*" (1945), Journal of Applied Mechanics, Vol. 67, pp. A159-A164, 1945.
6. PN-B-0326 (2002). *Konstrukcje betonowe, żelbetowe i sprężone. Obliczenia statyczne i projektowanie.*
7. PN-EN 1992-1-1:2005+AC:2008 *Eurokod 2: Projektowanie konstrukcji z betonu, Część1-1: Reguły ogólne i reguły dla budynków.*
8. PN-EN 1992-2:2005+AC:2008 *Eurokod 2: Projektowanie konstrukcji z betonu, Część 2:Mosty z betonu. Obliczanie i reguły konstrukcyjne.*
9. PN-EN 206-1:2003+AP1:2004 *Beton Część 1: Wymagania, właściwości, produkcja i zgodność.*

10. PN-91/S-10042 *Obiekty mostowe. Konstrukcje betonowe, żelbetowe i sprężone. Projektowanie.*
11. Schijve, J. (2003). "*Fatigue of structures and materials in the 20th century and the state of the art*", Materials Science, Vo. 39, no 3, pp. 307-333.
12. Siwowski T., Michalak E. (2013). *Projektowanie mostów wg Eurokodów. Mosty żelbetowe cz. II*. Mosty, Nr 2/2013, 68-73.
13. Woliński S. (1998). *Opis i analiza zjawiska zmęczenia konstrukcji z betonu w normach projektowania*. Inżynieria i Środowisko, R.54, Nr 8, 418-422.
14. Woliński S. (1999). *Stan graniczny zmęczenia konstrukcji z betonu w normach projektowania*. Inżynieria i Środowisko, R.55, Nr 4, 220-224.

Acknowledgments

The studies were co-financed by the Rector Project S/WBiIŚ/2/12

WATERPROOF IMPREGNATION OF CERAMIC BRICK WITH EMULSIONS OF LOW VOC CONTENT

[1]Stanisław Fic, [1]Danuta Barnat – Hunek, [2]Agnieszka Karwacka

[1]Lublin University of Technology, Faculty of Civil Engineering and Architecture,
Department of Building Construction, Nadbystrzycka St. 40, 20-618 Lublin, Poland
e-mail:d.barnat-hunek@pollub.pl, s.fic@pollub.pl
[2]Pope John Paul II State School Higher Education in Biala Podlaska,
Department of Engineering Sciences, Department of Civil Engineering
Sidorska St. 95/97, 21-500 Biała Podlaska, Poland

Summary:
The aim of the research presented in the paper was to evaluate the feasibility of using hydrophobizing preparations based on organosilicon compounds for impregnation of ceramic bricks. The process of surface hydrophobization both using solvents and water substances was analyzed. The effectiveness of four preparations which differed in terms of hydrolytic polycondensation degree, viscosity and concentration, as these are the factors that are decisive as far as the end result of hydrophobization is concerned.
The following laboratory tests were performed: the analysis of physical properties of the tested materials, water drop absorption test, water absorption by weight of the hydrophobized samples, water vapour diffusion, frost resistance, the analysis of silica gel properties in electron microscopy.
Based on the results of the above mentioned, the analysis of effectiveness and desirability of hydrophobization using emulsion with a low VOC content was carried out.

Keywords: hydrophobization, organosilicon compounds, absorbability, frost-resistance

Introduction

The use of hydrophobizing preparations for impregnating the building materials has been increasing over the last few years. This has been proved by not only an increase in the use of preparations for hydrophobization in building engineering, particularly in relation to historic buildings, but also a large number of new hydrophobizing products appearing on the market. An important advantage of hydrophobization is the fact that preparations used for this purpose form a thin, colorless coating showing good adhesion properties and resistance to aging (Łukaszewicz J., 2002). The hydrophobic coating should be impermeable to water and aqueous solutions, while ensuring evaporation of water contained in the material (Płuska I., 2005).

Nowadays organosilicone compounds are used for hydrophobization. Silicones belong to the most effective and safe agents for hydrophobization. As silicone hydrophobizing agents are used alkyl-potassium silicates, alkoxysilanes, siloxanes and hydrated siloxanes and siloxanes in the form of hydroxide. Alkyl-potassium silicates as the only ones are available on the market in the form of a strongly alkaline aqueous solution, (pH=14) (Barnat-Hunek D i in., 2013). Other compounds are soluble only in organic solvents.

A controversial component of hydrophobizing preparations are organic solvents. The volatiles contained in hydrocarbon preparations, can be toxic, carcinogenic or mutagenic. The most important legislation act regulating the VOC emission in the EU is Council Directive 2004/42/EC (Directive 2004) on the limitation of emissions of volatile organic compounds due to the use of organic solvents in certain paints and varnishes. It limits the VOC content in products for decorative painting and renovation. For the purpose of renovation and maintenance of the buildings, Member States may grant individual licenses for sale and use of specific quantities of products which do not meet the VOC limits set out in the Directive.

Solvent impregnating agents play an important role in a range of hydrophobizing substances, and due to the high efficiency, their use is mostly preferred in comparison to water-based preparations.

Nowadays, manufacturers of building chemicals need to face necessity to protect natural environment which is related to amendments to regulations requiring the limitation of emissions of volatile organic solvents (Osterholtz F. D., Pohl E. R., 1992, Kaesler K. H., 2006, Barnat-Hunek D, 2010). The most important ways to decrease the VOC emissions from the impregnating agents are: the use of water-based instead of solvent-based preparations, decreasing the solvent content, decreasing the VOC content in water-based preparations. The law regulations made the chemical concerns develop and manufacture water-based impregnating emulsions. Water-based emulsions of silanes are suspensions composed of two insoluble liquids. Silane is mixed with water and an emulsifier.

The most suitable hydrophobizing preparations with good properties of penetration into the stone (Łukaszewicz, J., 2002, Krzywobłocka - Laurów R., 2001, Sasse R., 2001, Płuska I., 2005, Bai Y, i in., 2003) and those which do caused sealing the surface. Waterproof impregnation is only effective when the critical depth of penetration has been reached, and the surface has taken an appropriate amount of impregnating agents. Penetration depends on such factors as: the duration of contact between the silane and the surface of the material, the chemical reactivity of the silanes used, the type of solvent, the viscosity of the solution (Borgia G. C. i in., 2001).

Water-based preparations may sometimes cause swelling of clay minerals contained in building materials which, by narrowing the capillary lumen are limiting penetration of the solution into the structure of the material (Łukaszewicz J. 2002).

Experimental investigations

Scope of studies

The paper analyzes the effectiveness of four organosilicone agents recommended for ceramic building materials

The following preparations have been selected to laboratory tests:

P1 — water-based solution of methylosilicone resin in the potassium hydroxide
P2 – water-dilutable siloxane
P3 – organic solvent based methylosilicone resin
P4 – organic solvent based alkiloalkoksysiloxane oligomer.

Preparations of well-known manufacturers which differed in the type of solvent and physical characteristics were adopted to tests. The concentration of the product and the amount of layers applied were not subjected to the analysis due to the fact that the samples had been hydrophobized according to the manufacturers' instructions by using a brush. In order to perform a thorough analysis of the impact of concentration of the active substance on the effectiveness of brick hydrophobization, some additional tests would have to be performed. The P1 preparation was diluted according to the instructions in proportion of 1:6 respectively, other hydrophobizing agents are not subject to dilution.

In order to perform the test, samples of cubic bricks were prepared with dimensions of 4 x 4 x 4 cm. All samples, before being subjected to hydrophobization treatment, had undergone seasoning for 30 days in the laboratory at room temperature of 20 ± 2°C and relative humidity of 60 ± 5%. Six samples were taken for each test.

The analysis of physical characteristics of bricks prior to impregnation was performed. A direct water drop absorption test and water absorbability test were conducted. In addition, water vapor diffusion outflow test was carried out in order to check whether hydrophobization does not cause sealing the pores of the materials tested and whether it does not interfere with the diffusion of gases and liquids. Based on the analysis results, the effectiveness of brick hydrophobization was performed.

Physical characteristics of the materials

According to the PN-EN 1936:2010 determination of bulk density, density, open and total porosity was performed.

The results were as follows: bulk density ρ_b = 1,75 g/cm³, density ρ_r = 2,61 g/cm³, open porosity ρ_o = 18,31 %, total porosity P = 27,37 %.

Water drop absorption ratio WA

Water drop absorption test was carried out according to ZUAT 15/VI.11-2/2001 ITB (Krzywobłocka – Laurów R., 2001). Adsorption time through the hydrophobized surfaces is calculated based on the formula (2.1),

$$WA = \left(1 - \frac{t_x - t_n}{t_x}\right) \cdot 100 \qquad (2.1)$$

where:

WA – water drop adsorption ratio, (%)
$\mathbf{t_x}$ – adsorption time into the hydrophobized surface, (s or min.)
$\mathbf{t_n}$ – adsorption time into the into the sample taken for a model one, (s or min.).

During the test, one could have observed spherical droplets which showed no adhesion to the base tested. Extreme angle of a waterdrop on the surface of the brick samples impregnated with the chemical agents based on silicones did not change significantly until the time when water has evaporated. However, the water-based P2 preparation has got a small wetting angle. Droplets applied into such coating are characterized by flat surface. The minimum adsorption time for the hydrophobic surface was 133 minutes for P2 preparation. Other chemicals have reached the time t = 193 minutes, which proves a decreased porosity of the brick.

ZUAT requirements regarding the value of WA have been met by the tested preparations with respect to all the bricks involved in the tests (WA ≤ 5%, WR ≥ 95%). The highest WA ratio (0,53%) for the brick was obtained at the surface hydrophobization using the P2 preparation. The lowest WA ratios were achieved at hydrophobization by the use of other preparations (0,3%). The duration of water drop absorption in the non-hydrophobized brick which was less than one minute.

The preliminary test of the effectiveness of hydrophobization showed that all hydrophobized samples were fully water-resistant.

Water absorption coefficient

Measurement of water absorbability of bricks by weight for the four periods: after 0.5 h, 6 h, 24 h, 48 h (Krzywobłocka – Laurów R., 2001). In order to check the effectiveness of hydrophobization in conditions of dampness which lasts for a long period of time, two additional times of water absorbability test were introduced: after 7 and 14 days. Long-lasting dampness may occur in horizontal parts of the walls (cornices, stains due to faulty flashing) and in the period of continuous rain.

A measure of the effectiveness of surface impregnation is wettability of the protected base, expressed by the following formula:

$$W_n = 100 - \frac{n_h}{n_b} \cdot 100 \tag{2.2}$$

in which:

$\mathbf{W_n}$ –hydrophobization effectiveness, (%)
$\mathbf{n_h}$ – wettability of the hydrophobized sample by weight, (%)
$\mathbf{n_b}$ – wettability of the non-hydrophobized sample by weight, (%).

Test results are shown in Tab. 1.

Tab. 1. Hydrophobization effectiveness for ceramic brick, [%]

	P1	**P2**	**P3**	**P4**
30 min	97,47	95,49	99,85	99,87
6 h	97,03	89,12	97,69	98,62
24h	92,56	82,44	98,78	97,05
48 h	83,23	77,49	98,06	96,87
7 days	78,57	64,35	89,73	94,55
14 days	64,79	56,27	82,14	93,19

After 48 hours from actually having applied the coating, a decrease in brick resistance to water action has been observed. The P4 sample which was subjected to hydrophobization by means of oligomers is an exception thereto.

The difference in the effectiveness of impregnating the brick after the period of 14 days from protecting the material is clearly visible. The effectiveness of hydrophobization after the period of 14 days ranges from 56,27% to 93,19%, depending on the impregnating agent used. Preparations based on organic solvents are found to be more effective.

The longer the contact of the preparation with water, the weaker the effectiveness of impregnation becomes.

Capability to diffusion of water vapor of impregnated samples of ceramic bricks

In order to verify whether hydrophobization does not disturb the diffusion of vapor and gas, vapor permeability test of the brick were carried out.

After having completed the wettability test, the samples were dried, and then left in laboratory conditions at 20 ± 5°C and relative humidity of 60 ± 5% to get dry. At this time, the rate of drying the samples was determined by measuring the weight loss of the samples, which indicated the amount of evaporated water.

Percent decrease in moisture content was determined as the humidity indicator of the brick prior to and after hydrophobization after the period of 14 days of drying the samples (Table 2).

Tab. 2. Percent decrease in moisture after 14 days of drying the samples, [%]

PERCENT DECREASE IN MOISTURE				
PREPARATION	**P1**	**P2**	**P3**	**P4**
MOISTURE DECREASE [%]	90,52	85,45	51,45	69,18

Water has evaporated the fastest from the non-impregnated material. After 14 days of drying, P3 samples achieved the lowest average humidity decrease equal to 51,45%.

The P1 water-based preparation achieved the biggest decrease in humidity – 90,52% at water absorbability by weight n_w equal to 1,36%.

Hydrophobizing preparations based on organic solvents (P3, P4) cause the biggest sealing of the surface of the tested material, which makes it slightly difficult to evaporate moisture from ceramic materials.

Frost-resistance by means of a direct method

Frost-resistance of bricks was determined based on the PN-EN 12012:2007 and EN 13581:2004. The brick was subjected to 50 cycles of freeze-thaw. After 50 cycles thereof, the samples were dried again until they have reached a constant weight and then the percentage weight loss of the sample was determined.

The smallest weight loss was observed for ceramic brick in the case of P4 preparation, which amounted to 0,10%, while the P2 samples were characterized by the biggest weight loss of 0,60% among the hydrophobizing preparations. The weight loss of reference samples was 0,67%.

This means that hydrophobization by means of oligomers (P4) had a considerable impact on the frost-resistant properties of the brick. However, impregnation by the use of macromolecular siliconates does not protect the brick against damage caused by frost to a sufficient degree.

Silicone resin distribution in the microstructure of ceramic brick

The analysis of hydrophobic coating distribution in the pores of ceramic bricks using scanning electron microscopy SEM was performed. The resin texture at the brick fracture has been shown in Figure 1 and 2.

Macromolecular methylosilicone resins and alkyl alkoxysilane oligomers produced a coating evenly distributed in the microstructure of the brick. Polysiloxane coating (Fig. 1a, b), compared to the reference brick (Figure 2b) does not cause sealing the pores, and thus it should not interfere with the diffusion of gases and vapors.

a) b)

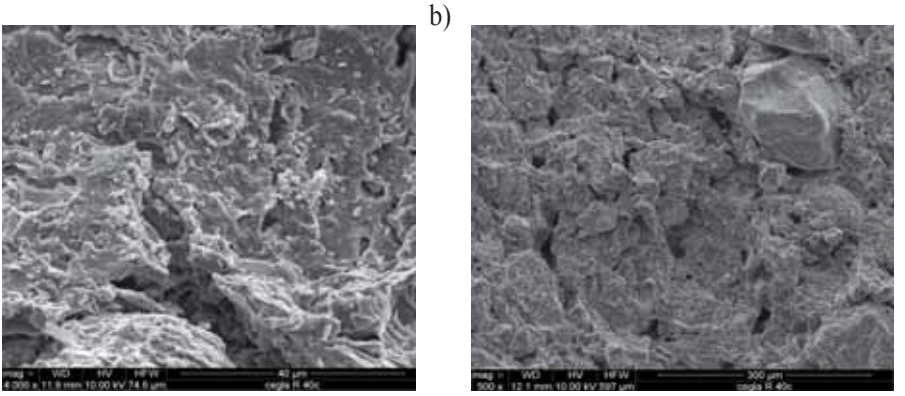

Fig. 1. Water-soluble preparations in the structure of ceramic bricks: a) P4 preparation in the structure of ceramic bricks: a) magnified by 4000x, b) magnified by 500x.

Water-dilutable macromolecular P2 siliconates formed a thick coating of silicone that covers the microstructure of ceramics and shows cracks in many places (Fig. 2a). This did not disturb normal diffusion of water vapor from the ceramic material, however it did not protect against water and frost action effectively, as proved by previous studies.

a) b)

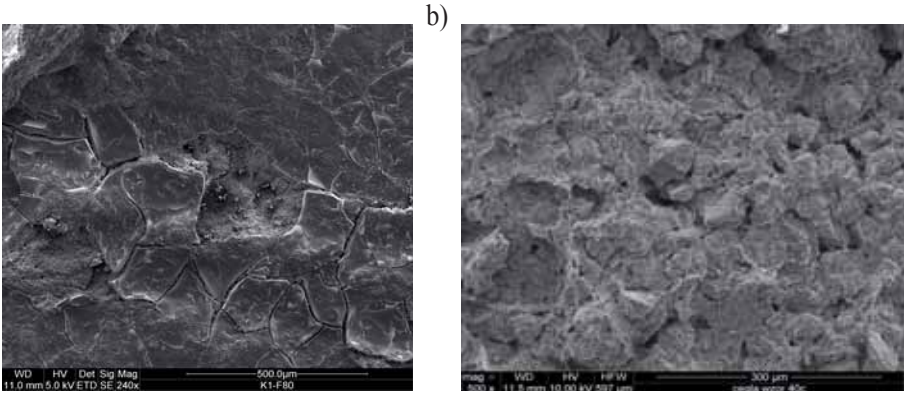

Fig. 2. Microstructure of the tested ceramic brick: a) P2 preparation (240x), b) reference brick (500x).

Conclusions

The following conclusions are drawn based on the studies performed on brick hydrophobization: The best effect in protecting solid ceramic brick against penetration of water was obtained using P4 preparation based on small molecule oligomers. This preparation makes hydrophobic properties of the brick increase by 99%.

The weakest protection against water absorption for bricks are water-based preparations such as P1, P2. The use of these preparations increased hydrophobicity of the brick by 95%. Test results of hydrophobization effectiveness of the brick after 14 days showed a decrease in absorbability by weight from 56% to 93%. Organic solvent based hydrophobizing preparations cause the biggest sealing of the surface, which makes evaporation of moisture difficult. In the context of the afore said observations one should not disregard hydrophobization treatment by means of hydrocarbon solvents based preparations. Despite sealing the rock structure, these preparations have the best hydrophobizing properties (Łukaszewicz J., 2002, Sobkowiak D., Zapałowski G., 2000, Sobkowiak D., Zapałowski G., 1997, Meinhardt – Degen J., 2004) and they do not make clay minerals swell. The amount of vaporized water as well, what is very important, absorbed water in the same moisture conditions will be relatively low as compared with water-diluted coatings.

The best protection against frost for ceramic brick is provided by small molecular oligomers. Application of these preparations resulted in a decrease in weight equal to 0.10% after 50 cycles of freeze-thaw actions.

Organic solvent based hydrophobizing preparations, such as methylosilicone resins in white spirit or oligomers cause the most effective hydrophobization. Despite the fact that, in practice, these preparations often cause sealing surface which hinders diffusion of water vapor from materials, water vapor permeability tests showed a decrease of moisture from 51,45-69,18% after 14 days.

A Guarantee of good hydrophobic effect are: low density, viscosity, low concentration of the active substance and large quotient of surface tension to the viscosity of the solution. This is confirmed by the presented studies and the research of other scientific centers (Domasłowski W., 1993, J. Lukaszewicz, 2002).

The effectiveness of hydrophobization is affected by: the nature of silica gel, its distribution in the pores, aggregates, the effect of "spilling" as well as cracking net of the coating. These features are found in electron microscopy SEM. Resins are composed of fine particles, which are evenly distributed in the brick microstructure. A thin silicon film provides effective hydrophobization.

The resin obtained from macromolecular siliconate (P2) cannot guarantee a satisfactory hydrophobic effect. The preparation does not "rise" in brick, but seals, clogs surface pores. Siliconate does not form a thin hydrophobic film, but a thick cracked layer. A thin hydrophobic coating should slightly cover the capillary walls, and not to fill the entire volume of the pores (Domasłowski W., 1993, J. Łukaszewicz 2002 Geih H., 2004). Then, hydrophobization does not significantly alter vapor permeability of the material, and smooth two-way movement of gases and vapors is not disturbed.

In practice, prior to taking decision regarding hydrophobization, it is necessary to carry out a preliminary analysis of the effectiveness of material hydrophobization to determine whether the anticipated effect will be proportional to the costs incurred.

For the purpose of a more precise analysis of the impact of organosilicon compounds on building ceramics, one should conduct additional studies on, among others concentration of the preparation, the number of layers of hydrophobizing agents applied, the effect of coating aging on the effect of hydrophobic effect, qualitative and quantitative analysis of ions and anions present in ceramics after hydrophobization (Barnat-Hunek D., Klimek B, 2012).

When deciding on hydrophobization treatment not only technical, but also ecological and economical aspects play an important role. The selection of impregnating agents cannot be accidental, one should not rely solely on recommendations of the technical advisors, but it should be considered in the context of the impact on the environment. This is only feasible through the use of water-based or solvent-based impregnating agents which have a reduced content of organic solvents.

The research conducted so far have shown that low molecule alkyloalkoxysiloxane oligomers penetrate the most deeply into the structure of porous materials, the weakest penetration are those of water-diluted polymer preparations.

However, in many cases, modern emulsions with a low VOC content are as effective as the products containing organic solvents.

References:

1. Łukaszewicz J. W., 2002: Badania i zastosowanie związków krzemoorganicznych w konserwacji zabytków kamiennych. UMK Toruń.
2. Płuska I., 2005: Konserwacja kamienia w architekturze i sztuce. Renowacje i Zabytki 1 (13)/2005
3. Barnat-Hunek D., Góra J., Brzyski P. 2013: Ocena skuteczności hydrofobizacji powierzchniowej betonu. Izolacje 6/2013.
4. DYREKTYWA 2004/42/WE PARLAMENTU EUROPEJSKIEGO I RADY z dnia 21 kwietnia 2004 r. w sprawie ograniczeń emisji lotnych związków organicznych w wyniku stosowania rozpuszczalników organicznych w niektórych farbach i lakierach oraz produktach do odnawiania pojazdów, a także zmieniająca dyrektywę 1999/13/WE.
5. Osterholtz F. D., Pohl E. R., 1992: Kinetics of the hydrolysis and condensation of organofunctional alkoxysilanes: a review, Journal of Adhesion Science Technology 6/1992.
6. Kaesler K. H., 2006: Powłoki silanowe i siloksanowe. Skuteczna ochrona przed wodą i zabrudzeniami. Rynek chemii budowlanej 5/2006.
7. Barnat-Hunek D. 2010: Hydrofobizacja opoki wapnistej w obiektach zabytkowych Kazimierza Dolnego. Monografia Wydziału Budownictwa i Architektury. Wydawnictwo Politechniki Lubelskiej, Lublin 2010.
8. Krzywobłocka – Laurów R., 2001: ZUAT -15/VI.11-2/01 wyd. I. Preparaty do powierzchniowej hydrofobizacji wyrobów budowlanych. Część 2. Wyroby ceramiczne. ITB, Warszawa.
9. Sasse R., 2001: Inżynierskie problemy ochrony budowli zabytkowych. Materiały Budowlane 8/2001.

10. Bai Y., Thompson G. E., Martinez – Ramirez S., Brüeggerhoff S., 2003: Mineralogical study of salt crusts formed a historic building stones. The Science of the Total Environment 302.
11. Borgia G. C., Bortolotti V., Camaiti M., Cerri F., Fantazzini P., Piacenti F., 2001: Performance evolution of hydrophobic treatments for stone conservation investigated by MRI. Elsevier Science Inc. Magnetic Resonance Imaging 19/2001.
12. PN-EN 1936:2010 Metody badań kamienia naturalnego. Oznaczanie gęstości i gęstości objętościowej oraz całkowitej i otwartej porowatości.
13. PN-EN 12012:2007 Metody badań elementów murowych – Określanie odporności na zamrażanie-odmrażanie elementów murowych ceramicznych.
14. PN-EN 13581:2004 Wyroby i systemy do ochrony i napraw konstrukcji betonowych – Metody badań – Oznaczanie ubytku masy betonu hydrofobizowanego przez impregnację po działaniu zamrażania – rozmrażania w obecności soli.
15. Sobkowiak D., Zapałowski G., 2000: Badania środka Sarsil W produkcji Instytutu Chemii Przemysłowej, Zakładu Doświadczalnego Silikonów w Nowej Sarzynie do wzmacniania i hydrofobizacji materiałów budowlanych w obiektach zabytkowych. Pracownie Konserwacji Zabytków, Laboratorium Naukowo – Badawcze w Toruniu.
16. Sobkowiak D., Zapałowski G., 1997: Badania środków Ahydrosil K, Ahydrosil KT/K, Sarsil H-14/R, Sarsil H-15, Sarsil ME-25 – produkcji Instytutu Chemii Przemysłowej, Zakładu Doświadczalnego Silikonów – do impregnacji wodoodpornej materiałów budowlanych. Pracownie Konserwacji Zabytków, Laboratorium Naukowo – Badawcze w Toruniu.
17. Meinhardt – Degen J., 2004: Durability of hydrophobic treatment of sandstone facades – investigations of the necessity and effects of re – treatment. 10th International Congress on Deterioration and Conservation of Stone. Stockholm June 27 – July 2 2004.
18. Domasłowki W., 1993: Profilaktyczna konserwacja kamiennych obiektów zabytkowych. UMK skrypty i teksty pomocnicze.
19. Geih H., 2004: Recent developments in protecting facades with silicones. 10th International Congress on Deterioration and Conservation of Stone. Stockholm June 27 – July 2. 2004.
20. Barnat-Hunek D., Klimek B.2012: Hydrofobizacja cegły ręcznie formowanej. Materiały Budowlane 3/2012, str. 19-20.
21. Krzywobłocka – Laurów R., Rościszewski P., Zielecka M.: Badania trwałości zabezpieczeń hydrofobowych środkami krzemoorganicznymi obiektów zabytkowych. Instytut Techniki Budowlanej.

SELF-STRESSED CONCRETE MEMBERS REINFORCED WITH FRP-BARS

Victor Tur, Volha Semianiuk

Brest State Technical University, Department of Concrete Technology and Building Materials,
Faculty of Civil Engineering, Republic of Belarus
e-mail: vvtur@bstu.by

Summary:
Problem of usage fiber reinforced polymer as reinforcing bars in self-stressed flexuring structural elements is considered. Comparison of reaching degree of self-stress in concrete, which was got on the stage of self-stressing and was got like result of calculation with usage theoretical equations is produced.

Keywords: reinforcement, FRP bars; self-stressing (expansive) concrete; value of the self-stress; reinforcement ratio.

Introduction

Concrete members with reinforcement made of fiber reinforced polymer (FRP) bars find a wide application in the world practice of manufacturing building structures, exploting under the influence of the aggressive environment and industrial buildings of special purpose. As a polymer matrix for manufacturing FRP bars use different thermoreactive, thermoplastic or hybrid polymers and for it's reinforcing use different types of fibers: glass, polymer, basalt, carbon and others.

High strength, low density, high corrosion resistance in comparison with steel, possibility of regulation in wide range of conductance and radioparency depending on the type of reinforcing fiber.

It should be noted, that FRP bars have high strength characteristics (the ultimate tensile strength comes up to 1 200 N/mm^2) and low modulus of elasticity (it's about 32 000 – 55 000 MPa). This feature of FRP bars creates difficulties with it's utilization. The main problems appear at service limit state (SLS) analysis (deflection and cracking control). According with sufficiently conservative guidelines of (*fib* 2005) the partial factor γ_{cf} shall be set equal to 1,5 for ULS, that substantially reduces it's design strength in comparison with value of characteristic strength; and for SLS stresses in FRP bars shall be limited under $0,3 \cdot f_{frpu}$.

The possibility of creation prestressed structures by means of usage FRP bars (in this case rise up the effectiveness of FRP reinforcement) exists due to perfectly elastic behavior of FRP bars. At the same time, as experience has shown, it's rather laborious and even somethimes impracticable to realize pretensioning of FRP bars with the usage of traditional technology (because of necessity of manufacturing special anchorage systems, tensioning devices and creating special conditions of concrete hardening by means of temperature limitation when heat treatment is applying etc.).

In this case could be effective the utilization of physicochemical method of prestressing, based on the usage of self-stressing (expansive) concrete. Experimentally-theoretical grounds of self-stressing structures are presented in work (Mihajlov, Litver 1974). In work (Tur 1998) is presented hypothesis of conditional reinforcement. In accordance

with this hypothesis anyone restriction, that restrains free expansion strains development, can be presented as a quantity of equivalent steel reinforcement. The equivalent steel reinforcement are determined on the basis of equality of the restrictive bars stiffness. Such an approach gives in the first approximation a possibility of usage multiplicative model, that was developed by prof. Mihajlov V.V., Litver S.L., Budagianec L.I. (Mihajlov, Litver 1974) and that was updated by prof. Tur V.V.

It must be noted, that in the case of utilization steel reinforcement could be reached rather high stresses, that are coupled with low restrictive bars strains. This restrictive bars strains can be compensated as a result of concrete shrinkage in the air-dry curing.

FRP bars that have low modulus of elasticity and as a result less stiffness than steel reinforcement, reach more restrained expansion strain in comparison with steel reinforcement coupled with the same with it grade of self-stressing. As a result, greater level of the self-stressing would be saved in FRP bar after development concrete shrinkage in the air-dry curing.

Experimental researches

With the aim of checking offered theoretical approaches for evaluating self-stress value in the concrete members reinforced with FRP bars, special laboratory researches were done. For this researches were done specimens-prisms of series I and series II. The specimens-prisms had square cross section (100x100 mm) and were reinforced uniaxially with single bar. The degree of restraint (it depends on longitudinal axial stiffness of the restrictive bars); kind of the expansive concrete and it's self-stressing grade were variables parameters during this researches. One specimen-prism (reference specimen) reinforced with traditional steel bar (diameter 8 mm) that is equivalent to GFRP bar (diameter 14 mm) in terms of equality of the axial stiffness in the series I and series II was done. It was done with the aim of checking all degrees of self-stressing, that were reached during concrete expansion in the all specimens-prisms of series I and series II.

Program of the experimental researches is presented in the table 1, schemes of the experimental specimens-prisms are presented on the figure 1.

Tab. 1 Program of the experimental researches

Series of specimens	Specimens-prisms designation	Reinforcement		
		Reinforcement area $A_{f(s)}$, mm^2	Reinforcement ratio $\rho_{f(s)}$, %	Equivalent reinforcement ratio $\rho_{l,eff}$, %
Series I	PECC-1	$\frac{12.56}{1Ø4}$	0,126	0,035
	PECC-2	$\frac{28.26}{1Ø6}$	0,283	0,078
	PECC-3	$\frac{50.24}{1Ø8}$	0,505	0,139
	PECC-4	$\frac{78.50}{1Ø10}$	0,791	0,218

Series I	PECC-5	$\frac{153.86}{1Ø14}$	1,563	0,430
	PECS-6	$\frac{50.24}{1Ø8}$	0,505	0,505
Series II	PEFC-1	$\frac{12.56}{1Ø4}$	0,126	0,035
	PEFC-2	$\frac{28.26}{1Ø6}$	0,283	0,078
	PEFC-3	$\frac{50.24}{1Ø8}$	0,505	0,139
	PEFC-4	$\frac{78.50}{1Ø10}$	0,791	0,218
	PEFC-5	$\frac{153.86}{1Ø14}$	1,563	0,430
	PEFS-6	$\frac{50.24}{1Ø8}$	0,505	0,505

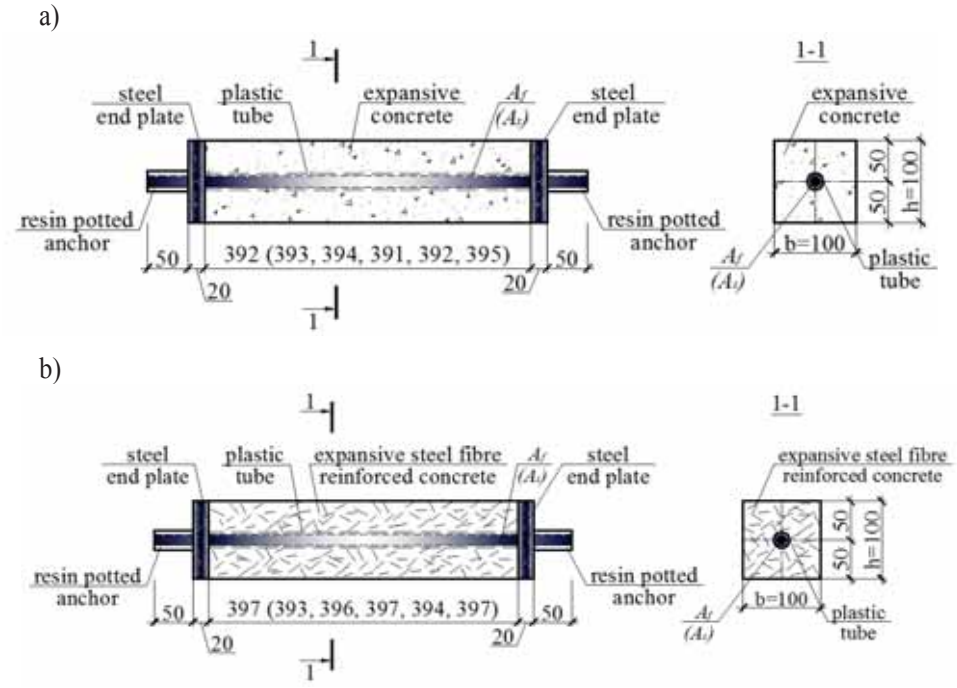

Fig. 1. Schemes of the experimental specimens-prisms
– specimens-prisms of the series I; b) – specimens-prisms of the series II)

For preparation of expansive concrete were used granite crushed stone (fraction 5-10 mm) and sand with fineness modulus equal to 3,4. Water-cement ratio was fixed equal to 0,4 (W/C=0,4). For preparation of 1 m^3 of expansive concrete were used: 500 kg of expansive cement; 960 kg of crushed stone and 750 kg of sand. Material consumption for preparation of 1 m^3 of the expansive concrete was the same as for preparation of 1 m^3 of steel fibre reinforced expansive concrete and was selected proceeding from the requirement of the efficient packing of the fractions (steel fibre consumption for preparation of 1 m^3 of the steel fibre reinforced expansive concrete was equal to 210 kg or 2,68% from the common volume content of the concrete mix or 8,4% from the common mass of the concrete mix). For the reaching required workability of the concrete mix hyper-plasticizer was used.

The main properties of the used expansive concrete were the next: the value of the self-stressing in the standard conductors was equal to 0,86 N/mm^2, the average concrete compressive strength in the free condition was equal to 36,3 N/mm^2. The main properties of the used steel fibre reinforced expansive concrete were the next: the value of the self-stressing in the standard conductors was equal to 0,63 N/mm^2, the average concrete compressive strength in the free condition was equal to 22,5 N/mm^2.

GFRP bars with diameters 4, 6, 8, 10, 14 mm (it's ultimate tensile strength was equal to 1 300 N/mm^2 and it's modulus of elasticity was equal to $E_{f(s)}$=55 000 N/mm^2) were used for restraint of the expansion strains of the self-stressing concrete and steel fiber reinforced self-stressing concrete. Steel reinforcing bars (S500) with diameter 8 mm (it's tensile strength was equal to 620 N/mm^2 and it's modulus of elasticity was equal to $E_{f(s)}$=200 000 N/mm^2) were used as equivalent to GFRP bars with diameter 14 mm in terms of equality of the uniaxial longitudinal stiffness.

Manufactured in accordance with accepted program of the experimental specimens-prisms researches were in the moist curing on the stage of self-stressing concrete expansion (before loading testing).

The following equation was used to compute the value of the self-stress ($\sigma_{CE,p}$) in the experimental specimens-prisms of series I and II expansive concrete:

$$\sigma_{CE,p} = \varepsilon_{CE,f(s)} \cdot E_{f(s)} \cdot \rho_{f(s)}, \quad (1)$$

where: $\varepsilon_{CE,f(s)}$ – GFRP (steel) reinforcing bars restrained strain at the moment of the experimental specimens-prisms of series I and II self-stressing concrete expansion stabilization; $E_{f(s)}$ – GFRP (steel) reinforcing bars modulus of elasticity; $\rho_{f(s)}$ – experimental specimens-prisms of series I and series II reinforcement ratio.

To compute the value of the theoretical self-stress ($\sigma_{CE,th}$) in the experimental specimens-prisms of series I and II expansive concrete were used equations from (TKP 45-5.03-158-2009 2010) and prof. Mihailov's formula (Mihajlov, Litver 1974).

In accordance with (TKP 45-5.03-158-2009, 2010) to compute the value of the theoretical self-stress ($\sigma_{CE,th}$) in the concrete of the experimental specimens-prisms the next equation was used:

$$\sigma_{CE,th} = \varepsilon_{CE,f(s)} \cdot E_s \cdot \rho_{l,eff}, \quad (2)$$

where: $\varepsilon_{CE,f(s)}$ – strain at the point of the centroid of reinforcing restrictive bars cross section (it is computed with usage of equation from (TKP 45-5.03-158-2009 2010)); E_s – steel reinforcement modulus of elasticity; $\rho_{l,eff}$ – equivalent reinforcement ratio, that was computed with usage of the next equation:

$$\rho_{l,eff} = \frac{A_{s,eff}}{A_c} = \frac{\alpha_f \cdot A_f}{A_c}, \quad (3)$$

where: $A_{s,eff}$ – cross sectional area of the steel reinforcement, equivalent to the cross sectional area of the FRP reinforcement; A_c – concrete section area; α_f – ratio, that takes in account steel reinforcement and FRP reinforcement stiffnesses ratio ($\alpha_f = \frac{E_f}{E_s}$); E_f – FRP reinforcement modulus of elasticity; A_f – cross sectional area of the FRP reinforcement.

In accordance with (Mihajlov, Litver 1974) to compute the value of the theoretical self-stress ($\sigma_{CE,th}$) in the concrete of the experimental specimens-prisms prof. V. V. Mihailov's formula was used:

$$\sigma_{CE,th} = 0.085 \cdot \left(f_{CE,d}\right)^{1,25} \cdot \left(\frac{1}{\varepsilon_{CE,f(s)}}\right)^{0,25}, \quad (4)$$

where: $f_{CE,d}$ – design value of the self-stressing; $\varepsilon_{CE,f(s)}$ – reinforcing bar restrained strain at the moment of the self-stressing concrete expansion stabilization.

Specimens-prisms of series I and series II value of the average concrete tensile strength (f_{ctm}) was computed with usage of the following equation:

$$f_{ctm} = \frac{\sigma_{flex}}{1,5}, \quad (5)$$

where: σ_{flex} – concrete flexural tensile strength that was got during specimens-prisms of series I and series II testing; 1,5 – conversion factor, applied for transition from concrete flexural tensile strength to concrete uniaxial tensile strength.

Results of the experimental studies

As was mentioned previously, specimens-prisms of series I and II were manufactured with various reinforcement ratio. Diagrams, shown restrained expansion strain development in uniaxially restrained expansive concrete of specimens-prisms of series I and series II (moist curing) are represented on the figure 2.

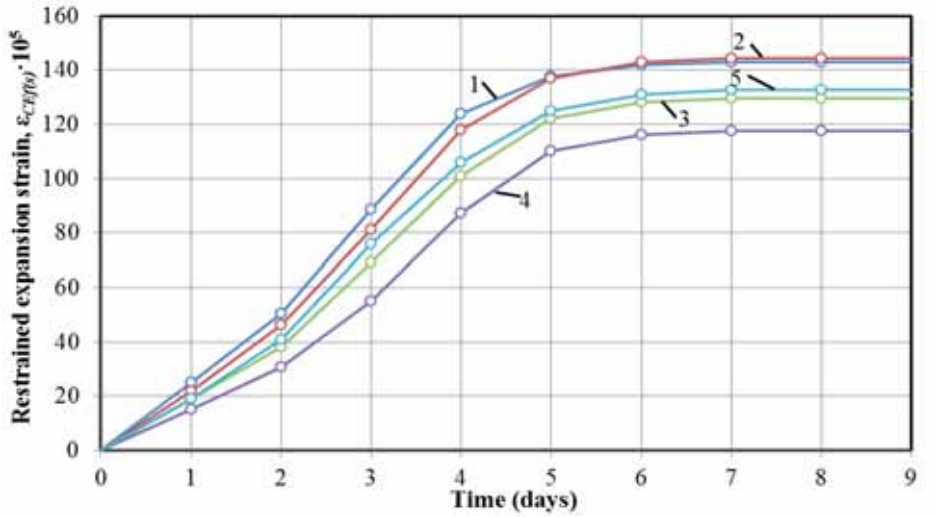

a)

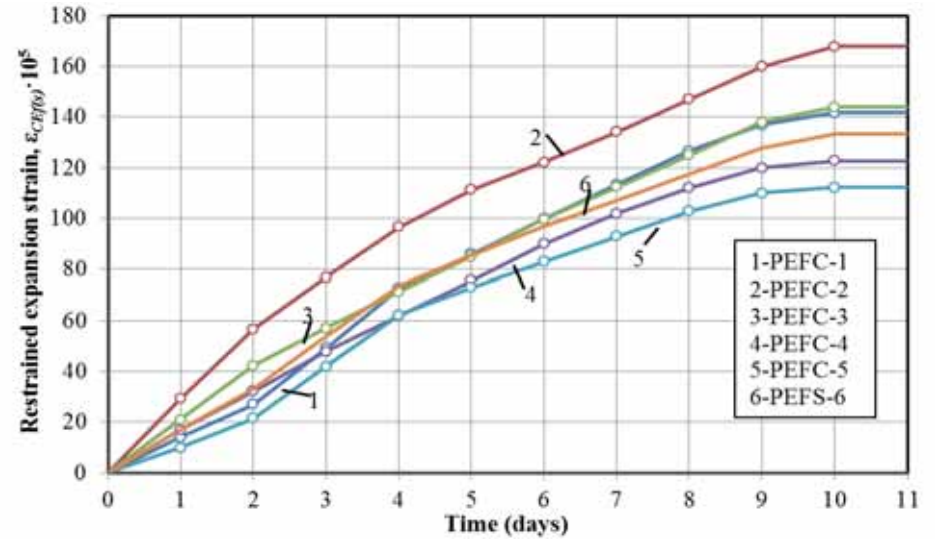

b)

Fig. 2. Restrained expansion strain development
in uniaxially restrained expansive concrete (moist curing)
(a) – for specimens-prisms of series I; б) – for specimens-prisms of series II)

Tab. 2 Testing results on the phase of specimens-prisms of series I and series II self-stressing concrete expansion stabilization

Series of specimens	Specimens-prisms designation	Reinforcement ratio $\rho_{f(s)}$, %	Equivalent reinforcement ratio $\rho_{l,eff}$, %	Restrained expansion strain $\varepsilon_{CE,f(s)} \cdot 10^5$ at the moment of the self-stressing concrete expansion stabilization	Self-stress in the concrete $\sigma_{CE,p}$, MPa	Theoretical self-stress in the concrete $\sigma_{CE,th}$, MPa	
						equation (2)	equation (4)
1	2	3	4	5	6	7	8
Series I	PECC-1	0,126	0,035	143	0,1	0,26	0,36
	PECC-2	0,283	0,078	144	0,22	0,37	0,36
	PECC-3	0,505	0,139	129	0,36	0,48	0,37
	PECC-4	0,791	0,218	118	0,51	0,57	0,38
	PECC-5	1,563	0,430	133	1,14	0,71	0,37
Series II	PEFC-1	0,126	0,035	142	0,10	0,19	0,25
	PEFC-2	0,283	0,078	168	0,26	0,27	0,24
	PEFC-3	0,505	0,139	144	0,40	0,35	0,24
	PEFC-4	0,791	0,218	118	0,54	0,42	0,26
	PEFC-5	1,563	0,430	112	0,96	0,52	0,26
	PEFS-6	–	0,505	133	1,34	0,54	0,25

As follows from the diagrams, presented on the figure 2, specimens-prisms restrained strains had almost even development up to the moment of the self-stressing concrete expansion stabilization.

It must be noted that almost all specimens-prisms, regardless of it's actual GFRP reinforcement ratio (r_f varies from 0,126 % to 1,563 %) had rather close restrained strains values at the moment of the self-stressing concrete expansion stabilization ($\varepsilon_{CE,f}$ 0.14%). This is explained by the fact that in terms steel reinforcement effective area (on the basis of uniaxial stiffness equality), equivalent steel reinforcement ratio $r_{l,eff}$ varied over the range from 0,035 % to 0,43 %. For traditional self-stressed structures presented equivalent steel reinforcement ratio are related to the restraint conditions similar to free expansion.

Expansive concrete cross-section of specimens-prisms of series I and II uniaxial stiffness development towards GFRP bars axial stiffness are presented on the figure 3.

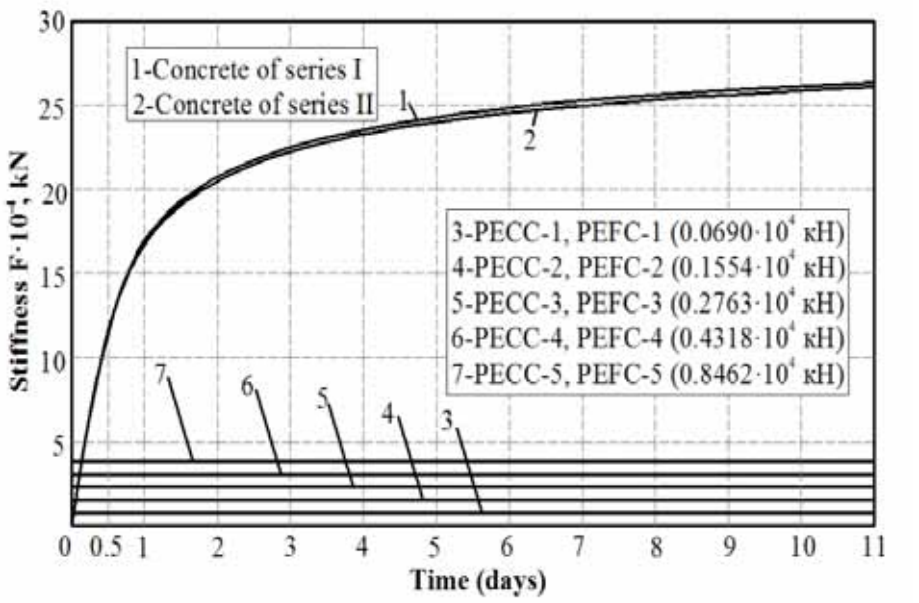

Fig. 3 Expansive concrete cross-section uniaxial stiffness development towards GFRP bars axial stiffness

As follows from the diagram on the figure 3 approximately at the age of 12 hours, concrete element stiffness becomes more than axial stiffness of GFRP bars and in the provided bond conditions (in the presence of steel end plates and resin potted anchors on the GFRP bars end zone) solid-phase expansion realizes. Whereby GFRP bars are exposed to tension that leads to concrete compression (self-stressing). It must be noted that extension of the expansion strains took place in the conditions of rather low compression stresses values. Values of the fixed in the course of experiments self-stresses at the moment of the self-stressing concrete expansion stabilization are presented in the

table 2 and self-stress development is presented on the figure 4. As follows from the presented in the table 2 and on the diagram (see figure 4) data, regardless of the GFRP bars reinforcement ratio development of the restrained strains was almost the same for all tested specimens-prisms and approached to the free expansion (specimens with value of the r_f under 0,5 %) strains.

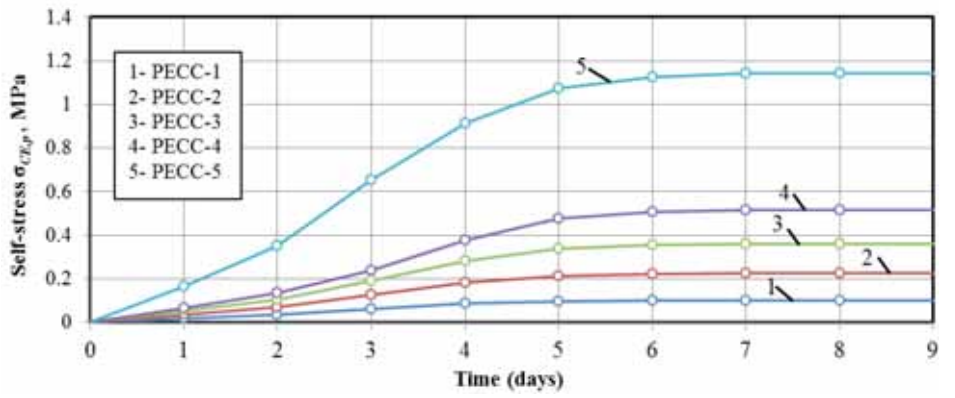

a)

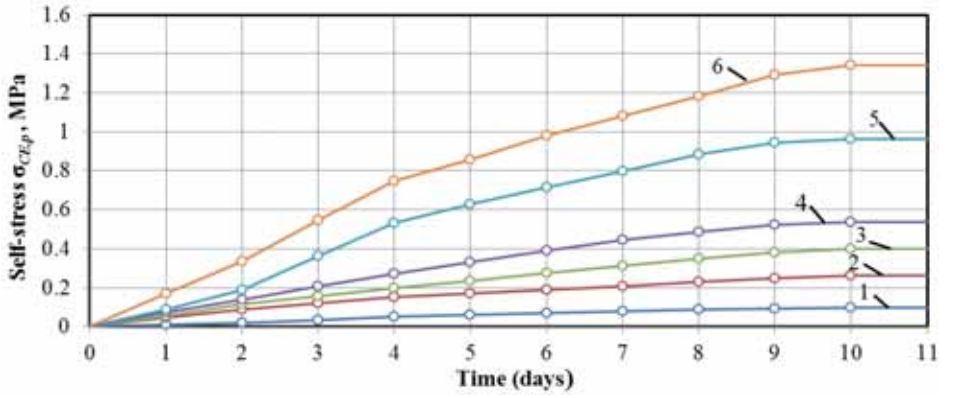

b)

Fig. 4 Self-stress development in uniaxially restrained expansive concrete
(a) – for specimens-prisms of series I; b) – for specimens-prisms of series II)

It means that in connection with GFRP reinforcement restraint low axial stiffness, concrete specimens-prisms expanded almost free. The main influence of the restrictive bond was observed at the early age concrete hardening and expansion (under 1 day). At the moment of the self-stressing concrete expansion stabilization the value of the concrete restrained strain for all specimens-prisms was equal to $\varepsilon_{CE,f} = 140 \times 10^{-5}$; at the same time the value of the restrained strain for specimens-prisms, hardened in the conditions of the standard restraint (power conductor with stiffness, equivalent to the steel

reinforcement restraint with stiffness equal to $r_1 = 1\%$) was up to $\varepsilon_{CE,d} = 43\times10^{-5}$ and to $\varepsilon_{CE,d} = 31,5\times10^{-5}$ for specimens-prisms of series I and II respectively. It must be noted, that for admitted restraint stiffness characteristics (GFRP reinforcement) were reached rather low self-stress values (under 0,4 MPa) in the concrete for both experimental specimens-prisms of series I and II (for specimens-prisms with r_f under 0,5 %); at the same time in specimens-prisms with $r_f = 1{,}563\%$ were reached rather high self-stress values – 1,14 MPa and 0,96 MPa for experimental specimens-prisms of series I (PTCC-5) and series II (PTCF-5) respectively.

Comparison self-stress values at the moment of self-stressing concrete expansion stabilization obtained in the result of the computation are represented in the table 2 and on the diagrams on the figure 5. Difference between self-stress values comes up to 3,6 times for specimens-prisms of series I and to 2,5 times for specimens-prisms of series II. It would be related with the next important effects: all equations, concerning estimation of the self-stress value are empirical and originally were received for steel reinforcement, coming out as free expansion strains restraint. During receiving this equations, low reinforcement ratio area (under 0,3%) was not considered. In this restraint area in accordance with (Mihajlov, Litver 1974) equation for evaluating self-stress value was received due to the test data from the area of high reinforcement ratio approximation and with taking into account fact, that function must pass through the origin of the axes $\frac{\sigma_{CE}}{f_{CE,d}} - r_e$.

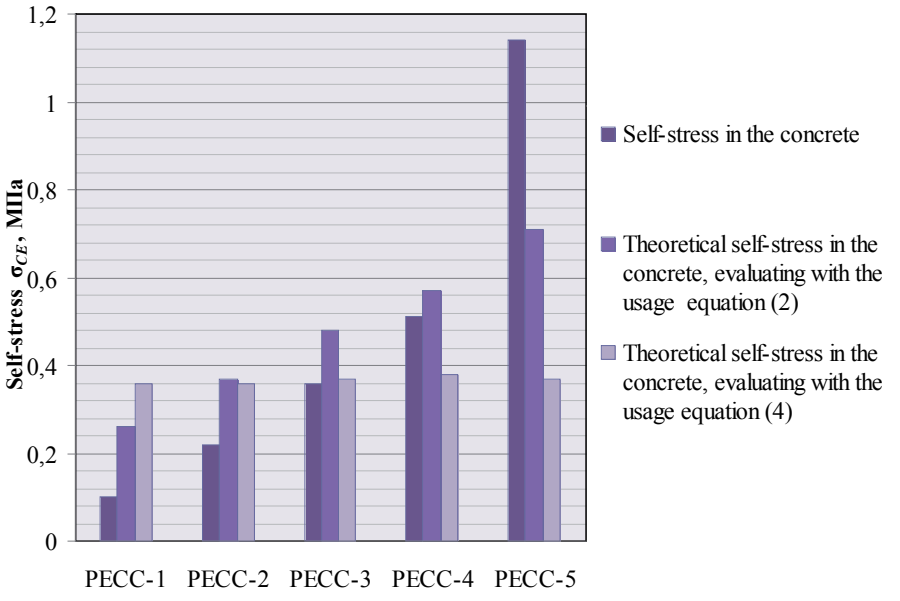

a)

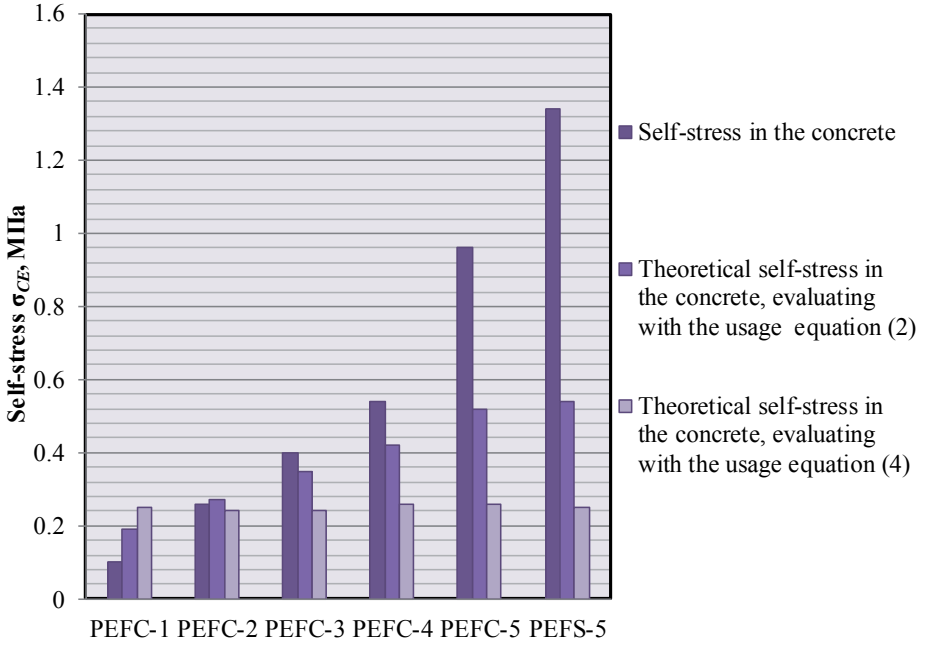

b)

Fig. 5 Comparison self-stress values obtained in the result of computations at the moment of self--stressing concrete expansion stabilization
(a) – for specimens-prisms of series I; b) – for specimens-prisms of series II)

In connection with this fact, conversion of the self-stress values for GFRP reinforcement with usage equivalent steel reinforcement ratio (it defines from the axial stiffness equality) is not quite reasonably in the low reinforcement ratio area. Approaches, based on the grounds from (Mihajlov, Litver 1974) in mind of restrained strains development, plastic strains progress in the result of creep of concrete at the young age and stress relaxation should be applied for adequate analytical model for evaluation of the self-stress values obtaining. Self-stressing process definition based on consideration values of the external restrictive bond fixed strains only don't allow take into account internal stresses, appeared in the concrete structure on the self-stressing phase. The following specimens-prisms loading tests results, presented in the table 3, sustain described above fact.

Tab. 3 Specimens-prisms loading tests results

Series of specimens	Designation of specimens-prisms	Restraint conditions $r_{f(s)}$, %	Cracking features		Axial tensile concrete strength σ_{ct}, MPa	$\Delta\sigma_{ct}$, MPa
			Force P, kN	Flexural tensile concrete strength S_{flex}, MPa		
	PEC-1	Free prism	8,98	4,04	2,69	
Series I	PECC-1	0,126 %	11,28	5,08	3,39	0,7
	PECC-2	0,283%	11,16	5,02	3,35	0,66
	PECC 3	0,505%	11,92	5,36	3,57	0,88
	PECC 4	0,791%	13,56	6,10	4,07	1,38
	PECC-5	1,563%	11,86	5,34	3,56	0,87*
	PECS-6	0,505%	7,5	3,38	2,25	–*
	PEF-1	Free prism	14,86	6,69	4,46	
Series II	PEFC-1	0,126 %	18,38	8,27	5,51	1,05
	PEFC-2	0,283%	14,04	6,32	4,21	–*
	PEFC-3	0,505%	23,24	10,46	6,97	2,51
	PEFC-4	0,791%	19,33	8,70	5,80	1,34*
	PEFC-5	1,563%	28,39	12,77	8,51	4.05
	PEFS-6	0,505%	21,05	9,47	6,31	1,85*
*Note. Within static tests in the experimental specimen-prism slipping of bar has happened.						

As follows from the specimens-prisms loading tests results (see table 3), reinforced experimental specimens-prisms had higher value of the flexural tensile strength in comparison with free specimens, hardened in the same with it conditions.

In addition it must be noted that hardening in restrained conditions (involving compression stresses effect) provided creation of the cleared conditions for structure formation, that in turn leads to average concrete axial tensile strength rising.

More important results were reached due to parthnering GFRP reinforcement and steel fibre reinforcement (specimens-prisms of series II).

Diagrams, shown restrained strains development of specimens-prisms of series II (with additional steel fibre reinforcement), presented on the figure 2 b) and values of the fixed self-stress at the moment of self-stressing concrete expansion stabilization are presented in the table 2.

It must be noted that experimental specimens-prisms of series II (made of steel fibre reinforced expansive concrete) strains were approximately the same with experimental specimens-prisms of series I (made of expansive concrete) strains (see table 2 and figure 2). Diagrams of self-stress development of specimens-prisms of series II, constructed in terms of fixed strains, are presented on the figure 4.

Conclusions

Due to completed stage researches following conclusions can be done:

1. Owing to restrictive bond made of FRP reinforcement bars low axial stiffness (it's modulus of elasticity almost commensurable with concrete modulus of elasticity) possibility of jacking with usage physicochemical method appears. Physicochemical method of the prestressing (by means of expansive concrete utilization) applies to the as it is called «soft» conditions of prestressing. Due to this method of prestressing the main shortcoming of the mechanical method of prestressing GFRP bars consisted in the limitation of the permissible stresses in the FRP tendons at jacking and transfer at the level of (30 – 50%) from it's ultimate tensile strength, otherwise creep strains (this strains inevitably led to tendons rupture) will indefinitely grow up and accumulate as a result of the FRP tendons low modulus of elasticity can be removed. In addition due to physicochemical method of prestressing it succeeded in minimizing of presrtess losses due to shrinkage of concrete.
2. In the course of self-stressing process research on the specimens-prisms of series I and series II was established that specimens with GFRP bars reinforcement ratio from 0 to 0,8% during self-stressing concrete expansion got strains almost the same with free specimens strains. As a result for such specimens comparable and rather low values of the self-stress were got. However though this fact specimens with GFRP reinforcement ratio from 0 to 0,8% tensile strength value (and as a result crack resistance) was higher in 1,4 times and in 1,6 times for specimens-prisms of series I and series II properly than free specimens from this series tensile strength value. At the same time we can say that specimens-prisms of series I and series II with GFRP reinforcement ratio in 1,563 % had rather massive restrictive bond, judging by the strains values it had at the moment of self-stressing concrete expansion stabilization. In turn it led to the obtaining by this experimental specimens rather sizeable values of it's practically self-stressing stresses: 1,14 MPa and 0,96 MPa for specimen from series I and series II properly. Mentioned specimens uniaxial tensile strength appeared in 1,9 times higher than proper free specimens uniaxial tensile strength.
3. As a result of additional restriction in the capacity of three-dimensional steel fibre reinforcement reduction of the longitudinal strains at the restrictive reinforcement depth were observed. Therewith completed loading tests showed that specimens-prisms of series I and series II made of steel fibre reinforced expansive concrete had the highest value of the axial tensile strength (specimens-prisms of series II cracking resistance moment was higher than specimens-prisms of series I made of expansive concrete cracking resistance moment in 2 times; was higher than specimen-prism with equivalent in terms of axial stiffness equality steel reinforcement ratio cracking resistance moment in 1,3 times; was higher than free specimen-prism made of steel fibre reinforced expansive concrete cracking resistance moment in 2 times).

4. Essential distinctions between theoretical self-stress value and obtained during experimental studies at the moment of self-stressing concrete expansion stabilization self-stress value must be noted (distinction between this values up to 3,6 times for specimens-prisms of series I and to 2,5 times for specimens-prisms of series II). It would be related with the next important effects: all equations concerning equation of self-stress value are impirical. In addition this equations were obtained for steel reinforcement as a restraint. Upon receipt this calculation equations was not considered the area of the low reinforcement ratio (under 0,3 %). Adequate analytical model can be developed taking into account the following values (some of this values are time-varying): self-stressing grade of concrete, restrictive bond stiffness, reinforcement ratio and surrounding it concrete stiffnesses, plastic strains in the result of creep of concrete and stress relaxation must also be taken into account.

References:

1. *fib* / Task Group 9.3 (Fiber Reinforced Polymer) Reinforcement for Concrete Structures. (2005), *FRP Reinforced for reinforced concrete structures.* Lausanne, Swithерland
2. Mihajlov V., Litver S. (1974), *Expansive and self-stressing cements and self-stressed structures.* Stroyizdat, Moscow.
3. Tur V. (1998), *Experimental-theoretical grounds of prestressing structures with the usage of expansive concrete.* BPI publishing house, Brest.
4. TKP 45-5.03-158-2009. (2010), *Concrete and reinforced concrete structures made of expansive concrete.*

ANALYSIS OF SHEAR CAPACITY OF STEEL FIBER REINFORCED CONCRETE BEAMS

Julita Krassowska, Andrzej Łapko

Bialystok University of Technology, Faculty of Civil and Environmental Engineering,
Wiejska St.45 E, 15-351 Bialystok, Poland
e-mail: j.krassowska@pb.edu.pl; lapko@pb.bialystok.pl,

Summary:
Fibers may be used in the flexural members like beams or slabs as a full or partial replacement of flexural or shear reinforcement. In the last case we have to do with combined reinforcement for shear. The methods for determining the shear capacity for SFRC elements are defined in scientific literature and also in Model Code 2010 and Russian Standard. In the paper there are presented and discussed two recent standard models and methods of calculation of shear loads in steel fiber reinforced concrete beams with combined flexural and shear reinforcement. Some chosen results of experimental investigation on shear capacity in SFRC beams including own research of flexural SFRC members tested under flexure are also presented and discussed. The tests results confirmed that steel fibers in reinforced concrete beams can partially replace (in certain cases) the traditional steel stirrups calculated for shear.

Keywords: Steel fiber reinforced concrete, shear load, shear capacity, Model Code 2010

Introduction

Near to support of the beams shear forces have significant value, and at the same regions can occur the bending moments. As a result, of shear forces exist shear stress and the bending moment causes the normal stress (compression and tension), the summation of the stresses working are formed principal stresses tension $s_1 = s_{max}$ and compression $s_2 = s_{min}$. In the reinforced concrete element compressive principal stresses are generally safely transferred through the concrete, which is characterized by high compressive strength. Principal tensile stresses tend to reach values exceeding the tensile strength of concrete. Through the use of transverse reinforcement (stirrups or bent bars), the most shear forces are safely transferred.

In the conventional RC beams steel stirrups work effectively only after formation of diagonal cracks. Their main role is to take the tensile stresses from shearing. Transfer of shear stress in the gaping crack is through the interaction of the four components of the shear force transfer: tensile component of longitudinal reinforcement, the resultant of compressive stress in the concrete, the interlocking aggregate effect and the resultant tensile stress in the stirrups.

The use of conventional steel stirrups causes additional costs associated with the consumption of reinforcing steel, installation costs for construction, during the formation of beam short distance between the stirrups also cause technological problems of uniform distribution of the aggregate in the concrete mix, which may lead to presence of voids and weak bond between the concrete and the reinforcing rods.

An alternative solution might be to apply in concrete beams distributed fibers. In practice the use of such a solution is still not sufficiently confirmed by research. Recently such studies have been undertaken on a large scale for single span beams (Aoude et al. 2012), (Haslam 2011), (Dinh et al. 2010), (Dinh 2009), (Salò, Marciukaitis 2007), (Parra-Montesinos 2006), (Domanski, Czkwianianc 2004); (Hanzlová et al. 2011). At the Department of Building Structures of the Bialystok University of Technology a research was conducted on the effects of steel and basalt fibers for single-supported beams (Krassowska, Lapko 2011) and also for two-span beams (Krassowska, Lapko 2012, 2013).

Theoretical evaluation of shear load in steel fiber reinforced concrete beams

The shear resistance of conventionally RC flexural elements are calculated using model of truss analogy according to the standard PN-EN 1992. The appropriate calculation formulas determining the capacity of:

$V_{Rd,c,}$ - Design shear resistance of the member without shear reinforcement (effect of design strength of concrete for tension and some other effects);

$V_{Rd,s}$ - Design value of shear force which can be sustained by the yielding shear reinforcement;

$V_{Rd,max}$ - Design value of maximum shear force which can be sustained by the member, limiting by crushing of the compression concrete struts (in the truss model).

Unfortunately Eurocode does not provide how to calculate the elements made of SFRC (with steel fibers). Methods for determining the shear capacity of SFRC elements are defined in (Model Code 2010), (Russian Standard 2007) and some papers (Lim and Oh 1999) and also by Aouda et al 2012).

Shear capacity of SFRC members according to Model Code 2010

With regard to the behavior in tension, which is the most important aspect of SFRC, various test methods are possible.

Bending tests can be carried out aiming at determining the load-deflection relation. The results can be used for deriving the stress – crack width relations by inverse analysis, performing equilibrium calculations for numerous crack openings. Nominal values of the material properties can be determined by performing a 3-point bending test on a notched beam as showed in Fig. 1. The deformation is generally expressed in terms of Crack Mouth Opening Displacement (CMOD).

The characteristic value of the residual ultimate tensile strength of SFRC is calculated according to the formula:

$$f_{Ftuk} = f_{Fts} - (w_u/CMOD_3)(f_{Fts} - 0{,}5\, f_{R3} + 0{,}2\, f_{R1}) \geq 0 \quad (1)$$

where: w_u is the maximum crack opening accepted in structural design, f_{Fts} serviceability residual strength (post-cracking strength for serviceability crack opening), f_{R3} residual strength of fiber reinforced concrete significant for serviceability conditions, f_{R1} residual strength of fiber reinforced concrete significant for ultimate conditions.

The value of *CMOD*,=2,5 mm.

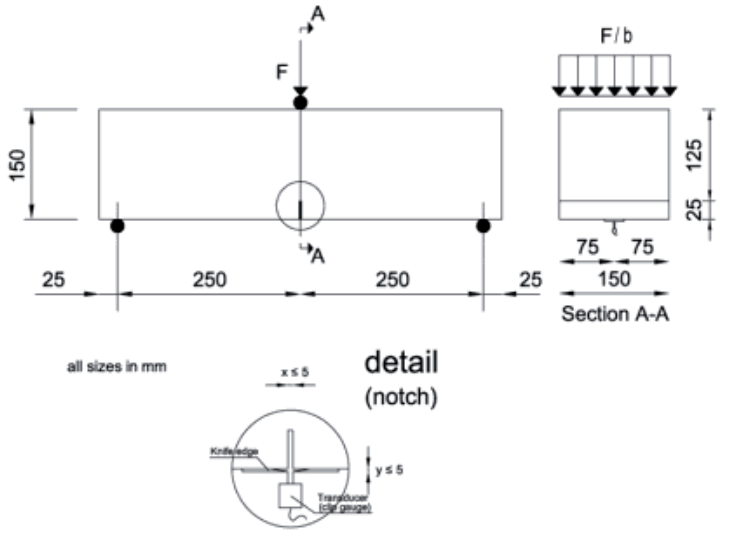

Fig. 1 Test set-up required

Beams without longitudinal and shear reinforcement

For SFRC members without both longitudinal and transverse reinforcement, the principal tensile stress s_1, shall not be higher than the design tensile strength of steel fiber:

$$s_1 \leq f_{Ftuk}/\gamma_F \tag{2}$$

where: f_{Ftuk} [MPa] is the characteristic value of the ultimate residual tensile strength of FRC
γ_F is is the partial safety factor for fiber steel.

The design value for the shear resistance in SFRC members with conventional longitudinal reinforcement and without shear reinforcement is given by the formula:

$$V_{Rd,F} = \{\frac{0,18}{\gamma_C}\ k\,[100\,\rho_l\,(1+7,5\,\frac{f_{Ftuk}}{f_{ctk}})\,f_{ck}]^{1/3}\ + 0,15\sigma_{cp}\ \}b_w\,d(1+x)^n \tag{3}$$

where:
γ_c is the partial safety factor for the concrete without fibers;
k is a factor that which takes into account the size effect and it is equal to:

$$1+\sqrt{\frac{200}{2d}} \leq 2,0 \tag{4}$$

d is the effective depth of the cross section, in mm
ρ_l is the reinforcement ratio for longitudinal reinforcement equal to:

$$\rho_l = A_{sl}/\,b_w d \tag{5}$$

A_{sl} is the cross sectional area of the reinforcement which extends $\geq l_{bd}+d$ beyond the considered section; in mm^2;

f_{Ftuk} is the characteristic value of the ultimate residual tensile strength for FRC, by considering w_u = 1.5 mm [MPa];

f_{ctk} is the characteristic value of the tensile strength for the concrete matrix, in MPa;

f_{ck} is the characteristic value of concrete cylindrical compressive strength, in MPa;

$s_{cp} = N_{Ed}/A_c < 0.2 f_{cd}$ [MPa] is the average stress acting on the concrete cross section, A_c [mm^2], for an axial force N_{Ed} [N], due to loading or prestressing force ($N_{Ed} > 0$ for compression);

b_w is the smallest width of the cross-section in the tensile area, in mm.

The shear resistance, $V_{Rd,F}$ is assumed to be not smaller than the minimum value, $V_{Rd,Fmin}$, defined as:

$$V_{Rd,Fmin} = (\nu_{min} + 0{,}15\, s_{cp})$$

$$\nu_{min} = 0{,}035 k^{3/2} f_{ck}^{1/2} \tag{6}$$

Beams with shear and longitudinal reinforcement

For the design of members with conventional shear reinforcement applies formula,

$$V_{Rd} = V_{Rd\,c} + V_{Rd\,s} \tag{7}$$

In the case of FRC members this equation is extended to:

$$V_{Rd} = V_{Rd\,c} + V_{Rd\,s} + V_{Rd\,F} \tag{8}$$

where:

$V_{Rd\,F}$ - is the contribution of the steel fibers, intersecting the design shear crack.

Shear capacity of SFRC beams according to the Russian Code

Russian Code SP-52-104-2007 proposes the formulas to calculate the tensile strength of SFRC elements. When calculating the tensile strength, it is assumed that the tensile stresses are evenly distributed throughout the cross-section of the tension. Also, it is assumed that the fiber is uniformly distributed in a volume element.

A tensile strength of steel fiber reinforced concrete is denoted as f_{fct}.

For determination of *ffct* strength there are two models of element destruction:

- The first model: the tension element is destroyed as a result of the interruption of certain fiber and pulling the rest:

$$l_{f,an} < \frac{l_f}{2} \tag{9}$$

The second type: the tension element is destroyed, assuming that all the fibers

have been drawn from concrete

$$l_{f,an} \geq \frac{l_f}{2} \tag{10}$$

where $l_{f,an}$ is anchorage length

If it is the first element the mode of failure, use the formula

$$f_{fct}\ R_{fbt} = m_1\left[K_T k_{or}^2 \mu_{fv} R_f (1 - \frac{l_{f,an}}{l_f}) + 0{,}1 R_b (0{,}8 - \sqrt{2\mu_{fv} - 0{,}005})\right] \tag{11}$$

where:

m_1 – coefficient depending on the work of fibers in concrete,

k_{or} – coefficient taking into account fiber orientations of in a volume element, depending on the dimensions of element cross section and length of the fibers, acc. taken from the standard SP-52-104-2007

μ_{fv} – ratio of the ratio of fibers in the concrete volume (v);

K_T – coefficient calculated using the formula:

$$K_T = \sqrt{1 - (1{,}2 - 80\mu_{fv})^2} \tag{12}$$

If there is the second model of damage element, it should be used the following formula:

$$f_{fct}\ R_{fbt} = m_2 R_b \left(K_T \frac{k_{or}^2 \mu_{fv} l_f}{8\eta_f d_{f,red}} + 0{,}8 - 0{,}5\mu_{fv}\right) \tag{13}$$

where:

m_2 – coefficient depending on the work of fibers in concrete

The coefficients m_1 and m_2 for engineering structures are based on experimental studies.

Shear model for SFRC concrete elements

Shear load capacity of steel fiber-reinforced concrete members with combined reinforcement (steel fibers and stirrups) may be defined on the basis of model diagonal cross-sections, presented in Russian Code SP-52-104-2007. The presented model is based on the equilibrium conditions of forces and bending moments in the inclined sections created by the inclined crack in the shear zone (see Fig.2 and 3).

Calculation of shearing strength must be checked separately considering the effect of bending moment and shear force. Strength diagonal cross-sections determined by the equations of equilibrium of external and internal forces and bending moments acting on the assumed cross section. Design shear force V_{Ed} is defined in cross -section perpendicular to the longitudinal axis and design moment M_{Ed} is obtained from the summary of the moments of all the design forces to the center of gravity of compression zone.

Calculation of shear capacity V_{Rd} for steel fiber-reinforced concrete elements without stirrups in the zone of inclined crack (Fig.2) in the beam is based on the formula

$$V_{Rd} = V_{fcc} + V_{fct} \tag{14}$$

where: V_{Rd} - shear capacity in a cross-section perpendicular to the longitudinal axis in the element, V_{fcc} - shear force, carried by compression zone of fiber-reinforced concrete in this section; V_{fct} - shear force, carried by tensile zone of steel fiber-reinforced concrete in the section.

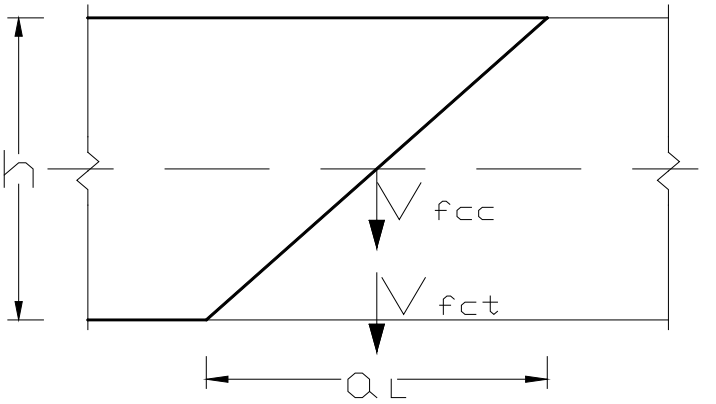

Fig. 2. Superposition of shear force in the fiber-reinforced concrete beam without stirrups (SP-52-104-2007)

The value of shear force V_{fcc} for flexural members may be determined by the formula:

$$V_{fcc} = \frac{0{,}75 f_{fct} b h^2}{a_L \sin(90^0 - \beta)} \tag{15}$$

where: f_{fct} - defined by the formulas with the substitution of two coefficients k_{or} or $k_{n,w}$

k_{or} - coefficient taking into account the orientation of the fibers relative to the direction of principal tensile stresses; $k_{n,w}$ - coefficient taking into account the influence of the orientation of the fibers sectional dimensions perpendicular to the direction of an external force, b and h - the width and height of cross-section of the calculated member; a_L - the projection of an inclined crack (the angle is assumed to be 45°); β - angle of the vertical axis of element to the vertical.

The value of shear force V_{fct} is given by:

$$V_{fct} = q_{fcc} a_L \tag{16}$$

where:
$$q_{fcc} = \frac{f_{fcc} b}{a_L \sin(90^0 - \beta)} \tag{17}$$

f_{fcc} is the characteristic value of compressive strength steel fiber-reinforced concrete

Calculation of shear capacity V_{Rd} for fiber-reinforced concrete members with flexural reinforcement (stirrups), see Fig.3, is based on the formula

$$V_{\mathrm{Rd}} = V_{fcc} + V_{fct} + V_{sw} \tag{18}$$

where: V_{sw} - shear force, carried by the shear reinforcement in the cross-section.

Transverse force taken by the stirrups V_{sw} is determined by the formula

$$V_{sw} = \varphi_{sw} q_{sw} a_q \tag{19}$$

where:
φ_{sw} – a coefficient taken equal to 0.75;
qsw - force in the transverse reinforcement per unit length of the element, determined by the formula:

$$q_{sw} = \frac{f_{sw} A_{sw}}{s_w} \tag{20}$$

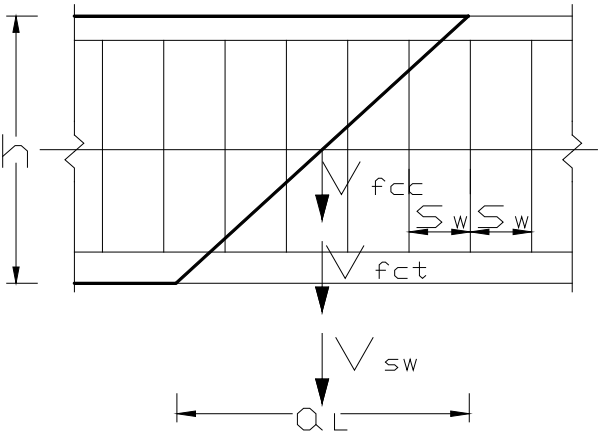

Fig. 3. Composition of shear forces in the fiber-reinforced concrete beam having flexural and shear reinforcement

Calculation of shear capacity of SFRC beams on the basis of experimental studies

Lim and Oh (Lim, Oh 1999) conducted the first tests on the shear capacity of flexural beams made of steel fiber reinforced concrete. Theoretical and experimental research has been carried out on 9 beams by testing varied fraction of steel fibers and the ratios of steel stirrups required to shear reinforced. On this basis they formulated the formula for the total shear force for the simply supported beams:

$$V=V_c+V_A+V_d+V_F \tag{21}$$

where V_c is the shearing force across the compression zone, V_a is the interlocking aggregate force, V_d is the dowel action force, V_f is the vertical components of the fiber pull out force along the inclined crack, as showed in Fig 4.

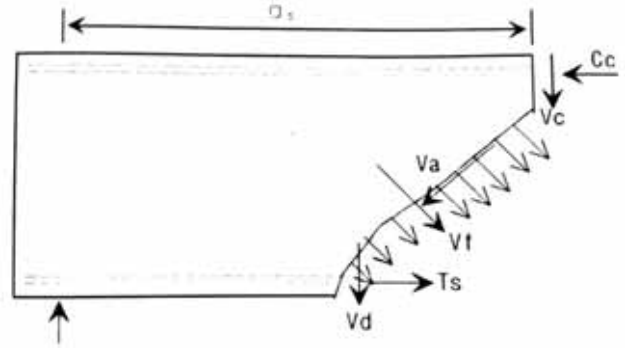

Fig.4. A part of shear span of a simply supported SFRC beam (Lim, Oh 1998)

Recent studies on the effect of fiber on shear capacity of the fiber are presented by Aouda, and others (Aoude, et al. 2012). Experimental program involving 9 series of RC and SFRC beams. Investigated shear capacity, failure mode and crack openings. Based on performed research there was carried out theoretical research to establish the formula for the shear capacity considering the effect of fibers. Presented model lead to equation (22) where the shear resistance of an SFRC bream was assumed to be equivalent to the expected shear strength of traditional RC beam V_{no} plus the additional shear resistance V_{fib} provided by the fibers.

$$V_{nf}= V_{no} + V_{fib} \tag{22}$$

Shear resistance V_{no} - is general design method of CSA A23.3-04 showed in equation (23).

$$V_{no}=V_c+V_s \tag{23}$$

The V_c and V_s are the concrete and transverse steel (stirrup) contributions to shear resistance.

The fiber contribution the shear resistance V_{fib} can be related to the pullout strength F_P of the fibers crossing this cracking plane, as shown in eq. (24).

$$V_{fib} = (N_{fib} 0{,}83 F_p)\, b_w\, d_v \cot\Theta \tag{24}$$

The effective number of fibers per unit area N_{fib} for fibers randomly oriented in three dimensions can be calculated using eq. (25)

$$N_{fib} = V_f / A_f\, \alpha\, \eta_1 \tag{25}$$

where A_f is the cross-sectional area of the fiber, v_f - the volume fraction of fibers in the matrix, α - the orientation factor and η_1 - the length factor.

Own experimental investigation on shear capacity of SFRC

Team of Bialystok University of Technology conducted a study in order to clarify the possibility of partial or total replacement of stirrups with steel fibers in flexural model beams. The beams were performed of concrete mix using steel fibers with a length of 50 mm and a diameter of 1 mm made of round wire, cold drawn, low carbon steel. Steel fibers were dispensed to the concrete mix in an amount of 1.5% by volume of concrete. For preparation of SFRC model beams Portland cement CEM I 32.5 R and natural aggregates, having grain size of 0.125-4 mm. To improve the workability of the composite mixture a superplasticizer was used. In the mix water to cement ratio was equal to 0.67. Single-span reinforced concrete beams with a cross section 80 mm × 120 mm and the span 1,100 mm were loaded till failure. The reinforcing flexural steel bars are made of steel with a yield strength f_y of 500 MPa, and the steel of stirrups have the yield strength f_y of 220 MPa. The details of SFRC model beams are presented in Fig. 5. Depending on steel fiber content and arrangement of steel stirrups the 3 series of model SFRC beams have been performed containing three samples in each series (Iwaniuk, 2012). In any series, the spacing of steel stirrups was differed at the left and right half span of each model beam (as shown in Fig. 5).

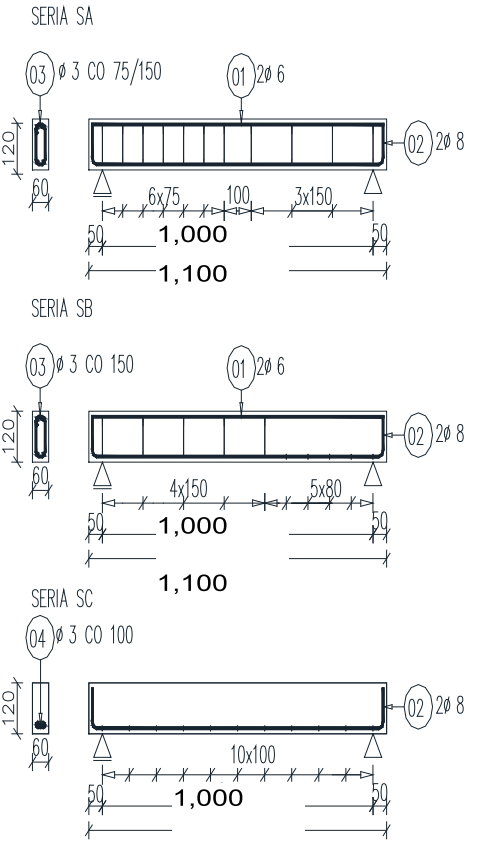

Fig. 5 Details of three Series of tested SFRC beams: SA, SB and SC (Iwaniuk, 2012)

Eight of the nine tested SFRC model beams were failed in shear. Only one beam has failed due to flexure. Fig. 6 shows the destructive diagonal cracks in the tested beams. The failures caused by the shear force occurring on this side of the beam, where the stirrups was used at twice increased spacing of stirrups or they were not used at all.

Fig. 6 The failure modes of selected SFRC beams after testing (Iwaniuk, 2012)

The test results obtained for SFRC model beams are presented in Table 2. The tested model beams with steel fibers for all the test series showed an increase shear capacity by about 45%.

Tab. 1 Critical forces for each series of model SFRC beams (Iwaniuk, 2012)

Series of beams	Maximum critical experimental load	Experimental critical shear capacity	Increase of theoretical shear capacity
	(kN)	(kN)	(%)
SA-0	24	12	-
SA-1	34*fail in bending	17	42.0
SA-2	34	17	42.0
SB-0	22	11	-
SB-1	32	16	45.0
SB-2	32	16	45.0
SC-0	20	10	-
SC-1	28	28	40.0
SC-2	30	30	50.0

Comparison of experimental results and theoretical

The calculation of the effect of longitudinal forces will be carried out in accordance with PN-EN 1992.

Tab. 2. Load theoretical and experimental beams of model (Iwaniuk, 2012)

Capacity on	Series	Theoretical destructive force [kN]	Destructive force of experimental studies [kN]	Increase in shear capacity for experimental research [%]
Bending	A, B, C	17	17*	-
Shear	A	12	17**	42,0
	B	10	16**	60,0
	C	7	15**	114,0

The values of critical shear forces evaluated from the tests for each series of test were significantly higher than the calculated theoretical shear capacities. The largest increase was obtained for beams of series C, where there was no stirrups.

Summary and conclusions

Model Code 2010 proposes separately the methods of calculation of shear capacity for beams with or without shear and longitudinal reinforcement. In the case without shear reinforcement fibers supplement is taken into account by determining the characteristic value of the residual ultimate tensile strength of FRC in accordance with the principles of fracture mechanics. For elements with steel shear reinforcement and longitudinal fibers also are included as a contribution of the fibers increasing the design shear cracks.

Russian standard specifies shear capacity of SFRC beams taking into account the impact of cross-diagonal dividing the fiber in tension and compression zones. The standard calculation formulas are presented in function of strength of fiber concrete in tension, taking into account the amount, type, length and diameter of the fibers. Unfortunately, these models are suitable only for fibers produced in Russia.

In all the reporting methods of computing the impact of fiber on shear capacity included as a component of the shear force. In view of the many factors the Model Code 2010 method is the most accurate method. The parameters used in the calculation are universal and do not depend on the country of origin of fibers, as in the case of the Russian method. However, the method of calculation laid down in the Russian standard is much simpler.

From own research done on model SFRC beams with and without stirrups shows that experimental values of destructive shear forces are much higher than theoretical ones.

For better understanding of the problem of determination of shear capacity of SFRC members a further experimental investigations of FRC beams are needed.

References:

1. Aoude H et all.: Response of Steel Fiber- Reinforced Concrete Beams with and without Stirrups. ACI Structural Journal. May-June 2012. 359-367.
2. CAN/CSA-A23.3-04. Design of Concrete Structures. 2010.
3. Dinh H. H.: Shear Behavior of steel fiber reinforced concrete beams without stirrup reinforcement", doctoral dissertation, Department of Civil and Environmental Engineering, University of Michigan, Ann Arbor, MI 2009.
4. Dinh H.H., Parra-Montesinos G.J., Weght J.K.: *Shear Behavior of Steel Fiber - Reinforced Concrete Beams without Stirrup Reinforcement*, ACI Structural Journal, September-October 2010, 597-607.
5. Domański T. Czkwianianc A.: Influence of steel fibers on the strains in shear zones in two-span beams, *Proceedings of the National Conference on the Research Problems in Civil Engineering*, Krynica, pp. 26-19, 2004.
6. Hanzlova H., Kratky J., Heran R.: ‚Analysis of shear failure of flexural fiber concrete beams reinforced with rebar of two ductility classes, 4th WSEAS International Conference on Engineering Mechanics, Structures, Engineering Geology, Greece 2011.
7. Hasam E. Yakoub: Shear Stress Prediction: Steel Fiber-Reinforced Concrete Beams without Stirrups, ACI Structural Journal, May-June 2011).
8. Iwaniuk P.: Strengthening of reinforced concrete beams shear zones using the local fibre-cement with steel fibre, Master Thesis, Department of Civil and Environmental Engineering, Bialystok University of Technology, Poland, 2011 (in Polish).
9. Krassowska J., Lapko A.: The Influence of the Basalt Fiber on the Shear and Flexural Capacity of Reinforced Concrete Continuous Beams, 1st International Conference for PhD Students in Civil Engineering, Cluj-Napoca, Romania 2012.
10. Krassowska J., Lapko A.: The Influence of Steel and Basalt Fibers on the Shear and Flexural Capacity of Reinforced Concrete Beams. Journal of Civil Engineering and Architecture, Vol. 7, No 7, 2013, pp. 789-798.

11. Lapko A., Krassowska J.: *Shear effects in steel fibre reinforced concrete beams*. International Conference on Engineering, UBI2011, Portugal 2011.
12. Lim D.H., Oh B.H.: Experimental and theoretical investigation on the shear of steel fiber reinforced concrete beams, Engineering Structures, 1999.
13. Model Code 2010: First Complete Draft. Vol.2. CEB - *fib*. October 2011.
14. Parra-Montesinos G.J.: Shear Strength of beams with deformed steel fibers, Concrete International, November 2006.
15. EN 1992-1-1 Design of concrete structures. Part 1-1: General rules and rules for buildings, 2004.
16. Salna R. Marciukaitis G.: The influence of shear span ratio an load capacity of steel fiber reinforced concrete elements with various steel fiber volumes. Journal of Civil Engineering and Management, Vol. XIII, No 3, 2007. pp. 215-209, 2007.
17. SP 52-104-2006. Steel Fiber Reinforced Concrete. Moscow, Russian Standard (2007).

DETERMINATION OF SATURATED WATER CONDUCTIVITY COEFFICIENT IN BUILDING MATERIALS

Zbigniew Suchorab, Ewa Zarzeka-Raczkowska

Lublin University of Technology, Faculty of Environmental Engineering
Nadbystrzycka St. 40B, 20-618 Lublin, Poland
e-mail: Z.Suchorab@wis.pol.lublin.pl

Summary:
Capillary water uptake is a serious phenomenon influencing the functioning of old and newly raised buildings, thus modeling of this process is very important for prediction of the behavior of building objects. Among many models of water transport in building barriers Richards model of unsaturated water flow can be distinguished. This model of water transport in porous materials can be seriously applied for capillary uptake simulations and can be useful to predict behavior of the walls which are prone to groundwater influence. One of the most important empirical parameters which are applied in the above mentioned model is hydraulic conductivity coefficient k, which, depending on type of water flow can be expressed in saturated state (saturated water conductivity coefficient k_s) and water conductivity in relation to moisture for unsaturated water transport model.
This article presents basic information about water transport models in saturated and unsaturated states that can be applied for prediction of capillary rise phenomenon in building barriers and determination of one of most important parameters – saturated water conductivity k_s. Saturated water conductivity coefficient was determined for red ceramic brick, aerated concrete and autoclaved calcium silicate using a modified Wit apparatus, which normally is applied for soil hydraulic conductivity coefficient determination.
Obtained results confirmed the lowest conductivity feature of red brick which is expressed in the lowest value of saturated conductivity coefficient. Aerated concrete and autoclaved calcium silicate are more porous materials and thus are more hydraulically conductive.

Keywords: capillary uptake, Richards model, water transport in porous media, saturated water conductivity coefficient

Introduction

One of the models describing water transport in porous materials is a Richards equation. It is based on Darcy's law (Zaradny 1990) of saturated water transport in porous medium. According to Darcy's law, water transport is a relation of sample cross-section, hydraulic gradient and saturated conductivity coefficient k, determined in the described research. Darcy's model of water transport can be described with the following formula:

$$V = k_s \Delta h \tag{1}$$

Where:

k_s – saturated conductivity coefficient (Darcy's constant) [cm/s, cm/h, cm/d],
Δh – pressure gradient [cm H_2O, m H_2O].

Saturated conductivity is a characteristic feature of each material and it depends mainly on its porosity, granulometry and temperature. Values of saturated conductivity coefficient are determined experimentally and they may differ for each material many times.

Darcy's model of water transport in porous media described in this paper is mainly applied in soil water movement description, where water flow is expressed in volume units [m^3/s] and transporting force is hydraulic gradient caused by pressure difference. Anyhow it should be underlined that this model is also applied in building physics (Černý et al., 2001; Grunewald, 2000) especially in states near saturation, which may occur in the bottom parts of the buildings like funds or walls in contact to ground water, without suitable water-proof isolation.

Building materials and barriers are hardly ever in saturated states, that's why application of Darcy's model is strongly limited in building physics and more practical is to use Richards model, where water transport depends not only on the hydraulic gradient and water conductivity but also on water content. That's why in unsaturated states water velocity should be described by the following formula (van Genuchten 1980, Feddes 1997, Kowalik 1995):

$$V = -k(\theta)\nabla h \tag{2}$$

Where:

θ – volumetric water content [cm^3/cm^3],

$k(\theta)$ – hydraulic water conductivity in relation to water volumetric content [cm/s, cm/h, cm/d],

h – water pressure [cm H_2O, m H_2O].

Above formula is a Darcy's model for unsaturated states, where $k(\theta)$ is a hydraulic conductivity in relation to moisture. Water content and water pressure are combined by water retention characteristics (Mualem 1976, van Genuchten 1980, Mallants, 1997) that's why water conductivity in the above formula can be also treated as a relation of water pressure h.

Formula describing water transport in unsaturated materials is called Richards model and requires to determine hydraulic conductivity in unsaturated states - $k(\theta)$ or $k(h)$.

In the first case, hydraulic conductivity depends on volumetric water conductivity and Richards formula can be described in the following form:

$$\frac{\partial\theta}{\partial t} = \frac{\partial}{\partial x}\left[D(\theta)\frac{\partial\theta}{\partial x}\right] + \frac{\partial}{\partial y}\left[D(\theta)\frac{\partial\theta}{\partial y}\right] + \frac{dk(\theta)}{d\theta}\frac{\partial\theta}{\partial y} \tag{3}$$

Where:

$D(\theta)$ – moisture diffusivity, the product of hydraulic conductivity and moisture characteristics $k(\theta)\frac{dh}{d\theta}$.

Final element of the above formula is gravitation, which does not strongly influence the process of capillary rise. From the point of view of the building physics it may be worth to mention here, that without gravitation part this formula is equivalent to heat conductivity equation in relation to temperature (Kowalik 1995).

Another form of Richards equation is a formula in relation to hydraulic potential, which, from computational reasons is more often used in simulations, especially in multilayered objects like building envelopes:

$$C(h)\frac{\partial h}{\partial t} = \frac{\partial}{\partial x}\left[k(h)\frac{\partial h}{\partial x}\right] + \frac{\partial}{\partial y}\left[k(h)\frac{\partial h}{\partial y}\right] + \frac{dk(h)}{dh}\frac{\partial h}{\partial y} \tag{4}$$

Where:

$C(h) = \frac{d\theta}{dh}$ - differential water capacity of the material [m^{-1}].

Hydraulic conductivity coefficient described in this article is determined for only saturated states, which are not typical for most of circumstances connected to water flow in building barriers, thus there are applied many mathematical and empirical models relating hydraulic conductivity to pressure potential (or moisture). Currently the most popular models are the following:

- in relation to moisture (van Genuchten 1980):

$$k(\theta) = k_s\sqrt{\theta}\cdot\left[1-(1-\theta^{\frac{1}{m}})^m\right]^2 \tag{5}$$

- in relation to pressure potential (van Genuchten 1980):

$$k(h) = k_s\frac{\left[\left(1+|\alpha h|^n\right)^m - |\alpha h|^{n-1}\right]^2}{\left(1+|\alpha h|^n\right)^{\frac{5}{2}m}} \tag{6}$$

Where:

k_s – saturated water conductivity [cm/d],

θ – volumetric water content [cm^3/cm^3],

α, n, m – empirical parameters depending on type of the porous medium.

As visible in the above formulas, determination of water conductivity coefficient in intermediate states requires determination of this parameter in saturation and then recalculation into unsaturated states using above presented formulas.

Materials and Methods

The aim of the described research was to determine saturated water conductivity coefficient (Darcy's constant). The research was conducted using laboratory technique with Wit apparatus (Wit 1967) modified by Zawadzki (Zawadzki et al. 1981) presented at Fig. 1.

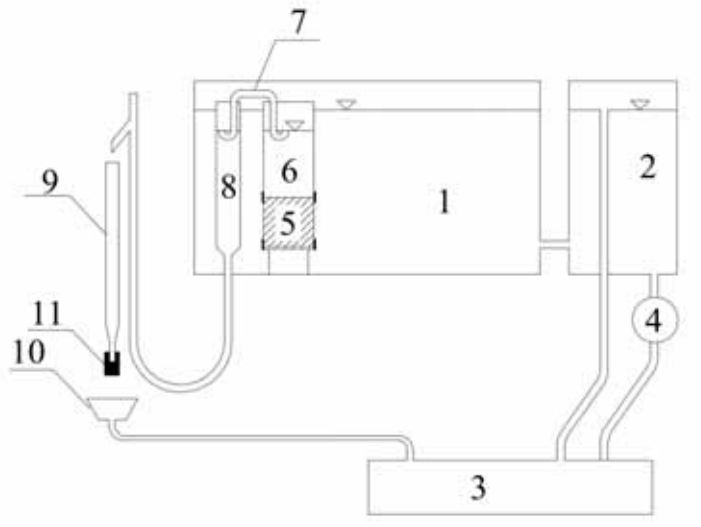

Fig. 1. Schematic of modified Wit aparatus (Iwanek 2005, Zawadzki et al. 1981): 1 – main container, 2 – overflow vessel, 3 – closed water container, 4 – electric pump, 5 – measured sample, 6 – measurement cylinder, 7 – overflow siphon, 8 – outflow siphon, 9 – burette, 10 – outflow through, 11 – rubber heel

The details of modified Wit apparatus and its service are in detail presented in [Zawadzki et al. 1981].

For the experiment a set of the following building material samples was prepared: red ceramic brick (apparent density 1600g/dm^3), cellular concrete (apparent density 400g/dm^3) and autoclaved calcium silicate (apparent density 180g/dm^3). The samples were precisely placed in measurement cylinders and sealed with bitumen insulation to eliminate any potential leaking.

In case of red ceramic brick it was necessary to modify the sample preparation methodology due to impossibility of insertion of the hard material in the traditional cylinder cover. For that aim the cuboid samples were prepared with the following dimensions: 5×5×5.8cm and externally insulated with epoxy resin to prevent unexpected water inflow to the measured material from the outside.

The whole experiment was repeated six times. Saturated water conductivity coefficient k_s was calculated using the following formula (Zawadzki et al. 1981, Iwanek 2005):

$$k_s = \frac{Q\Delta l}{F\Delta H} \tag{7}$$

Where:

Q – amount of water in time [cm^3/s],

Δl – vertical length of the sample [cm],

F – sample cross-section area perpendicular to water flow direction [cm^2],

ΔH – hydraulic loss at Δl length [cm].

Results and discussion

Below presented table shows average saturated conductivity coefficients of three examined building materials expressed in [cm/min] and [cm/day] together with standard deviations (δ).

Table 1. Saturated conductivity coefficients of examined building materials

Material	Saturated conductivity k_s			
	[cm/min]	δ [cm/min]	[cm/day]	δ [cm/day]
Red Ceramic Brick	0.00078	0.00006	1.125	0.0821
Cellular Concrete	0.00198	0.00036	2.845	0.5219
Autoclaved Calcium Silicate	0.00226	0.00042	3.253	0.6045

On the basis of the conducted research it is visible that the building material with the lowest hydraulic saturated conductivity is red ceramic brick. It is caused by the dense structure and the biggest share of solid phase in the whole volume. Cellular concrete and autoclaved calcium silicate are the materials with greater porosity and thus the value of saturated conductivity coefficient is significantly greater (two times in case of autoclaved calcium silicate).

Comparing the obtained results with the values found in the literature it should be noticed that it is hard to find values of this parameters. It is mainly caused by the fact that Richards equation is not popular model of water transport in building materials. According to data presented by Hall et all. (2001) value of this parameter varies between $3.2 \cdot 10^{-8}$ to $3.8 \cdot 10^{-9}$cm/s which means that red brick is a very inhomogeneous material with hydraulic saturated conductivity coefficient varying even 10 times.

Conclusions

Basing on the conducted experiment and obtained results, the following conclusions may be drawn:

- Richards model applied for water transport in unsaturated, porous materials is not popular in building physics to describe water movement in building materials and barriers.
- Modified Wit apparatus enables determination of saturated conductivity coefficient of building materials which is an important factor in Richards model of water transport.
- Saturated conductivity coefficients determined in the presented research can be successfully applied for water uptake simulating in building materials and barriers using Richards model.
- Among examined materials, the greatest value of saturated conductivity coefficient was determined for autoclaved calcium silicate and the lowest for ceramic brick, which means that brick is less permeable material from the other examined media.

References:

1. Černý R., Drchalova J., Rovnanikova P. (2001), *The effect of thermal load and frost cycles on the water transport in two high-performance concretes*. Cement and Concrete Research 31, pp. 1129-1140.
2. Feddes R.A., Koopmans R.W.R., van Dam J.C. (1997), Agrohydrology, Wageningen.
3. Grunewald J. (2000), Documentation of the Numerical Simulation Program DIM3.1, Volume 2, User's Guide.
4. Hall C., Hoff W.D. (2001), Water Transport in Brick, Stone and Concrete, Spon Press, Londyn and New York.
5. Iwanek M. (2005), *Badanie współczynnika filtracji gleb metodą polową i w laboratorium*, Acta Agrophysica, 5(1), pp. 39-47.
6. Kowalik P. (1995), Obieg wody w ekosystemach lądowych, Monografie Komitetu Gospodarki Wodnej PAN, Warszawa, Zeszyt 9.
7. Mallants D., Jacques D., Tseng P-H., van Genuchten M. Th., Feyen J (1997), *Comparison of three hydraulic property measurement methods*, Journal of Hydrology 199, pp. 295-318.
8. Mualem, Y., (1976), *A new model for predicting the hydraulic conductivity of unsaturated porous media*. Water Resour. Res., 12, pp. 513-522.
9. Van Genuchten T.Th., (1980), *A closed form equation for predicting the hydraulic conductivity of unsaturated soils*. Soil Sci. Soc. Am. J., 44, pp. 892-898.
10. Wit K.E. (1967), *Aparatus for measuring hydraulic conductivity of undisturbed soil samples*. Inst. For Land and Water Management Reearch Tech. Bubl. 52. Wagningen.
11. Zaradny H. (1990), Matematyczne metody opisu i rozwiązań zagadnień przepływu wody w nienasyconych i nasyconych gruntach i glebach. Prace IBW PAN nr 23, Gdańsk.
12. Zawadzki S., Olszta W. (1981), *Zmodyfikowany aparat Wita do laboratoryjnego oznaczania przepuszczalności wodnej gleb*. Wiadomości IMUZ, t. XIV z. 2, 187-194.

MODELING OF AIR-FLOW IN ASSEMBLY HALL SUPPORTED BY MECHANICAL VENTILATION SYSTEM

[1]Andrzej Raczkowski, [2]Zbigniew Suchorab, [2]Grzegorz Kucharczyk

[1]Pope John Paul II State School Higher Education in Biala Podlaska, Department of Engineering Sciences, Sidorska St. 95/97, 21-500 Biała Podlaska, Poland
[2]Lublin University of Technology, Faculty of Civil Engineering and Architecture, Nadbystrzycka St. 40, 20-618 Lublin, Poland

Summary:
The aim this paper is to present the results of simulations of mechanical ventilation system performance in assembly hall of the Faculty of Environmental Engineering, Lublin University of Technology. Simulation was conducted using Autodesk CFD Simulation 2013. 3D model of the assembly hall was created in Autodesk Revit Architecture application, which is directly connected to CFD Simulation program. There were conducted two variants of simulations: for winter conditions and for the summer performance. Obtained results enable to verify temperature values and air-flow velocities in the modeled room in each place and time. Conducted simulations showed that there are the areas with air parameters do not satisfying the design assumptions, required for thermal comfort and the correction of the applied solutions is needed. Air flow velocity distribution in the examined assembly hall, determining the indoor air parameters depends on many factors that were not considered in the described system solutions. The most important factor is temperature of the external barriers and the particular geometry of the room. Their consideration was only possible after creating the spatial model of the room and the ventilation system.

Keywords: Indoor air quality, Computational Fluid Dynamics, CFD

Introduction

Quickly developing civilization and changing way of human livings caused that most of time people spend in the artificial indoor climate. Currently more pressure is put on creation of optimal indoor air conditions and the possibility to control the microclimate parameters (Afshari A., Bergsoe N.C 2003). Progress of modern technique enables to provide almost all microclimate conditions on suitable level (Fanger, P. Ole, 1974).

Indoor environment designing requires such information as airflow pattern, velocity, temperature, humidity. To study indoor air flow at small-scale or full-scale, suitable models can be built, but they need coefficients for heat transfer and air flow or they are expensive and time consuming. Various numerical methods have been developed to simulate the indoor environment (Chang 2011). The most popular approach of computational simulation is Computational Fluid Dynamics (CFD) methods. CFD can be used for prediction of internal and external flow within and around the buildings.

Autodesk CFD Simulation uses the Finite Element Method (FEM). The space occupied by the fluid is divided into the discrete elements. This allows the temperature, velocity, and other fluid properties to be determined. FEM is used in structural analysis of the solids, but is also applicable to fluids. The FEM formulation has been adapted to be also used for fluid dynamics equations solving (Surana, K.A. et al. 2007, Huebner, K. H. et al. 1995).

The possibility to regulate the indoor air parameters leads to obtain such thermal conditions, that would be satisfying to each person present inside the room. Biological variety of people causes, that it is not possible to guarantee suitable comfort parameters to all individuals, anyhow it should be possible to feel comfortably by the greatest amount of people present. Creation of thermal comfort state is only possible when the neutral status of thermal parameters is obtained which means that men do not require wormer or colder conditions. Anyhow such state does not guarantee thermal comfort (Fanger P.O. et al. 2003, Baker N., Standeven M. 1993).

Still aiming to create thermal comfort is caused by the need to satisfy human needs to feel comfortably. Also, creation of thermal comfort at workplace positively influences work efficiency. Each individual obtains the greatest physical and intellectual efficiency only when suitable thermal comfort status is provided. There were conducted a lot of examinations aimed on determination what conditions were the most satisfactory at particular workplace but it was not determined if thermal comfort is required to maintain the optimal health status of human individuals (Burek R. et al. 2006, Fanger P.O. et al. 2003, Popiołek 2005).

Model assumptions

This paper presents the analysis – simulation of air-conditioning system performance in the room of the assembly hall of the Faculty of Environmental Engineering, Lublin University of Technology. Assembly hall model was elaborated basing on the real object stocktaking and air-conditioning system basing on the executive design of the installation. To create the 3D model Autodesk Revit Architecture 2012 program was applied. Geometry of the assembly hall is presented at Fig. 1. Modeled external envelopes and internal equipment determine the calculation area. Due to the necessity to limit the number of the nodes in the calculation mesh, shape of most of elements was simplified. Such simplifications are widespreadly applied for numerical calculations, because rounded shapes or too many details do not increase calculations quality, but significantly increase the duration of calculations and the volume of the result files (Chang 2011).

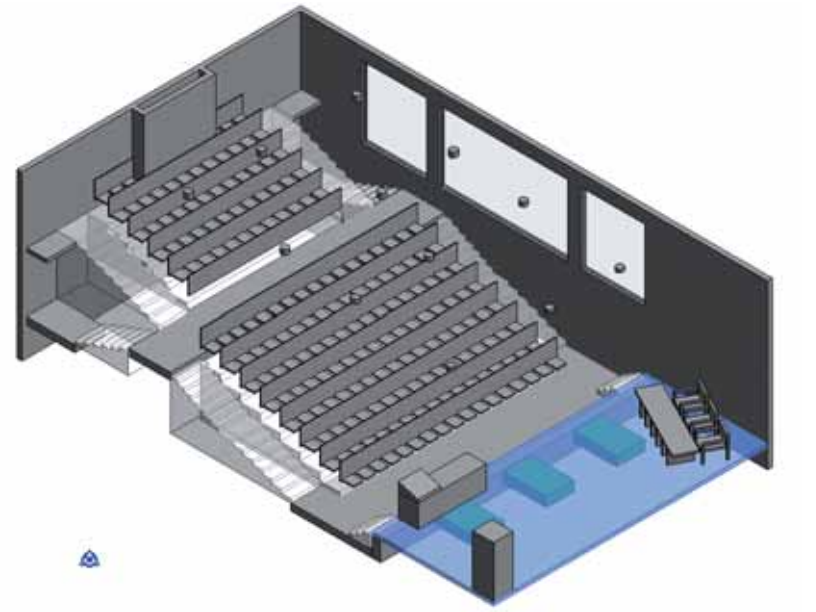

Fig. 1. Three dimensional model of the described assembly hall

The dimensions of the assembly hall are the following: 11m × 20m and the room height depends on place. Maximum height is about 7m and minimum height – 2.5m.

According to fire regulations, in the design it was assumed the maximal number of people inside the room n = 150 persons. Air ventilation is supported by the inlet-exhaust central unit. Ventilation unit productivity is 7200m^3/h. Inlet elements are TROX VDR 315 type ventilators. They are assembled at the suspended ceiling. These ventilators have the possibility to change slope angle of the delivered air. Depending on position the ventilators have the following slope angle: 45°, 65°, 75°, 90°. Each of 12 ventilators delivers the same amount of fresh air equal to 600m^3/h. Single exhaust is placed below the stand for the lecturers. It removes totally 7200m^3/h of polluted air and consists of three exhaust grills made by TROX, AWT type.

System of air-conditioning of the assembly hall should enable maintenance of temperature level at 22°C during winter season and 23°C in summer (Fanger P.O., et al., 2003).

Materials and methods

The basic tool used in the described paper is Autodesk Simulation CFD packet which can be used for thermal analyses and fluid mechanics simulations. It consists of tools enabling simulation of turbulent flows but also heat conduction and convection (Chang 2011).

To create model for simulation procedure it is necessary to determine the types of materials of the modeled object and assign the suitable parameters like temperature etc. Next step is determination of points of air delivery and the exhaust. For simulations of indoor thermal

comfort the most important is to present air temperature and velocity distribution. To obtain this results it is required to assign such values as: the amount of air delivered to the room, the amount of exhausted air but also its temperature and velocity. Intake air velocity can be omitted, but only if the dimensions of intake and exhaust ventilators are suitably defined – in these cases the program will calculate suitable velocities of air intake and exhaust itself. In rooms with equal amount of delivered and exhausted air it is not required to set the amount of the exhausted air by the ventilator, it is only required to sign this element with 0 Pa air flow. The final step to be defined before simulation procedure is to set up the calculation mesh. CFD Simulation packet has a very big potential for calculation mesh settings. The only criterion that limits the extend of the details is the CPU computational efficiency and thus duration of calculations but also the size of the outcome file, which great dimensions sometimes disable the possibility to verify the results even on very effective computers.

Described application enables to present the obtained results in many formats: for example the diagrams with averaged results from the default period of calculations, results in graphical form for any layer of the room, particular place or the area. From generated graphics it is also possible to create animations.

Available computer efficiencies enabled to conduct simulations reaching 120 minutes of simulated process with possibility to visualize every 10 minute steps in the most significant stage of air conditioning system – start of the process.

Simulation was divided into two variants: one for winter period and the second one for summertime:

- Winter, empty room, intake air temperature 22°C, windows temperature 10°C, external envelopes temperature 18°C,
- Summer, empty room, intake air temperature 19°C, windows temperature 40°C, external envelopes temperature 22°C (Fanger P.O., et al., 2003).

Results analysis

The aim of the conducted simulation was to verify the possibility to provide suitable values of temperature and air velocities in the people's zone in the assembly hall of the Faculty of Environmental Engineering, Lublin University of Technology.

Obtained simulation results unequivocally show places where calculated indoor air parameters significantly differ from the assumed ones, which were required to satisfy the thermal comfort conditions. Air temperature distribution in winter period after 120 minutes of system start is not satisfactory – areas with unfavorable temperature below 20°C can be found in the people's zone. Fig. 2 presents temperature distribution at the level of ankles of the audience. In the middle part of the hall there are visible the areas with temperature 18°C which is unacceptable (Fanger P.O., et al., 2003).

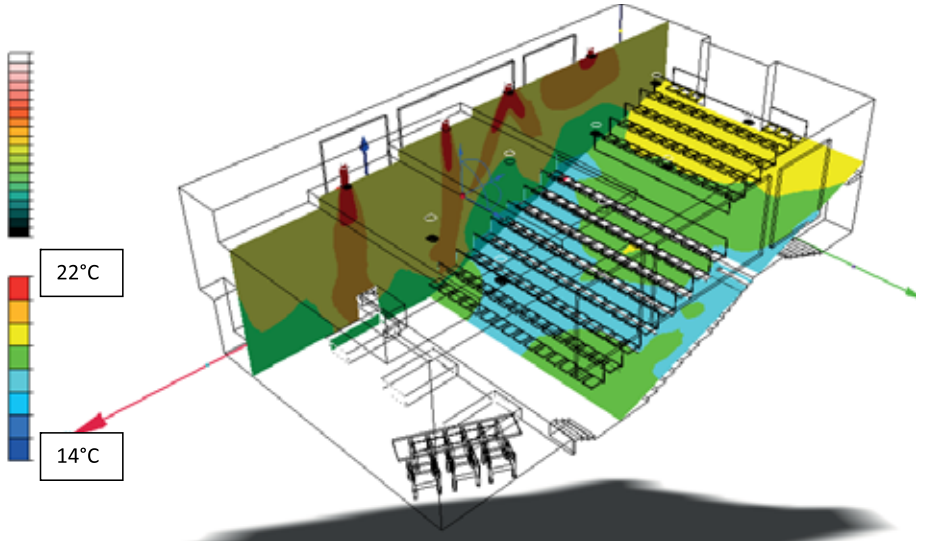

Fig. 2. Air temperature distribution at the level of ankles in the 120 minute of air-conditioning system working

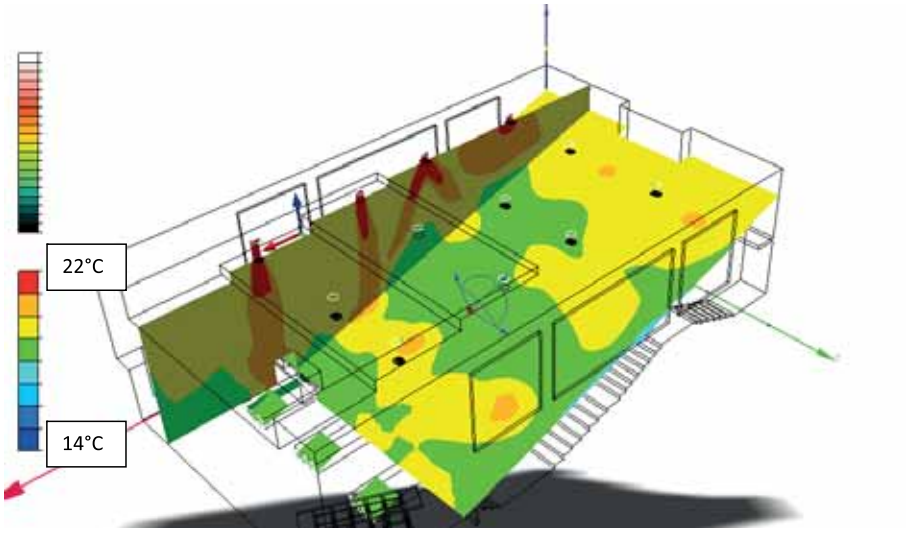

Fig. 3. Air temperature distribution at the level of heads in the 120 minute of air-conditioning system working

In winter period, air velocity at the level of head of sitting people maximally equals 0.6 m/s (Fig. 4) with temperature 19°, which is unfavorable phenomenon from the point of view of thermal comfort (Fanger P.O., Popiołek Z., Wargocki P. 2003).

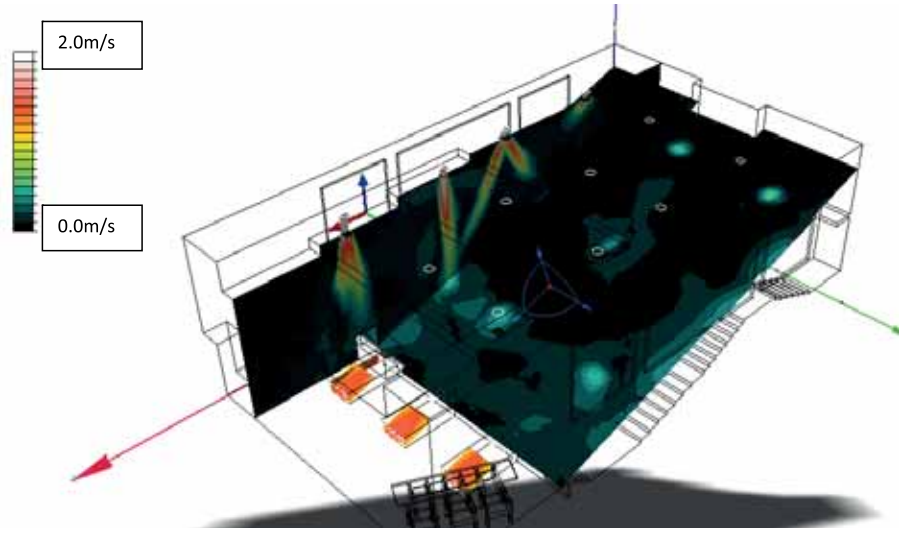

Fig. 4. Air velocities distribution at the level of head after 120 minutes of system functioning

Unfavorable conditions were also noticed in the lecturers podium – air velocity exceeds the maximal values (Fig 5).

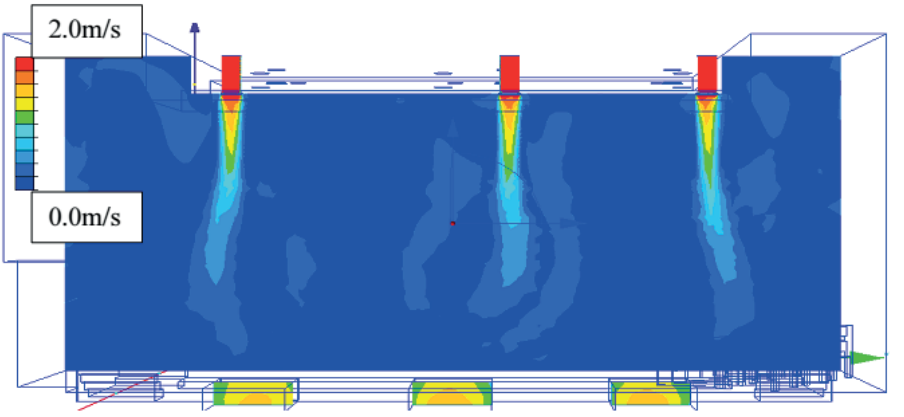

Fig. 5. Air velocities distribution at lecturers podium

In summertime temperature distribution at whole room is suitable and is equal about 27°C, with the assumed outdoor temperature equal 36°C. Unfavorable conditions spread close to the intake ventilators with the following inflow angles: 75° and 90°, where air flow velocity close to people's heads is significantly too high and reaches about 1.3 m/s (Fig. 7) and air temperature equal 29°C (Fig. 6).

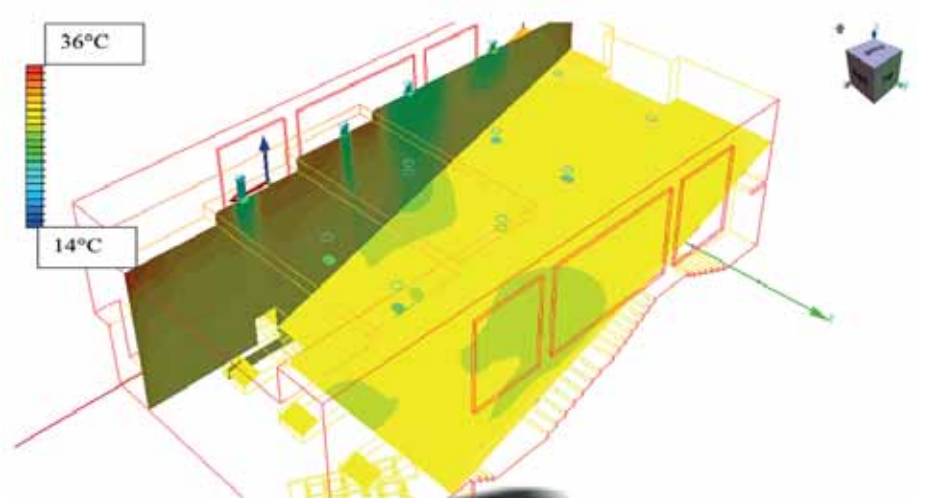

Fig. 6. Temperature distribution at heads level, summertime period

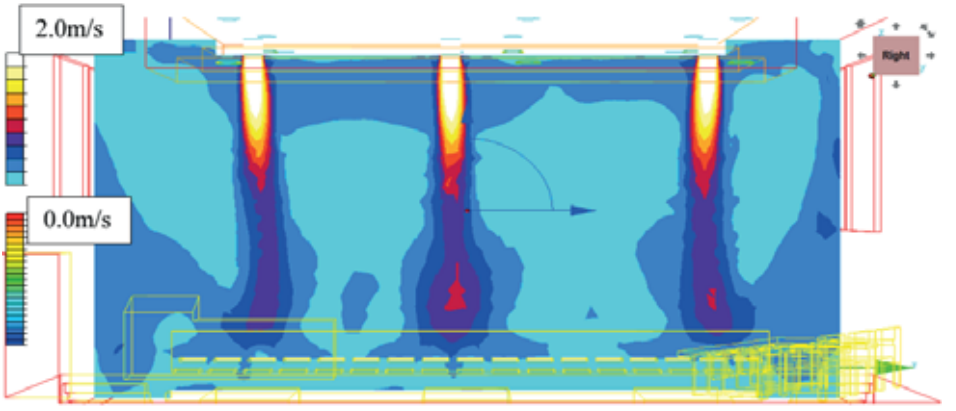

Fig. 7. Air velocity distribution at lecturers stage

At the upper part of the assembly hall, under the intake ventilators with blades angle equal 45° there occur places with air flow velocities equal zero, which also, especially during summertime, may result in discomfort sensation (Fig.8).

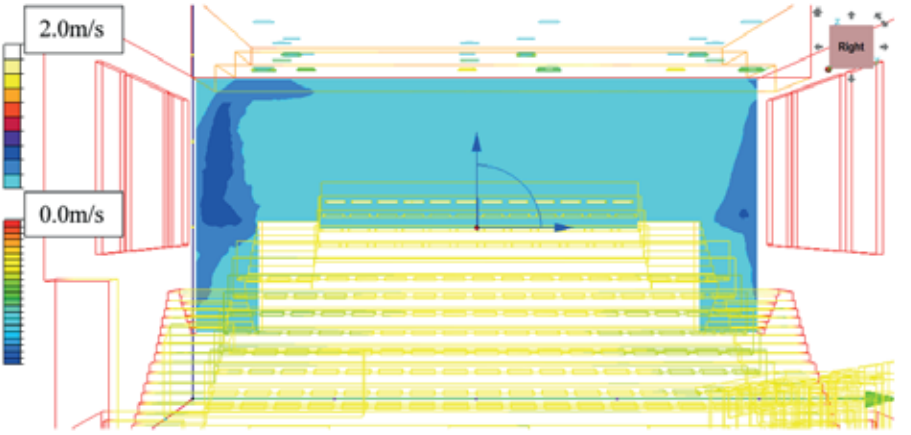

Fig. 8. Air velocity distribution in the last row of the seats

Air temperature and velocities at the rest part of the assembly hall are at the suitable levels. Main factor which would enable to obtain suitable temperature and air velocity in the whole people's zone would be to set different blades angle of the intake ventilators or application of a different type of ventilators.

Conclusions

Simulation of functioning of the air-conditioning installation in the assembly hall of the Faculty of Environmental Engineering, Lublin University of Technology designed in the traditional way, according to all assumed rules revealed the possibilities of occurrence of situations, when the designed system does not fulfills its assumptions. Disturbances of the described system performance were not possible to be predicted at the stage of designing. Air velocity distribution determining the maintenance of thermal comfort depends on many factors which were not considered at the designing stage, but were possible to be considered in presented simulations. The most important factors are: temperature of external envelopes and the detailed geometry of the room itself. Their consideration was only possible by creation of the spatial model of the room and thus installation. Due to the benefits provided by modeling, computer simulation will become obligatory stage of the whole building designing process and installations.

References:

1. Afshari A., Bergsoe N.C. (2003), Humidity as a Control Parameter for Ventilation, Indoor and Built Environment, No 12, 215-216.
2. Baker N., Standeven M. (1993), Thermal comfort for free-running buildings, Energy and Buildings, No 23, 175-182.

3. Burek R., Połednik B., Raczkowski A. (2006), Study of the relationship between the perceived air quality and the specific enthalpy of air polluted by people, Archiwum Ochrony Środowiska, vol. 32, No 2, 21-26.
4. Chang R. (2011), High Performance Building Design Using Computational Fluid Dynamics (CFD). Autodesk University 2011.
5. Fanger P.O., Popiołek Z., Wargocki P. (2003), Środowisko Wewnętrzne, Wyd. Politechniki Śląskiej, Gliwice.
6. Huebner, K. H., Thornton, E. A., Byron, T. D. (1995), The Finite Element Method for Engineers. Wiley Interscience.
7. PN-78/B-03421 - Wentylacja i klimatyzacja. Parametry obliczeniowe powietrza wewnętrznego w pomieszczeniach przeznaczonych do stałego przebywania ludzi.
8. PN-78/B-03421 – Wentylacja i klimatyzacja. Parametry obliczeniowe powietrza wewnętrznego w pomieszczeniach przeznaczonych do stałego przebywania ludzi.
9. PN-EN 13779:2008 - Wentylacja budynków niemieszkalnych. Wymagania dotyczące właściwości instalacji wentylacji i klimatyzacji.
10. Popiołek Z (2005), Energooszczędne kształtowanie środowiska wewnętrznego, Wydawnictwo Politechniki Śląskiej, Gliwice.
11. Surana, K.A.; Allu, S.; Tenpas, P.W.; Reddy, J.N. (2007), "k-version of finite element method in gas dynamics: higher-order global differentiability numerical solutions". International Journal for Numerical Methods in Engineering 69.